

Award Number: W81XWH-04-1-0001

TITLE: SignalingPathwaysthatMediateNeurotoxin-InducedDeathofDopamineNeurons

PRINCIPAL INVESTIGATOR: Kim A. Heidenreich, Ph.D.

CONTRACTING ORGANIZATION: University of Colorado Health Sciences Center
Aurora, CO 80045

REPORT DATE: November 2008

TYPE OF REPORT: Final

PREPARED FOR: U.S. Army Medical Research and Materiel Command
Fort Detrick, Maryland 21702-5012

DISTRIBUTION STATEMENT: Approved for Public Release;
Distribution Unlimited

The views, opinions and/or findings contained in this report are those of the author(s) and should not be construed as an official Department of the Army position, policy or decision unless so designated by other documentation.

REPORT DOCUMENTATION PAGE			<i>Form Approved</i> <i>OMB No. 0704-0188</i>		
Public reporting burden for this collection of information is estimated to average 1 hour per response, including the time for reviewing instructions, searching existing data sources, gathering and maintaining the data needed, and completing and reviewing this collection of information. Send comments regarding this burden estimate or any other aspect of this collection of information, including suggestions for reducing this burden to Department of Defense, Washington Headquarters Services, Directorate for Information Operations and Reports (0704-0188), 1215 Jefferson Davis Highway, Suite 1204, Arlington, VA 22202-4302. Respondents should be aware that notwithstanding any other provision of law, no person shall be subject to any penalty for failing to comply with a collection of information if it does not display a currently valid OMB control number. PLEASE DO NOT RETURN YOUR FORM TO THE ABOVE ADDRESS.					
1. REPORT DATE 1 Nov 2008		2. REPORT TYPE Final		3. DATES COVERED 1 Nov 2003 – 31 Oct 2008	
4. TITLE AND SUBTITLE SignalingPathwaysthatMediateNeurotoxin-InducedDeathofDopamineNeurons			5a. CONTRACT NUMBER		
			5b. GRANT NUMBER W81XWH-04-1-0001		
			5c. PROGRAM ELEMENT NUMBER		
6. AUTHOR(S) Kim A. Heidenreich, Ph.D. E-Mail: kim.heidenreich@ucdenver.edu			5d. PROJECT NUMBER		
			5e. TASK NUMBER		
			5f. WORK UNIT NUMBER		
7. PERFORMING ORGANIZATION NAME(S) AND ADDRESS(ES) University of Colorado Health Sciences Center Aurora, CO 80045			8. PERFORMING ORGANIZATION REPORT NUMBER		
9. SPONSORING / MONITORING AGENCY NAME(S) AND ADDRESS(ES) U.S. Army Medical Research and Materiel Command Fort Detrick, Maryland 21702-5012			10. SPONSOR/MONITOR'S ACRONYM(S)		
			11. SPONSOR/MONITOR'S REPORT NUMBER(S)		
12. DISTRIBUTION / AVAILABILITY STATEMENT Approved for Public Release; Distribution Unlimited					
13. SUPPLEMENTARY NOTES					
14. ABSTRACT Parkinson's disease (PD) is characterized by progressive loss of dopaminergic neurons in the nigrostriatal pathway resulting in significant motor dysfunction. The pathology of PD is mimicked by exposure to 1-methyl-4-phenyl-1,2,3,4-tetrahydropyridine (MPTP) or the pesticide rotenone. These neurotoxins inhibit complex I of the mitochondrial respiratory chain resulting in the production of reactive oxygen species (ROS) and increased cytosolic calcium. We hypothesize that ROS promotes opening of the mitochondrial permeability transition pore which triggers the death pathway. In parallel, increases in cytosolic calcium leads to oxidative stress and activation of c-Jun-NH2-terminal kinase (JNK). JNK/c-Jun signaling augments activation of the mitochondrial apoptotic cascade by suppressing Bcl-2 pro-survival signals via phosphorylation of Bcl-2 or transcription of the BH3-only, Bcl-2 antagonist Bim. The interactions between the oxidative stress pathway, the JNK/c-Jun signaling cascade, and the mitochondrial apoptotic machinery ultimately determine the fate of dopamine neurons. We will utilize primary ventral mesencephalic cultures obtained from E15 embryonic rats to investigate our hypothesis. The data obtained should lead to the identification of promising therapeutic strategies to slow or halt the dopaminergic neurodegeneration that occurs during progression of PD.					
15. SUBJECT TERMS neurodegeneration, apoptosis, dopamine neuron, MPTP, rotenone, intrinsic death pathway					
16. SECURITY CLASSIFICATION OF:			17. LIMITATION OF ABSTRACT	18. NUMBER OF PAGES	19a. NAME OF RESPONSIBLE PERSON USAMRMC
a. REPORT U	b. ABSTRACT U	c. THIS PAGE U			19b. TELEPHONE NUMBER (include area code)
			UU	95	

Table of Contents

Introduction.....	4
Key Research Accomplishments.....	17
Reportable Outcomes.....	18
Conclusions.....	20
Appendices.....	6 manuscripts attached

Final Progress Report- #W81XWH-04-1-0001, “Signaling Pathways that Mediate Neurotoxin-induced Death of Dopamine Neurons”. November 1, 2003-October 31, 2008

Introduction

The overall goal of our studies is to better understand the cellular proteins and signaling pathways that control neuronal death so that we can identify new therapeutic targets for slowing or preventing neurodegenerative diseases, particularly Parkinson’s disease. Our approach has been to study primary neurons in culture where we attempt to create *in vitro* conditions that are relevant to neurodegenerative disease. That is, we create conditions that cause the death of neurons in culture in order to identify the cellular proteins that mediate death and also to understand how neurotrophic factors like GDNF and IGF-1 prevent neuronal death.

The overall working hypothesis of this research proposal was that the Parkinsonian neurotoxins, MPP+ and rotenone, share a common mechanism of action to induce death in dopaminergic neurons. By inhibiting complex I of the mitochondrial respiratory chain, these toxins result in the production of reactive oxygen species (ROS) that leads to opening of the mitochondrial permeability transition pore (mitoPTP) and activation of a JNK/c-Jun signaling cascade. Opening of the mitoPTP induces Bax translocation to mitochondria and Bax-dependent cytochrome C release that initiates the intrinsic apoptotic cascade. Activation of the intrinsic death pathway is augmented by JNK/c-Jun-dependent inhibition of Bcl-2 pro-survival signals. Neurotrophic factors, like GDNF, prevent cell death by regulating the activity the death machinery.

To study primary differentiated dopamine neurons *in vitro*, we cultured cells obtained from embryonic rat or mouse ventral mesencephalon (the location of most dopamine neurons in the CNS). One major limitation of the ventral mesencephalic cultures is that the percentage of dopamine neurons in the cultures is very low (generally less than 3% of total cells). A second problem inherent to ventral mesencephalic cultures centers on the methods that are currently available to identify dopamine neurons in culture. To date, most investigators stain the ventral mesencephalic cultures for tyrosine hydroxylase (TH, the rate-limiting enzyme in the dopamine biosynthetic pathway) to identify dopamine neurons. The staining procedure, however, kills the neurons and limits the types of experiments that can be done with the cultures. To circumvent this issue, we used a GFP-TH reporter construct to identify living dopamine neurons in culture. This allowed us to study dopamine neurons (GFP-positive cells) using live-cell imaging techniques. Most of the data obtained in the first two years of study was obtained by delivering the GFP-reporter construct using the Helios gene-delivery system. This method was successful for dopamine neurons, however, the yield of transfected cells was low (less than 5%). The low transfection efficiency combined with the low numbers of dopamine neurons in the cultures made it extremely difficult to obtain large numbers of single-cell measurements for quantitative analysis. For these reasons, we spent a lot of effort in the next two years investigating new ways of transfecting dopamine neurons. Unfortunately, none of the transfection methods have yielded optimal results. Despite these technical difficulties we learned information about the nature of cultured dopamine neurons, the process by which they die, and the limitations of using GDNF as a factor to prevent dopamine cell death in response to neurotoxins like MPP+ and rotenone.

Specific Aim 1. To investigate the role of the mitochondrial (intrinsic) death pathway in the apoptosis of primary dopamine neurons induced by the neurotoxins MPP+ and rotenone.

Throughout these studies, primary cultures derived from E15 rat ventral mesencephalon were prepared in $\text{Ca}^{2+}/\text{Mg}^{2+}$ -free Hanks' balanced salt solution by mechanically dispersing tissue pieces with a 1 ml pipet. Subsequently, cells were centrifuged at 200x g for 4 min and resuspended in F12 medium containing 5% heat-inactivated human placental serum, 2 mM L-glutamine, 100 $\mu\text{g}/\text{ml}$ streptomycin, 100 U/ml penicillin and (in some cases) 2.2 $\mu\text{g}/\text{ml}$ ascorbic acid. Cells were seeded on polyethylenimine-coated 24-well plates in 0.5 ml of medium at 6×10^4 viable cells/ cm^2 . Culture medium was changed every two days. In the ventral mesencephalic cultures, approximately 2-5% of the cells were tyrosine hydroxylase (TH)-positive dopaminergic neurons.

To examine the toxicity of MPP+ in cultured dopamine neurons, day 5 cultures were treated with MPP+ (time course and dose response experiments were performed). After treatment, cells were fixed with 4% paraformaldehyde and then permeabilized and blocked in PBS containing 0.2% Triton X-100 and 5% bovine serum albumin. Cells were then incubated overnight at 4 °C with a monoclonal antibody to TH (1:500). The primary antibody was aspirated, and cells were washed five times with PBS. Cells were then incubated with a donkey anti-mouse Cy3-conjugated secondary antibody (1:500) and DAPI for 2 h at room temperature. The cells were then washed 5 times with PBS, and coverslips were adhered to glass slides with mounting medium. Fluorescent images were captured on a Zeiss Axioplan-2 microscope equipped with a Cooke Senciam deep-cooled CCD camera. All imaging data collection and analysis were carried out using the Intelligent Imaging Innovations Slide book software program. Data were obtained from at least five coverslips from five different cell preparations. Results showed that the MPP+ treatment resulted in a time- and dose-dependent loss of TH+ neurons (Fig. 1).

**MPP+ toxicity in primary dopamine neurons
is time- and dose- dependent**

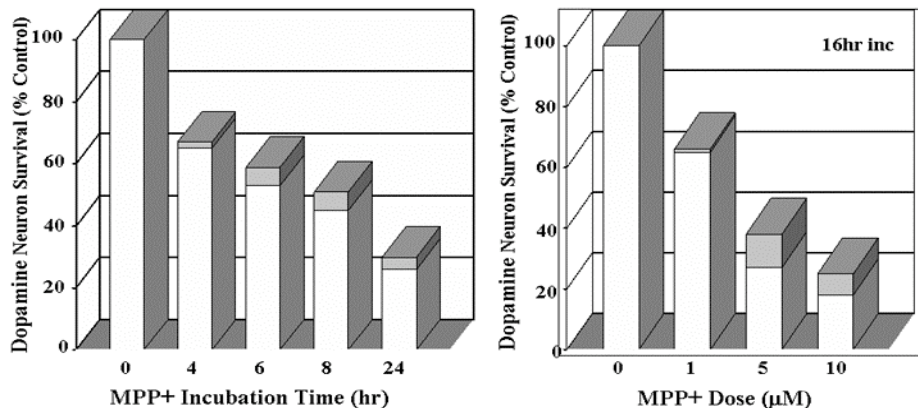
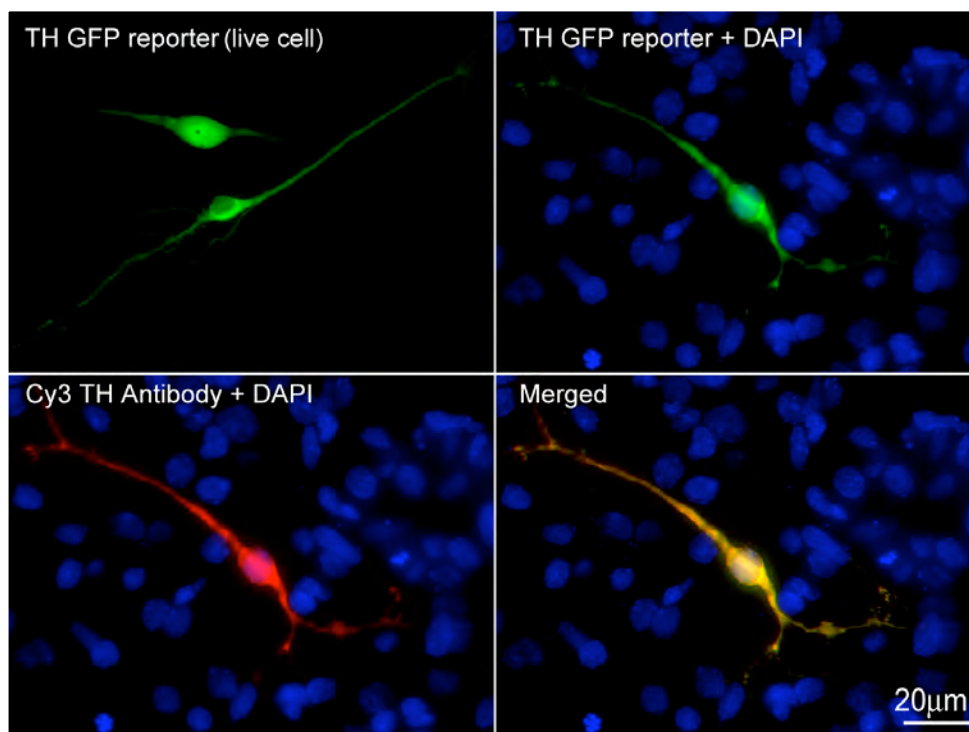


Fig. 1

Our results were in agreement with previously reported findings. A finding worth noting and often overlooked was that MPP⁺ killed the other cells in the culture at about a ten-fold higher concentration than that used for dopamine neurons. MPP⁺ is not selective in killing dopamine neurons in vitro even though it appears more selective in vivo. The same is true for rotenone.

To determine the mechanism of cell death in response to MPP⁺, we assessed an early step in the intrinsic apoptotic cascade, mitochondrial membrane depolarization ($\Delta\psi_m$). For these technically difficult experiments, dopamine neurons were identified by transfecting the cultures with a GFP-TH reporter using the Helios gene-gun. Typically 48 h after transfection, 10 to 50 GFP-positive neurons were apparent on each coverslip and 100% of these cells stained positively with an antibody against TH, indicating that TH reporter activity was only detected in dopamine neurons. See Figure 2 below.

Fig. 2



To measure mitochondrial membrane potential ($\Delta\psi_m$), cells were washed with Ringer's solution containing 130 mM NaCl, 5 mM KCl, 0.5 mM MgCl₂, 2 mM CaCl₂, 25 mM HEPES, 5 mM glucose, pH 7.4. The cells were loaded with 500 nM of tetramethylrhodamine ethyl ester (TMRE) for 30 min at room temperature. TMRE fluorescence was excited at 545 nm using excitation light provided by a HBO 100 W lamp in a computer-controlled filter wheel. Emitted fluorescence light was reflected through a 590 nm long-pass filter to the camera. Changes in $\Delta\psi_m$ were monitored in single GFP⁺ neurons over time. Results show that MPP⁺ induced rapid mitochondrial depolarization and that pretreatment with GDNF partially protected dopamine neurons from the effects of MPP⁺. These results supported our working hypothesis that MPP⁺

kills dopamine neurons by activating the mitochondrial death pathway, a finding that was expected since MPP⁺ is known to block mitochondrial complex I.

To determine if the intrinsic initiator caspase-9 and the executioner caspase-3 were activated in primary dopamine neurons following incubation with MPP⁺. We used antibodies that specifically recognize the active (cleaved) forms of caspase-9 (rabbit polyclonal, rat-specific, Cell Signaling Technology) or caspase-3 (rabbit polyclonal, Promega), and DAPI to distinguish normal vs. apoptotic nuclei. It appeared that many of the dopamine neurons undergo apoptosis after MPP⁺ treatment. But whether or not all of the cells that detached after 24 hr of MPP⁺ treatment died by apoptosis was less clear. We examined shorter periods of time after MPP⁺ treatment or trophic factor withdrawal (an inducer of intrinsic apoptosis) to determine morphological characteristics of the dying TH neurons. It appeared that at high concentrations of MPP⁺ (greater than 10-100uM) or longer treatment periods, a lot of the cell death was necrotic.

To examine the apoptosis question in more detail, the effects of a caspase-3 selective inhibitor on the death of primary dopamine neurons induced by MPP⁺. Rat ventral mesencephalic cultures were treated with MPP⁺ or subjected to trophic factor withdrawal in the absence or presence of the cell permeable, caspase-3 selective inhibitor, z-DEVD-FMK (Calbiochem). Cultures were fixed and stained with anti-TH antibodies to identify dopaminergic neurons and DAPI to distinguish normal vs. apoptotic nuclei. Caspase-3 inhibitors blocked cell death by both MPP⁺ and trophic factor withdrawal, but the inhibition of cell death was not complete. So again, the data raised the question as to whether some cells die by a non-caspase dependent mechanism.

We also examined the effects of a caspase-9 selective inhibitor on cell death induced by MPP⁺. Rat ventral mesencephalic cultures were treated with MPP⁺ or subjected to trophic factor withdrawal in the absence or presence of the cell permeable, caspase-9 selective inhibitor, z-LEHD-FMK (Calbiochem). Cultures were fixed and stained with anti-TH antibodies to identify dopaminergic neurons and DAPI to distinguish normal vs. apoptotic nuclei. The caspase-9 inhibitors blocked cell death to a similar extent as the caspase-3 inhibitors indicating that most of the apoptotic death was mediated by the intrinsic mitochondrial pathway. But again, the blockade of cell death was incomplete, raising the possibility that other death pathways are involved.

We were ultimately interested in determining whether Bax translocates to mitochondria of dopamine neurons after MPP⁺ treatment. Towards that goal we first established a procedure for measuring Bax translocation in primary cultured granule neurons that are 97% homogeneous and easier to transfect than dopamine neurons. We obtained a plasmid encoding an amino-terminal GFP fusion protein of human Bax_a from Dr. R. J. Youle (NINDS, NIH). Neurons were transfected with Bax-GFP via particle-mediated gene transfer using a Helios gene gun (Biorad). At 48 h post-transfection, cells were either maintained in control medium or switched to apoptotic medium. After a further 4 h incubation, neurons were fixed in paraformaldehyde and nuclei were stained with Hoechst dye. The localization of GFP or GFP-Bax_a and nuclear morphology were examined by fluorescence microscopy. GFP displayed a diffuse distribution over the entire cell body in neurons cultured in either control or apoptotic medium. In contrast, the localization of GFP-Bax_a changed from a diffuse pattern in control medium to a punctate distribution in neurons cultured in apoptotic medium. To confirm that the punctate distribution of

GFP-Bax_a corresponded to its translocation to mitochondria, neurons were stained for the integral mitochondrial membrane protein, cytochrome c oxidase subunit IV (COX IV). In control medium, there was little specific overlap between the localization of GFP-Bax_a and COX IV. While in apoptotic medium, GFP-Bax_a showed substantial co-localization with COX IV. Examination of the kinetics of GFP-Bax_a translocation revealed a rapid movement of the expressed fusion protein to mitochondria upon induction of apoptosis. In control medium, less than 30% of the CGNs expressing GFP-Bax_a showed a mitochondrial localization of the fusion protein. Within 1 h of an apoptotic stimulus, a significant increase in mitochondrial GFP-Bax_a was detectable. After 4 h of incubation in apoptotic medium, approximately 70% of the transfected neurons demonstrated a mitochondrial distribution of GFP-Bax_a. We next analyzed the activation of the endogenous Bax protein by immunostaining neurons with a monoclonal antibody that specifically recognizes the active Bax conformation (clone 6A7). Neurons maintained in control medium showed little-to-no detectable 6A7 staining, whereas neurons in apoptotic medium showed active Bax immunoreactivity. Moreover, the 6A7 staining often coincided with condensed and/or fragmented chromatin. These experiments were published in the Journal of Neuroscience, 24: 9993-10002, 2004. We began similar studies in rat ventral mesencephalic cultures, but the number of dopamine neurons that got transfected with the Bax-GFP plasmid was extremely low. So we deferred these experiments in hopes of obtaining better transfections (discussed below).

Specific Aim 2. To determine if neurotoxins activate the mitochondrial death pathway via a mechanism that involves the formation of reactive oxygen and/or reactive nitrogen species.

Experiments indicated that rotenone-induced death of dopamine neurons was completely reversed by the addition of n-acetylcysteine (NAC) to the cultures at the time of rotenone addition (see Fig.3). This supported our hypothesis that ROS is an activator of the intrinsic apoptotic cascade. The effect of NAC is seen at high doses of rotenone under conditions where GDNF is unable to protect against death (explained in more detail later).

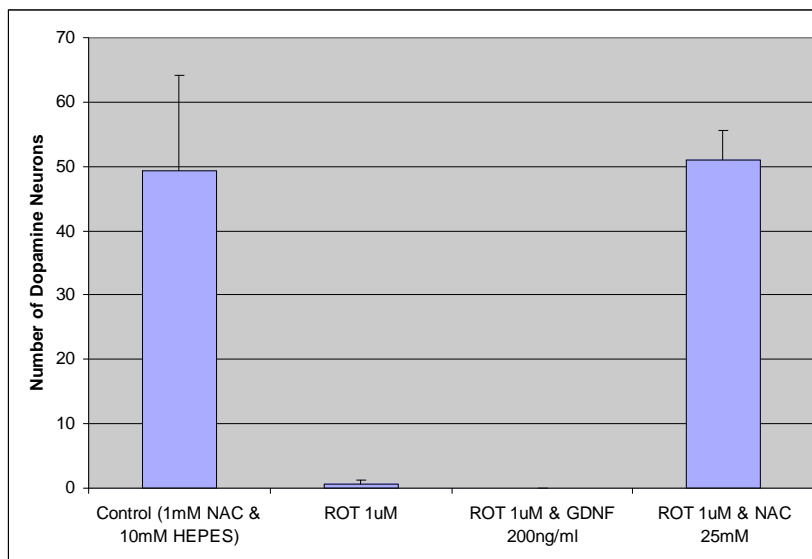


Fig. 3. Primary cultures derived from E15 rat ventral mesencephalon. On day 4, cultures were treated with or without rotenone (48hr) in the absence or presence of NAC. After treatment, cells were fixed with 4% paraformaldehyde and then permeabilized and blocked in PBS containing 0.2% Triton X-100 and 5% bovine serum albumin. Cells were then incubated overnight at 4 °C with monoclonal mouse anti-tyrosine hydroxylase (TH, 1:500). The primary antibody was aspirated, and cells were washed five times with PBS. Cells were then incubated with the appropriate Cy3-conjugated antibody (diluted 1:500) and DAPI for 2 h at room temperature. The cells were then washed 5 times with PBS, and cover slips were adhered to glass slides with mounting medium (0.1% *p*-phenylenediamine in 75% glycerol in PBS). Fluorescence measurements were obtained on Zeiss Axioplan 2 microscope equipped (63x objective) with a Cooke Sensicam deep-cooled CCD camera.

The plan was to continue these experiments once we had a more efficient way of labeling live dopamine neurons so that the generation of ROS induced by rotenone (and MPP+) could be measured in GFP-positive dopamine neurons using the redox-sensitive dye CM-H2-DCFA (Molecular Probes) in the absence and presence of various inhibitors to determine the relationship between ROS and mitochondrial mPTP opening. Because we were unsuccessful in improving transfection techniques for dopamine neurons, we never completed these experiments.

Specific Aim 3. To determine if neurotoxin-induced oxidative stress signals through stress-activated protein kinase pathway to activate mitochondrial apoptotic death in primary neurons.

We examined the effects of two novel inhibitors of JNK/c-Jun signaling on both MPP+ and rotenone induced cell death of dopamine neurons. The first inhibitor examined was the cell penetrating JNK inhibitor VII containing the TAT-cell entry sequence linked to the JBD20 sequence from JIP1 (Calbiochem). The second inhibitor, JNK inhibitor IX, was a thienyl-naphthamide compound that potently blocks the ATP-binding site of JNK2 and JNK3 with little activity against JNK1, p38 α and a panel of 30 other kinases. Ventral mesencephalic cultures were incubated with either MPP+ or rotenone alone or in combination with two inhibitors described. The results showed that 500, 100, and 50 nM rotenone, the cell-permeable inhibitor of JNK (JNK inh VII) has no effect on dopamine neuronal survival (Fig.4).

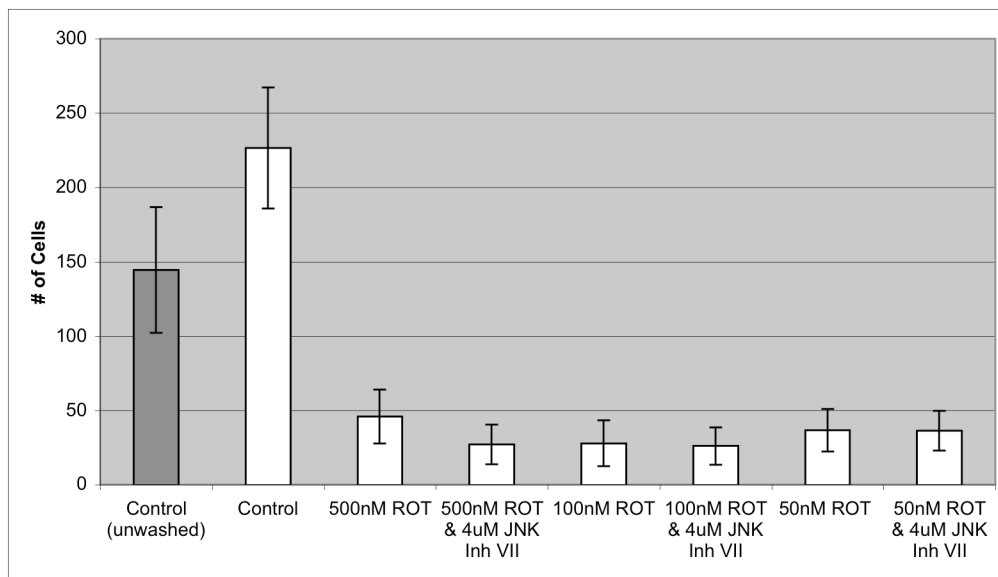


Fig.4

These results were surprising since similar concentrations of the JNK VII inhibitor were shown to offer neuroprotection *in vivo* in a rat ischemic brain injury model and *in vitro* in an NMDA excitotoxicity model. The JNK IX inhibitor also failed to block rotenone-induced dopamine neuronal cell loss at concentrations up to 20uM. These results suggest that JNK2 and JNK3 are not involved in mediating cell death at the concentrations of rotenone used. The results do not rule out the involvement of JNK1. The interpretation of the data are also complicated by the finding that rotenone kills dopamine neurons by more than one pathway. It is thought that low concentrations of rotenone kill by an apoptotic mechanism, whereas, high concentrations kill by a necrotic mechanism. We did additional experiments at 10 nM rotenone where there was a partial loss of dopamine neurons and again there was no significant effect of the JNK inhibitors.

We next examined the effects of the JNK inhibitors on MPP+-induced cell death. Results indicated that at the lowest concentration of MPP+ (30uM), there was a trend showing partial inhibition of cell death by the JNK inhibitor VII. Repeated experiments showed no significant effect of either JNK inhibitor on dopamine cell death.

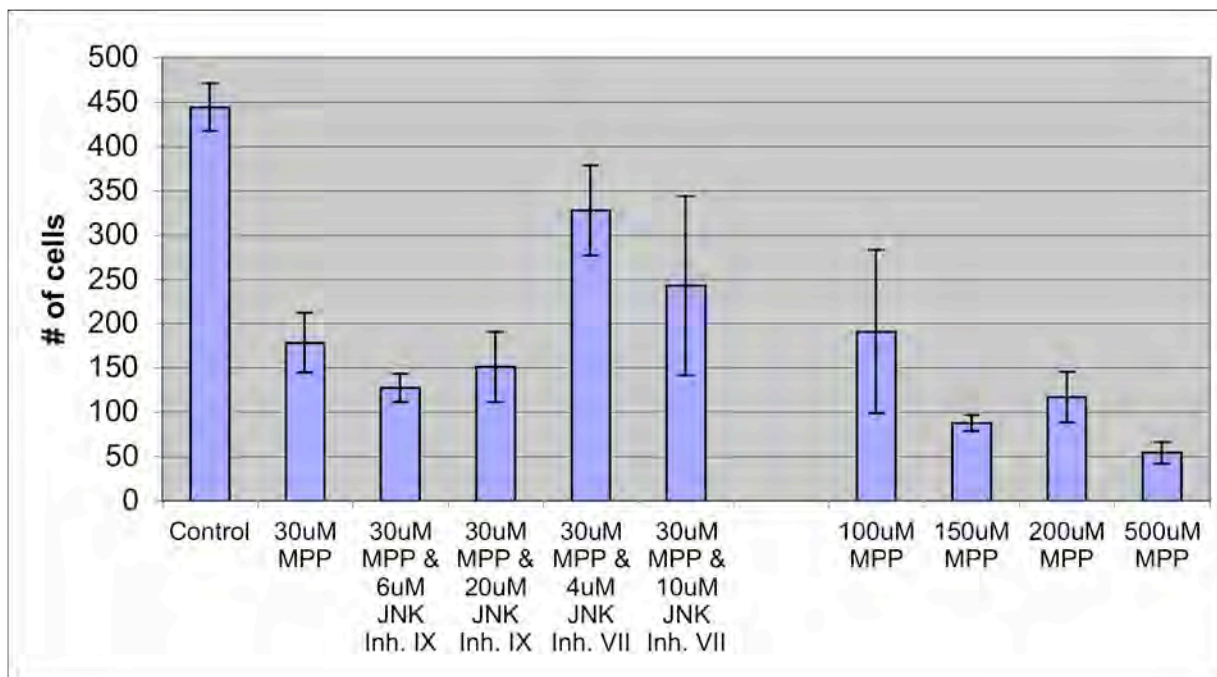


Fig.6

The only compound that consistently and significantly blocked dopamine cell death was N-acetylcysteine. These findings suggest that oxidative stress kills the neurons upstream of JNK activation. Perhaps the mitochondria is a source of most of the oxidative stress that kills the cells. This goes against our hypothesis that oxidative stress activates JNK and they in turn activate the mitochondrial apoptotic pathway. More experiments need to be carried out to determine if JNK is indeed activated in dopamine neurons in response to low concentrations of MPP+ and rotenone and whether the activation is blocked by N-acetylcysteine.

Specific Aim 4. To evaluate the effects of glial cell line-derived neurotrophic factor (GDNF) on neurotoxin-induced generation of reactive oxygen and nitrogen species, activation of JNK/c-Jun, and mitochondrial death signaling.

During the first two years of the project, we investigated the effects of GDNF on the loss of mitochondrial membrane potential triggered by MPP⁺ in primary dopamine neurons. Ventral mesencephalic cultures from E15 rats were transfected with a TH promoter-driven GFP construct using a helium-powered gene-gun. After transfection, cultures were exposed to MPP⁺ alone or following pre-incubation with GDNF. Live dopamine neurons were identified by GFP fluorescence and mitochondrial membrane potential was measured continuously using TMRE. Incubation with MPP⁺ induced a rapid (within 3 hr) collapse of mitochondrial membrane potential which was prevented by pretreatment with GDNF. The effects of GDNF were partially antagonized by the ERK pathway inhibitor, PD98059. Inhibitors of oxidative stress (glutathione), the classical mitoPTP inhibitor (cyclosporin A), or a Ca²⁺-triggered permeability transition inhibitor (2-APB), were each less effective than GDNF at blocking mitochondrial depolarization induced by MPP⁺. Collectively, these data suggest that GDNF inhibits multiple pathways that induce mitochondrial depolarization in dopaminergic neurons. GDNF blocks both the classical, cyclosporin A-sensitive permeability transition pore and a Ca²⁺-triggered permeability transition activated by complex I inhibition. Moreover, GDNF partially inhibits a redox-sensitive, but cyclosporin A/2-APB-insensitive, pathway that is regulated by Bcl-2. These results are the first to show that GDNF acts at the level of mitochondrial depolarization to protect dopamine neurons from MPP⁺-induced toxicity.

The protection by GDNF required pretreatment of the neurons (8 hr) prior to addition of MPP⁺. We hypothesized that GDNF counteracts the changes in expression of pro- and anti-apoptotic Bcl-2 family members induced in dopamine neurons by exposure to MPP⁺. Although, not proposed in the original grant, we ultimately wanted to use Affymetrix analysis to measure changes in the gene expression of primary dopaminergic neurons exposed to MPP⁺ in the absence or presence of GDNF. Towards this goal, we spent considerable effort developing laser capture microdissection methods for isolating dopamine neurons from ventral mesencephalic cultures. We developed an ultra-rapid TH⁺ staining procedure that allows for the identification of dopamine neurons within 20 minutes (see Fig.7). Left upper panel shows differential staining for TH with immunoreactive dopamine neurons indicated by the arrows. Following TH staining, dopamine neurons are captured by LCM using an Arcturus AutoPixTM LCM instrument indicated by the loss of cell bodies in upper right panel and lower left panel (white arrows). The captured dopamine neurons are shown on the surface of the harvest cap (lower right panel). RNA was isolated from the captured cells using the RiboAMP RNA amplification kit provided by Arcturus. The quality and quantity of RNA was analyzed with the NanoDrop ND-1000 instrument available at the UCHSC microarray core. We were able to capture approximately 100 dopamine neurons within 1 hr. We performed PCR analysis of tyrosine hydroxylase in isolated dopamine neurons and non-dopamine neurons and the procedure was successful with the capture of 100 dopamine neurons. The costs to use the laser capture instrument prevented us from optimizing the technique and moving forward to Affymetrix analysis.

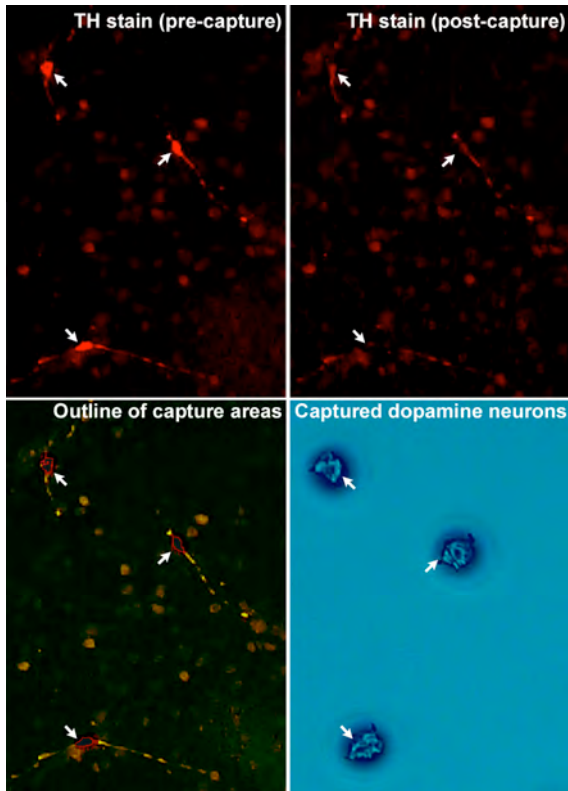


Fig. 7

During the course of GDNF experiments, we determined that GDNF exerts two actions in ventral mesencephalic cultures. The first effect is a trophic or survival effect on dopamine neurons. When GDNF is added to the cultures at the time of plating (even in the presence of serum), approximately 50 % more dopamine neurons survive in culture (see Fig.8). This effect is selective to dopamine neurons. The second effect of GDNF is to protect dopamine neurons from neurotoxin exposure.

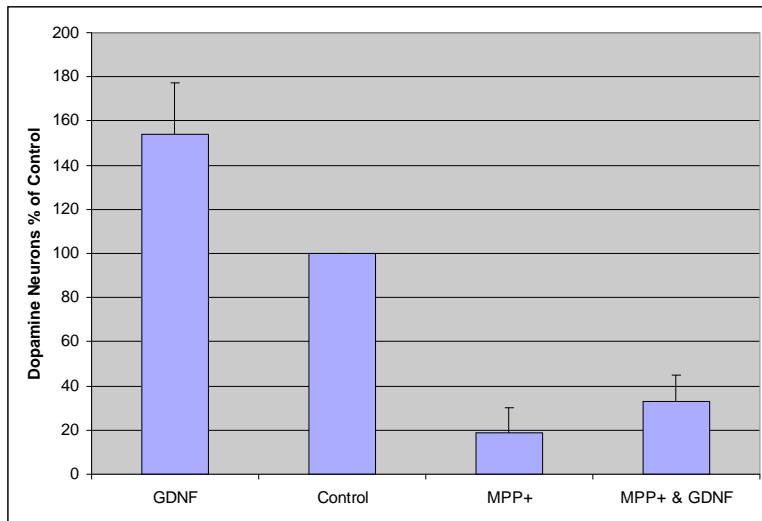


Fig. 8 Primary cultures derived as described in Figure 1 except GDNF (200ng/ml) was added to the culture medium in on experimental group (column 1). On day 4, cultures not subjected to GDNF were treated with or without MPP+ (48hr) in the absence or presence of GDNF. After treatment, cells were fixed and stained with monoclonal mouse anti-tyrosine hydroxylase as described in Figure 1. Fluorescence measurements were obtained on Zeiss Axioplan 2 microscope equipped (63x fluorite objective) with a Cooke Sensicam deep-cooled CCD camera.

The neuroprotective effects of GDNF on neurotoxin exposure were quite variable and were dependent on the dose of neurotoxin used. As mentioned previously this is related to the type of cell death that occurs after rotenone and MPP+ exposure. At low doses of both toxins, death occurs largely by an apoptotic mechanism dependent on the presence of ATP. Once ATP is depleted as a result of inhibition of complex I, the neurons die by a non-apoptotic mechanism that is insensitive to GDNF.

Even at low doses of MPP+, the protection by GDNF (200 ng/ml) is never complete. During the course of these experiments, the PI read a report that the neurotrophic actions of GDNF require TGF-beta. Experiments were carried out to determine if pretreatment or addition of TGF-beta with GDNF would enhance the neuroprotective effects of GDNF following MPP+ or rotenone exposure. The results were conclusively negative. TGF-beta had no effect on the ability of GDNF to protect against MPP+ or rotenone in ventral mesencephalic cultures.

Efforts to increase the delivery of the TH reporter construct and other genes into primary dopamine neurons.

I. Amaxa Nucleofector Technology using rat ventral mesencephalic neurons.

Many laboratories, including the PI's, have had success using Nucleofector technology for gene-transfer in primary cells and hard-to-transfect cell lines. The technology involves modified electroporation parameters and specific solutions that permit gene transfer into the nucleus. We have been successful in optimizing conditions that result in 60-70% transfection efficiency of primary cerebellar granule neurons. Conditions that proved successful for granule neurons were found to be toxic for dopamine neurons in ventral mesencephalic cultures. We tried different settings (Amaxa programs G13 and O-03) and different cell densities and had no success with dopamine neurons. Last year, Amaxa representatives introduced us to a new 96-well shuttle system that has many more electrical programs available to the user and a modified cuvette that apparently results in less cell toxicity. With the assistance of Amaxa technicians, we spent 2 months investigating parameters (DNA quality, cell density, different proprietary solutions, and multiple electrical programs) that would result in efficient transfection of primary dopamine neurons. These were labor-intensive experiments since they required 2-4 million cells per reaction. We found that all of the optimized programs used for other cell types, including other types of primary neurons, lead to the death of dopamine neurons, assessed by TH staining. A few conditions that resulted in transfection of non-dopamine cells and low toxicity to dopamine neurons, resulted in no transfection of dopamine neurons. At 2-4 million cells per reaction, we decided to abort these experiments, although the Amaxa technicians were confident that the nucleofector technology would eventually be successful for dopamine neurons.

II. Exploration and development of viral vectors for gene delivery to dopamine neurons.

Upon hiring a new molecular biologist halfway through the project and the establishment of a viral core in the Neuroscience program, we focused on the use of viral vectors to establish a more efficient and reliable method for the identification of live dopamine neurons in primary culture. We developed a new strategy based on lentiviral transformation of rat mesencephalic cells using vectors containing a TH reporter driving the expression of GFP.

A lentiviral expression system was chosen over adenoviral and adeno-associated virus (AAV) expression vectors to deliver the GFP-TH reporter construct into primary dopamine neurons because lentiviral transduction resulted in the lowest amount of cellular toxicity and the highest amount of expression of GFP in preliminary studies (see Fig. 9). Adenoviral GFP expression vectors were very toxic to dopamine neurons, although we use them for other primary neurons in the lab. AAV transduction was not toxic to dopamine neurons, but transduction efficiency was less than with lentivirus and AAV is more limited by insert capacity (less than 4.5 kb). The major challenging factor in making a lentiviral GFP-TH expression vector relates to the fact that lentiviral vectors can only incorporate DNA fragments less than 8 kb and the established 9 kb rat promoter coupled to GFP (Patankar *et al.*, 1997) is consequently too large.

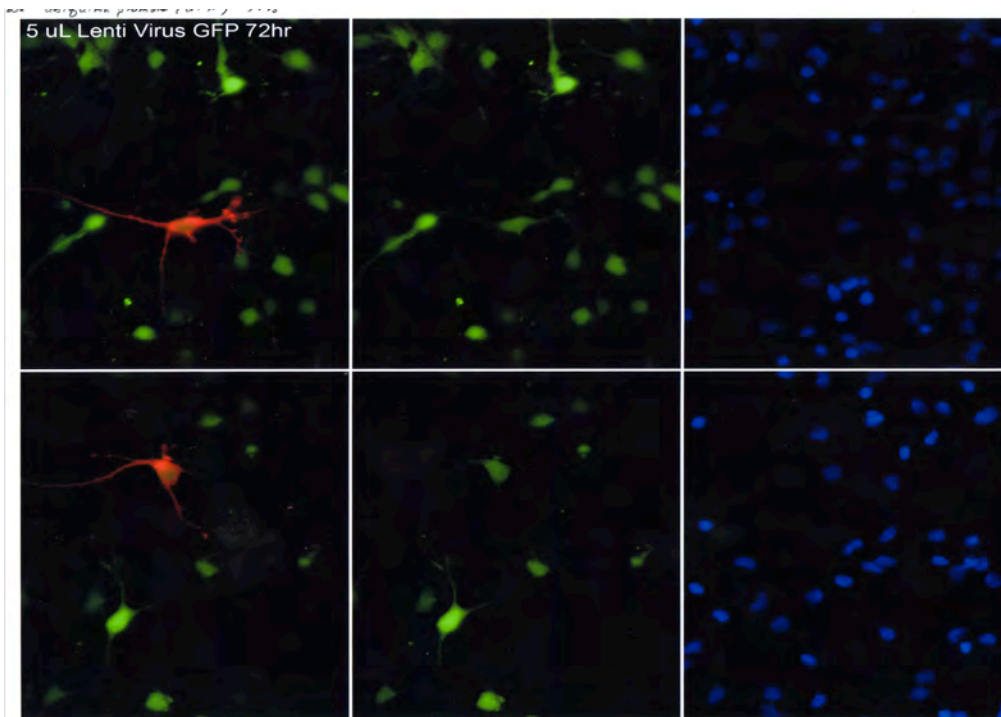
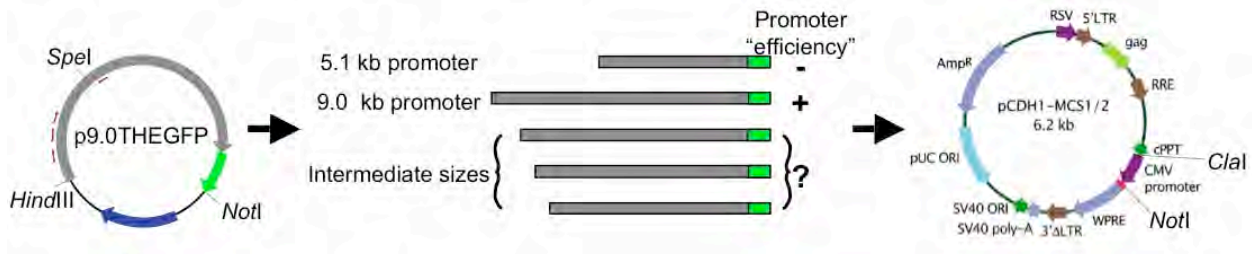


Figure 9. Lentiviral transduction of dopamine neurons. E15 rat ventral mesencephalic cultures (3 days in culture) were infected with a lentivirus -GFP at a MOI of approximately 50. Seventy two hours later, the cultures were fixed and immunostained with a primary antibody against TH (rabbit polyclonal from Pel-Freeze) followed by a secondary goat anti-rabbit antibody conjugated to Alexa Fluor555 and DAPI. Left panels display TH staining and GFP expression, middle panels display GFP alone, and right panels display DAPI alone. Dopamine neurons (shown in red) were GFP positive.

Preliminary experiments showed that a 9kb (8660 bp) but not a 5kb (5280 bp) TH promoter generates GFP expression in primary dopamine neurons. We hypothesized that generation of fragments of intermediate length will successfully work as TH reporter constructs in lentiviral vectors. Our hypothesis was supported by the fact that a putative binding site for a transcription factor of the Pitx family, expressed in the midbrain at ED 10.5, is found at the position – 6840 (Sclafani *et al.*, 2006). To optimize our chances of obtaining a useful lentiviral vector that will deliver an efficient TH-GFP reporter construct, we designed a pool of sequences of intermediate sizes ranging from 6.9 to 8 kb. The cloning strategy that was used to obtain these mutant clones is shown on the figure below.

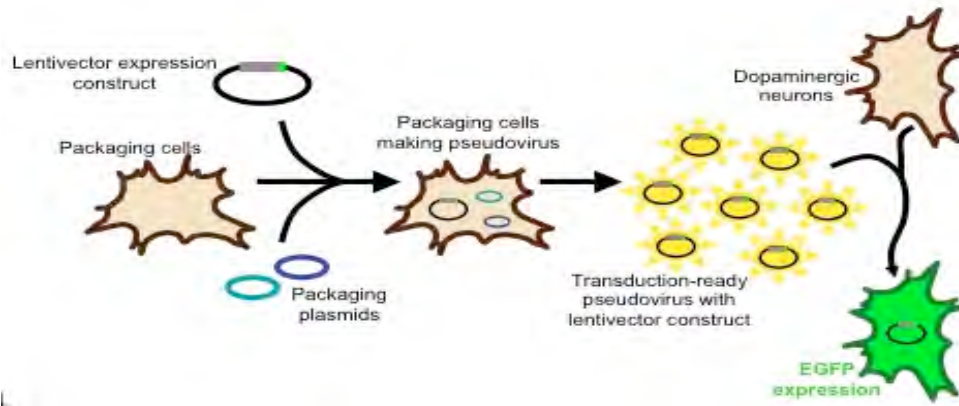


The starting vector p9.0THEGFP, containing the GFP coding sequence downstream of the 9.0 kb rat TH promoter served as the template for several PCR amplifications, in which the primers located in the distal part of the promoter contained at their 5' extremity an additional *HindIII* restriction site. This allowed the use of the *HindIII* and *SpeI* unique restriction sites to re-insert the amplified fragments in the p9.0THEGFP plasmid cut beforehand with the same enzymes and gel purified. This procedure resulted in the construction of 3 new pEGFP plasmids carrying TH promoters of 6.8, 7.3 and 7.8 kb. After complete sequencing of the new constructs, The ability of the newly obtained constructs to drive the expression of GFP was tested in PC12 cells transformed using the Effectene Transfection Reagent (Qiagen). All three shortened promoters lead to the expression of GFP at a rate comparable to the full length promoter.

The next stage involved cutting the promoter-GFP fusions obtained using the *HindIII* and *NotI* restriction sites, in order to isolate the genetic material to be transferred to the lentiviral expression plasmid. This pCDH1 plasmid was cut using the *NotI* and *ClaI* restriction sites, in order to remove the constitutive CMV promoter. Since the *HindIII* and *ClaI* restriction sites are not compatible, we needed to blunt the single strand extremities of the purified fragments, using the T4 DNA polymerase. Finally, after a dephosphorylation step carried out to avoid the recircularization of the pCDH1 vector without insert, the promoter-GFP fusions and the lentiviral expression plasmid deprived of the CMV promoter were subjected to ligation. Unfortunately, the blunt ligations never worked.

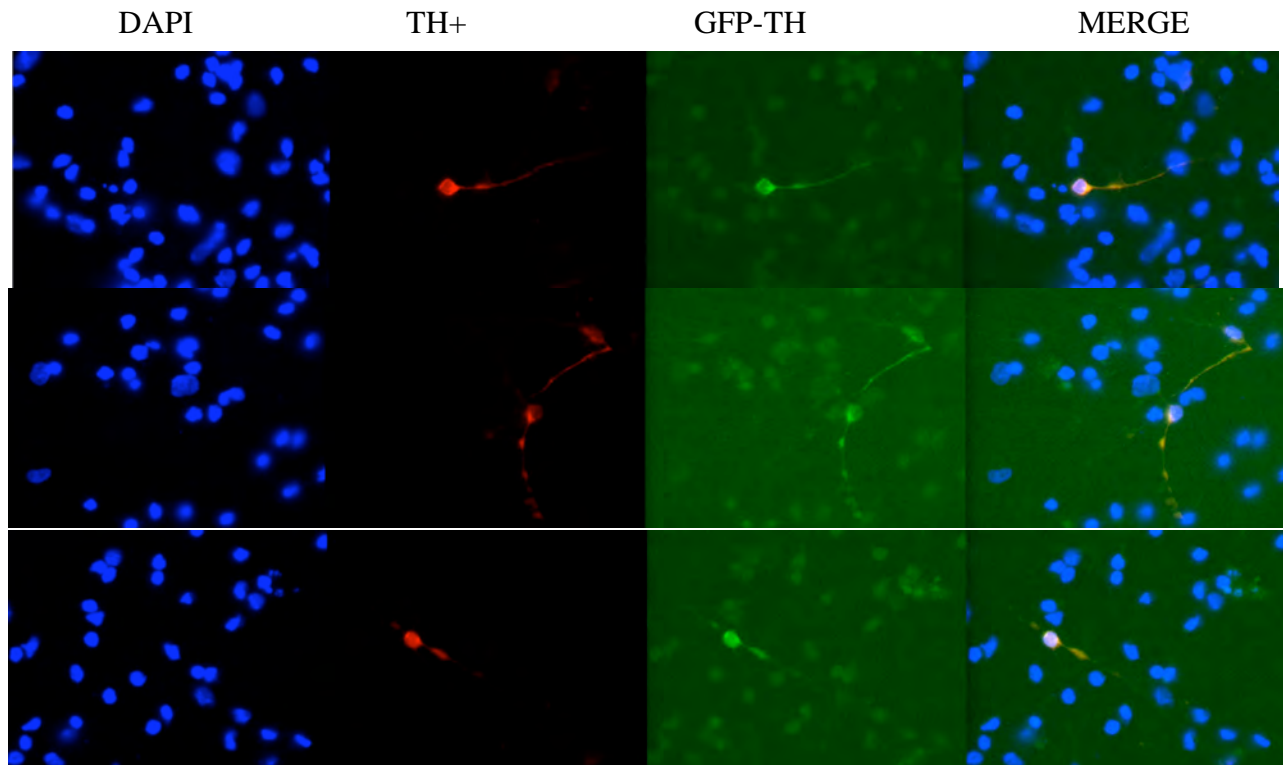
We redesigned the cloning strategy by inserting an adapter in the lentiviral expression plasmid, which allowed the use of cohesive restriction sites. This approach was successful and yielded three new lentiviral plasmids.

As shown in the next schematic, the next step of the project consisted of packaging the newly obtained expression constructs into pseudo viral particles.



In order to obtain the three lentiviruses containing the TH promoters of intermediate size, we used the pPACKH1 Lentivector Packaging Kit from System Biosciences. Briefly, 293TN cells (a human kidney cell line) were co-transformed with our different expression constructs and the pPACKH1-GAG, pPACKH1-REV, and pVSV-G packaging plasmids. Following the co-transformation, the pseudo-viral particles obtained were collected, purified and titrated.

The final step consisted in testing our lentiviruses carrying the TH reporter constructs. We infected primary mesencephalic cultures using different amounts of viral particles. It appeared that only 1 to 5 out of the 250 TH positive neurons were expressing GFP, representing a 0.4 to 2 % transfection rate



In order to enhance the sensitivity of our detection method, we immunostained the transfected cells with an anti-GFP antibody, but again, without significant results. We hypothesized that the low expression level of the TH promoter conjugated with the low copy number provided by lentiviral transfection does not allow the synthesis of a detectable level of GFP protein.

Key Research Accomplishments

The key research accomplishments were to establish the primary ventral mesencephalic cultures and develop live-cell imaging techniques to explore death pathways in dopamine neurons. These experiments were technically difficult since such a small percentage of the cells are dopaminergic neurons. We were able to identify living dopamine neurons by transfecting a GFP-TH reporter construct using gene-gun delivery. This allowed us to measure mitochondrial depolarization using fluorescence microscopy in real time. The experiments suggested that MPP⁺ leads to a loss in mitochondrial membrane potential by activating several channels in the outer mitochondrial membrane that lead to the release of apoptogenic factors that cause cell death. A novel finding of our studies was that GDNF blocks activation of several of these channels, thereby, blocking dopamine neuron death at a very early step in the intrinsic apoptotic cascade. We also developed laser capture methods to isolate dopamine neurons from rat ventral mesencephalic neurons so that we can eventually identify gene targets of GDNF. We established a method for measuring Bax translocation in primary neurons, hoping eventually to adapt the procedure to dopamine neurons after transfection issues were resolved. The study showed that GSK-3 β , a potent pro-apoptotic serine threonine protein kinase, phosphorylates Bax and drives it to the mitochondria during neuronal apoptosis.

In 2005, I had unforeseen circumstances involving the departure of three individuals that worked on the DOD project. Dr. Chunhe Chen, the postdoctoral fellow who performed the embryonic rat mesencephalic cell cultures and most of the live cell imaging, resigned in May 2005 to care for her 16-year old son who was in a near fatal car accident, paralyzed from the neck down. Dr. Daniel Linseman, who trained in my lab and acted as co-investigator on this grant, left my laboratory to establish his own research program at the VA Eastern Colorado Health Care System end of Dec 2005. Ron Bouchard, our microscopy technician, also left my lab in June of 2005. I hired a technician (Jacqui Kulbe) after Dr. Chen's departure who was subsequently trained in primary culture of dopamine neurons, immunocytochemical detection of dopamine neurons, and some imaging techniques. Unfortunately, she left after several months to apply for graduate schools. Since progress was greatly slowed in 2005 and I asked for a no-cost extension to make up for time lost. I hired a new technician (Janna Mize-Berge) who mastered the primary cultures and worked on several aspects of the proposal until its end. A new postdoc started in February 07 (Dr. Vince Zaegel). Dr. Zaegel, a well trained molecular biologist, worked on lenti-virus expression systems for dopamine neurons and other transfection approached like the Amaxa nucleofector technology. Much to our disappointment, neither method proved satisfactory for delivering the TH reporter construct into dopamine neurons. This limited the type of experiments that could be carried out.

Reportable Outcomes

Publications

Heidenreich KA and DA Linseman. Myocyte enhancer factor-2 (MEF2) transcription factors in neuronal differentiation and survival. Mol. Neurobiol. 29: 155-166, 2004.

Chen, C, DA Linseman, BD Butts, RJ Bouchard, ML McClure, **KA Heidenreich**. GDNF protects primary dopamine neurons from MPP+ induced toxicity by blocking diverse pathways to mitochondrial depolarization. Society for Neuroscience , San Diego, CA 2004.

McClure ML, DA Linseman, CT Chu, RJ Bouchard, TA Laessig, SS Le, and **KA Heidenreich**. Neurotrophins and death receptors regulate autophagic death in cerebellar Purkinje neurons. J. Neuroscience 24: 4498-4509, 2004.

Linseman, DA*, BD Butts*, TA Precht, RA Phelps, SS Le, TA Laessig, RJ Bouchard, ML McClure, and KA Heidenreich. Glycogen synthase kinase-3b phosphorylates Bax and promotes its mitochondrial localization during neuronal apoptosis. *co-first authors J. Neuroscience 24: 9993-10002, 2004.

Precht, TA, RA Phelps, DA Linseman, BD Butts, RJ Bouchard, SS Le, TA Laessig, and **KA Heidenreich**. Bax translocation to mitochondria is triggered by permeability transition pore opening in cerebellar granule neurons undergoing apoptosis. Cell Death and Differentiation, 12: 255-265, 2005.

Zimmermann, AK, FA Loucks, SS Le, BD Butts, M McClure, RJ Bouchard, **KA Heidenreich**, DA Linseman. Bcl-2 interacting mediator of cell death (Bim) induces cerebellar granule neuron apoptosis via a mechanism that is independent of Bcl-2 antagonism. J. Neurochem.94: 22-36, 2005.

Butts BD, HR Hudson, DA Linseman, SS Le , and **KA Heidenreich**. Proteasome inhibition elicits a biphasic effect on neuronal apoptosis via differential regulation of pro-survival and pro-apoptotic transcription factors. Mol. Cell. Neurosci. 30: 279-289, 2005.

Le, SS, FA Loucks, H Udo, S Richardson-Burns, RA Phelps, RJ Bouchard, H Barth, K Aktories, KL Tyler, ER Kandel, **KA Heidenreich**, and DA Linseman. Inhibition of Rac GTPase triggers a c-jun -and Bim-dependent mitochondrial apoptotic cascade in cerebellar granule neurons. J. Neurochem. 94: 1025-1039, 2005.

Brewster JL, Linseman DA, Bouchard RJ, Loucks FA, Esche E, Precht T, and **Heidenreich KA**. Endoplasmic reticulum stress and trophic factor withdrawal activate distinct signaling

cascades that converge at GSK-3 β to trigger mitochondrial apoptosis in neurons. Mol. Cell. Neurosci. 32:242-253, 2006.

Allen, MP, S M Nielsen-Preiss, M Xu, DA Linseman, JE Pawlowski, R Bouchard, BC Varnum, **KA Heidenreich**, and ME Wierman. Adhesion related kinase induction of GnRH neuronal migration involves PI-3kinase stimulation of Rac activity. Endocrinology 148(6):2806-2814, 2007.

Farias, SE, S Zarini, T Precht, RC Murphy, and **KA Heidenreich**. Transcellular biosynthesis of cysteinyl-leukotrienes in the rat neuronal and glial cells. J. Neurochem. 103 (4): 1310-1318, 2007.

Klionsky, DJ et al. Guidelines for monitoring autophagy in higher eukaryotes. Autophagy 4 (2): 151-175, 2008.

Farias, SE , M Basselin, L Chang, **KA Heidenreich**, SI Rapoport, and RC Murphy. Simultaneous formation of eicosanoids and docosanoids following global ischemia, measured in high-energy microwaved rat brain. J. Lipid Res. 49: 1990-2000, 2008.

Mona Bains and **KA Heidenreich**. Live-cell imaging of autophagosome-lysosome fusion in primary neurons. Methods of Enzymology: Autophagy, ed D.L. Klionsky *Invited chapter*, (in press).

Grants Funded

American Parkinson Disease Association (APDA), “Neurotoxin-induced Changes in BH3-only Protein Expression Analyzed by Real-time PCR in Primary Dopaminergic Neuronal Cultures”, P.I.: Daniel A. Linseman, Ph.D. (Effective: September 1, 2004 – August 31, 2005) Total direct costs - \$50,000 per year

Invited talks

Kim A. Heidenreich, Plenary talk, New York Academy of Science Symposium “ PD: Life Cycle of the Dopamine Neuron”, Princeton, N.J. 2003.

Kim A. Heidenreich, Chairperson and Invited Speaker, Gordon Conference on Insulin-like Growth Factors, Ventura, CA. 2003.

Kim A. Heidenreich, Department of Pharmacology Retreat, Copper Mountain, CO, “Molecular Mechanisms of Neuronal Death” 2003.

Daniel A. Linseman, University of Colorado Health Sciences Center, Neuroscience Training Program Seminar, “Regulation of Bax by phosphorylation during neuronal apoptosis” 2003.

Daniel A. Linseman, Gordon Research Conference, Insulin-like Growth Factors in Physiology and Disease. “IGF-I blocks neuronal apoptosis by inhibiting Bim induction and Bax translocation to mitochondria” 2003.

Kim A. Heidenreich, Neuroscience program, University of Michigan, Ann Arbor, “Molecular Mechanisms of Neuronal Death”, MI, 2004.

Kim A. Heidenreich, Department of Pathology, University of Pittsburgh, Pittsburgh, PA, “Molecular Mechanisms of Neuronal Cell Death”, PA, 2005

Kim A. Heidenreich, Invited symposium speaker, Gordon Conference on IGFs, “The Neuroprotective Actions of IGFs, Ventura, CA, 2005

Kim A. Heidenreich , Department of Neurology, “Mechanisms of Neuronal Cell Death”, Johns Hopkins University, Baltimore, MD, 2006

Kim A. Heidenreich , Invited speaker, Gordon Research Conference, Insulin-like Growth Factors in Physiology and Disease, Ventura, CA, 2007

Kim A. Heidenreich , Department of Pharmacology, University of Texas Health Science Center, San Antonio, TX, “Different Ways that Neurons Die”, 2007

Kim A. Heidenreich , Department of Physiology, Colorado State University, Fort Collins, CO, “Apoptotic and autophagic death of neurons”,2007

Kim A. Heidenreich , Symposium speaker, Winter Conference for Brain Research, “New Pistes for IGF Signaling in the Brain”, Salt Lake City, Utah,2008

Conclusions

Despite the technical difficulties centered around gene transfer to dopamine neurons and the loss of research personnel, we gained information about the complexity of dopamine neuron death in response to MPP+ and rotenone. There appear to be multiple pathways involved in cell death induced by rotenone and MPP+. At low doses of both neurotoxins, part of the cell death was apoptotic, inhibited by caspase inhibitors and growth factors, including GDNF and IGF-I. At higher doses of neurotoxin, these factors had little effect, but N-acetylcysteine protected suggesting that oxidative stress kills the neurons by a non-apoptotic mechanism under these conditions. These findings support the notion that multiple pathways need to be targeted to prevent cell death induced by neurotoxins. Although the lentivirus did not work well in dopamine neurons, the learned skills will enable us to apply this techniques to other types of neurons. We also have a better understanding of the critical factors required for viral expression in neurons. The success with laser capture techniques opens a door for numerous experiments that rely on separating dopamine neurons from other cell types in the cultures.

Myocyte Enhancer Factor-2 (MEF2) Transcription Factors in Neuronal Differentiation and Survival

Kim A. Heidenreich* and Daniel A. Linseman

Department of Pharmacology, University of Colorado Health Sciences Center and the Denver Veterans Affairs Medical Center, Denver, Colorado 80262

Abstract

Myocyte enhancer factor-2 (MEF2) transcription factors regulate genes that control critical cellular processes including proliferation, differentiation, and survival. Although MEF2 proteins were first identified as transcription factors that bound A/T rich DNA sequences and controlled muscle-specific genes during myogenic development, it is now apparent that MEF2 transcription factors are also highly expressed in neurons and are critical determinants of neuronal differentiation and fate. Here we focus our discussion on the role of MEF2 proteins in nervous tissue and the regulation of these transcription factors by calcium and phosphorylation signaling pathways.

Index Entries: Neuron; apoptosis; brain; MADS-box; protein kinases; calcium signaling; muscle; development.

MEF2 Family of Transcription Factors

The MEF2 proteins are members of the MADS (MCM1-agamous-deficiens-serum response factor) family of transcription factors (1,2). A hallmark of MADS-box proteins is their combinational association with other MADS

domain factors and additional heterologous classes of transcriptional regulators (3). Vertebrate MEF2 proteins are encoded by 4 genes (MEF2-A, -B, -C, and -D), each of which gives rise to alternatively spliced transcripts (1,4-7). The MEF2 isoforms are expressed in distinct, but overlapping patterns during embryogenesis and in adult tissues. Posttranslational regulation is largely responsible for the functional pattern of expression of the MEF2 proteins (1).

MEF2 transcription factors contain a N-terminal 56 amino acid MADS-box domain that serves as a minimal DNA-binding domain

Received 7/1/03; Accepted 10/1/03

* Author to whom all correspondence and reprint requests should be addressed. E-mail: Kim.Heidenreich@UCHSC.edu

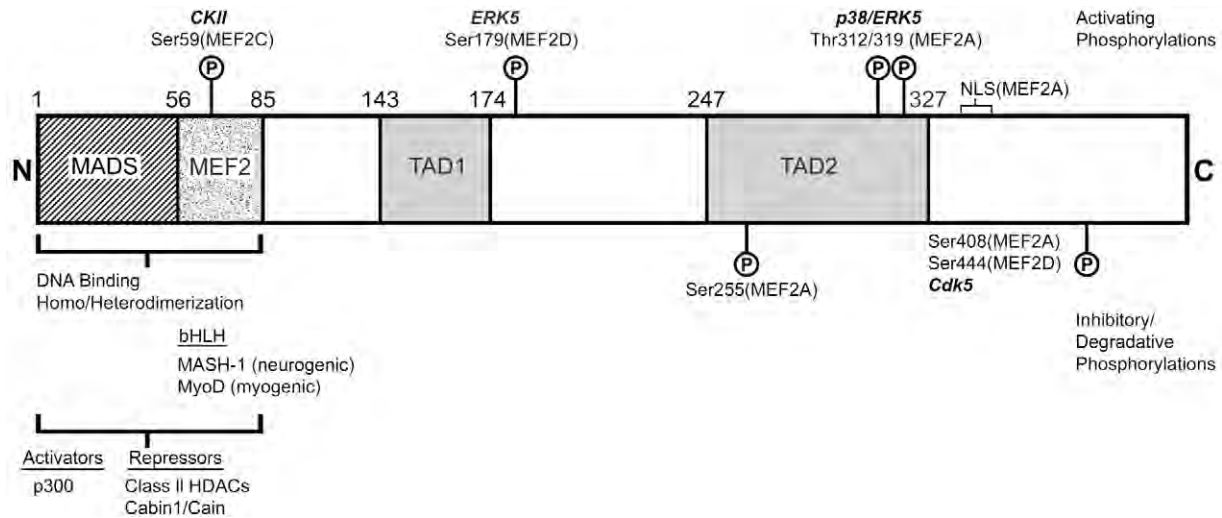


Fig. 1. Structural schematic of a MEF2 transcription factor. MEF2 proteins contain a highly conserved N-terminal MADS box and MEF2 domain. These elements are involved in DNA binding, dimerization with other MEF2 proteins and basic helix-loop-helix (bHLH) transcription factors, and interaction with various coactivators and repressors. The C-terminal region of MEF2 contains the transcriptional activation domains (TADs) as well as a nuclear localization sequence (NLS). MEF2 proteins are substrates for many protein kinases that regulate both DNA binding and transcriptional activity. For example, a conserved casein kinase II (CKII) site lies within the MEF2 domain and its phosphorylation enhances DNA binding. Multiple residues within the C-terminus are substrates for MAP kinase family members, p38 and/or ERK5, and phosphorylation of these sites generally enhances transcriptional activation. In contrast, phosphorylation at the extreme C-terminus by Cdk5 or at Ser255, by an as yet unidentified kinase, leads to inhibition of transcriptional activity and degradation, respectively.

(see Fig. 1). The MADS box is a highly conserved structural motif involved in the regulation of homeotic fate, growth, and differentiation in many organisms (1,8–10). Adjacent to the MADS box is a 29 amino acid MEF2 domain that mediates high-affinity DNA binding and homo- and heterodimerization with other MEF2 proteins. The vertebrate MEF2 proteins share about 50% amino acid identity overall and about 95% similarity in the highly conserved MADS box and MEF2 domain (11). MADS box proteins generally bind A/T rich DNA sequences, whereas MEF2 binds preferentially to the consensus sequence CTA(A/T)₄ TAG/A (11). The MADS box and MEF2 domain are necessary and sufficient for DNA binding but lack transcriptional activity on their own. The C-terminal half of MEF2 proteins contains the transcriptional activation domain, as well as, a number

of regulatory domains including a nuclear localization sequence and multiple phosphorylation motifs (12). There is relatively low amino acid homology between the C-terminal regions of the various MEF2 isoforms and the C-terminus is subject to complex patterns of alternative splicing (11). The structural organization of MEF2 proteins allows them to receive and respond to multiple inputs from various intracellular signaling pathways. In this way, MEF2 activity is profoundly influenced by developmental cues and signals from the extracellular environment.

MEF2 Transcription Factors in Muscle and Immune Cells

The MEF2 family of genes is highly expressed in cells of muscle lineage, where they have been

shown to be important regulators of gene expression during development of skeletal, cardiac, and smooth muscle (6,7,13). In these tissues, MEF2 proteins interact with myogenic basic helix-loop-helix (bHLH) transcription factors such as Myo D to activate myogenesis (14–16). MEF2 factors are thought to activate transcription by binding to individual E-box or MEF2 consensus sites or via adjacent E-box/MEF2 elements. During myogenesis, MEF2 transcription factors activate the expression of structural genes, as well as maintain and amplify the expression of other transcription factors that initiate muscle differentiation (17). Loss-of-function mutations of the mouse MEF2C (18) and the *Drosophila* MEF2 gene (19,20) have demonstrated an essential role of MEF2 proteins in myogenesis and morphogenesis of striated and nonstriated muscle cell types. In addition to their critical role in muscle development, MEF2 proteins are involved in adult cardiac hypertrophy (21–23).

MEF2 proteins are also present in cells of the immune system where they mediate cell fate decisions. T-cell activation leads to MEF2-mediated transcriptional activation of Nur77, an orphan nuclear steroid receptor that activates apoptosis in these cells (24). MEF2 binds directly to regulatory elements in the Nur77 gene and also cooperates with NFAT to drive Nur77 expression (25). The increase in MEF2 transcriptional activity on the Nur77 regulatory element occurs in the absence of changes in DNA binding, implicating other regulatory mechanisms such as cofactor binding and/or changes in phosphorylation of the transactivation domain.

MEF2 Transcription Factors in Brain

MEF2 family members are also highly expressed in neurons of the central nervous system (5,6,26–29). In vertebrates, each MEF2 isoform shows a unique temporal expression pattern in different regions of the brain. The timing of MEF2 expression in neurons is consistent with a role of MEF2 transcription factors in neu-

ronal differentiation and maintenance. In human brain, MEF2C is preferentially expressed in certain neuronal layers of the postnatal cerebral cortex in a temporal manner declining from postnatal d 2 to adult (5,6). These immunocytochemical data suggest that MEF2C regulates the laminar differentiation of central neurons. Of note, is the absence of MEF2C in dividing neurons in the subventricular zones (6). An alternative splice variant of MEF2C is found exclusively in the brain and contains a unique SEDVDLLL peptide sequence in the transactivation domain that may serve to mediate tissue-specific protein–protein interactions (26).

In the mouse brain where more extensive regions have been examined by *in situ* hybridization, the timing of MEF2 gene expression is also associated with neurons exiting the cell cycle and entering differentiation (27). Mef2C mRNA is first detected in the mouse telencephalon at postnatal d 11.5. This region of the brain is one of the first to begin neuronal differentiation. At postnatal d 13.5, Mef2C is expressed in a layer of cells in the intermediate zone of the frontal cortex and in the olfactory bulb. At this time MEF2 transcripts are also localized in different regions of the neural tube. Mef2A is distributed in a gradient with highest levels in the dorsal portion and lowest levels in the ventral portion. Mef2C is expressed only in the dorsal region, whereas, Mef2D is distributed throughout the neural tube. At postnatal d 14.5, Mef2C and Mef2D are detected in frontal cortex, hippocampus, amygdala, midbrain, olfactory bulb, and cerebellum. Mef2B is abundant in frontal cortex, present at lower levels in the hippocampus, midbrain, and amygdala, and absent in cerebellum. At postnatal d 16.5, low levels of Mef2A overlap with high levels of Mef2C in the hippocampus, midbrain, and frontal cortex. Mef2B is also present in both frontal and midbrain cortex. Mef2D is the most widely distributed of the four genes at this time. At birth, the expression pattern of Mef2B and Mef2C overlap in frontal cortex and olfactory bulbs. Mef2B transcripts appear in the cerebellum. In the 2 wk postnatal brain, all four gene transcripts are present in dentate gyrus.

Mef2C, -D, and -A appear in neurons of the horn of Ammon. Mef2C and Mef2D are expressed equally throughout the layers of the frontal cortex. Between 2 and 6 wk after birth, Mef2 transcripts show a striking pattern of differential expression in the mature cerebellum. Mef2A and Mef2D are found predominantly in the granule layer of the cerebellum. Mef2C is expressed primarily in Purkinje neurons and Mef2B is very low or absent. This dynamic pattern of mRNA expression during pre- and postnatal development in the mouse suggests that different MEF2 isoforms may perform unique roles at different stages of neuronal maturation.

To date, there have not been extensive immunocytochemical studies performed to localize the specific MEF2 proteins in the brain partly due to the scarcity of high affinity isoform-specific antibodies. The data thus far indicate that MEF2 protein expression in the brain correlates with mRNA expression (30). For example, in the developing mouse cerebellum (postnatal d 7), MEF2A protein expression occurs primarily in the internal granule layer where the final differentiation and maturation of granule neurons occurs. Levels of MEF2A are very low in the external granule layer where granule neuron precursors are still dividing. This pattern of expression matches that of mRNA localization (27,31). In the developing rat cerebral cortex, MEF2C protein expression is detectable at embryonic d 17 and peaks around E21 (29). MEF2C is expressed in the cortical plate but not in the ventricular zone where dividing neuronal precursors reside. Cortical cells expressing MEF2C also express β -tubulin type III, but not glial fibrillary acidic protein, indicating that MEF2C expression is restricted to neurons. Again, the pattern of expression of MEF2C protein in cerebral cortex correlates with the pattern of expression of Mef2C mRNA. The immunocytochemistry data taken together with the *in situ* hybridization studies indicate that MEF2 transcription factors are primarily expressed in differentiating neurons but not in dividing neuronal precursors. Distinct MEF2 isoforms may mediate similar functions in different populations of

neurons, but because of their structural variations they might be regulated in cell type-specific and isoform-specific manners.

In Vitro Studies of Neuronal MEF2

Studies of primary neuronal cultures support the hypothesis that MEF2 transcription factors regulate neuronal survival and differentiation. In cultures of cerebral cortical neurons where proliferating precursor cells and postmitotic differentiating neurons can be distinguished, MEF2C is selectively expressed in newly generated postmitotic neurons and is not detectable in BrdU-positive precursor cells (31). Blocking the function of MEF2C in the postmitotic cortical neurons, by introducing a dominant-interfering form of MEF2, results in apoptotic cell death. Similar results have been obtained in cultures of cerebellar granule neurons where expression of a dominant-interfering form of MEF2 reduces the survival of granule neurons grown in the presence of depolarizing potassium (32). Conversely, expression of a constitutively-active form of MEF2 promotes the survival of granule neurons grown in the absence of depolarizing potassium, conditions that normally trigger apoptosis (32). Additional evidence that MEF2 regulates activity-dependent survival of granule neurons comes from gene silencing experiments demonstrating that RNA interference (RNAi) of MEF2A in primary cerebellar cultures markedly decreases the survival of granule neurons (33). The loss of MEF2 activity also contributes to the death of cortical neurons subjected to excitotoxic stress (34). Exposure of primary cortical neurons to excitotoxic concentrations of NMDA leads to caspase-mediated cleavage of MEF2 that yields dominant-interfering forms of MEF2 (34). Caspase-mediated cleavage of MEF2A and MEF2D also contributes to the death of granule neurons when deprived of trophic support (32).

In P19 neuronal precursor cells, expression of MEF2C induces a mixed neuronal/myogenic phenotype (35). During retinoic acid-induced

neurogenesis of these cells, a dominant-negative form of MEF2C enhances apoptosis but does not affect cell division. On the other hand, P19 cells induced to undergo apoptosis can be rescued from cell death by expression of constitutively-active MEF2C. In addition, over-expression of MEF2C in P19 cells results in induction of neurofilament protein, the nuclear antigen NeuN, and MASH-1, a neural-specific bHLH transcription factor known to interact with MEF2s (36). These data suggest that MEF2 proteins regulate neuronal development not only by promoting survival but by also inducing differentiation.

Other examples of a differentiation role of MEF2 during neuronal development include MEF2C activation of the NMDA receptor subunit 1 (NR1) gene in cerebral cortical cultures (37) and the role of the MEF2B/2C heterodimer to mediate adhesion related kinase repression of the GnRH gene in GnRH neuronal cells (38). In the former case, MEF2C interacts with Sp1 proteins to activate transcription. This mechanism of transcriptional activation represents a nonclassical mode of gene regulation by MEF2 proteins that may not involve bHLH binding partners. In the case of the GnRH promoter, the putative homeodomain partner interacting with MEF2B/2C heterodimer has not yet been identified.

Activation of MEF2 Proteins by Protein Kinases

Direct phosphorylation of MEF2 proteins plays an important role in the regulation of MEF2 function. A casein-kinase II (CKII) phosphorylation site is conserved in the MEF2 domain of all MEF2 proteins. Phosphorylation of this site by CKII enhances DNA binding of MEF2 (39). This site appears to be constitutively phosphorylated *in vivo* with no evidence for its regulation. It is likely that phosphorylation by CKII induces a conformational change that enhances the ability of the MADS box and MEF2 domain to contact DNA.

Phosphorylation of the transactivation domain of MEF2 transcription factors has also been shown to increase MEF2 activity. At least two isoforms of p38 MAP kinase (p38 α and p38 β) activate MEF2A and MEF2C by phosphorylating residues located in their activation domains (40,41). In the case of MEF2A, p38-mediated phosphorylation of T312 and T319 within the transactivation domain is required for transcriptional activation in muscle cells (42). Additional serine residues including S355, S453, and S479 are phosphorylated *in vitro* by p38 but their relevance to transcriptional activation is questionable (40,41,43). Activation of MEF2C by p38 seems more complex than for MEF2A and is subject to cell-type specific regulation. Three prominent residues (T293, T300, and S387) in the activation domain of MEF2C are phosphorylated by p38 *in vitro* (41). Phosphorylation of these residues has been shown to be important for MEF2C activation by p38 in T lymphocytes (44). However, only phosphorylation of T293 is induced in differentiating myocytes and is required for MEF2C activation by p38 during muscle differentiation (45). Introduction of dominant-interfering mutants of p38 in primary neurons and differentiating P19 neurons has been shown to reduce MEF2-dependent transcription and induce apoptosis (31,35), suggesting that p38 mediates the activation of MEF2 in neurons. The isoforms of MEF2 that are phosphorylated by p38 in neurons and the sites that are critical for enhanced transactivation are not yet understood. Moreover, whether activation of Mef2 proteins by p38 is a common mechanism shared by diverse types of neurons is unclear.

In addition to p38 MAP kinase, the serine/threonine kinase ERK5 is capable of phosphorylating the transactivation domains of MEF2A, -C, and -D resulting in increased transcriptional activity (46–49). Interestingly, ERK5 has also been shown to possess a transactivation domain and may stimulate MEF2-dependent transcription by functioning as a coactivator that facilitates recruitment of the basal transcription machinery (50). In T lymphocytes,

ERK5-MEF2 interactions are stimulated by increases in intracellular calcium and inhibited by Cabin (50). Recent studies indicate that ERK5 activation of MEF2 plays an important role in BDNF-mediated survival of primary cortical neurons (51). Similarly, the temporal survival effects of BDNF in cerebellar granule neurons appear to be mediated by an ERK5/MEF2 signaling pathway that induces transcription of neurotrophin-3 (52).

Inactivation of Neuronal MEF2 Proteins by Phosphorylation and Regulation by Calcium Signaling

MEF2 transcription factors in muscle cells are sensitive to calcium signals that act through multiple mechanisms to modulate transcriptional activity (12). Recent work suggests that MEF2 activity in neurons is similarly regulated by intracellular calcium. Calcineurin is a serine/threonine phosphatase that is activated by the binding of calcium and calmodulin. Recent studies have shown that calcineurin promotes the DNA binding and activity of MEF2 transcription factors in neurons that depend on depolarization-mediated calcium influx for their survival (31,32). Cultured cerebellar granule neurons survive in the presence of high intracellular calcium, a condition that mimics activity-dependent neuronal survival during development. The neurons are cultured in elevated (25 mM) potassium that promotes an influx of calcium by opening L-type voltage sensitive calcium channels resulting in persistent activation of calcineurin. Removal of depolarization induces hyperphosphorylation of MEF2D and MEF2A on serine/threonine residues, resulting in decreased DNA binding and susceptibility to caspase cleavage (29,32). The subsequent loss of MEF2 dependent gene transcription leads to apoptosis of granule neurons (see Fig. 2). The hyperphosphorylation of MEF2 is mimicked by the addition of calcineurin inhibitors to depolarizing medium,

indicating that calcineurin maintains MEF2 in a hypophosphorylated state that has enhanced DNA binding and transcriptional activity (29,32). The kinase(s) responsible for phosphorylating the sites that calcineurin keeps dephosphorylated in healthy neurons is unknown. Recent findings, however, indicate that a MEF2 kinase activated during neuronal apoptosis is lithium-sensitive but is distinct from glycogen synthase kinase-3 (GSK-3) (53). Additional studies, discussed in the following section, have shown that Cdk5 phosphorylates and inactivates MEF2 in cerebral cortical neurons undergoing apoptosis (54). Whether or not Cdk5 regulates MEF2 phosphorylation in granule neurons during removal of depolarization signals remains to be determined.

In primary cortical neurons, phosphorylation of MEF2 by Cdk5 results in inhibition of MEF2 transcriptional activity (54). The Cdk5 phosphorylation site is conserved in MEF2A, -C, and -D and lies within the transactivation domain of MEF2. Oxidative stress and excitotoxic concentrations of glutamate increase nuclear Cdk5 activity leading to Cdk5-dependent phosphorylation of MEF2 and inhibition of function. Moreover, MEF2 mutants that are resistant to Cdk5 phosphorylation rescue neurons from neurotoxin-induced apoptosis. In light of accumulating evidence that Cdk5 activity is dysregulated in a number of neurodegenerative disorders including, Alzheimer's disease, amyotrophic lateral sclerosis, and Parkinson's disease (55–58), these data raise the possibility that decreased function of the survival-promoting transcription factor MEF2 contributes to the neuronal loss observed in neurodegenerative diseases.

The mechanism by which phosphorylation by Cdk5 inhibits MEF2 function is not understood. Phosphorylation by Cdk5 may target MEF2 for cleavage and/or degradation. Whether or not Cdk5 phosphorylation of MEF2 is related to the caspase cleavage of MEF2 proteins that occurs during neuronal apoptosis remains to be investigated. Another possibility is that phosphorylation changes the conformation of MEF2 which in turn alters its

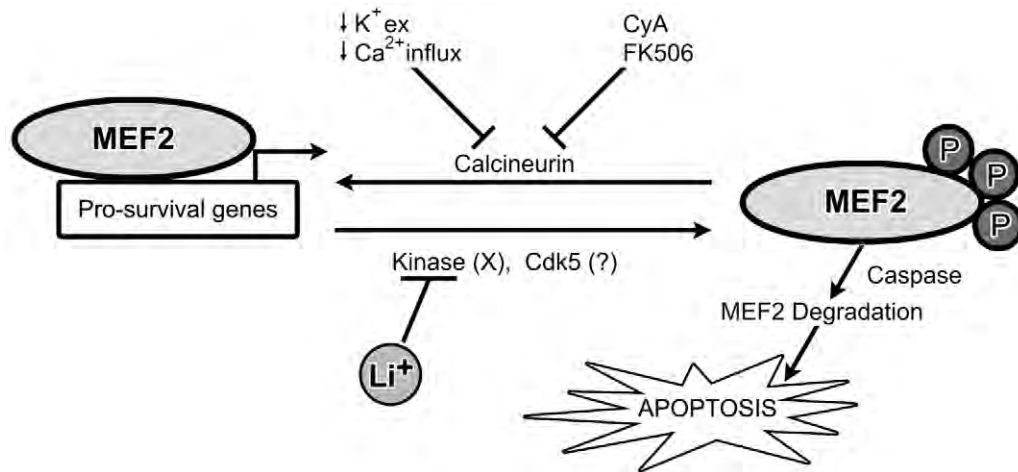


Fig. 2. Regulation of neuronal MEF2 function by calcium signaling. Primary cultures of cerebellar granule neurons require depolarization-stimulated MEF2 activity for their survival. Removal of extracellular depolarizing potassium leads to a decrease in calcium influx and subsequent inactivation of calcineurin phosphatase activity. The loss of calcineurin activity acts in a coordinated manner with activation of a pro-apoptotic MEF2 kinase (X), resulting in a marked hyperphosphorylation of MEF2 proteins. Hyperphosphorylation of MEF2 decreases its DNA binding and enhances its susceptibility to caspase-mediated degradation. The loss of MEF2-dependent transcription of pro-survival genes contributes to granule neuron apoptosis. The hyperphosphorylation of MEF2 can be partially mimicked under depolarizing conditions by addition of calcineurin inhibitors (cyclosporin A and FK506), demonstrating a key role for calcineurin in maintaining MEF2 proteins in a hypophosphorylated (DNA-bound) state in healthy neurons. Neither the sites of hyperphosphorylation induced on MEF2 during neuronal apoptosis, nor the kinase responsible, are currently known. However, the MEF2 kinase (X) is a lithium-sensitive kinase distinct from the known lithium target, glycogen synthase kinase-3. Whether or not Cdk5, a pro-apoptotic kinase that phosphorylates and inactivates MEF2 in cortical neurons, plays a role in the hyperphosphorylation of MEF2 in cerebellar granule neurons remains to be investigated.

interaction with cofactors or the basal transcription machinery.

Indirect Mechanisms of MEF2 Regulation by Protein Kinases

In addition to the direct phosphorylation of MEF2 proteins that regulate their activity, there are also indirect mechanisms by which protein kinases influence MEF2 function. In particular, serine phosphorylation of two repressors of MEF2 activity, class II histone deacetylases (HDACs) and MEF2-interacting transcription repressor (MITR), leads to their nuclear export and association with cytoplasmic scaffolding

proteins of the 14-3-3 family (59–62). In this manner, a serine kinase acts indirectly to derepress MEF2 activity. In all of the studies cited above, overexpression of active calcium/calmodulin-dependent kinases (CaMKs) I and IV was utilized to stimulate phosphorylation of the HDACs in muscle cells and nonmuscle cells (e.g., COS or NIH3T3 fibroblasts). However, the identity of the endogenous kinase responsible for phosphorylation of HDACs in muscle is currently unknown. We have recently shown that class II HDACs (HDAC4 and HDAC5) are excluded from the nuclei of cerebellar granule neurons cultured in depolarizing medium (Linseman et al., in press). Either removal of the depolarization stimulus

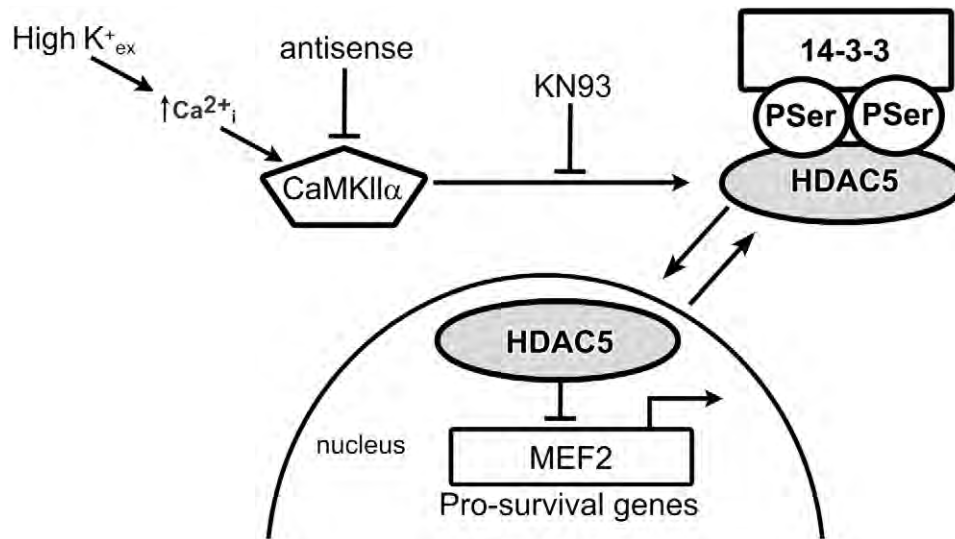


Fig. 3. Derepression of neuronal MEF2 activity by CaMKII-mediated phosphorylation of HDAC. In cerebellar granule neurons cultured in depolarizing extracellular potassium, the MEF2 repressor histone deacetylase-5 (HDAC5), is excluded from the nucleus. Under these conditions it is retained in the cytoplasm in a phosphorylated state, likely associated with scaffolding proteins of the 14-3-3 family. Removal of the depolarization stimulus induces a rapid translocation of HDAC5 into the nucleus where it interacts with MEF2 to repress its transcriptional activity. The nuclear translocation of HDAC5 can also be stimulated under depolarizing conditions either by the addition of a calcium/calmodulin-dependent kinase (CaMK) inhibitor, KN93, or by the antisense-mediated depletion of CaMKII α . These data suggest a mechanism by which depolarization-mediated calcium influx acts through CaMKII to induce phosphorylation and nuclear export of HDAC5, resulting in derepression of MEF2 activity in healthy neurons.

or addition of CaMK inhibitors (KN93 or KN62) stimulates a rapid translocation of HDACs into the nucleus, resulting in repression of MEF2 activity and induction of cerebellar granule neuron apoptosis. Furthermore, HDAC nuclear translocation and apoptosis are induced by antisense-mediated depletion of CaMKII α , a neuronal specific CaMK isoform. These results are the first to identify an endogenous kinase capable of regulating HDAC localization and suggest a mechanism by which depolarization-mediated calcium influx acts through CaMKII to phosphorylate HDAC, promoting its nuclear export and derepression of MEF2 activity (see Fig. 3). In further support of this mechanism in neurons, Chawla et al. (63) recently showed that CaMK inhibitors similarly attenuate HDAC nuclear

export in hippocampal neuronal cultures. Thus, CaMK-mediated inactivation of HDACs may act in a cooperative manner with kinases that directly phosphorylate and activate MEF2 proteins to regulate this important transcription factor in neurons.

Summary and Future Directions

The MEF2 family of transcription factors act as effectors of diverse signaling pathways that regulate fundamental cellular processes. It seems paradoxical that MEF2 could control such diverse and opposing functions such as proliferation, differentiation, and apoptosis. A likely explanation lies in the identity of tissue-specific DNA binding partners and coactiva-

tors, as well as, cell-type and isoform-specific regulation by a variety of protein kinases. The identities of the MEF2 target genes that mediate many of the cellular responses, particularly in neurons, remain to be determined. Future studies using conditional gene inactivation to assess the *in vivo* functions of specific MEF2 isoforms in neuronal development will further our understanding of MEF2 function in the nervous system.

Acknowledgments

This work was supported by a Department of Veterans Affairs Merit Award (Kim A. Heidenreich), a Department of Defense Grant DAMD17-99-1-9481 (K.A.H.), an NIH Grant NS38619-01A1 (Kim A. Heidenreich), and a Department of Veterans Affairs Research Enhancement Award Program (Kim A. Heidenreich and Daniel A. Linseman).

References

1. Yu Y.T., Breitbart R.E., Smoot L.B., Lee Y., Mahdavi V., Nadal-Ginard B. (1992) Human myocyte-specific enhancer factor 2 comprises a group of tissue-restricted MADS box transcription factors. *Genes Dev.* **6**, 1783–1798.
2. Naya F.S., Olson E. (1999) MEF2: a transcriptional target for signaling pathways controlling skeletal muscle growth and differentiation. *Curr. Opin. Cell Biol.* **11**, 683–688.
3. Shore P., Sharrocks A.D. (1995) The MADS-box family of transcription factors. *Eur. J. Biochem.* **229**, 1–13.
4. Breitbart R.E., Liang C.S., Smoot L.B., Laheru D.A., Mahdavi V., Nadal-Ginard B. (1993) A fourth human MEF2 transcription factor, hMEF2D, is an early marker of the myogenic lineage. *Development* **118**, 1095–1106.
5. Leifer D., Krainc D., Yu Y.T., et al. (1993) MEF2C, a MADS/MEF2-family transcription factor expressed in a laminar distribution in cerebral cortex. *Proc. Natl. Acad. Sci. USA* **90**, 1546–1550.
6. McDermott J.C., Cardoso M.C., Yu Y.T., et al. (1993) hMEF2C gene encodes skeletal muscle- and brain-specific transcription factors. *Mol. Cell Biol.* **13**, 2564–2577.
7. Martin J.F., Miano J.M., Hustad C.M., Copeland N.G., Jenkins N.A., Olson E.N. (1994) A Mef2 gene that generates a muscle-specific isoform via alternative mRNA splicing. *Mol. Cell Biol.* **14**, 1647–1656.
8. Moore S., Vrebalov J., Payton P., Giovannoni J. (2002) Use of genomics tools to isolate key ripening genes and analyse fruit maturation in tomato. *J. Exp. Bot.* **53**, 2023–2030.
9. Ng M., Yanofsky M.F. (2001) Function and evolution of the plant MADS-box gene family. *Nat. Rev. Genet.* **2**, 186–195.
10. Yun K., Wold B. (1996) Skeletal muscle determination and differentiation: story of a core regulatory network and its context. *Curr. Opin. Cell Biol.* **8**, 877–889.
11. Black B.L., Olson E.N. (1998) Transcriptional control of muscle development by myocyte enhancer factor-2 (MEF2) proteins. *Annu. Rev. Cell. Dev. Biol.* **14**, 167–196.
12. McKinsey T.A., Zhang C.L., Olson E.N. (2002) MEF2: a calcium-dependent regulator of cell division, differentiation and death. *Trends Biochem. Sci.* **27**, 40–47.
13. Molkentin J.D., Firulli A.B., Black B.L., et al. (1996) MEF2B is a potent transactivator expressed in early myogenic lineages. *Mol. Cell Biol.* **16**, 3814–3824.
14. Molkentin J.D., Olson E.N. (1996) Combinatorial control of muscle development by basic helix-loop-helix and MADS-box transcription factors. *Proc. Natl. Acad. Sci. USA* **93**, 9366–9373.
15. Ornatsky O.I., McDermott J.C. (1996) MEF2 protein expression, DNA binding specificity and complex composition, and transcriptional activity in muscle and non-muscle cells. *J. Biol. Chem.* **271**, 24927–24933.
16. Puri P.L., Sartorelli V. (2000) Regulation of muscle regulatory factors by DNA-binding, interacting proteins, and post-transcriptional modifications. *J. Cell. Physiol.* **185**, 155–173.
17. Puri P.L., Wu Z., Zhang P., et al. (2000) Induction of terminal differentiation by constitutive activation of p38 MAP kinase in human rhabdomyosarcoma cells. *Genes Dev.* **14**, 574–584.
18. Lin Q., Schwarz J., Bucana C., Olson E.N. (1997) Control of mouse cardiac morphogenesis and myogenesis by transcription factor MEF2C. *Science* **276**, 1404–1407.
19. Bour B.A., O'Brien M.A., Lockwood W.L., et al. (1995) *Drosophila* MEF2, a transcription factor

- that is essential for myogenesis. *Genes Dev.* **9**, 730–741.
20. Prokop A., Landgraf M., Rushton E., Broadie K., Bate M. (1996) Presynaptic development at the *Drosophila* neuromuscular junction: assembly and localization of presynaptic active zones. *Neuron* **17**, 617–626.
 21. Kolodziejczyk S.M., Wang L., Balazsi K., DeRopentigny Y., Kothary R., Megeney L.A. (1999) MEF2 is upregulated during cardiac hypertrophy and is required for normal post-natal growth of the myocardium. *Curr. Biol.* **9**, 1203–1206.
 22. Passier R., Zeng H., Frey N., et al. (2000) CaM kinase signaling induces cardiac hypertrophy and activates the MEF2 transcription factor in vivo. *J. Clin. Invest.* **105**, 1395–1406.
 23. Zhang C.L., McKinsey T.A., Chang S., Antos C.L., Hill J.A., Olson E.N. (2002) Class II histone deacetylases act as signal-responsive repressors of cardiac hypertrophy. *Cell* **110**, 479–488.
 24. Youn H.D., Sun L., Prywes R., Liu J.O. (1999) Apoptosis of T cells mediated by Ca²⁺-induced release of the transcription factor MEF2. *Science* **286**, 790–793.
 25. Youn H.D., Chatila T.A., Liu J.O. (2000) Integration of calcineurin and MEF2 signals by the coactivator p300 during T-cell apoptosis. *Embo J.* **19**, 4323–4331.
 26. Leifer D., Golden J., Kowall N.W. (1994) Myocyte-specific enhancer binding factor 2C expression in human brain development. *Neuroscience* **63**, 1067–1079.
 27. Lyons G.E., Micales B.K., Schwarz J., Martin J.F., Olson E.N. (1995) Expression of *mef2* genes in the mouse central nervous system suggests a role in neuronal maturation. *J. Neurosci.* **15**, 5727–5738.
 28. Ikeshima H., Imai S., Shimoda K., Hata J., Takano T. (1995) Expression of a MADS box gene, MEF2D, in neurons of the mouse central nervous system: implication of its binary function in myogenic and neurogenic cell lineages. *Neurosci. Lett.* **200**, 117–120.
 29. Mao Z., Wiedmann M. (1999) Calcineurin enhances MEF2 DNA binding activity in calcium-dependent survival of cerebellar granule neurons. *J. Biol. Chem.* **274**, 31102–31107.
 30. Lin X., Shah S., Bulleit R.F. (1996) The expression of MEF2 genes is implicated in CNS neuronal differentiation. *Brain Res. Mol. Brain Res.* **42**, 307–316.
 31. Mao Z., Bonni A., Xia F., Nadal-Vicens M., Greenberg M.E. (1999) Neuronal activity-dependent cell survival mediated by transcription factor MEF2. *Science* **286**, 785–790.
 32. Li M., Linseman D.A., Allen M.P., et al. (2001) Myocyte enhancer factor 2A and 2D undergo phosphorylation and caspase-mediated degradation during apoptosis of rat cerebellar granule neurons. *J. Neurosci.* **21**, 6544–6552.
 33. Gaudilliere B., Shi Y., Bonni A. (2002) RNA interference reveals a requirement for myocyte enhancer factor 2A in activity-dependent neuronal survival. *J. Biol. Chem.* **277**, 46442–46446.
 34. Okamoto S., Li Z., Ju C., Scholzke M.N., Mathews E., et al. (2002) Dominant-interfering forms of MEF2 generated by caspase cleavage contribute to NMDA-induced neuronal apoptosis. *Proc. Natl. Acad. Sci. USA* **99**, 3974–3979.
 35. Okamoto S., Krainc D., Sherman K., Lipton S.A. (2000) Antiapoptotic role of the p38 mitogen-activated protein kinase-myocyte enhancer factor 2 transcription factor pathway during neuronal differentiation. *Proc. Natl. Acad. Sci. USA* **97**, 7561–7566.
 36. Skerjanc I.S., Wilton S. (2000) Myocyte enhancer factor 2C upregulates MASH-1 expression and induces neurogenesis in P19 cells. *FEBS Lett.* **472**, 53–56.
 37. Krainc D., Bai G., Okamoto S., et al. (1998) Synergistic activation of the N-methyl-D-aspartate receptor subunit 1 promoter by myocyte enhancer factor 2C and Sp1. *J. Biol. Chem.* **273**, 26218–26224.
 38. Allen M.P., Xu M., Linseman D.A., et al. (2002) Adhesion-related kinase repression of gonadotropin-releasing hormone gene expression requires Rac activation of the extracellular signal-regulated kinase pathway. *J. Biol. Chem.* **277**, 38133–38140.
 39. Molkentin J.D., Li L., Olson E.N. (1996) Phosphorylation of the MADS-Box transcription factor MEF2C enhances its DNA binding activity. *J. Biol. Chem.* **271**, 17199–17204.
 40. Yang S.H., Galanis A., Sharrocks A.D. (1999) Targeting of p38 mitogen-activated protein kinases to MEF2 transcription factors. *Mol. Cell. Biol.* **19**, 4028–4038.
 41. Zhao M., New L., Kravchenko V.V., et al. (1999) Regulation of the MEF2 family of transcription factors by p38. *Mol. Cell. Biol.* **19**, 21–30.
 42. Wu Z., Woodring P.J., Bhakta K.S., et al. (2000) p38 and extracellular signal-regulated kinases regulate the myogenic program at multiple steps. *Mol. Cell. Biol.* **20**, 3951–3964.
 43. Ornatsky O.I., Cox D.M., Tangirala P., et al. (1999) Post-translational control of the MEF2A

- transcriptional regulatory protein. *Nucleic Acids Res.* **27**, 2646–2654.
44. Han J., Jiang Y., Li Z., Kravchenko V.V., Ulevitch R.J. (1997) Activation of the transcription factor MEF2C by the MAP kinase p38 in inflammation. *Nature* **386**, 296–299.
 45. Wu H., Naya F.J., McKinsey T.A., et al. (2000) MEF2 responds to multiple calcium-regulated signals in the control of skeletal muscle fiber type. *Embo J.* **19**, 1963–1973.
 46. Kato Y., Kravchenko V.V., Tapping R.I., Han J., Ulevitch R.J., Lee J.D. (1997) BMK1/ERK5 regulates serum-induced early gene expression through transcription factor MEF2C. *Embo J.* **16**, 7054–7066.
 47. Yang C.C., Ornatsky O.I., McDermott J.C., Cruz T.F., Prody C.A. (1998) Interaction of myocyte enhancer factor 2 (MEF2) with a mitogen-activated protein kinase, ERK5/BMK1. *Nucleic Acids Res.* **26**, 4771–4777.
 48. Kato Y., Zhao M., Morikawa A., et al. (2000) Big mitogen-activated kinase regulates multiple members of the MEF2 protein family. *J. Biol. Chem.* **275**, 18534–18540.
 49. Marinissen M.J., Chiariello M., Pallante M., Gutkind J.S. (1999) A network of mitogen-activated protein kinases links G protein-coupled receptors to the c-jun promoter: a role for c-Jun NH2-terminal kinase, p38s, and extracellular signal-regulated kinase 5. *Mol. Cell. Biol.* **19**, 4289–4301.
 50. Kasler H.G., Victoria J., Duramad O., Winoto A. (2000) ERK5 is a novel type of mitogen-activated protein kinase containing a transcriptional activation domain. *Mol. Cell. Biol.* **20**, 8382–8389.
 51. Liu L., Cavanaugh J.E., Wang Y., Sakagami H., Mao Z., Xia Z. (2003) ERK5 activation of MEF2-mediated gene expression plays a critical role in BDNF-promoted survival of developing but not mature cortical neurons. *Proc. Natl. Acad. Sci. USA* **100**, 8532–8537.
 52. Shalizi A., Lehtinen M., Gaudilliere B., et al. (2003) Characterization of a neurotrophin signaling mechanism that mediates neuron survival in a temporally specific pattern. *J. Neurosci.* **23**, 7326–7336.
 53. Linseman D.A., Cornejo B.J., Le S.S., et al. (2003) A myocyte enhancer factor 2D (MEF2D) kinase activated during neuronal apoptosis is a novel target inhibited by lithium. *J. Neurochem.* **85**, 1488–1499.
 54. Gong X., X. T., Wiedmann M., Wang X., et al. (2003) Cdk-5 mediated inhibition of the protective effects of transcription factor MEF2 in neurotoxicity-induced apoptosis. *Neuron* **38**, 33–46.
 55. Grant P., Sharma P., Pant H.C. (2001) Cyclin-dependent protein kinase 5 (Cdk5) and the regulation of neurofilament metabolism. *Eur. J. Biochem.* **268**, 1534–1546.
 56. Bajaj N.P. (2000) Cyclin-dependent kinase-5 (CDK5) and amyotrophic lateral sclerosis. *Amyotroph Lateral Scler Other Motor Neuron Disord.* **1**, 319–327.
 57. Maccioni R.B., Otth C., Concha I.I., Munoz J.P. (2001) The protein kinase Cdk5. Structural aspects, roles in neurogenesis and involvement in Alzheimer's pathology. *Eur. J. Biochem.* **268**, 1518–1527.
 58. Takahashi M., Iseki E., Kosaka K. (2000) Cyclin-dependent kinase 5 (Cdk5) associated with Lewy bodies in diffuse Lewy body disease. *Brain Res.* **862**, 253–256.
 59. Lu J., McKinsey T.A., Zhang C.L., Olson E.N. (2000) Regulation of skeletal myogenesis by association of the MEF2 transcription factor with class II histone deacetylases. *Mol. Cell.* **6**, 233–244.
 60. McKinsey T.A., Zhang C.L., Lu J., Olson E.N. (2000) Signal-dependent nuclear export of a histone deacetylase regulates muscle differentiation. *Nature* **408**, 106–111.
 61. Kao H.Y., Verdel A., Tsai C.C., Simon C., Juguilon H., Khochbin S. (2001) Mechanism for nucleocytoplasmic shuttling of histone deacetylase 7. *J. Biol. Chem.* **276**, 47496–47507.
 62. Zhang C.L., McKinsey T.A., Olson E.N. (2001) The transcriptional corepressor MITR is a signal-responsive inhibitor of myogenesis. *Proc. Natl. Acad. Sci. USA* **98**, 7354–7359.
 63. Chawla S., Vanhoutte P., Arnold F.J., Huang C.L., Bading H. (2003) Neuronal activity-dependent nucleocytoplasmic shuttling of HDAC4 and HDAC5. *J. Neurochem.* **85**, 151–159.

Distinct mechanisms of neuronal apoptosis are triggered by antagonism of Bcl-2/Bcl-x(L) versus induction of the BH3-only protein Bim

Angela K. Zimmermann,^{*,1} F. Alexandra Loucks,^{†,1} Shoshona S. Le,[†] Brent D. Butts,[‡] Maria L. Florez-McClure,[‡] Ron J. Bouchard,[†] Kim A. Heidenreich^{*,†,‡} and Daniel A. Linseman^{*,†,‡}

^{*}Neuroscience Program, University of Colorado Health Sciences Center, Denver, Colorado, USA

[†]Research Service, Veterans Affairs Medical Center, Denver, Colorado, USA

[‡]Department of Pharmacology, University of Colorado Health Sciences Center, Denver, Colorado, USA

Abstract

Primary cerebellar granule neurons (CGNs) require depolarizing extracellular potassium for their survival. Removal of depolarizing potassium triggers CGN apoptosis that requires induction of Bim, a BH3-only Bcl-2 family member. Bim is classically thought to promote apoptosis by neutralizing pro-survival Bcl-2 proteins. To determine if this is the principal function of Bim in CGNs, we contrasted Bim-mediated apoptosis to neuronal death induced by HA14-1, a BH3-domain mimetic that antagonizes Bcl-2 and Bcl-x(L). HA14-1 elicited CGN apoptosis characterized by caspase 3 and 9 activation, cytochrome *c* release, conformational activation of Bax, and mitochondrial depolarization. HA14-1 provoked CGN apoptosis in the absence of Bim induction and negative regulators of Bim transcription did not prevent HA14-1-induced cell death. However, the antioxidant glutathione and its precursor, *N*-acetyl-

L-cysteine, suppressed HA14-1-induced apoptosis. Similarly, apoptosis induced by either a structurally distinct Bcl-2/Bcl-x(L) inhibitor (compound 6) or Bcl-2 antisense oligonucleotides was diminished by glutathione. In contrast, antioxidants had no effect on CGN apoptosis provoked by either removal of depolarizing potassium or overexpression of a GFP–Bim fusion protein, two models of Bim-dependent death. These data show that antagonism of Bcl-2/Bcl-x(L) function elicits oxidative stress-dependent CGN apoptosis that is mechanistically distinct from Bim-mediated cell death. These results further indicate that, although Bcl-2/Bcl-x(L) antagonism is sufficient to induce neuronal apoptosis, Bim likely promotes neuronal death by interacting with additional proteins besides Bcl-2/Bcl-x(L).

Keywords: apoptosis, Bcl-2, Bim, cerebellar granule neuron, glutathione, oxidative stress.

J. Neurochem. (2005) **94**, 22–36.

Although apoptosis (programmed cell death) plays an essential role in the normal development of the central nervous system (Lossi and Merighi 2003), unchecked apoptotic cell death has been implicated in the progression of several neurodegenerative disorders (Ekshyyan and Aw 2004). For instance, with the advent of new techniques to identify apoptotic cells *in situ*, evidence supporting a significant apoptotic component of neuronal degeneration in Parkinson's disease is compelling (Fiskum *et al.* 2003; Tatton *et al.* 2003). Investigations into the molecular mechanisms underlying Parkinsonian neuronal death have identified a principal pathway involving Bax-dependent mitochondrial apoptosis (Vila *et al.* 2001; Viswanath *et al.* 2001). Similarly, diverse morphological and immunocytochemical markers have been implemented to identify activation of a mitochondrial apoptotic cascade in other

Resubmitted manuscript received January 18, 2005; accepted February 10, 2005.

Address correspondence and reprint requests to Daniel A. Linseman PhD, Veterans Affairs Medical Center, Research Service-111H, 1055 Clermont Street, Denver, CO 80220, USA.

E-mail: Dan.Linseman@UCHSC.edu

¹These authors contributed equally to this work.

Abbreviations used: BH3, Bcl-2 homology-3; CGN, cerebellar granule neuron; $\Delta\psi_m$, mitochondrial membrane potential; ER, endoplasmic reticulum; GFP, green fluorescent protein; GSH, glutathione; HA14-1, ethyl 2-amino-6-bromo-4-(1-cyano-2-ethoxy-2-oxoethyl)-4H-chromene-3-carboxylate; IGF-I, insulin-like growth factor-I; 5K, serum-free culture medium containing 5 mM KCl; 25K, serum-free culture medium containing 25 mM KCl; mPTP, mitochondrial permeability transition pore; NAC, *N*-acetyl-L-cysteine; TMRE, tetramethylrhodamine ethyl ester; VDAC, voltage-dependent anion channel.

neurodegenerative diseases, including amyotrophic lateral sclerosis and Huntington's disease (Guegan *et al.* 2001; Jana *et al.* 2001; Inoue *et al.* 2003). These *in vivo* findings illustrate the importance of elucidating the regulation of mitochondrial apoptosis in the context of neurodegenerative diseases

Primary cultures of cerebellar granule neurons (CGNs) undergo apoptosis when deprived of depolarizing extracellular potassium and have consequently been utilized as a primary neuronal model to study this process (D'Mello *et al.* 1993). CGNs die by a mitochondrial apoptotic pathway that requires Bax activation and induction of the BH3-only protein, Bim (Harris and Johnson 2001; Linseman *et al.* 2002; Linseman *et al.* 2004). Bim is a pro-apoptotic Bcl-2 family member that plays a key role in neuronal apoptosis (Putchá *et al.* 2001; Whitfield *et al.* 2001; Putchá *et al.* 2002). BH3 domain-only proteins, like Bim, are commonly thought to promote mitochondrial apoptosis primarily by interacting with and neutralizing anti-apoptotic members of the Bcl-2 family [e.g. Bcl-2 and Bcl-x(L)] (reviewed in Strasser *et al.* 2000; Bouillet and Strasser 2002). For example, using techniques such as the yeast two-hybrid assay, Bim has been shown to interact directly with multiple anti-apoptotic Bcl-2 family members and inhibit their pro-survival functions in non-neuronal cells (Hsu *et al.* 1998; Wilson-Annan *et al.* 2003). Moreover, Bim gene deletion prevents a host of non-neuronal degenerative disorders, including fragility of the lymphoid system and polycystic kidney disease, observed in Bcl-2-deficient mice, suggesting that Bim acts as an endogenous antagonist of Bcl-2 in some tissues (Bouillet *et al.* 2001). Finally, anti-apoptotic Bcl-2 family proteins promote survival principally by sequestering and inhibiting the function of Bax and Bak, multidomain Bcl-2-like proteins that permeabilize the outer mitochondrial membrane to permit the release of cytochrome *c* (Wei *et al.* 2001; Degenhardt *et al.* 2002). Consistent with this, BH3-only proteins require the presence of Bax or Bak to trigger the mitochondrial apoptotic cascade (Zong *et al.* 2001). Despite the above findings, there is currently sparse evidence demonstrating that the major pro-apoptotic function of Bim in neurons is to directly antagonize Bcl-2/Bcl-x(L) function.

In order to study the principal role of Bim in neuronal apoptosis, we contrasted the mechanism of Bim-dependent CGN death to that induced by the Bcl-2/Bcl-x(L) antagonist, HA14-1. HA14-1 is a novel organic compound that was a product of a rational drug design effort to find small molecules that could compete with the Bak BH3-domain for binding to a hydrophobic surface pocket on Bcl-2 (Wang *et al.* 2000). HA14-1 has micromolar affinity for Bcl-2 and Bcl-x(L) and acts as a mimetic of BH3-only proteins by antagonizing the anti-apoptotic Bcl-2 proteins and triggering Bax-dependent apoptosis (Wang *et al.* 2000; Chen *et al.* 2002; An *et al.* 2004). In addition, we utilized another BH3 domain mimetic that is structurally distinct from HA14-1, compound 6

[2,9-dimethoxy-11,12-dihydrodibenzo-[c,g][1,2]-diazocine 5,6-dioxide (A) and 5'-dimethoxy-2,2'-dinitrosobenzyl (B)]. Compound 6, like HA14-1, interacts with the hydrophobic surface pocket of Bcl-2 and Bcl-x(L) proteins, preventing them from binding to pro-apoptotic family members (Enyedý *et al.* 2001). Finally, one other means of inhibiting Bcl-2 function is to interfere with its synthesis by using antisense oligonucleotides. These three tools complement one another and allow for a comparison of the apoptotic pathway induced by inhibition of Bcl-2 and/or Bcl-x(L) function versus the mechanism of Bim-dependent neuronal death.

Experimental procedures

Materials

HA14-1, compound 6, FITC-labeled phosphorothioate antisense oligonucleotides to Bcl-2, Bcl-2 antisense oligonucleotide negative control, SB203580, NAC, and GSH monoethyl ester were purchased from Calbiochem (San Diego, CA, USA). Bcl-2, Bcl-x(L), and Bcl-w (each C-terminal truncated, His-Tag, human recombinant proteins) were purchased from Oncogene Research Products (San Diego, CA, USA). BimEL-GST recombinant protein was purchased from Upstate Biotechnology (Lake Placid, NY, USA). Monoclonal antibody to β -tubulin, Hoechst dye number 33258, and 4,6-diamidino-2-phenylindole (DAPI) were from Sigma (St Louis, MO, USA). Glutathione-agarose beads and rabbit polyclonal antibodies to Bcl-2, Bcl-x(L), Bcl-w, cleaved caspase 9, cleaved caspase 3, cytochrome *c*, and Bim were obtained from Santa Cruz Biotechnology (Santa Cruz, CA, USA). Rabbit polyclonal antibody to active (cleaved) caspase 3 for immunocytochemistry was from Promega (Madison, WI, USA). Monoclonal antibody (clone 6A7) to the active conformation of Bax was purchased from Alexis Biochemicals (San Diego, CA, USA). FITC- and Cy3-conjugated secondary antibodies for immunocytochemistry were purchased from Jackson ImmunoResearch Laboratories (West Grove, PA, USA). Rabbit polyclonal antibody to 6X His-tag was purchased from Abcam (Cambridge, MA, USA). Horseradish peroxidase-linked secondary antibodies and reagents for enhanced chemiluminescence detection were obtained from Amersham Pharmacia Biotech (Piscataway, NJ, USA). Rhodamine-phalloidin and tetramethylrhodamine ethyl ester (TMRE) were from Molecular Probes (Eugene, OR, USA). Recombinant human IGF-I was provided by Margarita Quiroga (Chiron, Emeryville, CA, USA).

CGN culture

As previously described (Linseman *et al.* 2002), primary CGNs were isolated from 7-day-old Sprague-Dawley rat pups (15–19 g). Neurons were plated on 35-mm-diameter plastic dishes coated with poly-L-lysine at a density of 2.0×10^6 cells/mL in basal modified Eagles medium containing 10% fetal bovine serum, 25 mM KCl, 2 mM L-glutamine, and 100 U/mL penicillin/100 μ g/mL streptomycin (Invitrogen, Grand Island, NY, USA). At 24 h after plating, cytosine arabinoside (10 μ M) was added to the culture medium in order to limit the growth of non-neuronal cells. Cultures were almost entirely pure for granule neurons (~95–99%). All experiments were performed after 6–8 days in culture.

Quantitation of apoptosis

Apoptosis was induced by the addition of varying concentrations of either HA14-1, compound 6, or Bcl-2 antisense oligonucleotides to serum-free culture medium containing 25 mM KCl. In some experiments, cultures were switched from high potassium medium to that containing only 5 mM KCl. CGNs were incubated under the above conditions for 24 h and were subsequently fixed in 4% paraformaldehyde. Chromatin was stained with Hoechst dye to visualize nuclear morphology. Criteria for apoptosis included condensed or fragmented nuclei. In general, approximately 500 CGNs from at least two different fields of a 35-mm well were counted. Data are presented as the percentage of cells in a given treatment condition that were scored as apoptotic based on the aforementioned criteria. Experiments were performed in triplicate.

Preparation of CGN cell extracts

CGNs were incubated for the times specified and with the reagents described in Results. After the incubation period, the medium was aspirated and the cells were washed once with 2 mL of ice-cold phosphate-buffered saline (PBS), pH 7.4. Cells were then placed on ice and scraped into lysis buffer (200 μ L/35-mm well) containing (in mM): 20 HEPES, pH 7.4, 50 NaCl, 1 EGTA, 5 β -glycerophosphate, 30 sodium pyrophosphate, and 1 phenylmethylsulfonyl fluoride, plus 1% Triton X-100, 100 μ M sodium orthovanadate, 10 μ g/mL leupeptin, and 10 μ g/mL aprotinin. Cell debris was removed by centrifugation at 6000 *g* for 3 min, and a commercially available protein assay kit (Pierce, Rockford, IL, USA) was used to determine the protein concentration of the supernatants. Next, aliquots (~80 μ g) of supernatant protein were diluted to a final concentration of 1 \times sodium dodecyl sulfate – polyacrylamide gel electrophoresis (SDS–PAGE) sample buffer, boiled for 5 min, and electrophoresed through 15% polyacrylamide gels. Proteins were then transferred to polyvinylidene difluoride (PVDF) membranes (Amersham Pharmacia Biotech) and processed for western blot analysis.

Western blotting

Non-specific binding sites were blocked by the addition of PBS, pH 7.4, containing 0.1% Tween 20 (PBS-T) and 1% bovine serum albumin (BSA) for 1 h at room temperature (22°C). Blocking solution was used to dilute primary antibodies and this solution was then incubated with the membranes for 1 h. Next, the membranes were washed three times (15 min intervals) with PBS-T in order to remove excess primary antibody. Horseradish peroxidase-conjugated secondary antibodies were diluted in PBS-T and membranes were incubated in this solution for 1 h. Again, membranes were washed three times with PBS-T to remove excess secondary antibody. Immunoreactive proteins were detected by enhanced chemiluminescence. Autoluminograms shown are representative of at least three independent experiments.

HA14-1 competition binding assay

His-tagged recombinant Bcl-2 family proteins (either Bcl-2, Bcl-x(L), or Bcl-w; 50 ng), Bim-GST (10 ng), and HA14-1 (when indicated; 500 μ M), were mixed in a microfuge tube in a total volume of 100 μ L cell lysis buffer (see above) containing 0.1% Triton X-100 for 30 min at 4°C. Next, 30 μ L of GSH-agarose beads were added to the samples to bind the Bim-GST fusion protein and tubes were rotated for an additional 20 min at 4°C. Each sample was

centrifuged for 90 s at 12 000 *g* and supernatants were removed. The GSH-beads were then washed twice with ice-cold 0.1% Triton X-100 lysis buffer. The supernatants and beads were then resolved on 12.5% polyacrylamide gels and proteins were transferred to PVDF membranes for western blotting. A polyclonal antibody to Bcl-2 was used to detect the Bcl-2 protein and a polyclonal antibody that recognizes a 6X His-tag was employed to detect Bcl-x(L) and Bcl-w.

Immunofluorescence microscopy

CGNs were cultured on polyethyleneimine-coated glass coverslips at a density of approximately 2.5×10^5 cells per coverslip. After appropriate incubation as described in Results, CGNs were fixed in 4% paraformaldehyde and were subsequently permeabilized and blocked in PBS, pH 7.4, containing 0.2% Triton X-100 and 5% BSA. Coverslips were then incubated for 16 h at 4°C with primary antibody diluted in PBS containing 0.2% Triton X-100 and 2% BSA. The primary antibody solution was aspirated and cells were washed five times with PBS. Then, CGNs were incubated with FITC- or Cy3-conjugated secondary antibodies and DAPI for 1 h at room temperature. Again, cells were washed five times with PBS and coverslips were then adhered to glass slides in mounting medium (0.1% *p*-phenylenediamine in 75% glycerol in PBS). Fluorescent images were captured using either a 63 \times or 100 \times oil immersion objective on a Zeiss Axioplan 2 microscope equipped with a Cooke Sencicam deep-cooled CCD camera and a Slidebook software analysis program for digital deconvolution (Intelligent Imaging Innovations, Denver, CO, USA).

Measurement of mitochondrial membrane potential

CGNs were grown on glass coverslips and incubated in the absence or presence of HA14-1, as described in Results. TMRE (500 nm) and Hoechst dye were added directly to the cells 30 min prior to the end of the incubation period. Afterwards, the coverslips were inverted onto slides into a small volume of phenol red-free medium containing TMRE (500 nm). Cells were imaged live under a Cy3 filter to detect TMRE fluorescence using a 100 \times oil objective. All images were acquired at equal exposure times for TMRE fluorescence to determine relative mitochondrial membrane potentials.

Preparation of GFP-Bim cDNA

BimEL cDNA was excised from a pCMS-EGFP/Bim bicistronic plasmid (kindly provided by Dr Lloyd Greene and Dr Subhas Biswas, Columbia University, NY) with *Xho*I and *Kpn*I restriction enzymes. The excised cDNA was ligated into *Xho*I/*Kpn*I-cleaved pEGFP-C3 (Promega). The ligation reaction resulted in an N-terminal fusion of GFP onto the BimEL protein. Successful construction of the pEGFP-Bim was verified by DNA sequencing.

Gene gun transfection of primary CGNs

CGNs were transiently transfected using the Helios Gene-Gun system (Bio-Rad, Hercules, CA, USA). Briefly, 60 μ g of either pEGFP or pEGFP-Bim plasmid DNA was precipitated onto 30 mg of 0.6 μ m-diameter gold beads in a CaCl₂/spermidine mixture. The gold/DNA precipitates were washed three times in 100% ethanol, and re-suspended in 3 mL of ethanol containing 0.05 mg/mL polyvinylpyrrolidone. After thoroughly re-suspending the gold/DNA precipitate, it was drawn into approximately 74 cm of Tefzel

tubing and the beads were allowed to settle to the bottom of the tubing. After 5 min, the ethanol was slowly drawn off while the beads adhered to the tubing. The tubing was dried under nitrogen for an additional 5 min and was then cut into approximately 1.3-cm pieces. CGNs to be transfected were seeded at a density of 8×10^5 cells/well on polyethyleneimine-coated glass coverslips in 24-well plates. After 5 days in culture, the medium was removed from the wells and the 1.3-cm lengths of tubing containing the DNA-bound beads were loaded into the Gene Gun and shot with a burst of 100 p.s.i. helium through a 40 μ m nylon cell strainer placed over the well. The medium was immediately replaced and cells were incubated for an additional 24 h before image analysis.

Data analysis

The results that are shown represent the means \pm SEM for the number (n) of independent experiments that were performed. Statistical differences between the means of unpaired sets of data were evaluated by one-way ANOVA, followed by a post-hoc Dunnett's or Tukey's test. A p -value of <0.05 was considered statistically significant.

Results

HA14-1 specifically antagonizes Bcl-2 and Bcl-x(L) and induces apoptosis of CGNs

To assess the specificity of the BH3 domain mimetic, HA14-1, for binding to various pro-survival Bcl-2 family members, we examined its ability to interfere with the interaction between recombinant His-tagged Bcl-2, Bcl-x(L), or Bcl-w and a Bim-GST fusion protein in an *in vitro* binding assay. When GSH-agarose beads were added to a solution containing recombinant His-Bcl-2 alone, a small amount of non-specific binding of Bcl-2 was observed in the pellet while most remained in the supernatant (Fig. 1a, left blot, first lane). Inclusion of Bim-GST with Bcl-2 resulted in significant pull-down of the Bcl-2 protein, presumably bound to Bim, in the pelleted GSH-agarose beads (Fig. 1a, left blot, second lane). The ability of Bim-GST to bind to recombinant Bcl-2 was significantly antagonized by addition of HA14-1, resulting in a loss of Bcl-2 in the GSH-agarose pellet and a corresponding increase of Bcl-2 in the supernatant (Fig. 1a, middle blot, compare second lane to first lane). In agreement with the data obtained for Bcl-2, addition of HA14-1 similarly resulted in an increase in Bcl-x(L) detected in the supernatant fraction (i.e. less binding to Bim-GST) (Fig. 1a, right blot, upper panel). However, HA14-1 did not compete with Bim-GST for binding to Bcl-w as evidenced by no change in the amount of Bcl-w detected in the supernatant fraction (i.e. no change in binding to Bim-GST) (Fig. 1a, right blot, lower panel). These data indicate that HA14-1 competes with Bim for binding to the hydrophobic surface of both Bcl-2 and Bcl-x(L), elucidating its specificity for these proteins. HA14-1 did not, however, affect the binding of Bcl-w to Bim.

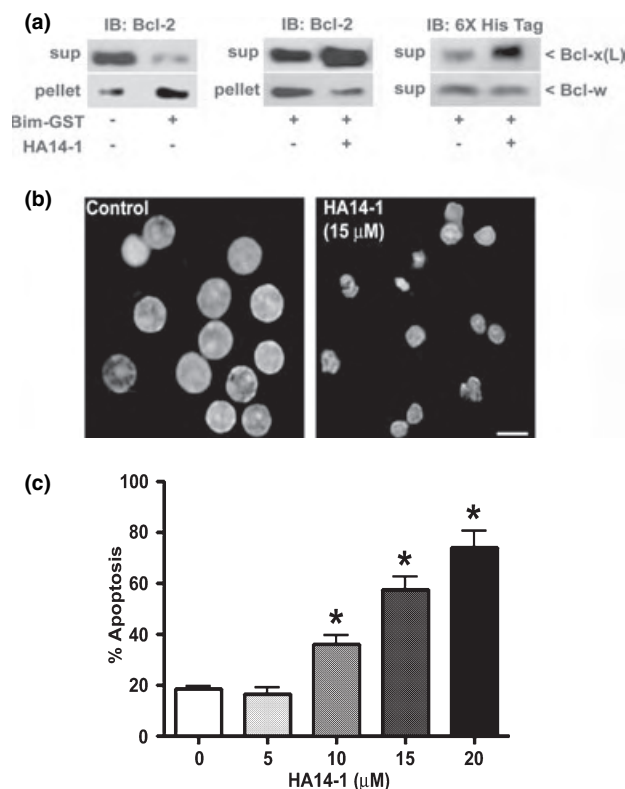


Fig. 1 The BH3-domain mimetic, HA14-1, antagonizes Bcl-2 and Bcl-x(L) and induces apoptosis of CGNs in a dose-dependent manner. (a) 50 ng His-tagged recombinant Bcl-2 protein was incubated in the presence or absence of 10 ng recombinant Bim-GST. Glutathione-agarose beads were used to pull down the Bim-GST (along with any protein bound to it) and then the supernatant was removed. Both supernatant and pellet were loaded onto a 12.5% polyacrylamide gel, transferred to a PVDF membrane, and blotted for Bcl-2 with a polyclonal antibody (left panel). The addition of 500 μ M HA14-1 was able to compete the Bcl-2 off of the Bim-GST and therefore less Bcl-2 was detected in the pellet and more in the supernatant (middle panel). His-tagged recombinant Bcl-x(L) or Bcl-w (50 ng) were substituted for Bcl-2 in separate experiments to determine whether HA14-1 could specifically bind either of these other pro-survival Bcl-2 family members. HA14-1 did compete Bcl-x(L) off of the Bim-GST but had no effect on the binding of Bcl-w to Bim (right panel). The data shown for each pro-survival protein are representative of at least two independent experiments that yielded similar results. (b) CGNs were incubated for 24 h in serum-free culture medium containing 25 mM KCl (25K) either in the absence (control condition) or presence of HA14-1 (15 μ M). After incubation, CGNs were fixed in 4% paraformaldehyde and nuclei were stained with Hoechst dye. Scale bar, 10 μ m. A large proportion of the CGNs exposed to HA14-1 were apoptotic as indicated by their condensed nuclei. (c) The fraction of CGNs scored as apoptotic following a 24 h incubation with varying concentrations of HA14-1 was quantified by counting \sim 250 CGNs per field in two 40 \times fields per condition. Values represent the means \pm SEM for three independent experiments, each performed in triplicate. *Significantly different from the control (25K) condition ($p < 0.01$).

We next evaluated the effects of the Bcl-2/Bcl-x(L) antagonist, HA14-1, on CGN survival. CGNs cultured in the presence of a depolarizing concentration (25 mM) of extracellular potassium (25K or control conditions) demonstrated large intact nuclei, as detected by staining with Hoechst dye (Fig. 1b, left panel). Addition of the Bcl-2/Bcl-x(L) antagonist, HA14-1 (15 μ M), to 25K medium for 24 h induced striking nuclear condensation, consistent with an apoptotic mechanism of cell death (Fig. 1b, right panel). Quantitation of the amount of apoptosis observed in CGNs incubated with increasing concentrations of HA14-1 for 24 h revealed a dose–response curve with no significant effect at 5 μ M and approximately 75% apoptosis at 20 μ M of the drug (Fig. 1c). The extent of CGN apoptosis observed with 20 μ M HA14-1 was comparable with that induced by the removal of depolarizing potassium (5K condition) for 24 h (Linseman *et al.* 2003).

Sensitivity to HA14-1 toxicity inversely correlates with cell density-dependent changes in pro-survival Bcl-2 family member expression

To verify that HA14-1-induced CGN death was dependent on antagonism of Bcl-2/Bcl-x(L), we analyzed the drug sensitivity of CGNs cultured at different cell densities. Increasing cell density has previously been shown to enhance the expression of Bcl-2 mRNA and protein in CGNs (Ohga *et al.* 1996). Consistent with this, increasing the plating density of CGNs in our cultures by fourfold produced substantial increases in the amounts of three pro-survival Bcl-2 proteins (Bcl-2, Bcl-x(L), and Bcl-w), detected by immunoblotting (Fig. 2a). Moreover, sensitivity of CGNs to HA14-1-induced apoptosis was inversely correlated with cell density and pro-survival Bcl-2 family member expression (i.e. increasing density of the cell culture led to an enhanced amount of the pro-survival Bcl-2 proteins, and consequently, decreased sensitivity to HA14-1) (Fig. 2b). This latter result is consistent with HA14-1-mediated neuronal death being dependent on antagonism of endogenous Bcl-2/Bcl-x(L) proteins.

HA14-1 stimulates activation of caspase 9 and caspase 3

Death induced by a Bcl-2/Bcl-x(L) antagonist can occur via activation of a mitochondrial apoptotic pathway (Wang *et al.* 2000; An *et al.* 2004). Although HA14-1 has been shown to be capable of inducing death in a caspase-independent manner (Chen *et al.* 2002), we observed a caspase-dependent mechanism of cell death in CGNs treated with this Bcl-2/Bcl-x(L) inhibitor. The principal downstream effectors of mitochondrial apoptosis are the intrinsic initiator, caspase 9, and the executioner, caspase 3. The zymogen, pro-caspase 9, is activated by a dATP-driven association with apoptosis-activating factor-1 (Apaf-1) and cytochrome *c* released from mitochondria. These molecules combine to form an oligomeric apoptosome structure containing the active protease

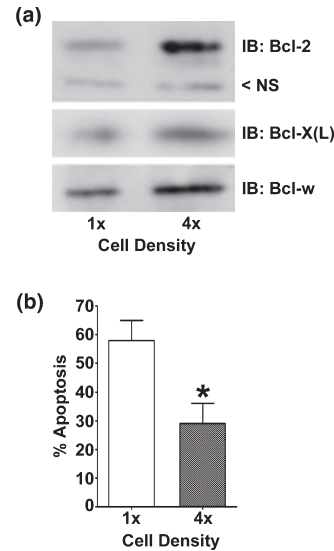


Fig. 2 The apoptosis-inducing effects of HA14-1 and the expression of the pro-survival Bcl-2 family members are cell density-dependent. (a) CGNs were plated into 12-well cluster plates at the following cell densities (cells/well): 1 x, 7.5×10^5 or 4 x, 3.0×10^6 . On day 7 *in vitro*, CGN lysates were prepared, equal amounts of cell protein (80 μ g) were electrophoresed through 12.5% polyacrylamide gels, and membranes were immunoblotted (IB) with specific antibodies to Bcl-2, Bcl-x(L) or Bcl-w. A non-specific (NS) protein band that was detected by the Bcl-2 antibody is shown as a loading control. (b) CGN cultures plated as described in (a) were incubated for 24 h with 15 μ M HA14-1 and apoptosis was quantitated by Hoechst staining. *Significantly different from the 1 x plating condition ($p < 0.05$, unpaired *t*-test). Note that CGNs plated at the higher density showed greater Bcl-2, Bcl-x(L) and Bcl-w content (a) and a corresponding lower sensitivity to the Bcl-2/Bcl-x(L) antagonist compound (b).

caspase 9 (Zou *et al.* 1999). Active caspase 9 subsequently cleaves and activates the executioner, caspase 3, leading to the proteolysis of critical cell proteins and ultimately death (Kuida *et al.* 1998; Slee *et al.* 1999). Incubation of CGNs for 6 h with at least 10 μ M HA14-1 induced a marked increase in the amounts of active (cleaved) caspase 9 detected by immunoblotting (Fig. 3a) and active (cleaved) caspase 3 visualized immunocytochemically (Fig. 3b). In addition to caspase activation and chromatin condensation, CGNs exposed to HA14-1 also showed significant disruption of the microtubule cytoskeletal network (Fig. 3b). Thus, antagonism of Bcl-2/Bcl-x(L) function is sufficient to trigger apoptosis of CGNs maintained in depolarizing medium via the activation of caspases 9 and 3.

HA14-1 elicits mitochondrial membrane depolarization, conformational activation of Bax, and cytochrome *c* release

During mitochondrial apoptosis, the activation of caspase 9 is typically preceded by several Bcl-2-inhibited mitochondrial events, including membrane depolarization (loss of $\Delta\psi_m$)

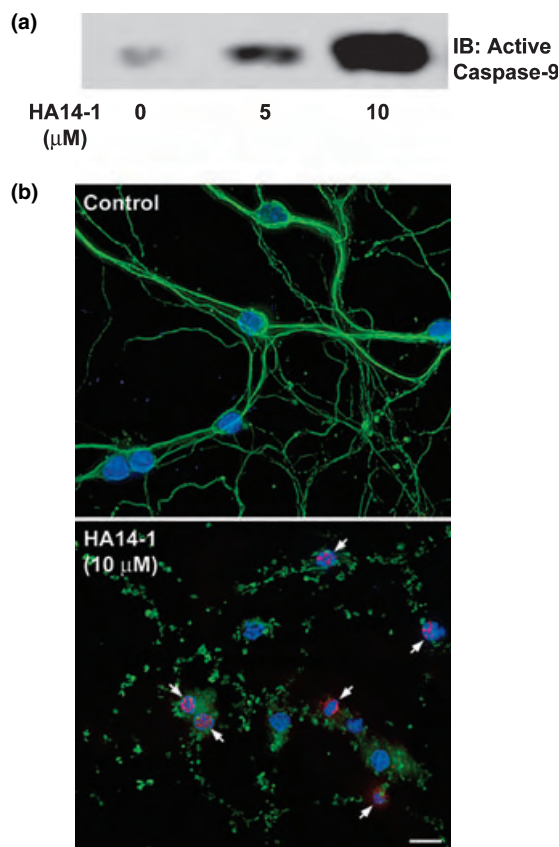


Fig. 3 HA14-1 elicits activation of the intrinsic initiator, caspase 9, as well as the executioner, caspase 3. (a) CGNs were incubated in control depolarizing (25K) medium containing 0, 5 or 10 μM HA14-1 for 6 h. Detergent-soluble CGN lysates were harvested and equivalent amounts of cell protein were subjected to SDS-PAGE on 15% polyacrylamide gels. The proteins were transferred to PVDF membranes and activation of caspase 9 was assessed by immunoblotting (IB) with a polyclonal antibody that recognizes only the active or cleaved form of caspase 9. The blot shown is representative of results obtained from three independent experiments. (b) CGNs were incubated for 6 h in 25K medium in either the absence (control) or presence of 10 μM HA14-1. Following incubation, cells were fixed in 4% paraformaldehyde, permeabilized with 0.2% Triton X-100, and blocked in 5% BSA. β -tubulin and active (cleaved) caspase 3 were immunostained by incubating the cells with a monoclonal antibody to tubulin and a polyclonal antibody that specifically recognizes the active fragment of caspase 3, followed by FITC-conjugated (green) and Cy3-conjugated (red) secondary antibodies, respectively. Nuclei were stained with DAPI (blue). Fluorescent images were captured using a $63\times$ oil objective. The images shown are representative of results obtained from three separate experiments. Scale bar, 10 μm . Arrows point to neurons that were immunoreactive for active caspase 3. Note the fragmented microtubule processes and the condensed nuclei in the HA14-1 condition, characteristic of apoptotic cell death.

(Dispersyn *et al.* 1999), conformational activation and translocation of Bax (Murphy *et al.* 2000), and cytochrome *c* release (Yang *et al.* 1997). Therefore, we next examined the

effects of HA14-1 on each of these mitochondrial events in CGNs. Live CGNs maintained in 25K control conditions showed healthy large nuclei and extensive mitochondrial labeling with the cationic dye, tetramethylrhodamine ethyl ester (TMRE), consistent with an intact mitochondrial membrane potential (Fig. 4a, left panel). After 6 h of incubation with HA14-1, CGNs displayed condensed nuclei and a nearly complete loss of TMRE, indicative of mitochondrial membrane depolarization (Fig. 4a, right panel). Moreover, CGNs incubated in control medium showed no detectable active Bax after staining with an antibody that specifically recognizes the active conformation of the protein (Fig. 4b, left panel). However, cells incubated with HA14-1 demonstrated substantial active Bax immunoreactivity that was localized predominantly in a perinuclear distribution consistent with mitochondria (Fig. 4b, right panel, see arrows). Finally, control CGNs stained for cytochrome *c* displayed a punctate mitochondrial distribution of the protein (Fig. 4c, left panel). In contrast, CGNs exposed to HA14-1 showed a marked re-localization of cytochrome *c* to a diffuse distribution over the majority of the cell body, indicative of release from mitochondria (Fig. 4c, right panel). Collectively, these data show that antagonism of Bcl-2/Bcl-x(L) function in CGNs promotes a rapid loss of $\Delta\psi_m$, Bax activation, and cytochrome *c* release, ultimately leading to caspases 9 and 3 activation and apoptotic cell death.

CGN apoptosis induced by HA14-1 is Bim independent

To clearly dissociate CGN apoptosis induced by the Bcl-2/Bcl-x(L) antagonist, HA14-1, from Bim-dependent death, we measured expression of the Bim protein by western blotting (Linseman *et al.* 2002). CGNs incubated for 6 h in depolarizing medium containing up to 15 μM HA14-1 showed no significant increase in the level of Bim protein, whereas cells deprived of depolarizing potassium (5K condition) for 6 h displayed a striking increase in Bim expression (Fig. 5a). To further exclude any role for Bim in CGN apoptosis induced by the small molecule Bcl-2/Bcl-x(L) antagonist, next we evaluated the effects of two distinct negative regulators of Bim transcription on HA14-1-stimulated cell death. First, the forkhead family transcription factor, FKHRL1 or FOXO3a, directly stimulates the Bim promoter in both hematopoietic cells and neurons (Dijkers *et al.* 2000; Gilley *et al.* 2003). We have recently shown that insulin-like growth factor-I (IGF-I) protects CGNs from 5K-induced apoptosis by stimulating an AKT-mediated phosphorylation of FKHRL1, resulting in its exclusion from the nucleus and suppression of Bim transcription (Linseman *et al.* 2002). In agreement with the Bcl-2/Bcl-x(L) antagonist compound triggering Bim-independent cell death, inclusion of IGF-I had no effect on HA14-1-induced death, whereas it significantly inhibited CGN apoptosis in non-depolarizing medium (Fig. 5b). In addition to FKHRL1, the *c-jun* transcription factor is also a potent activator of the Bim promoter in neurons and this

effect is blunted by both dominant-negative mutants of *c-jun* and inhibitors of the upstream kinase JNK (Harris and Johnson 2001; Whitfield *et al.* 2001). The pyridinyl imidazole compound, SB203580, was originally described as a selective inhibitor of p38 MAP kinase but has recently been shown to also block the activities of some neuronal isoforms of JNK (Coffey *et al.* 2002). Consequently, SB203580 suppresses Bim induction in CGNs undergoing 5K-induced apoptosis (Linseman *et al.* 2002). Like IGF-I, inclusion of SB203580 had no effect on CGN apoptosis induced by HA14-1 while it significantly protected cells from death in 5K medium (Fig. 5c). These results demonstrate that Bim is not involved in CGN apoptosis induced by the Bcl-2/Bcl-x(L) antagonist, HA14-1.

The GSH precursor, NAC, attenuates each step of the mitochondrial apoptotic cascade triggered by HA14-1

To further examine the mechanism of neuronal death induced by HA14-1, we focused on one of the initial mitochondrial events stimulated by antagonism of Bcl-2/Bcl-x(L),

mitochondrial membrane depolarization (see Fig. 4a). Previously, we showed that mitochondrial membrane depolarization elicited by withdrawal of extracellular depolarizing potassium from CGNs occurs in conjunction with significant mitochondrial swelling (Linseman *et al.* 2002). Moreover, both the mitochondrial depolarization and swelling induced in 5K medium are prevented by cyclosporin A (Precht *et al.* 2005), an inhibitor of the mitochondrial permeability transition pore (mPTP) (Waldmeier *et al.* 2003). In contrast, swollen mitochondria were not observed in CGNs exposed to HA14-1 and mitochondrial depolarization induced by the Bcl-2/Bcl-x(L) antagonist was not prevented by cyclosporin A (data not shown). Thus, as opposed to opening of the cyclosporin A-sensitive mPTP under non-depolarizing

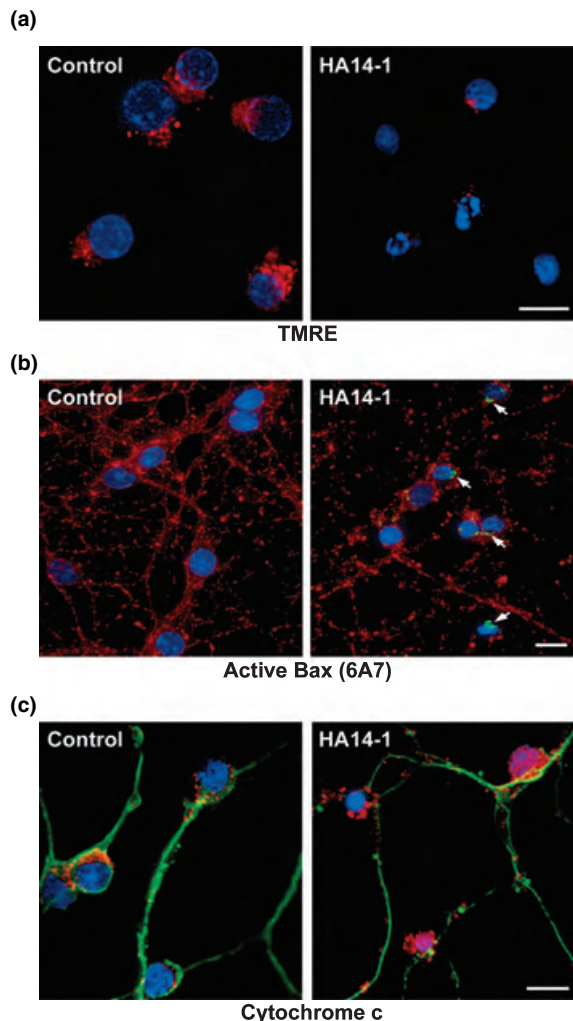


Fig. 4 HA14-1 triggers mitochondrial membrane depolarization, conformational activation of Bax, and release of cytochrome *c*. (a) CGNs were grown on glass coverslips and incubated for 6 h in depolarizing (25K) medium either in the absence (control) or in the presence of 10 μ M HA14-1. At 30 min prior to the end of the incubation period, TMRE (500 nm) and Hoechst were added directly to the cells. After incubation, the coverslips were inverted onto slides into a small volume of phenol red-free medium containing depolarizing potassium and TMRE (500 nm). Live cells were then imaged under a 100 \times oil objective. Nuclear staining with Hoechst is shown in blue; TMRE is shown in red. Scale bar, 10 μ m. In the control condition, CGNs exhibited many mitochondria stained intensely with TMRE, indicative of an intact mitochondrial membrane potential. In contrast, CGNs incubated in the presence of 10 μ M HA14-1 showed very little detectable mitochondrial TMRE staining, corresponding to a loss of mitochondrial membrane potential or depolarization. The images shown were acquired at equal exposure times for TMRE fluorescence and are representative of results obtained from three independent experiments, each performed in triplicate. (b) CGNs were incubated for 6 h exactly as described in (a). Following incubation, cells were fixed in 4% paraformaldehyde, permeabilized with 0.2% Triton X-100, and blocked in 5% BSA. Active Bax was detected immunocytochemically by incubating the cells with a monoclonal antibody that specifically recognizes the conformationally active form of Bax (clone 6A7), followed by a FITC-conjugated secondary antibody (green). Nuclei were stained with DAPI (blue). The actin cytoskeleton was stained with rhodamine-phalloidin (red). Fluorescent images were captured using a 63 \times oil objective. The images shown are representative of results obtained in three independent experiments. Arrows identify cells that were immunoreactive for active Bax. Scale bar, 10 μ m. (c) CGNs were incubated as described in (a). Cytochrome *c* was localized by incubating cells with a polyclonal antibody to cytochrome *c* and a Cy3-conjugated secondary antibody (red). Microtubule processes were stained with a monoclonal antibody to tubulin and a FITC-conjugated secondary antibody (green). Nuclei were stained with DAPI (blue). Images were captured using a 63 \times oil objective. The images shown are representative of results obtained in three separate experiments. Scale bar, 10 μ m. CGNs in the control condition exhibited intense cytochrome *c* staining in the perinuclear region consistent with localization to mitochondria. Whereas, CGNs incubated with HA14-1 showed a substantial redistribution of cytochrome *c* to a diffuse localization over the entire cell body.

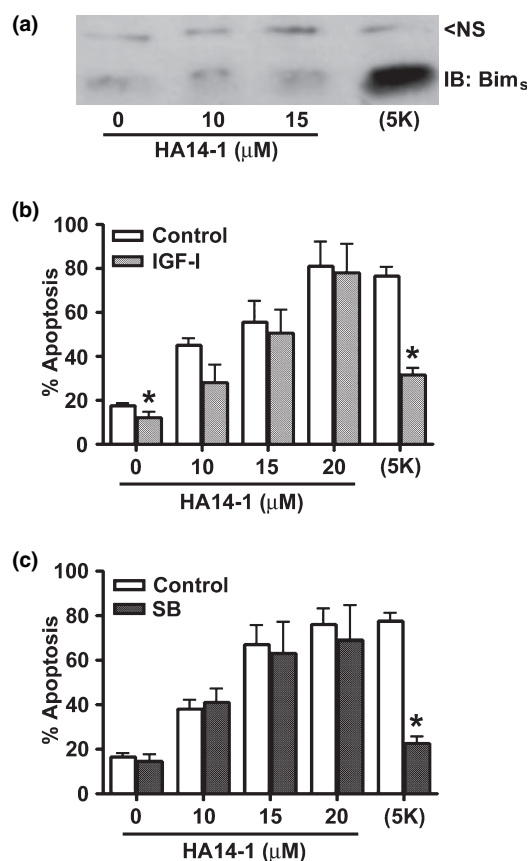


Fig. 5 CGN apoptosis induced by HA14-1 is Bim-independent. (a) CGNs were incubated for 6 h in either depolarizing (25K) medium containing 0, 10 or 15 μM HA14-1 or in medium lacking depolarizing potassium (5K). Detergent-soluble cell lysates were subjected to SDS-PAGE on 15% polyacrylamide gels, and the proteins were transferred to PVDF membranes. Induction of Bim was assessed by immunoblotting (IB) with a polyclonal antibody that recognizes the short isoform of Bim (Bim_s). The blot shown is indicative of results from three independent experiments. Bim expression was markedly induced in the 5K condition, but not in the presence of HA14-1. A non-specific (NS) protein band that was detected by the antibody is shown as a loading control. (b) The percentage of CGNs that were scored as apoptotic following incubation for 24 h in either 25K medium containing 0, 10, 15 or 20 μM HA14-1 or in 5K medium, with each treatment ± IGF-I (200 ng/mL), was quantified by counting ~250 CGNs per field in two fields per condition. Values represent the means ± SEM for three independent experiments, each performed in triplicate. *Significantly different from the same condition in the absence of IGF-I ($p < 0.01$). (c) The percentage of CGNs that were identified as apoptotic under the conditions described in (b) above, but with each treatment ± SB203580 (SB; 20 μM), was quantified as described in (b). *Significantly different from the same condition in the absence of SB ($p < 0.01$).

conditions, mitochondrial depolarization induced by HA14-1 occurs via a distinct mechanism.

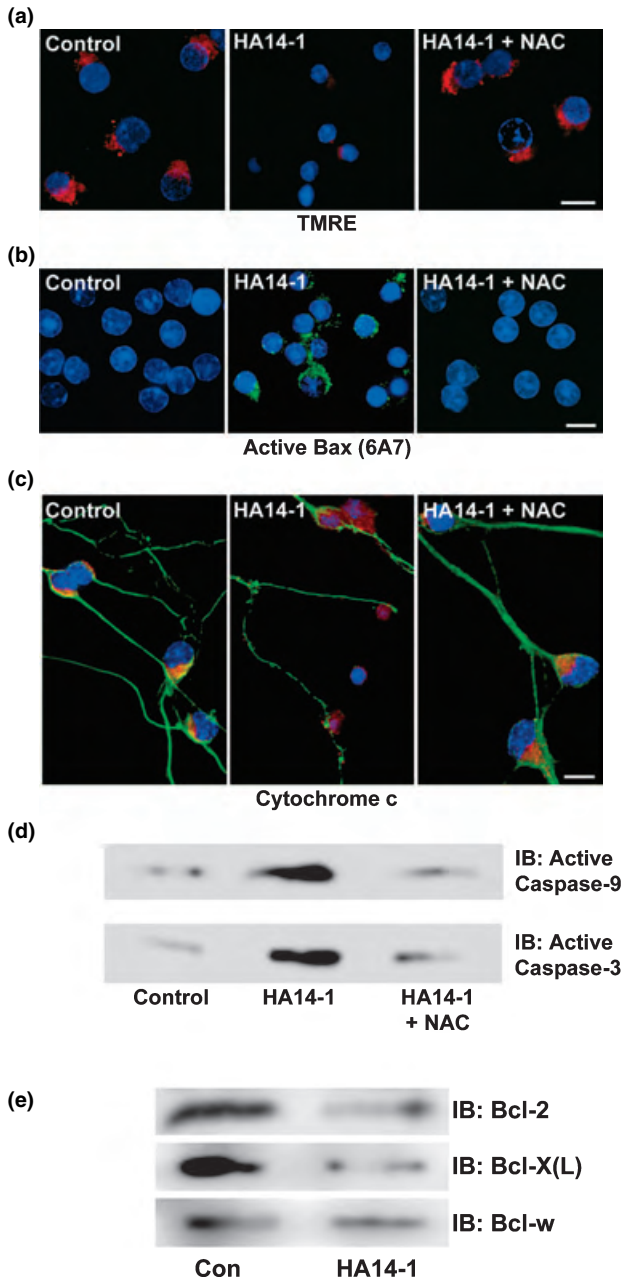
In addition to the mPTP, there exists a low-conductance mitochondrial membrane channel that, when opened,

similarly leads to mitochondrial depolarization. However, unlike the mPTP, mitochondrial depolarization activated by this channel is insensitive to cyclosporin A and occurs in the absence of significant mitochondrial swelling (Scanlon and Reynolds 1998; Kushnareva and Sokolove 2000). Moreover, the low conductance channel is robustly activated by oxidative stress and is potently inhibited by antioxidants including NAC (Scanlon and Reynolds 1998; Mukherjee *et al.* 2002). Bcl-2 is known to regulate the redox status of cells (reviewed in Voehringer and Meyn 2000). The best evidence for this comes from the observation of enhanced susceptibility to oxidative stress in the brains of Bcl-2 knockout mice (Hochman *et al.* 1998). These mice demonstrate substantial alterations in their antioxidant enzyme profiles and, in particular, show significant changes in the expression of enzymes that regulate the GSH content of the cell (Hochman *et al.* 1998). Given this apparent connection between Bcl-2 function and cellular GSH content, we hypothesized that the mitochondrial depolarization observed with HA14-1 was triggered by oxidative stress-dependent opening of a low conductance mitochondrial membrane channel. In support of this, co-incubation of CGNs with HA14-1 and NAC (an antioxidant and GSH precursor) largely prevented the mitochondrial depolarization induced by the Bcl-2/Bcl-x(L) antagonist alone (Fig. 6a). In agreement with mitochondrial depolarization being an initiating signal for cell death, inclusion of NAC also significantly attenuated HA14-1-stimulated Bax activation, cytochrome *c* release, and caspase activation (Figs 6b–d). These data suggest that antagonism of Bcl-2/Bcl-x(L) with HA14-1 compromises the GSH status of CGNs, leading to oxidative stress-dependent opening of a low-conductance channel in the mitochondrial membrane. Opening of this channel subsequently leads to loss of the mitochondrial membrane potential, resulting in Bax activation and initiation of a mitochondrial apoptotic cascade.

To further establish that HA14-1 induces apoptosis in an oxidative stress-dependent manner, we examined levels of Bcl-2, Bcl-x(L), and Bcl-w proteins in neurons treated with HA14-1 versus control conditions because reactive oxygen species have been shown to decrease the expression of pro-survival Bcl-2 family members (Hildeman *et al.* 2003; Li *et al.* 2004). Bcl-2 and Bcl-x(L), but not Bcl-w, were substantially down-regulated as a result of incubating the cells with HA14-1 (Fig. 6e). These results add further support that addition of the Bcl-2/Bcl-x(L) inhibitor induces CGN apoptosis via an oxidative stress-dependent mechanism.

Differential effects of antioxidants on CGN apoptosis induced by HA14-1 or removal of depolarizing potassium

Consistent with the oxidative stress-dependent pathway described above, co-incubation of CGNs with HA14-1 and either NAC or a cell-permeable monoethyl ester of GSH



significantly inhibited apoptosis induced by the Bcl-2/Bcl-x(L) antagonist (Figs 7a and b). In accord with NAC acting primarily as a GSH precursor, NAC (10 mM) had only a partial protective effect at all concentrations of HA14-1 tested (Fig. 7a). In comparison, GSH (2 mM) was much more potent than NAC and gave complete protection from 10 or 15 μM HA14-1 and nearly full protection from 20 μM HA14-1 (Fig. 7b). When the effects of these antioxidants were assessed on CGN apoptosis induced by removal of the depolarization stimulus (Bim-dependent death), neither NAC nor GSH offered any significant protection in non-depolarizing (5K) medium (Figs 7a and b). Bright-field (DIC)

Fig. 6 The glutathione precursor, *N*-acetyl-L-cysteine (NAC), protects CGNs from HA14-1-induced, oxidative stress-dependent apoptosis by inhibiting each step in the intrinsic death pathway. (a) CGNs were grown on glass coverslips and incubated for 6 h in depolarizing (25K) medium either alone (control condition) or in the presence of HA14-1 (10 μM) \pm NAC (10 mM). At 30 min before the end of the incubation period, TMRE (500 nm) and Hoechst were added directly to the cells. After incubation, the coverslips were inverted onto slides into a small volume of phenol red-free medium containing depolarizing potassium and TMRE (500 nm). Living cells were then imaged under a 100 \times oil objective. Nuclear staining with Hoechst is shown in blue; TMRE is shown in red. Scale bar, 10 μm . The mitochondrial depolarization induced by HA14-1, indicated by a loss of TMRE fluorescence, was prevented by inclusion of NAC. (b) CGNs were incubated as described in (a). Following incubation, cells were fixed in 4% paraformaldehyde, permeabilized with 0.2% Triton X-100, and blocked in 5% BSA. Active Bax was immunocytochemically identified by incubating the cells with a monoclonal antibody to the conformationally active form of Bax (6A7), followed by a FITC-conjugated secondary antibody (green). Nuclei were stained with DAPI (blue). Fluorescent images were captured using a 63 \times oil objective. The images shown are representative of results obtained in three independent experiments. Scale bar, 10 μm . The increase in conformationally active Bax induced by HA14-1 was blocked by NAC. (c) CGNs were incubated as described in (a). Cytochrome *c* was localized by incubating cells with a polyclonal antibody to cytochrome *c* and a Cy3-conjugated secondary antibody (red), while microtubules were stained with a monoclonal antibody to tubulin and a FITC-conjugated secondary antibody (green). Nuclei were stained with DAPI (blue). Fluorescent images were captured using a 63 \times oil objective. The images shown are representative of results obtained in three independent experiments. Scale bar, 10 μm . Cytochrome *c* release and microtubule disruption induced by HA14-1 were significantly inhibited by the addition of NAC. (d) CGNs were incubated as described in (a). Detergent-soluble cell lysates were harvested and subjected to SDS-PAGE on 15% polyacrylamide gels, and the proteins were transferred to PVDF membranes. Activation of caspase 9 and caspase 3 was assessed by immunoblotting (IB) with specific polyclonal antibodies that recognize only the active (cleaved) forms of the enzymes. The blots shown are representative of results from three independent experiments. The activation of both caspase 9 and caspase 3 induced by HA14-1 was attenuated by inclusion of NAC. (e) CGNs were treated with either 0 or 15 μM HA14-1 for 24 h and cell lysates were resolved on a 12.5% polyacrylamide gel, transferred to a PVDF membrane and blotted with polyclonal antibodies to Bcl-2, Bcl-x(L) or Bcl-w. Expression of Bcl-2 and Bcl-x(L) was down-regulated as a result of treatment with HA14-1.

images of CGNs incubated for 24 h with either HA14-1 (20 μM) or 5K medium in the absence or presence of GSH are shown in Fig. 7(c). In the absence of GSH, both HA14-1 and 5K conditions induced massive CGN death compared with the 25K control (upper panels). However, in the presence of GSH, CGNs exposed to HA14-1 looked remarkably like control cells, whereas those incubated in 5K medium still underwent severe apoptosis (lower panels). These findings illustrate a marked difference in the mechanism of CGN death induced by Bcl-2/Bcl-x(L) antagonism (oxidative stress-dependent apoptosis) as compared with the

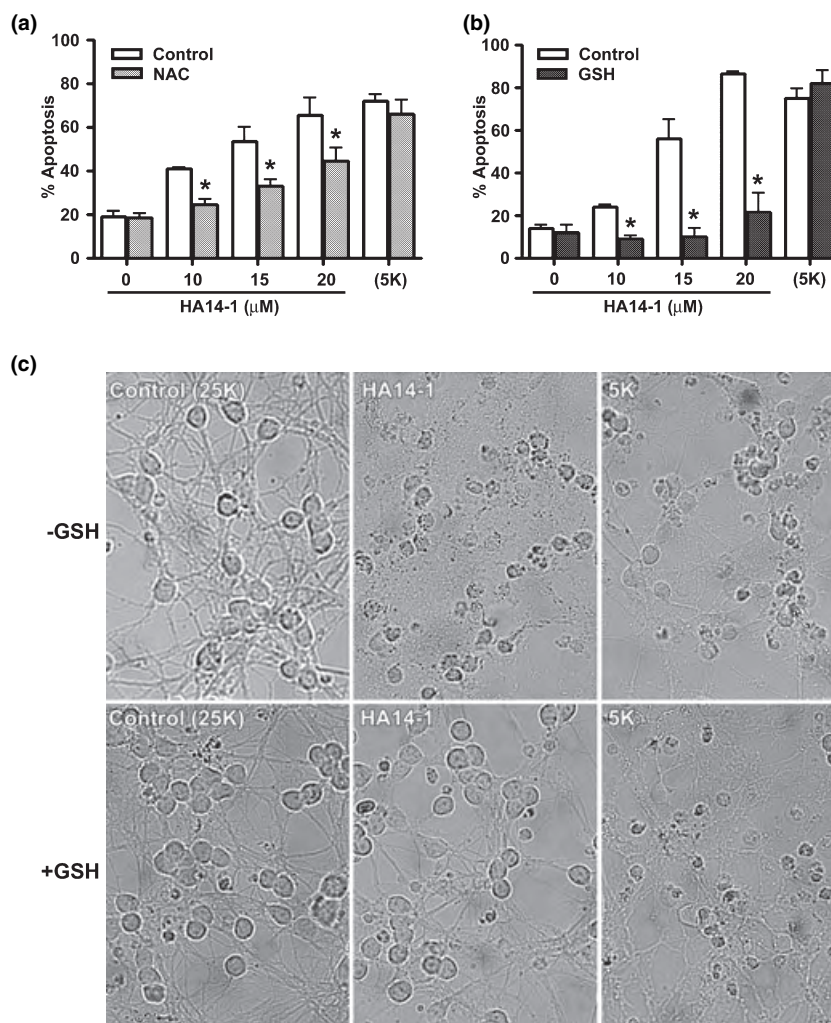


Fig. 7 The Bim-dependent apoptosis of CGNs induced by removal of depolarizing potassium is insensitive to antioxidants. (a) The fraction of CGNs that underwent apoptosis following incubation for 24 h in either depolarizing (25K) medium containing 0, 10, 15 or 20 μM HA14-1 or non-depolarizing (5K) medium, ±NAC (10 mM), is shown. CGN apoptosis in each condition was quantified by counting ~250 cells per field in two 40 × fields per condition. Values represent the means ± SEM for three independent experiments, each performed in triplicate. *Significantly different from the same treatment in the absence of NAC ($p < 0.01$). NAC inhibited apoptosis of CGNs treated with HA14-1, but did not protect CGNs from 5K-induced apoptosis. (b) Cells were incubated as described in (a), except ± glutathione (GSH;

2 mM) rather than NAC. Values represent the means ± SEM for three independent experiments, each performed in triplicate. *Significantly different from the same condition in the absence of GSH ($p < 0.01$). GSH protected CGNs from apoptosis induced by HA14-1 but not from the removal of depolarizing potassium (5K). (c) Bright-field images of live CGNs incubated for 24 h in either 25K alone (control), 25K containing 10 μM HA14-1, or 5K. Cells were imaged both in the absence and presence of 2 mM GSH. Living cells were imaged under a 63 × water objective with differential interference contrast (DIC) microscopy. Inclusion of GSH protected cells from apoptosis in the HA14-1 condition, but had no protective effect on CGNs in the 5K condition. Scale bar, 10 μm.

Bim-mediated (oxidative stress-independent) cell death elicited in non-depolarizing medium.

Inhibition of pro-survival Bcl-2 family proteins by two approaches distinct from HA14-1 mimic the oxidative stress-dependent apoptotic pathway

The addition of a structurally distinct Bcl-2/Bcl-x(L) antagonist, compound 6, that also binds the hydrophobic surface pocket of Bcl-2 and Bcl-x(L) with micromolar affinity

(Enyedy *et al.* 2001), induced marked CGN apoptosis that was significantly inhibited by co-incubation with GSH (Figs 8a and b). Figure 8(b) shows bright-field images of CGNs that were incubated for 24 h in either control conditions (25K-serum) or in the presence of 75 μM compound 6. The left panels show the effect of the Bcl-2/Bcl-x(L) inhibitor in CGNs without the addition of an antioxidant, while the right panels reveal the protective effects of 2 mM GSH on compound 6-induced apoptosis.

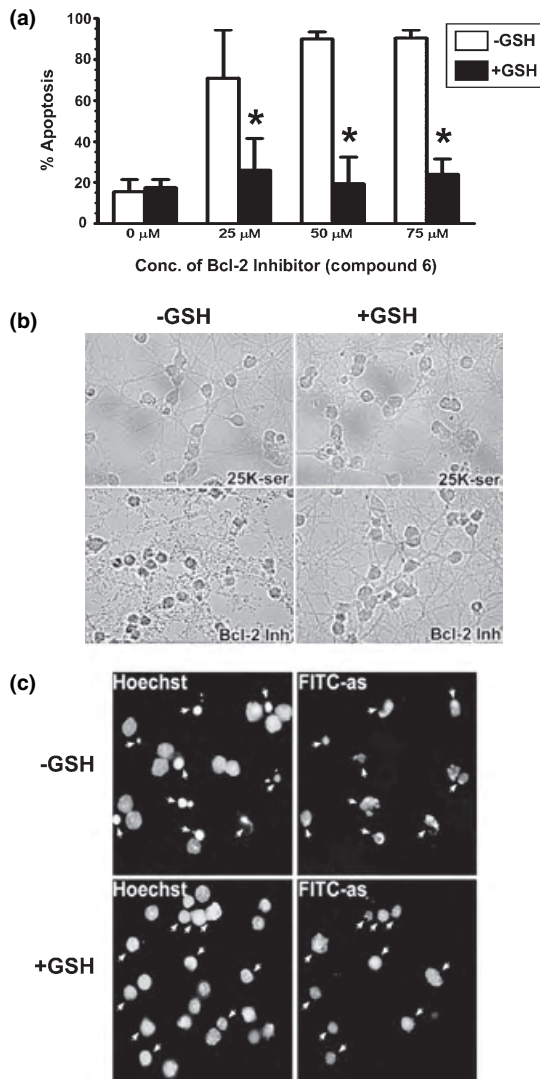


Fig. 8 Distinct inhibitors of the pro-survival Bcl-2 family members induce apoptosis in an oxidative stress-dependent manner. (a) Compound 6, a Bcl-2/Bcl-x(L) inhibitor, was added to CGNs at varying μM concentrations (0, 25, 50 or 75) in either the presence or absence of the antioxidant glutathione (2 mM). Compound 6-induced apoptosis was significantly inhibited by GSH at all concentrations tested. Values represent the means \pm SEM for three independent experiments. *Significantly different from the same condition in the absence of GSH ($p < 0.01$). (b) Bright-field (DIC) images of CGNs in control conditions (25K-serum) or in the presence of 75 μM compound 6 (Bcl-2/Bcl-x(L) inhibitor) \pm 2 mM GSH. (c) CGNs treated with FITC-labeled Bcl-2 antisense oligos \pm 2 mM GSH were stained with Hoechst dye (nuclear stain). Arrows indicate FITC-antisense (as)-positive cells. Note the highly condensed and fragmented nuclei in the -GSH condition and the much less condensed and intact nuclei in the protective +GSH condition. Each panel represents a composite of approximately five different fields of antisense-positive CGNs. The images shown are indicative of two independent experiments that yielded similar results.

Thus, two structurally dissimilar Bcl-2/Bcl-x(L) inhibitors, HA14-1 and compound 6, each elicit GSH-sensitive CGN apoptosis.

In addition to small molecule inhibitors, we also utilized cell-permeable phosphorothioate, FITC-labeled Bcl-2 antisense oligonucleotides as a tool to antagonize Bcl-2 function. CGNs incubated with Bcl-2 antisense oligos for 24 h (indicated by the FITC label) underwent significant apoptosis characterized by striking chromatin condensation and fragmentation (Fig. 8c, upper panels). No significant apoptosis was observed with a negative control oligo (data not shown). Inclusion of 2 mM GSH during the Bcl-2 antisense incubation resulted in partial protection of the CGNs (Fig. 8c, lower panels). While some nuclear condensation was detectable in Bcl-2 antisense-positive CGNs incubated with GSH, it wasn't nearly as extensive as that observed in neurons exposed to the antisense alone. Moreover, nuclear fragmentation was almost never observed in Bcl-2 antisense-treated CGNs incubated in the presence of GSH, whereas it was prominent in the absence of GSH. The oxidative-stress dependent nature of CGN apoptosis induced by inhibition of Bcl-2 and/or Bcl-x(L) function is evidenced by the use of three different approaches to antagonize these pro-survival proteins.

CGN apoptosis induced by overexpression of a GFP-Bim fusion protein is insensitive to antioxidants

We have shown that CGN apoptosis induced by removal of depolarizing extracellular potassium is insensitive to the antioxidants, NAC and GSH (see Fig. 7). Because 5K-induced CGN apoptosis requires induction of the BH3-only protein Bim (Harris and Johnson 2001; Linseman *et al.* 2002), these data suggest a dissociation of Bcl-2/Bcl-x(L) antagonism and Bim-dependent apoptosis. However, CGN apoptosis elicited by potassium deprivation is complex and involves many pathways in addition to Bim induction (Vaudry *et al.* 2003). To definitively establish the antioxidant resistance of Bim-mediated death, we analyzed the effects of NAC and GSH on CGN apoptosis induced by overexpression of a GFP-Bim fusion protein. These experiments were carried out in CGNs maintained in depolarizing (25K) medium to limit the contributions of other potential pro-apoptotic signals. Briefly, cells were transfected via a helium-powered gene gun with plasmid-coated gold particles containing cDNA for either GFP alone or GFP-Bim. Immediately after transfection, CGNs were returned to the incubator for 24 h in 25K medium alone or containing either 10 mM NAC or 2 mM GSH. Following incubation, nuclei were stained with Hoechst dye and apoptosis was assessed in GFP-positive cells by fluorescence microscopy. As shown in Fig. 9, cells transfected with GFP alone were healthy, whereas CGNs expressing the GFP-Bim fusion protein displayed apoptotic nuclear morphology (upper panels). Note that untransfected cells remained healthy in either

condition. Similar to the antioxidant insensitivity of 5K-induced death discussed above, CGN apoptosis evoked by the overexpression of GFP-Bim was not inhibited by incubation with either NAC or GSH (lower panels). When the apoptosis of GFP-Bim-expressing CGNs was quantified at 24 h post-transfection, greater than 95% of the Bim-positive cells were apoptotic regardless of whether they were incubated in 25K medium alone or containing antioxidants. Thus, CGN apoptosis induced by the overexpression of Bim occurs by a different mechanism than that elicited by antagonists of Bcl-2/Bcl-x(L) function.

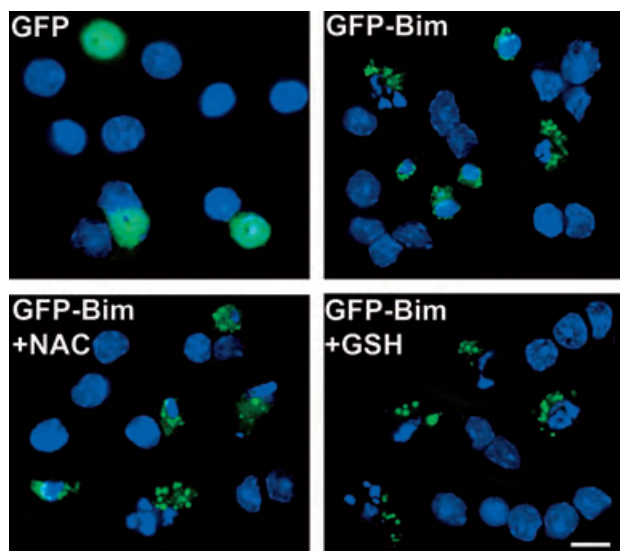


Fig. 9 CGNs transfected with GFP-Bim undergo apoptosis that is resistant to antioxidants. CGNs were transiently transfected using the Helios Gene-Gun system, as described in Experimental procedures. Briefly, CGNs to be transfected were seeded at a density of 8×10^5 cells/well on polyethyleneimine-coated glass coverslips in 24-well plates. After 5 days in culture, the medium was removed from the wells and the cells were shot with plasmid-coated gold beads (0.6 μm diameter) containing cDNA for either GFP-Bim or GFP alone as a control. CGNs were shot with a burst of ~ 100 p.s.i. helium through a 40- μm nylon mesh placed over the well. Depolarizing (25K) medium, either alone or containing NAC (10 mM) or GSH (2 mM), was immediately replaced and cells were incubated for an additional 24 h before image analysis. Following incubation, CGNs were fixed in 4% paraformaldehyde and nuclei were stained with Hoechst dye (blue). CGNs in the control condition (transfected with GFP alone) remained healthy after the 24 h incubation period, while CGNs transfected with GFP-Bim uniformly underwent apoptosis (upper panels). The addition of either NAC or GSH had no discernible protective effect on CGN apoptosis induced by expression of the GFP-Bim fusion protein (lower panels). Images shown are composites of several fields as so few cells (< 1% of the cell culture) were actually transfected using the gene gun method. The images are representative of transfected cells from three independent experiments. Scale bar, 10 μm . Note that non-transfected cells in the GFP-Bim panels remained healthy.

Discussion

The principal aim of the current study was to determine if the BH3-only protein, Bim, promotes CGN apoptosis by directly antagonizing pro-survival Bcl-2 family members. To examine this question, we first elucidated the specificity and mechanism of neuronal death induced by the small molecule Bcl-2/Bcl-x(L) antagonist, HA14-1, and then contrasted it to two models of Bim-dependent CGN apoptosis. In an *in vitro* binding assay, HA14-1 competed with a Bim-GST fusion protein for binding to Bcl-2 and Bcl-x(L), but not Bcl-w. Although each of these pro-survival proteins have a highly conserved hydrophobic surface pocket that binds BH3 domain proteins, and therefore should bind HA14-1, a unique C-terminal alpha helix blocks this surface pocket in the native conformation of the Bcl-w protein (Hinds *et al.* 2003). This intramolecular interaction apparently interferes with the ability of HA14-1 to access its binding site on the Bcl-w protein. Thus, we observed specificity of HA14-1 for antagonizing Bcl-2 and Bcl-x(L).

HA14-1 provoked Bim-independent CGN apoptosis that was characterized by mitochondrial membrane depolarization, conformational activation of Bax, cytochrome *c* release, proteolytic cleavage of caspases 9 and 3, and chromatin condensation. Consistent with an oxidative stress-dependent mechanism of cell death, as was recently reported for HA14-1 treatment of HL-60 cells (An *et al.* 2004), all of the above events observed in CGNs were significantly inhibited by co-incubation with the sulfhydryl-containing antioxidants NAC or GSH. In a similar manner, CGN apoptosis induced by a structurally distinct, small molecule Bcl-2/Bcl-x(L) inhibitor, compound 6, was also prevented by GSH. Moreover, GSH provided partial protection against Bcl-2 antisense-mediated apoptosis of CGNs. Although this latter protective effect of GSH was not as complete as that observed with HA14-1 or compound 6, this may be attributed to the fact that, while these small molecules inhibit the function of endogenous Bcl-2/Bcl-x(L), the proteins are presumably still present in the mitochondrial membrane. In contrast, addition of Bcl-2 antisense disrupts translation of the endogenous protein and therefore prevents the physical presence of Bcl-2 at the mitochondria, perhaps resulting in a secondary death mechanism as a result of loss of a possible membrane stabilizing effect of Bcl-2.

In contrast to the GSH-sensitive neuronal death induced by antagonism of Bcl-2 and/or Bcl-x(L) function, Bim-dependent CGN apoptosis, elicited by either removal of the depolarization stimulus (Linseman *et al.* 2002) or overexpression of a GFP-Bim fusion protein (Harris and Johnson 2001), was completely resistant to treatment with either NAC or GSH. These results demonstrate that Bim triggers CGN apoptosis via a mechanism that is markedly different from that induced by antagonism of Bcl-2/Bcl-x(L) function. Although these data do not completely exclude a putative

interaction between Bim and Bcl-2 or Bcl-x(L) in CGNs undergoing apoptosis, they do suggest that any such interaction is dispensable for Bim-mediated death. Moreover, these findings indicate that Bim must target additional proteins besides Bcl-2/Bcl-x(L) to induce CGN apoptosis.

Some clues about the alternative, Bcl-2/Bcl-x(L)-independent mechanism(s) utilized by Bim to induce CGN apoptosis may be found by comparing the upstream signals activated by the different death stimuli examined in this study. Although the canonical mitochondrial death pathway (i.e. mitochondrial depolarization \rightarrow Bax activation \rightarrow cytochrome *c* release \rightarrow caspases 9 and 3 activation) was triggered by either HA14-1 or the removal of depolarizing potassium, the proximal signals leading to the initial loss of $\Delta\psi_m$ were clearly distinct for these two cell death stimuli. For example, mitochondrial depolarization induced by HA14-1 occurred in the absence of mitochondrial swelling and was cyclosporin A-insensitive, but redox-sensitive (i.e. blocked by NAC). In contrast, mitochondrial depolarization elicited by removal of extracellular depolarizing potassium happened in conjunction with mitochondrial swelling (Linseman *et al.* 2002) and was cyclosporin A-sensitive (Precht *et al.* 2005), but redox-insensitive. These results suggest that antagonism of Bcl-2/Bcl-x(L) triggers an oxidative stress-dependent opening of a mitochondrial permeability channel that is distinct from the classical mPTP (Scanlon and Reynolds 1998; Kushnareva and Sokolove 2000; Mukherjee *et al.* 2002). Conversely, the induction of Bim that occurs in response to withdrawal of depolarizing potassium is associated with opening of the cyclosporin A-inhibited mPTP (Martinou and Green 2001; Waldmeier *et al.* 2003).

The above differences in the mechanism of mitochondrial depolarization elicited by either antagonism of Bcl-2/Bcl-x(L) or induction of Bim may reflect a propensity for Bim to interact with components of the mPTP. Consistent with this idea, Bim has recently been shown to interact with the voltage-dependent anion channel (VDAC) in isolated mitochondrial preparations, leading directly to opening of the mPTP and mitochondrial depolarization (Sugiyama *et al.* 2002). Alternatively, a selective interaction between Bim and VDAC2 (a low abundance isoform of VDAC) could act to dissociate VDAC2 from the multidomain Bcl-2 family member, Bak (Cheng *et al.* 2003). This latter effect could indirectly promote Bak oligomerization, insertion into the mitochondrial membrane, and an ensuing mitochondrial permeabilization. Finally, the potential for Bim to associate with other components of the mPTP, like the adenine nucleotide translocator (ANT) or cyclophilin D, is currently unknown.

In addition to mPTP proteins, it is also possible that Bim could trigger cell death by directly interacting with Bax or Bak at mitochondria. For example, the BH3-only protein, tBid, formed by the caspase 8-mediated cleavage of full

length Bid (Li *et al.* 1998), is known to interact directly with Bax at mitochondria to promote a conformational activation of this protein (Perez and White 2000). In a similar manner, some small isoforms of Bim, including Bim_s and Bim_{AD}, have recently been shown to elicit a conformational activation of Bax *in vitro* (Marani *et al.* 2002). Moreover, mutants of Bim_{AD} that bind Bax, but not Bcl-2, are still capable of triggering apoptosis, providing independent confirmation that Bim-mediated cell death does not necessarily require direct antagonism of Bcl-2 (Marani *et al.* 2002).

Besides a possible interaction of Bim with Bax or Bak at mitochondria, Bim could also associate with these multidomain family members at an extra-mitochondrial site to promote cell death. For example, Bax and/or Bak activation at the endoplasmic reticulum (ER) has been shown to induce the release of ER calcium that is subsequently taken up by mitochondria (Nutt *et al.* 2002; Scorrano *et al.* 2003). Mitochondrial calcium loading ultimately results in a loss of mitochondrial membrane potential and cytochrome *c* release. Consistent with this mechanism, SH-SY5Y neuroblastoma cells exposed to the ER stressor, tunicamycin, show induction of the BH3-only protein, PUMA, which is coincident with mitochondrial cytochrome *c* release and caspase activation (Reimertz *et al.* 2003). The potential for Bim to mediate a similar ER-dependent apoptotic response in primary neurons has not yet been investigated.

Lastly, one should consider the possibility that Bim may have multiple cellular targets, perhaps including some combination of Bcl-2/Bcl-x(L), VDAC or ANT, Bax or Bak, and other, as yet, unidentified proteins. If this is the case, then it could be the combined effects of several of these interdependent interactions that ultimately triggers cell death. Alternatively, multiple Bim-mediated actions may occur simultaneously, such as Bcl-2/Bcl-x(L) antagonism and Bax activation, that essentially act in a redundant manner. In the latter case, inhibition of one pathway (e.g. alleviating the consequences of Bcl-2/Bcl-x(L) antagonism with antioxidants) may be compensated for by the redundant pathway (e.g. direct Bax activation), such that the apoptotic cascade is still initiated. This scenario of redundant Bim-dependent death signals may underlie the observations of the current study in which Bim-mediated apoptosis persists in CGNs treated with antioxidants. It is also important to consider the role of other BH3-only proteins in CGN death. Although the focus of this paper is on Bim, we acknowledge that other BH3-only proteins like DP5 may also contribute to 5K-induced CGN apoptosis (Harris and Johnson 2001).

In summary, we have shown that CGN apoptosis triggered by the small molecule Bcl-2/Bcl-x(L) antagonists, HA14-1 and compound 6, as well as antisense oligos to Bcl-2, occurs via an oxidative stress-dependent pathway that is inhibited by the antioxidants, NAC and GSH. In contrast, Bim-mediated CGN death, induced by either the removal of depolarizing potassium or overexpression of Bim, is insensitive to

antioxidant treatment. We conclude that Bim promotes CGN apoptosis by a mechanism that does not require direct antagonism of Bcl-2/Bcl-x(L) and the consequential oxidative stress. Identification of additional molecular targets of Bim, besides Bcl-2/Bcl-x(L), is necessary to determine precisely how this BH3-only protein induces neuronal apoptosis.

Acknowledgements

This work was supported by a Department of Veterans Affairs Merit Review Entry Program (MREP) Award (to DAL) and a Department of Defense Grant USAMRMC no. 03281009 (to DAL and KAH). AKZ was supported by a Neuroscience Program Training Grant (T32 HD041697-03) from the National Institutes of Health. Molecular Biology Core Services were supported by the NIH DERC grant P30-DK57516.

References

- An J., Chen Y. and Huang Z. (2004) Critical upstream signals of cytochrome *c* release induced by a novel Bcl-2 inhibitor. *J. Biol. Chem.* **279**, 19 133–19 140.
- Bouillet P., Cory S., Zhang L. C., Strasser A. and Adams J. M. (2001) Degenerative disorders caused by Bcl-2 deficiency prevented by loss of its BH3-only antagonist Bim. *Dev. Cell* **1**, 645–653.
- Bouillet P. and Strasser A. (2002) BH3-only proteins – evolutionarily conserved pro-apoptotic Bcl-2 family members essential for initiating programmed cell death. *J. Cell Sci.* **115**, 1567–1574.
- Chen J., Freeman A., Liu J., Dai Q. and Lee R. M. (2002) The apoptotic effect of HA14-1, a Bcl-2-interacting small molecular compound, requires Bax translocation and is enhanced by PK11195. *Mol. Cancer Ther.* **1**, 961–967.
- Cheng E. H., Sheiko T. V., Fisher J. K., Craigen W. J. and Korsmeyer S. J. (2003) VDAC2 inhibits BAK activation and mitochondrial apoptosis. *Science* **301**, 513–517.
- Coffey E. T., Smiciene G., Hongisto V., Cao J., Brecht S., Herdegen T. and Courtney M. J. (2002) c-Jun N-terminal protein kinase (JNK) 2/3 is specifically activated by stress, mediating c-Jun activation, in the presence of constitutive JNK1 activity in cerebellar neurons. *J. Neurosci.* **22**, 4335–4345.
- D'Mello S. R., Galli C., Ciotti T. and Calissano P. (1993) Induction of apoptosis in cerebellar granule neurons by low potassium: inhibition of death by insulin-like growth factor I and cAMP. *Proc. Natl Acad. Sci. USA* **90**, 10 989–10 993.
- Degenhardt K., Sundararajan R., Lindsten T., Thompson C. and White E. (2002) Bax and Bak independently promote cytochrome *c* release from mitochondria. *J. Biol. Chem.* **277**, 14 127–14 134.
- Dijkers P. F., Medema R. H., Lammers J. W., Koenderman L. and Coffey P. J. (2000) Expression of the pro-apoptotic Bcl-2 family member Bim is regulated by the forkhead transcription factor FKHR-L1. *Curr. Biol.* **10**, 1201–1204.
- Dispersyn G., Nuydens R., Connors R., Borgers M. and Geerts H. (1999) Bcl-2 protects against FCCP-induced apoptosis and mitochondrial membrane potential depolarization in PC12 cells. *Biochim. Biophys. Acta.* **1428**, 357–371.
- Ekshyyan O. and Aw T. Y. (2004) Apoptosis in acute and chronic neurological disorders. *Front. Biosci.* **9**, 1567–1576.
- Enyedy I. J., Ling Y., Nacro K. *et al.* (2001) Discovery of small-molecule inhibitors of Bcl-2 through structure-based computer screening. *J. Med. Chem.* **44**, 4313–4324.
- Fiskum G., Starkov A., Polster B. M. and Chinopoulos C. (2003) Mitochondrial mechanisms of neural cell death and neuroprotective interventions in Parkinson's disease. *Ann. NY Acad. Sci.* **991**, 111–119.
- Gilley J., Coffey P. J. and Ham J. (2003) FOXO transcription factors directly activate Bim gene expression and promote apoptosis in sympathetic neurons. *J. Cell Biol.* **162**, 613–622.
- Guegan C., Vila M., Rosoklija G., Hays A. P. and Przedborski S. (2001) Recruitment of the mitochondrial-dependent apoptotic pathway in amyotrophic lateral sclerosis. *J. Neurosci.* **21**, 6569–6576.
- Harris C. A. and Johnson E. M. Jr. (2001) BH3-only Bcl-2 family members are coordinately regulated by the JNK pathway and require Bax to induce apoptosis in neurons. *J. Biol. Chem.* **276**, 37754–37760.
- Hildeman D. A., Mitchell T., Aronow B., Wojciechowski S., Kappler J. and Marrack P. (2003) Control of Bcl-2 expression by reactive oxygen species. *Proc. Natl Acad. Sci. USA* **100**, 15 035–15 040.
- Hinds M. G., Lackmann M., Skea G. L., Harrison P. J., Huang D. C. and Day C. L. (2003) The structure of Bcl-w reveals a role for the C-terminal residues in modulating biological activity. *EMBO J.* **22**, 1497–1507.
- Hochman A., Sternin H., Gorodin S., Korsmeyer S., Ziv I., Melamed E. and Offen D. (1998) Enhanced oxidative stress and altered antioxidants in brains of Bcl-2-deficient mice. *J. Neurochem.* **71**, 741–748.
- Hsu S. Y., Lin P. and Hsueh A. J. (1998) Bcl-2-related ovarian death gene is an ovarian BH3-domain-containing pro-apoptotic Bcl-2 protein capable of dimerization with diverse anti-apoptotic Bcl-2 members. *Mol. Endocrinol.* **12**, 1432–1440.
- Inoue H., Tsukita K., Iwasato T. *et al.* (2003) The crucial role of caspase-9 in the disease progression of a transgenic ALS mouse model. *EMBO J.* **22**, 6665–6674.
- Jana N. R., Zemskov E. A., Wang G. and Nukina N. (2001) Altered proteasomal function due to the expression of polyglutamine-expanded truncated N-terminal huntingtin induces apoptosis by caspase activation through mitochondrial cytochrome *c* release. *Hum. Mol. Genet.* **10**, 1049–1059.
- Kuida K., Haydar T. F., Kuan C. Y., Gu Y., Taya C., Karasuyama H., Su M. S., Rakic P. and Flavell R. A. (1998) Reduced apoptosis and cytochrome *c*-mediated caspase activation in mice lacking caspase-9. *Cell* **94**, 325–337.
- Kushnareva Y. E. and Sokolove P. M. (2000) Pro-oxidants open both the mitochondrial permeability transition pore and a low-conductance channel in the inner mitochondrial membrane. *Arch. Biochem. Biophys.* **376**, 377–388.
- Li D., Ueta E., Kimura T., Yamamoto T. and Osaki T. (2004) Reactive oxygen species (ROS) control the expression of Bcl-2 family proteins by regulating their phosphorylation and ubiquitination. *Cancer Sci.* **95**, 644–650.
- Li H., Zhu H., Xu C. J. and Yuan J. (1998) Cleavage of Bid by caspase 8 mediates the mitochondrial damage in the Fas pathway of apoptosis. *Cell* **94**, 491–501.
- Linseman D. A., Phelps R. A., Bouchard R. J., Le S. S., Laessig T. A., McClure M. L. and Heidenreich K. A. (2002) Insulin-like growth factor-I blocks Bcl-2 interacting mediator of cell death (Bim) induction and intrinsic death signaling in cerebellar granule neurons. *J. Neurosci.* **22**, 9287–9297.
- Linseman D. A., Cornejo B. J., Le S. S., Meintzer M. K., Laessig T. A., Bouchard R. J. and Heidenreich K. A. (2003) A myocyte enhancer factor 2D (MEF2D) kinase activated during neuronal apoptosis is a novel target inhibited by lithium. *J. Neurochem.* **85**, 1488–1499.
- Linseman D. A., Butts B. D., Precht T. A., Phelps R. A., Le S. S., Laessig T. A., Bouchard R. J., Florez-McClure M. L. and Heidenreich K. A. (2004) Glycogen synthase kinase-3 β phosphorylates

- Bax and promotes its mitochondrial localization during neuronal apoptosis. *J. Neurosci.* **24**, 9993–10 002.
- Lossi L. and Merighi A. (2003) *In vivo* cellular and molecular mechanisms of neuronal apoptosis in the mammalian CNS. *Prog. Neurobiol.* **69**, 287–312.
- Marani M., Tenev T., Hancock D., Downward J. and Lemoine N. R. (2002) Identification of novel isoforms of the BH3-domain protein Bim which directly activate Bax to trigger apoptosis. *Mol. Cell Biol.* **22**, 3577–3589.
- Martinou J. C. and Green D. R. (2001) Breaking the mitochondrial barrier. *Nat. Rev. Mol. Cell Biol.* **2**, 63–67.
- Mukherjee S. B., Das M., Sudhandiran G. and Shaha C. (2002) Increase in cytosolic Ca²⁺ levels through the activation of non-selective cation channels induced by oxidative stress causes mitochondrial depolarization leading to apoptosis-like death in *Leishmania donovani* promastigotes. *J. Biol. Chem.* **277**, 24 717–24 727.
- Murphy K. M., Streips U. N. and Lock R. B. (2000) Bcl-2 inhibits a Fas-induced conformational change in the Bax N-terminus and Bax mitochondrial translocation. *J. Biol. Chem.* **275**, 17 225–17 228.
- Nutt L. K., Pataer A., Pahler J., Fang B., Roth J., McConkey D. J. and Swisher S. G. (2002) Bax and Bak promote apoptosis by modulating endoplasmic reticular and mitochondrial Ca²⁺ stores. *J. Biol. Chem.* **277**, 9219–9225.
- Ohga Y., Zirgiebel U., Hamner S., Michaelidis T. M., Cooper J., Thoenen H. and Lindholm D. (1996) Cell density increases Bcl-2 and Bcl-x expression in addition to survival of cultured cerebellar granule neurons. *Neuroscience* **73**, 913–917.
- Perez D. and White E. (2000) TNF- α signals apoptosis through a Bid-dependent conformational change in Bax that is inhibited by E1B 19K. *Mol. Cell* **6**, 53–63.
- Precht T. A., Phelps R. A., Linseman D. A., Butts B. D., Le S. S., Laessig T. A., Bouchard R. J. and Heidenreich K. A. (2005) The permeability transition pore triggers Bax translocation to mitochondria during neuronal apoptosis. *Cell Death Diff.* **12**, 255–265.
- Putcha G. V., Moulder K. L., Golden J. P., Bouillet P., Adams J. A., Strasser A. and Johnson E. M. Jr (2001) Induction of Bim, a pro-apoptotic BH3-only Bcl-2 family member, is critical for neuronal apoptosis. *Neuron* **29**, 615–628.
- Putcha G. V., Harris C. A., Moulder K. L., Easton R. M., Thompson C. B. and Johnson E. M. Jr (2002) Intrinsic and extrinsic pathway signaling during neuronal apoptosis: lessons from the analysis of mutant mice. *J. Cell Biol.* **157**, 441–453.
- Reimertz C., Kogel D., Rami A., Chittenden T. and Prehn J. H. (2003) Gene expression during ER stress-induced apoptosis in neurons: induction of the BH3-only protein Bbc3/PUMA and activation of the mitochondrial apoptosis pathway. *J. Cell Biol.* **162**, 587–597.
- Scanlon J. M. and Reynolds I. J. (1998) Effects of oxidants and glutamate receptor activation on mitochondrial membrane potential in rat forebrain neurons. *J. Neurochem.* **71**, 2392–2400.
- Scorrano L., Oakes S. A., Opferman J. T., Cheng E. H., Sorcinelli M. D., Pozzan T. and Korsmeyer S. J. (2003) Bax and Bak regulation of endoplasmic reticulum Ca²⁺: a control point for apoptosis. *Science* **300**, 135–139.
- Slee E. A., Adrain C. and Martin S. J. (1999) Serial killers: ordering caspase activation events in apoptosis. *Cell Death Differ.* **6**, 1067–1074.
- Strasser A., Puthalakath H., Bouillet P., Huang D. C., O'Connor L., O'Reilly L. A., Cullen L., Cory S. and Adams J. M. (2000) The role of Bim, a pro-apoptotic BH3-only member of the Bcl-2 family in cell-death control. *Ann. NY Acad. Sci.* **917**, 541–548.
- Sugiyama T., Shimizu S., Matsuoka Y., Yoneda Y. and Tsujimoto Y. (2002) Activation of mitochondrial voltage-dependent anion channel by a pro-apoptotic BH3-only protein Bim. *Oncogene* **21**, 4944–4956.
- Tatton W. G., Chalmers-Redman R., Brown D. and Tatton N. (2003) Apoptosis in Parkinson's disease: signals for neuronal degradation. *Ann. Neurol.* **53**, S61–S72.
- Vaudry D., Falluel-Morel A., Leuillet S., Vaudry H. and Gonzalez B. J. (2003) Regulators of cerebellar granule cell development act through specific signaling pathways. *Science* **300**, 1532–1534.
- Vila M., Jackson-Lewis V., Vukosavic S., Djaldetti R., Liberatore G., Offen D., Korsmeyer S. J. and Przedborski S. (2001) Bax ablation prevents dopaminergic neurodegeneration in the 1-methyl-4-phenyl-1,2,3,6-tetrahydropyridine mouse model of Parkinson's disease. *Proc. Natl Acad. Sci. USA* **98**, 2837–2842.
- Viswanath V., Wu Y., Boonplueang R., Chen S., Stevenson F. F., Yantiri F., Yang L., Beal M. F. and Andersen J. K. (2001) Caspase-9 activation results in downstream caspase-8 activation and Bid cleavage in 1-methyl-4-phenyl-1,2,3,6-tetrahydropyridine-induced Parkinson's disease. *J. Neurosci.* **21**, 9519–9528.
- Voehringer D. W. and Meyn R. E. (2000) Redox aspects of Bcl-2 function. *Antioxidants Redox Signaling* **2**, 537–550.
- Waldmeier P. C., Zimmermann K., Qian T., Tintelnot-Bolmley M. and Lemasters J. J. (2003) Cyclophilin D as a drug target. *Curr. Med. Chem.* **10**, 1485–1506.
- Wang J. L., Liu D., Zhang Z. J., Shan S., Han X., Srinivasula S. M., Croce C. M., Alnemri E. S. and Huang Z. (2000) Structure-based discovery of an organic compound that binds Bcl-2 protein and induces apoptosis of tumor cells. *Proc. Natl Acad. Sci. USA* **97**, 7124–7129.
- Wei M. C., Zong W. X., Cheng E. H., Lindsten T., Panoutsakopoulou V., Ross A. J., Roth K. A., MacGregor G. R., Thompson C. B. and Korsmeyer S. J. (2001) Pro-apoptotic Bax and Bak: a requisite gateway to mitochondrial dysfunction and death. *Science* **292**, 727–730.
- Whitfield J., Neame S. J., Paquet L., Bernard O. and Ham J. (2001) Dominant-negative c-Jun promotes neuronal survival by reducing Bim expression and inhibiting mitochondrial cytochrome *c* release. *Neuron* **29**, 629–643.
- Wilson-Annan J., O'Reilly L. A., Crawford S. A. *et al.* (2003) Pro-apoptotic BH3-only proteins trigger membrane integration of prosurvival Bcl-w and neutralize its activity. *J. Cell Biol.* **162**, 877–887.
- Yang J., Liu X., Bhalla K., Kim C. N., Ibrado A. M., Cai J., Peng T. I., Jones D. P. and Wang X. (1997) Prevention of apoptosis by Bcl-2: release of cytochrome *c* from mitochondria blocked. *Science* **275**, 1129–1132.
- Zong W. X., Lindsten T., Ross A. J., MacGregor G. R. and Thompson C. B. (2001) BH3-only proteins that bind pro-survival Bcl-2 family members fail to induce apoptosis in the absence of Bax and Bak. *Genes Dev.* **15**, 1481–1486.
- Zou H., Li Y., Liu X. and Wang X. (1999) An APAF-1 cytochrome *c* multimeric complex is a functional apoptosome that activates procaspase-9. *J. Biol. Chem.* **274**, 11 549–11 556.

The p75 Neurotrophin Receptor Can Induce Autophagy and Death of Cerebellar Purkinje Neurons

Maria L. Florez-McClure,¹ Daniel A. Linseman,¹ Charleen T. Chu,² Phil A. Barker,³ Ron J. Bouchard,¹ Shoshona S. Le,¹ Tracey A. Laessig,¹ and Kim A. Heidenreich¹

¹Department of Pharmacology, University of Colorado Health Sciences Center, and Denver Veterans Affairs Medical Center, Denver, Colorado 80262,

²Department of Pathology, Division of Neuropathology, and Pittsburgh Institute for Neurodegenerative Diseases, University of Pittsburgh School of Medicine, Pittsburgh, Pennsylvania 15213, and ³Center for Neuronal Survival, Montreal Neurological Institute, McGill University, Montreal, Quebec H3A 2B4, Canada

The cellular mechanisms underlying Purkinje neuron death in various neurodegenerative disorders of the cerebellum are poorly understood. Here we investigate an *in vitro* model of cerebellar neuronal death. We report that cerebellar Purkinje neurons, deprived of trophic factors, die by a form of programmed cell death distinct from the apoptotic death of neighboring granule neurons. Purkinje neuron death was characterized by excessive autophagic–lysosomal vacuolation. Autophagy and death of Purkinje neurons were inhibited by nerve growth factor (NGF) and were activated by NGF-neutralizing antibodies. Although treatment with antisense oligonucleotides to the p75 neurotrophin receptor (p75^{ntr}) decreased basal survival of cultured cerebellar neurons, p75^{ntr}-antisense decreased autophagy and completely inhibited death of Purkinje neurons induced by trophic factor withdrawal. Moreover, adenoviral expression of a p75^{ntr} mutant lacking the ligand-binding domain induced vacuolation and death of Purkinje neurons. These results suggest that p75^{ntr} is required for Purkinje neuron survival in the presence of trophic support; however, during trophic factor withdrawal, p75^{ntr} contributes to Purkinje neuron autophagy and death. The autophagic morphology resembles that found in neurodegenerative disorders, suggesting a potential role for this pathway in neurological disease.

Key words: autophagy; Purkinje neuron; p75^{ntr}; cell death; neurotrophin; vacuoles

Introduction

Chronic neurodegenerative diseases are characterized by a selective loss of specific neuronal populations over a period of years or even decades. Although the underlying causes of most neurodegenerative diseases are unclear, the loss of neurons and neuronal contacts is a key feature of disease pathology. Elucidation of the cellular mechanisms regulating neuronal cell death is critical for developing new therapeutic strategies to slow or halt the progressive neurodegeneration in these disorders.

Purkinje neurons in the cerebellum integrate input to the cerebellar cortex from the mossy fibers and climbing fibers and subsequently generate inhibitory output to the deep cerebellar nuclei (Ghez and Thach, 2000). In addition to their essential role in proper cerebellar function, Purkinje neurons provide critical trophic support to developing cerebellar granule neurons and inferior olivary neurons (Torres-Aleman et al., 1994; Zanjani et al.,

1994; Linseman et al., 2002a). Purkinje neurons are specifically lost in various neurodegenerative conditions such as spinocerebellar ataxias (Koeppen, 1998; Watase et al., 2002), ataxia telangiectasia (Gatti and Vinters, 1985; Borghesani et al., 2000), autism (Ritvo et al., 1986; Bailey et al., 1998), and certain prion encephalopathies (Ferrer et al., 1991; Watanabe and Duchon, 1993; Lamezas et al., 1997). Although Purkinje cell loss is a critical feature of disease pathology, the molecular mechanisms underlying Purkinje cell death remain poorly understood.

The Lurcher (Lc) mouse has been extensively used as an *in vivo* model of Purkinje neuron degeneration. The cell degeneration in the Lurcher cerebellum results from a single point mutation in the $\delta 2$ glutamate receptor (GluR $\delta 2$), whose expression is restricted to Purkinje neurons (Zuo et al., 1997). The degeneration and loss of Purkinje neurons in Lurcher cerebellum is followed by a secondary death of cerebellar granule neurons and inferior olivary neurons attributable to loss of trophic support normally provided by their afferent target Purkinje neurons (Wetts and Herrup, 1982). Because GluR $\delta 2$ ^{Lc} causes a constitutive depolarization of Purkinje neurons, it was originally thought that the death of Purkinje neurons in the Lc cerebellum was akin to excitotoxicity mediated by excessive calcium influx. However, a recent report suggested that the mechanism of GluR $\delta 2$ ^{Lc}-induced Purkinje cell degeneration can be dissociated from depolarization (Selimi et al., 2003). Instead, Lc Purkinje cell death is hypothesized to involve interactions between the mutant GluR $\delta 2$

Received Dec. 30, 2003; revised March 16, 2004; accepted March 17, 2004.

This work was supported by a Department of Veterans Affairs merit award (K.A.H.), Department of Defense Grant DAMD17-99-1-9481 (K.A.H.), National Institutes of Health Grants NS38619-01A1 (K.A.H.) and NS40817 (C.T.C.), a Department of Veterans Affairs Research Enhancement Program award (K.A.H., D.A.L.), and a National Research Service award (M.L.F.-M.). We thank Ardith Ries of the University of Pittsburgh electron microscopy laboratory for technical assistance and Dr. John Shelburne of the Duke University and Veterans Affairs Medical Centers (Durham, NC) for helpful discussion.

Correspondence should be addressed to Kim A. Heidenreich, Department of Pharmacology, C236, University of Colorado Health Sciences Center, 4200 East Ninth Avenue, Denver, CO 80262. E-mail: kim.heidenreich@uchsc.edu.

DOI:10.1523/JNEUROSCI.5744-03.2004

Copyright © 2004 Society for Neuroscience 0270-6474/04/244498-12\$15.00/0

receptor and the proteins nPIST and Beclin 1, because these protein–protein interactions can lead to cell death and increase autophagy when overexpressed in heterologous cells (Yue et al., 2002). Furthermore, both groups were able to demonstrate the appearance of autophagic vacuoles in Lc Purkinje neurons before degeneration, suggesting that upregulated autophagy is an early feature of dying Purkinje neurons (Yue et al., 2002; Selimi et al., 2003).

Autophagy is a degradative pathway responsible for the bulk of proteolysis in normal cells. Autophagy is an evolutionarily conserved pathway that leads to the degradation of proteins and entire organelles in cells undergoing stress; however, in extreme cases it can result in cellular dysfunction and cell death (Klionsky and Emr, 2000). Autophagy begins with the formation of double-membrane vesicles that sequester cytoplasm and organelles in autophagosomes (autophagic vacuoles in mammalian cells). The autophagosomes fuse with lysosomes, forming autophagolysosomes. The contents of autophagolysosomes are degraded by lysosomal enzymes into basic macromolecules, which are then recycled for use in essential cellular functions (Stromhaug and Klionsky, 2001).

Dysregulation of autophagolysosomal activity can lead to cell death and is implicated in several neurodegenerative conditions, including Parkinson's disease (Anglade et al., 1997), Alzheimer's disease (Cataldo et al., 1996; Nixon et al., 2000), Lewy body dementias (Zhu et al., 2003), Huntington's disease (Kegel et al., 2000; Petersen et al., 2001), and prion encephalopathies (Boellaard et al., 1991; Liberski et al., 2002). Nutrient deprivation, including withdrawal of serum (Mitchener et al., 1976), is one stimulus known to induce autophagy. In this report, we describe an *in vitro* model to investigate signaling pathways that regulate autophagy and survival in cerebellar Purkinje neurons. We used cerebellar cultures from early postnatal rats to investigate Purkinje neuron death in response to trophic factor withdrawal. In this model, Purkinje cell loss was characterized by extensive cytoplasmic vacuolation and a marked absence of nuclear condensation or fragmentation. The vacuoles stained with markers for autophagic vacuoles and lysosomes and the presence of abundant, enlarged autophago(lyso)somes was confirmed by transmission electron microscopy. The autophagy inhibitor 3-methyladenine diminished cytoplasmic vacuolation and moderately increased the survival of Purkinje neurons. Nerve growth factor (NGF) also inhibited autophagy and death of Purkinje neurons. The protective effects of NGF were mediated by the low-affinity p75 neurotrophin receptor (p75ntr). Our data support the hypothesis that p75ntr can regulate autophagy and death in Purkinje neurons.

Materials and Methods

Materials. Polyclonal antibodies to calbindin-D28k and p75ntr, monoclonal antibodies to NGF, and purified NGF were obtained from Chemicon (Temecula, CA). Polyclonal antibodies to NGF and monoclonal antibodies to phospho-TrkA were obtained from Santa Cruz Biotechnology (Santa Cruz, CA). The monoclonal phosphotyrosine antibody (Ab) was obtained from Upstate Cell Signaling Solutions (Lake Placid, NY). A polyclonal antibody to the intracellular domain of rat p75ntr was obtained from Covance (Berkeley, CA). Cy3- and FITC-conjugated secondary antibodies for immunocytochemistry were purchased from Jackson ImmunoResearch (West Grove, PA). Horseradish peroxidase-linked secondary antibodies and reagents for enhanced chemiluminescence detection were obtained from Amersham Biosciences (Piscataway, NJ). Lysosensor blue was obtained from Molecular Probes (Eugene, OR). Mono-dansylcadaverine, 3-methyladenine, and 4,6-diamidino-2-phenylindole (DAPI) were from Sigma (St. Louis, MO). Adenoviral cytomegalovirus (CMV; negative control adenovirus) was from Dr. Jerry Schack (University

of Colorado Health Sciences Center, Denver, CO). The adenoviral rat p75ntr myristylated intracellular domain (p75mICD) has been described previously (Roux et al., 2001).

Cell culture. Rat cerebellar granule neurons were isolated from 7-d-old Sprague Dawley rat pups as described previously (D'Mello et al., 1993). Briefly, neurons were plated at a density of 2.0×10^6 cells/ml in basal modified Eagle's medium (BME) containing 10% fetal bovine serum, 25 mM KCl, 2 mM L-glutamine, and penicillin (100 U/ml)-streptomycin (100 μ g/ml; Invitrogen, Gaithersburg, MD). Cytosine arabinoside (10 μ M) was added to the culture medium 24 hr after plating to limit the growth of non-neuronal cells. Experiments were performed after 7 d in culture. Death was induced by removing the serum- and high-potassium-containing media and replacing it with serum-free and 5 mM potassium BME.

Adenoviral infection. Five days after plating, neuronal cultures were infected with either control adenovirus (adenoviral CMV) or adenoviral p75ntr, full-length or truncated, mICD, each at the indicated multiplicity of infection. After infection, cells were returned to the incubator for 48 hr at 37°C and 10% CO₂. On day 7, neurons were processed for live cell imaging or fixed for immunocytochemistry.

Antisense. The p75ntr antisense and missense oligonucleotides (both at 5 μ M) were added to the cultures at the time of plating [day *in vitro* (DIV) 0] by repeatedly trituring the cells in the presence of the oligonucleotides before seeding. The oligonucleotides were present throughout the culture. Trophic factor withdrawal was performed on day 5 or 6 in culture (DIV 5 or 6) for either 24 or 48 hr. After this treatment, the cells were processed for live cell lysosensor experiments or fixed for immunocytochemistry to count Purkinje neurons. In all cases, the antisense was taken up by neurons with nearly 100% efficiency as assayed by visualization of the fluorescently labeled oligonucleotides. HPLC-purified phosphorothioate oligonucleotides were purchased from Integrated DNA Technologies (Coralville, IA). Sequences used were as follows: rat p75ntr 5' antisense, 5'-ACCTGCCCTCTCATTGCA-3'; and rat p75ntr 5' missense, 5'-CTCCCACTCGTCATTCGAC-3'. The rat 5' p75ntr antisense was also purchased with a 5' 56-FAM fluorescent label so that uptake by the neurons could be monitored. The antisense sequence used has been characterized previously and has been shown to be effective at inhibiting p75ntr-mediated cell death both *in vitro* and *in vivo* (Barrett and Bartlett, 1994; Cheema et al., 1996; Lowry et al., 2001).

Immunocytochemistry. Neuronal cultures were plated on polyethyleneimine-coated glass coverslips. Neurons were infected and induced to undergo death as indicated previously. After treatment, the neurons were fixed with 4% paraformaldehyde and then permeabilized and blocked with PBS, pH 7.4, containing 0.2% Triton X-100 and 5% BSA. Cells were then incubated with polyclonal antibodies against calbindin (1:250), active caspase-3 (1:500), or p75ntr (1:250) overnight at 4°C diluted in PBS containing 0.1% Triton X-100 and 2% BSA. Primary antibodies were then removed, and the cells were washed at least six times with PBS at room temperature. The neurons were then incubated with Cy3-conjugated donkey anti-rabbit secondary antibodies (1:500) and DAPI (1 μ g/ml) for 1 hr at room temperature. The cells were then washed at least six more times with PBS, and coverslips were adhered to glass slides with mounting medium (0.1% *p*-phenylenediamine in 75% glycerol in PBS). Imaging was performed on a Zeiss (Thornwood, NY) Axioplan 2 microscope equipped with a Cooke Sensicam deep-cooled CCD camera, and images were analyzed with the Slidebook software program (Intelligent Imaging Innovations Inc., Denver, CO).

Purkinje cell counts. Purkinje neuron numbers were measured by counting the number of calbindin-positive cells in 152 fields under 63 \times oil that were randomly selected by following a fixed grid pattern over the coverslip. The total area counted per coverslip was 14.6 mm² or ~13% of the coverslip. In addition to calbindin staining, cells were also judged on their morphology. Cells counted as Purkinje neurons had large rounded cell bodies, elaborate processes, and larger, more oval nuclei (in comparison with the smaller, rounder nuclei of granule neurons). Some very bright calbindin-positive cells that were either as small as the granule neurons, having bipolar processes, or very large flattened cells, lacking elaborate processes, were not counted because previous studies on *in vitro* differentiation of Purkinje neurons suggest that these cells may represent examples of delayed or aberrant development of Purkinje neu-

rons in culture (Baptista et al., 1994). At least three coverslips were counted per experimental condition. The numbers were averaged and expressed as a percentage of the average number counted in the appropriate controls. This was repeated for at least three independent experiments.

Live cell imaging and vacuolation measurements. Lysosensor blue and monodansylcadaverine (MDC) were added to the cultures at the end of the indicated treatments and returned to the incubator for 20 min. The cells were then washed three times with 37°C phenol red-free DMEM to remove nonspecifically bound dyes. The coverslips were mounted onto glass slides on ~10 μ l of phenol red-free DMEM; excess media were aspirated; and the coverslips were sealed and imaged immediately. Purkinje neurons were identified on the basis of their morphology (large, oval nuclei, large cell body, and multiple processes) by scanning the coverslips under bright-field differential interference contrast with a 63 \times oil objective. Images of the lysosensor blue and MDC fluorescence were captured on the DAPI and FITC channels, respectively, with the 100 \times oil objective. The lysosensor blue images were used to measure the diameters of all the visible lysosomes in at least six Purkinje neurons per condition. This was usually between 100 and 200 lysosomes. This was repeated for at least three independent experiments.

Transmission electron microscopy. Cultured cells were fixed in 2% paraformaldehyde and 2.5% glutaraldehyde for 1 hr, postfixed in 1% osmium tetroxide for 1 hr at 4°C, and processed for embedding in the culture dish. Cells were then gently scraped and embedded in blocks of Epon-araldite. Thin sections were stained with 4% aqueous uranyl acetate and lead citrate and examined on a Philips CM-12 electron microscope.

Lysate preparation. After incubation for the indicated times and with the reagents specified above, the culture medium was aspirated, cells were washed once with 2 ml of ice-cold PBS (PBS, pH 7.4), placed on ice, and scraped into lysis buffer (200 μ l/35 mm well) containing 20 mM HEPES, pH 7.4, 1% Triton X-100, 50 mM NaCl, 1 mM EGTA, 5 mM β -glycerophosphate, 30 mM sodium pyrophosphate, 100 μ M sodium orthovanadate, 1 mM phenylmethylsulfonyl fluoride, 10 μ g/ml leupeptin, and 10 μ g/ml aprotinin. Cell debris was removed by centrifugation at 6000 \times g for 3 min and the protein concentration of the supernatant was determined using a commercially available protein assay kit (Pierce, Rockford, IL). Equal amounts of supernatant protein were diluted to a final concentration of 1 \times SDS-PAGE sample buffer, boiled for 5 min, and electrophoresed through 7.5% polyacrylamide gels. Proteins were transferred to polyvinylidene membranes (Millipore, Bedford, MA) and processed for immunoblot analysis.

Immunoblot analysis. Nonspecific binding sites were blocked in PBS, pH 7.4, containing 0.1% Tween 20 (PBS-T) and 1% BSA for 1 hr at room temperature. Primary antibodies were diluted in blocking solution and incubated with the membranes for 1 hr. Excess primary Ab was removed by washing the membranes three times in PBS-T. The blots were then incubated with the appropriate horseradish peroxidase-

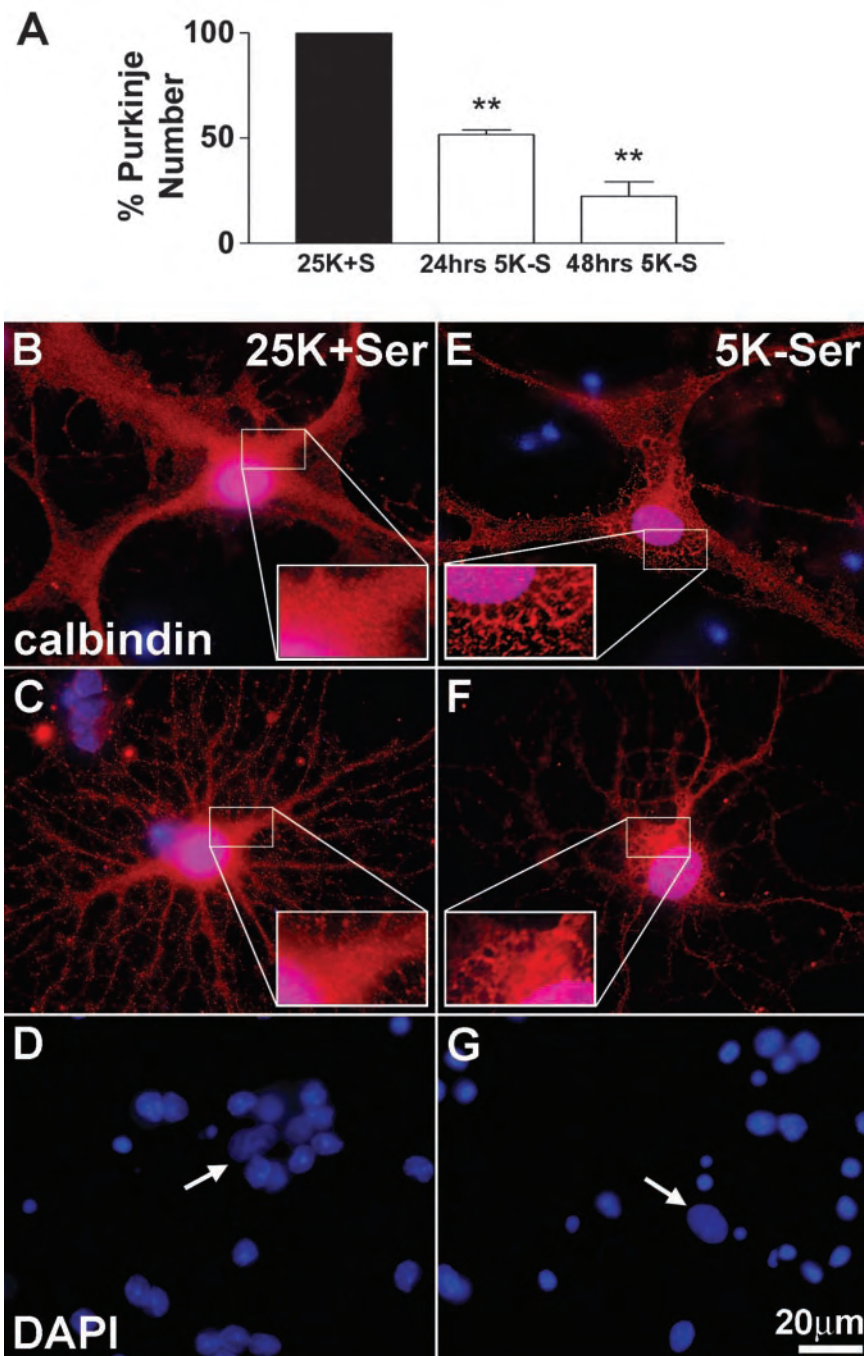


Figure 1. Trophic factor withdrawal induces a nonapoptotic death pathway in Purkinje neurons. Cultured cerebellar neurons were allowed to differentiate in medium containing 10% fetal calf serum and 25 mM potassium. On day 7, neurons were either maintained in control medium (25K + Ser) or subjected to trophic factor withdrawal medium (5K – Ser) for 24–48 hr. *A*, Purkinje number was quantified by counting the total number of calbindin-positive Purkinje cells in randomly chosen, equally sized areas per condition (total area, 14.6 mm²). Numbers are plotted as a percentage of control. Values represent the mean \pm SEM of three independent experiments each performed in triplicate. **Significant difference from 25K + S control at $p < 0.01$, one-way ANOVA, Tukey's *post hoc* test. *B–G*, Cells incubated in either control medium (*B–D*) or deprived of trophic factors (*E–G*) were fixed and stained with polyclonal antibodies against calbindin-D28k (a specific marker of Purkinje neurons; red) and the nuclear dye DAPI (blue). *B*, *C*, Purkinje neurons maintained in control medium demonstrate differentiated morphology. *D*, DAPI staining reveals the nuclei of healthy granule neurons and a Purkinje neuron (arrow). *E*, *F*, Trophic factor withdrawal induced extensive cytoplasmic vacuolation of Purkinje neurons (see magnified insets). *G*, DAPI staining reveals increased nuclear condensation and fragmentation in granule neurons, whereas there is a notable lack of nuclear condensation in Purkinje nuclei (arrow).

conjugated secondary Ab diluted in PBS-T for 1 hr and were subsequently washed three times in PBS-T. Immunoreactive proteins were detected by enhanced chemiluminescence. In some experiments, membranes were reprobbed after stripping in 0.1 M Tris-HCl, pH 8.0, 2% SDS, and

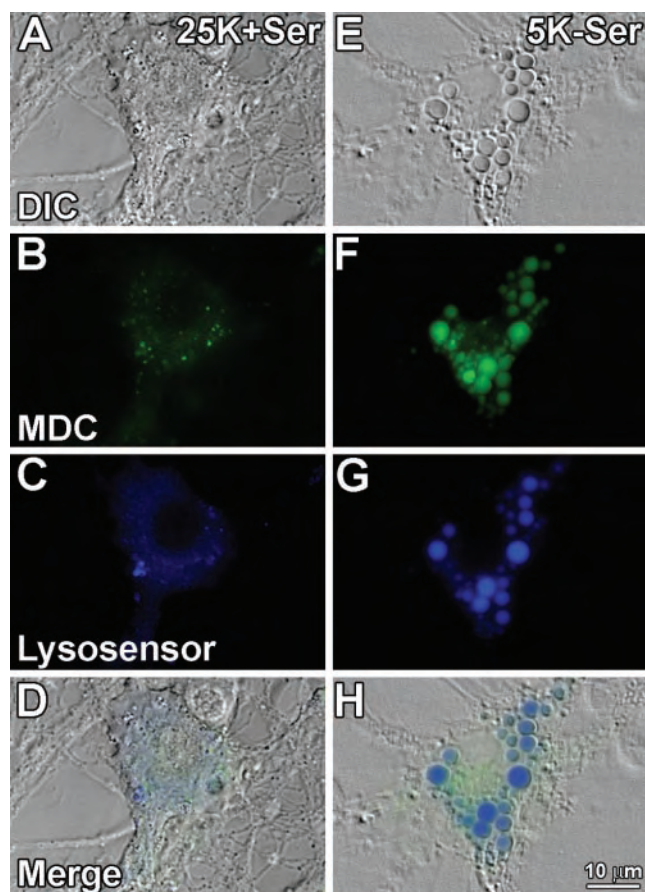


Figure 2. Autophagic and lysosomal markers stain vacuoles that form during Purkinje neuron degeneration. Purkinje neurons maintained in either control (25K+Ser) or trophic factor withdrawal (5K-Ser) media for 24 hr were stained with the autophagic marker MDC (green), and lysosensor blue, a pH-sensitive dye that fluoresces blue in acidic environments. Live cell imaging of control (A–D) and trophic factor-deprived (E–H) Purkinje neurons was performed. A, E, Bright-field images of cells identified as Purkinje neurons based on their morphology, characterized by a large cytoplasm (compared with granule neurons) and extensive neuronal processes. B, F, MDC staining demonstrating increases in autophagosomes in Purkinje neurons after trophic factor withdrawal. C, G, Lysosensor blue staining reveals acidic organelles (i.e., lysosomes) and demonstrates a marked increase in the size of lysosomes in Purkinje neurons after withdrawal of trophic factors. D, H, All three fields merged, demonstrating colabeling of some cytoplasmic vacuoles with both MDC and lysosensor blue indicative of autophagolysosomal fusion.

100 mM β -mercaptoethanol for 30 min at 52°C. The blots were rinsed twice in PBS-T and processed as above with a different primary Ab. Autoluminograms shown are representative of at least three independent experiments.

Data analysis. Results shown represent the means \pm SEM for the number of independent experiments performed. Statistical differences between the means of unpaired sets of data were evaluated using one-way ANOVA followed by *post hoc* Tukey's test; $p < 0.05$ was considered statistically significant.

Results

Trophic factor withdrawal results in a loss of Purkinje neurons that is morphologically distinct from apoptosis

We have investigated Purkinje neuron death induced by trophic factor withdrawal using primary cerebellar neuronal cultures. Although these cultures have been extensively used to study signaling pathways that regulate survival of cerebellar granule neurons (D'Mello et al., 1993; Linseman et al., 2002b; Vaudry et al., 2003), they also provide a model system for studying differentiated Purkinje neurons (Baptista et al., 1994). Primary neuronal cultures

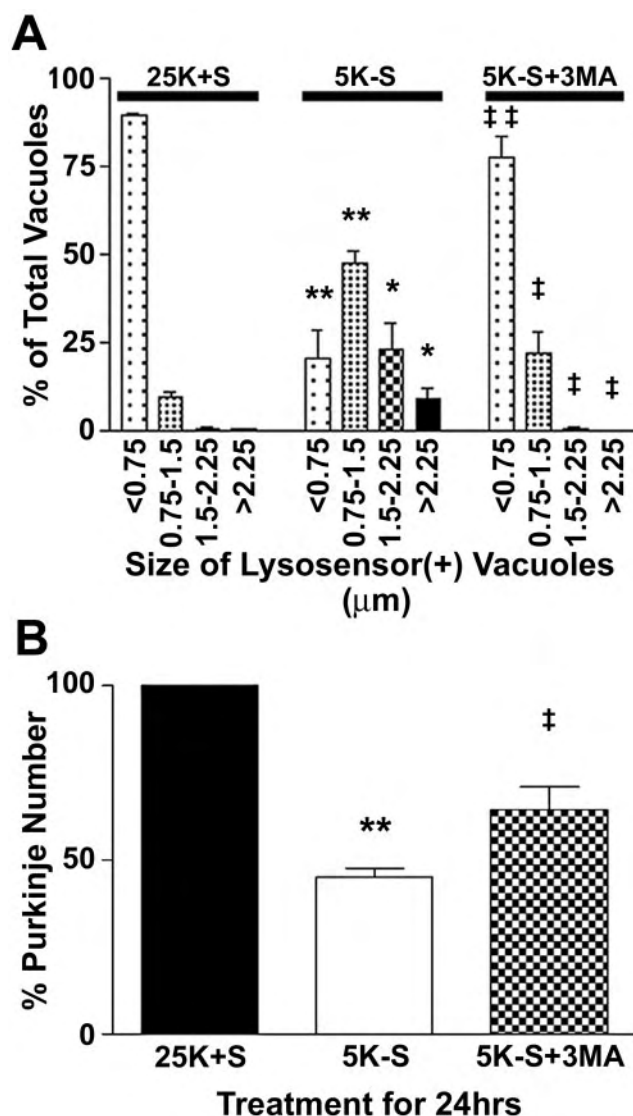


Figure 3. The autophagy inhibitor 3MA, blocks the increased vacuolation and loss of Purkinje neurons. Purkinje neurons were maintained in either control medium (25K+S) or trophic factor withdrawal medium (5K-S) in the absence or presence of 5 mM 3MA (5K-S+3MA) for 24 hr. A, The effects of the various treatments on vacuole size were quantified by measuring the diameters of all visible lysosensor blue-positive vacuoles in 6–12 Purkinje neurons per treatment condition in at least three independent experiments. Usually, the total number of vacuoles measured per condition was between 100 and 200. The size distribution was graphed as a percentage of total vacuoles that were within the indicated size ranges. B, Quantitation of the effects of 3MA on Purkinje neuron numbers demonstrate that addition of 5 mM 3MA to trophic withdrawal medium partially rescues Purkinje neurons from death after 24 hr of trophic factor withdrawal, compared with healthy controls. Numbers are mean \pm SEM values of seven independent experiments, each performed in triplicate. ***Significant difference from 25K+S (** $p < 0.01$; * $p < 0.05$). **†Significant difference from 5K-S († $p < 0.01$; † $p < 0.05$).

are derived from dissociated cerebella of early postnatal rats. These neuronal cultures survive and differentiate when maintained in medium containing 10% fetal calf serum and a depolarizing concentration of potassium (25 mM). Granule neurons, which constitute ~98% of the cell population, undergo classical apoptosis, characterized by chromatin condensation and caspase activation, when they are deprived of serum and depolarizing potassium (trophic factor withdrawal; (D'Mello et al., 1993; Linseman et al., 2002b).

In contrast, Purkinje neurons, which make up ~2% of the

culture, undergo a distinct nonapoptotic form of cell death in response to trophic factor withdrawal. Quantification of the number of Purkinje neurons after trophic factor withdrawal is shown in Figure 1A. Purkinje neurons were identified by staining with antibodies to the Purkinje marker calbindin-D28k. After 24 or 48 hr of trophic factor withdrawal, Purkinje numbers were 50.4 ± 1.4 and $22.3 \pm 7.0\%$ of controls, respectively. The remaining Purkinje neurons showed markedly different morphology from that of control cells, characterized by extensive cytoplasmic vacuolation (Fig. 1, compare control cells, *B, C*, with trophic factor-deprived cells, *E, F*). In contrast to granule neurons deprived of trophic support, which demonstrated substantial nuclear condensation and fragmentation characteristic of apoptosis (Fig. 1, compare *D, G*), Purkinje neurons showed no obvious signs of nuclear condensation or fragmentation (Fig. 1, compare nuclei indicated in *D, G*, arrows). The degenerating Purkinje neurons did not stain with propidium iodide, indicating that they retained membrane integrity throughout the death process (data not shown). The maintenance of membrane integrity suggested that Purkinje death did not occur by necrosis. Vacuole formation and subsequent loss of Purkinje neurons required new RNA synthesis because addition of the transcriptional inhibitor actinomycin D (ActD) decreased vacuolation and significantly increased the numbers of Purkinje cells to $78.7 \pm 1.5\%$ compared with $50.4 \pm 1.4\%$ ($p < 0.05$) after 24 hr of trophic factor withdrawal. The ability of ActD to protect Purkinje neurons further suggested that the mechanism of death was not necrotic but was rather a regulated program of cell suicide.

Purkinje neurodegeneration is associated with increased autophagy

Extensive cytoplasmic vacuolation was the most prominent morphological feature distinguishing healthy from degenerating Purkinje neurons in response to trophic factor withdrawal. To determine the mechanism underlying the loss of Purkinje neurons, we first characterized the nature of the vacuoles formed during withdrawal conditions. The formation of extensive cytoplasmic vacuoles is consistent with the upregulation of autophagy. The autofluorescent drug MDC has been shown to specifically accumulate in autophagic vacuoles (Biederbick et al., 1995; Munafò and Colombo, 2001). To determine whether autophagy was activated in Purkinje neurons subjected to trophic factor withdrawal, we incubated the cerebellar cultures with MDC and then visualized the MDC staining using live cell imaging techniques. In addition to MDC, the neurons were stained with lysosensor blue, a pH-sensitive dye that fluoresces in acidic compartments (pK_a , 5.2), thus specifically revealing lysosomes. These experiments demonstrated that control Purkinje neurons contained both lysosomal and autophagic vacuoles. However, in healthy

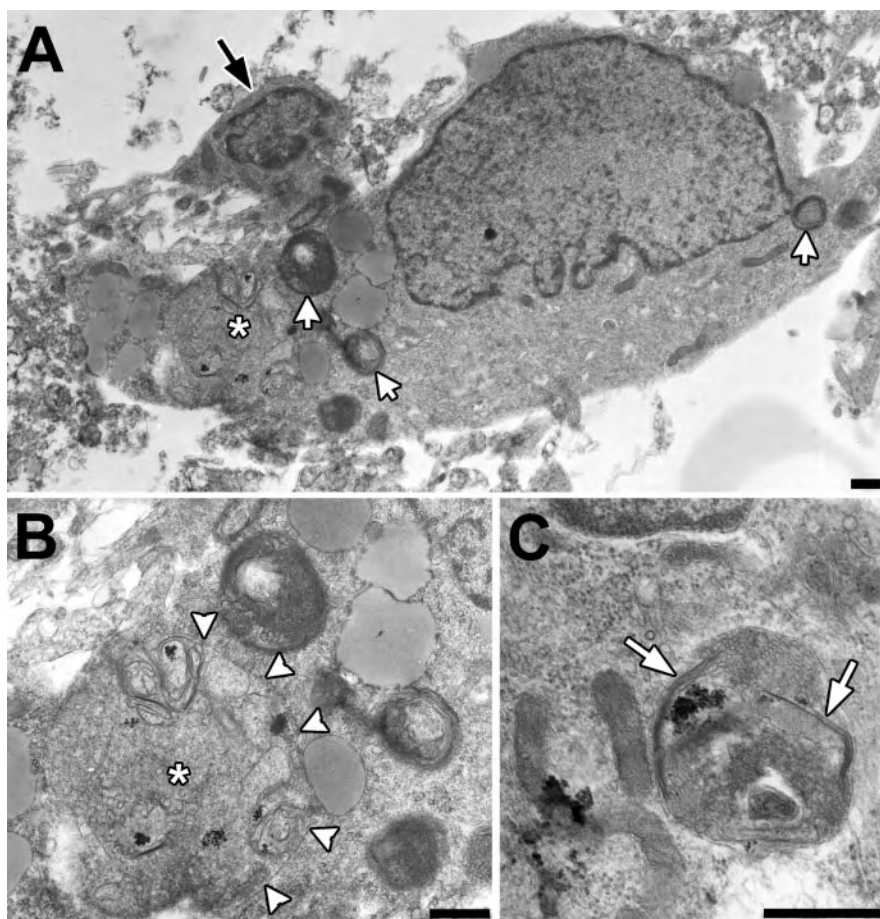


Figure 4. Transmission electron microscopy of Purkinje neurons after 24 hr of trophic factor withdrawal demonstrates ultrastructural features of autophagy. *A*, Low-power micrograph of a large Purkinje cell with multiple secondary lysosomes (white arrows) and a large autophagic vacuole (asterisk). In contrast, the smaller cerebellar granule neuron (black arrow) does not show these changes. *B*, Detail of the large autophagic vacuole indicated by the asterisk. There are disorganized membranous structures consistent with endoplasmic reticulum, ribosomes, and glycogen, delimited predominantly by a single membrane (white arrowheads). *C*, Micrograph showing an autophagosome delimited by a double membrane (white arrows). Note the similarity of the contents to adjacent mitochondria and cytoplasmic glycogen (lower left). Scale bars, 500 nm.

Purkinje neurons these vacuoles were on average very small (Fig. 2*A–D*). In contrast, 24 hr of trophic factor withdrawal induced a marked increase in the sizes of autophagic and lysosomal vacuoles, as detected by MDC and lysosensor blue staining, respectively (Fig. 2*E–H*).

To determine whether augmented autophagy contributed to Purkinje neuron death, we incubated the cultures with 5 mM 3-methyladenine (3MA), a drug known to inhibit the formation of autophagosomes (Seglen and Gordon, 1982). Quantitative analysis revealed that trophic factor withdrawal significantly increased the size of vacuoles in Purkinje neurons (Fig. 3*A*). In healthy Purkinje neurons, ~89% of the lysosensor blue-positive vacuoles were $<0.75 \mu\text{m}$ in diameter. After 24 hr of trophic factor withdrawal, most (~47%) of the lysosensor blue-positive vacuoles in the dying Purkinje neurons were much larger with a diameter, between 0.75 and $1.5 \mu\text{m}$, and a significant percentage (~32%) were $>1.5 \mu\text{m}$ in diameter. Addition of 5 mM 3MA to the cerebellar cultures almost completely maintained the lysosensor size profile of vacuoles in the range observed in control Purkinje neurons. The inhibition of autophagic activity by 3-methyladenine correlated with significantly increased numbers of Purkinje neurons that remained after 24 hr of trophic factor deprivation (Fig. 3*B*).

Electron microscopic analysis of autophagic vacuoles in trophic factor-deprived Purkinje neurons

Taken together, the above data suggested that autophagy is up-regulated in Purkinje neurons subjected to trophic factor withdrawal. Electron microscopy was performed on cerebellar cultures to confirm that the enlarged MDC- and lysosensor-positive vacuoles observed after trophic factor withdrawal were indeed autophagic vacuoles. The electron micrographs revealed that the cytoplasm of identified Purkinje cells showed multiple autophagosomes, multivesicular bodies, and other secondary lysosomes ranging in size from 0.7 to 3.0 μm after 24 hr of trophic factor withdrawal (Fig. 4). Some of these autophagic structures contained ribosomes, glycogen, and disorganized membranous organelles (Fig. 4A,B, asterisks, C). Occasionally, a double membrane was observed extending around cytoplasmic contents (Fig. 4C, white arrows), indicative of earlier stages of autophagy (Shelburne et al., 1973). The cytoplasm of Purkinje neurons also contained lipid droplets (Fig. 4A). In Purkinje neurons, the nuclear chromatin was uniformly dispersed (Fig. 4A). In contrast to the Purkinje neurons, large autophagolysosomes were absent from the granule neurons, which instead showed mild cytoplasmic condensation and peripheral chromatin clumping (Fig. 4A, black arrow).

Purkinje neuron autophagy and death are caspase-independent

Previous studies have shown that trophic factor withdrawal and other death-inducing stimuli can simultaneously induce both autophagy and apoptosis (Jia et al., 1997; Xue et al., 1999; Uchiyama, 2001). In these models, caspase activation and apoptosis occurred downstream of autophagy and could be blocked by 3MA. To determine whether the autophagic death pathway in Purkinje neurons acted in concert with caspase activation, we added the broad-spectrum caspase inhibitor zVAD-FMK to Purkinje neurons undergoing trophic factor withdrawal. Addition of zVAD-FMK (100 μM), which effectively inhibits caspase activity in cerebellar granule neurons, was unable to block Purkinje vacuolation or death. The numbers of Purkinje neurons remaining after 24 hr of trophic factor withdrawal in the absence and presence of zVAD-FMK were 55.7 ± 2.8 and 54.7 ± 3.5 , respectively. Furthermore, we were unable to detect increases in activated caspase-3 by immunocytochemical techniques in Purkinje neurons undergoing death induced by trophic factor withdrawal (data not shown). In contrast, activated caspase-3 immunoreactivity increases markedly in the granule neurons after trophic factor withdrawal (Linseman et al., 2003). These results suggest that neither autophagy nor death of Purkinje neurons required caspase activation.

NGF promotes survival and decreases autophagy in Purkinje neurons

Having established that trophic factor withdrawal induced autophagy and death of cerebellar Purkinje neurons, we next examined whether neurotrophin signaling could protect Purkinje neurons in this model. NGF is a neurotrophin known to promote the survival and differentiation of many types of neurons both *in vitro* and *in vivo*, including Purkinje neurons (Legrand and Clos, 1991; Cohen-Cory et al., 1993; Mount et al., 1998). We added NGF at various concentrations to the cultures at the time of trophic factor withdrawal and determined its effect on Purkinje survival. High concentrations of NGF (>50 ng/ml) significantly increased Purkinje numbers compared with trophic factor withdrawal alone (Fig. 5E). To determine whether NGF could

prevent extensive autophagic vacuolation, cultures were subjected to trophic factor withdrawal in the absence or presence of NGF, and quantitative analysis of vacuolation was performed using live cell lysosensor measurements (Fig. 5G). Again, in the presence of trophic support, the majority of Purkinje neurons contained small (<0.75 μm) lysosensor-positive vacuoles. After 24 hr of trophic factor withdrawal, most Purkinje neurons contained very large vacuoles, with 49% of vacuoles between 0.75 and 1.5 μm , $\sim 21\%$ of vacuoles between 1.5 and 2.25 μm , and $\sim 13\%$ of vacuoles >2.25 μm . The addition of NGF (2.5 $\mu\text{g/ml}$) to the trophic factor withdrawal media significantly decreased the overall vacuolation of Purkinje neurons. The lysosome size profile was shifted, with the majority of vacuoles ($\sim 76\%$) being <0.75 μm in diameter, $\sim 19\%$ of vacuoles between 0.75 and 1.5 μm , $\sim 4\%$ of vacuoles between 1.5 and 2.25 μm , and $<1\%$ of vacuoles >2.25 μm . Images shown are representative of the overall effects of the various treatments (Fig. 5A–C).

To determine whether decreasing NGF in the cerebellar cultures would be sufficient to induce autophagy and death of Purkinje neurons, we added NGF-neutralizing antibodies to the media and determined the effects on Purkinje survival and vacuolation. Addition of NGF-neutralizing antibodies to the cultures for 24 hr reduced the numbers of Purkinje neurons to $70.6 \pm 5.3\%$ of controls (Fig. 5F). Control IgG had no effect on the number of Purkinje neurons. The effect of the NGF-neutralizing antibodies was less than the effect of complete trophic factor withdrawal, which reduced Purkinje numbers to $45.2 \pm 2.7\%$ of control (Fig. 5F). To determine whether the NGF-neutralizing antibodies could induce autophagic vacuolation in Purkinje neurons, we performed live cell imaging experiments to measure the sizes of Purkinje lysosomes (Fig. 5H). Again, control Purkinje neurons contained mostly small lysosensor-positive vacuoles, whereas 24 hr of trophic factor withdrawal markedly induced the appearance of much larger vacuoles. Addition of NGF-neutralizing antibodies similarly increased the appearance of larger vacuoles in Purkinje neurons, although not to the same extent as trophic factor withdrawal. Control IgG had no effect on the size distribution of the vacuoles. The ability of NGF-neutralizing antibodies to induce the formation of vacuoles was also observed by calbindin staining (Fig. 5, compare A, D).

The protective effects of NGF on Purkinje neurons are independent of TrkA signaling

NGF exerts its effects by binding to two distinct receptors, the TrkA receptor and p75ntr. The high concentrations of NGF required to promote Purkinje survival suggested that the p75ntr receptor mediated the neuroprotective effects of NGF in these cultures. Further data supporting this hypothesis come from experiments showing that TrkA receptor tyrosine phosphorylation is high under basal conditions and does not change on trophic factor withdrawal (up to 6 hr) or on addition of high doses of NGF (Fig. 6A,B). Furthermore, Purkinje neurons demonstrated significantly increased autophagic vacuolation (within 3–4 hr of trophic factor withdrawal, as assessed by live cell lysosensor measurements of vacuole size; Fig. 6C) before any significant decrease in TrkA activation.

In the presence of trophic factors, the p75ntr supports Purkinje neuron survival

The p75 neurotrophin receptor is expressed throughout the developing cerebellum and demonstrates specific spatial and temporal regulation (Yan and Johnson, 1988; Carter et al., 2003). In

particular, p75^{ntr} is expressed in the developing Purkinje neurons by postnatal day 7, the time point at which we obtained our cerebellar cultures. p75^{ntr} immunoreactivity gradually decreases until it becomes absent from adult cerebellum; however, injury such as axotomy of Purkinje neurons results in marked re-expression of p75^{ntr} in the injured neurons (Martinez-Murillo et al., 1993). These data suggest that p75^{ntr} is involved in both the development of the cerebellum and injury responses in Purkinje neurons.

To determine whether p75^{ntr} was involved in mediating autophagy and death of Purkinje neurons, cerebellar cultures were incubated with antisense oligonucleotides directed against a 5' region spanning the initiation codon of the rat p75^{ntr} mRNA. This antisense sequence has been shown to be effective at preventing the NGF withdrawal or axotomy-induced death of dorsal root ganglion neurons (Barrett and Bartlett, 1994; Cheema et al., 1996) and the axotomy-induced death of spinal motor neurons (Lowry et al., 2001), which are mediated by p75^{ntr}. Dissociated cerebellar tissue was triturated with 5 μ M 56-FAM-labeled antisense or missense phosphorothioate oligonucleotides at the time of plating. The antisense entered both granule neurons and Purkinje neurons in the culture, with nearly 100% efficiency as assessed by fluorescence microscopy. The p75^{ntr} antisense had two distinct effects on the neurons in the culture. Inclusion of the antisense in the culture medium for 7 d resulted in a significant decrease in the basal survival of both cerebellar granule and Purkinje neurons. Purkinje neuron number with the p75^{ntr} antisense was $35 \pm 2.3\%$ of control cultures. The effect of the p75^{ntr} antisense on cell numbers was specific because cultures treated with scrambled missense oligonucleotides did not demonstrate diminished survival. Also, the loss of cells induced by p75^{ntr} antisense was not apparent until approximately day 4 or 5 in culture (as assessed by cell density by bright-field examination of the cultures). This corresponds to the time in culture when NGF production is first detectable by Western blot analysis (data not shown). These findings suggest that p75^{ntr} mediates survival in response to autocrine and paracrine neurotrophic factors such as NGF and possibly other neurotrophins such as brain-derived neurotrophic factor (BDNF) or neurotrophin-3 (NT-3), which are known to be secreted by cells in these cerebellar cultures (Favaron et al., 1993; Leingartner et al., 1994; Condorelli et al., 1998; Marini et al., 1998; Bhawe et al., 1999).

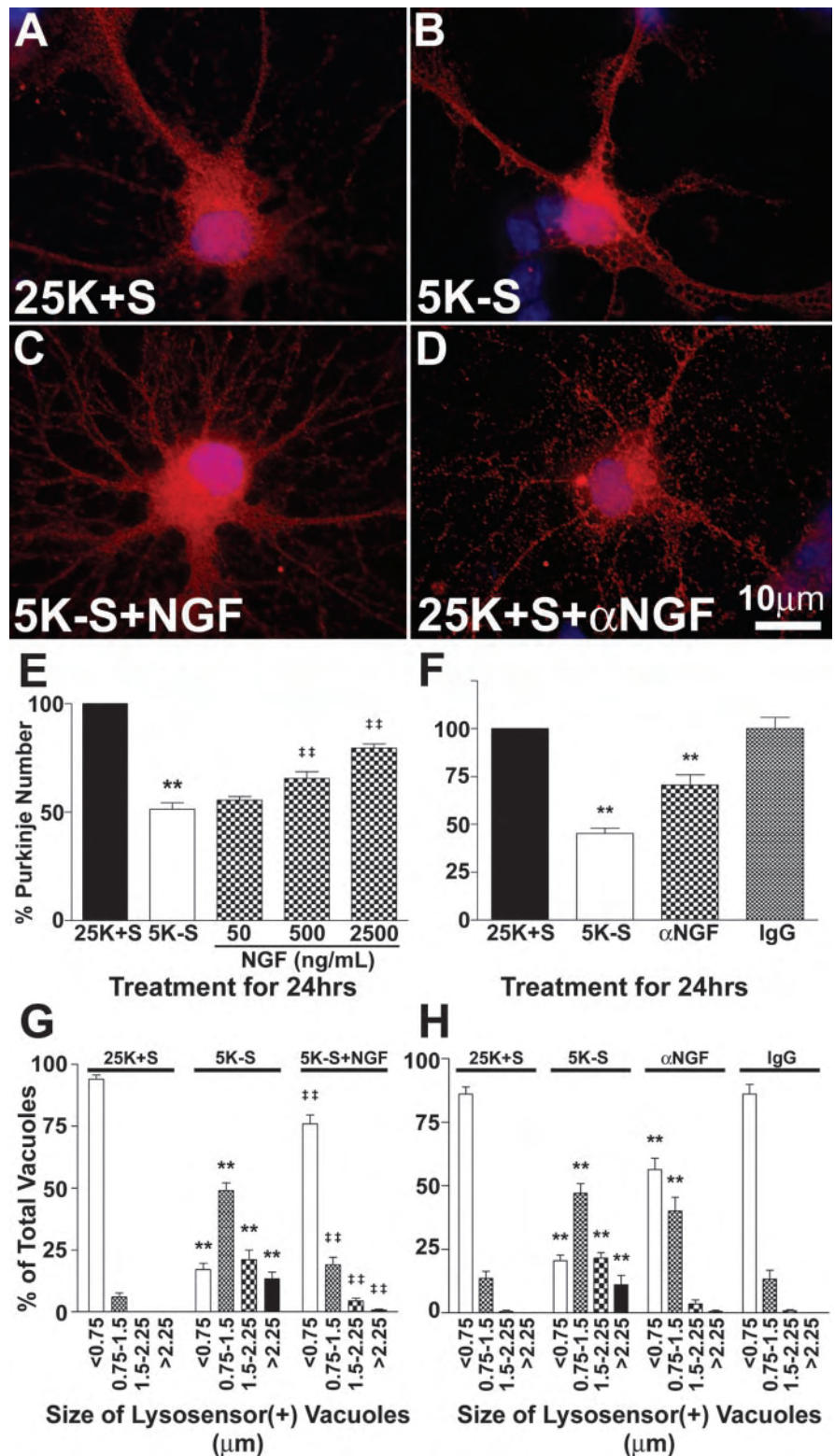


Figure 5. The neurotrophin NGF blocks the loss and the increased vacuolation of Purkinje neurons. *A–D*, Purkinje neurons maintained in various conditions were fixed and stained with antibodies to calbindin-D28k (a specific marker of Purkinje neurons; red) and the nuclear dye DAPI (blue). Images shown are representative of the effects of the various treatments. Purkinje neurons were maintained in control medium (*A*, 25K+S), trophic factor withdrawal medium (*B*, 5K–S), trophic factor withdrawal medium with 2500 ng/ml NGF (*C*, 5K–S+NGF), and control medium with 2 μ g/ml NGF-neutralizing antibodies (*D*, 25K+S+ α NGF) for 24 hr. *E*, Quantitation of the effects of NGF on Purkinje neuron numbers demonstrates that NGF partially rescues Purkinje neurons from death in a concentration-dependent manner after 24 hr of trophic factor withdrawal, compared with healthy controls. *F*, Quantitation of the effects of NGF-neutralizing antibodies on Purkinje neuron numbers demonstrates that depleting NGF from control media results in a loss of Purkinje neurons, whereas control antibodies had no effect on Purkinje survival. Numbers are mean \pm SEM values of at least three independent experiments, each performed in triplicate. *G*, *H*, The

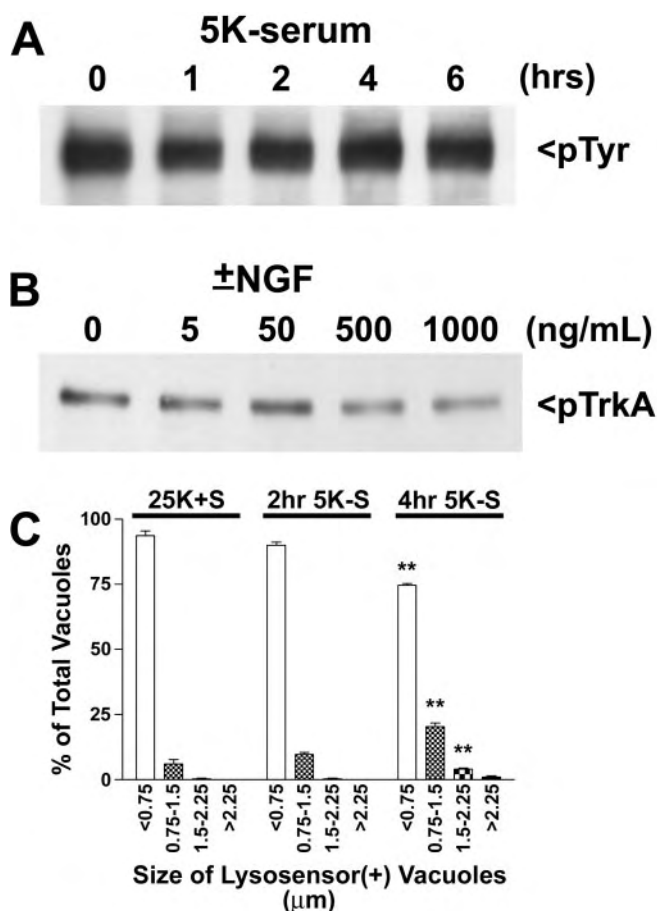


Figure 6. The protective effects of NGF are not mediated by TrkA. Immunoblot analysis was performed to determine the effects of trophic factor withdrawal and various doses of NGF on TrkA activation. *A*, Immunoblot of samples from cultures subjected to 0, 1, 2, 4, and 6 hr of trophic factor withdrawal with a phosphotyrosine-specific Ab. *B*, Immunoblot of samples from cultures subjected to acid wash, followed by 2 hr of trophic factor withdrawal and then incubation with 0, 5, 50, 500, or 1000 ng/ml of NGF for 10 min. *C*, The effects of a short time course of trophic factor withdrawal on vacuole size were quantified by measuring the diameters of all visible lysosensor blue-positive vacuoles in 6–12 Purkinje neurons per treatment condition in at least three independent experiments. Usually, the total number of vacuoles measured per condition was between 100 and 200. The size distribution was graphed as a percentage of total vacuoles that were within the indicated size ranges. ***Significant difference from 25K+S (** $p < 0.01$; * $p < 0.05$).

p75nr promotes autophagy and death of Purkinje neurons in the absence of trophic stimuli

In contrast to its effects on basal survival, the p75nr antisense completely blocked the death of Purkinje neurons induced by 48 hr of trophic factor withdrawal (Fig. 7A). Moreover, 5 μ M antisense decreased the autophagic vacuolation of Purkinje neurons elicited by 24 hr of trophic factor withdrawal (Fig. 7B). Again, in the presence of trophic support, most (~90%) of the Purkinje neuron lysosensor-positive vacuoles were <0.75 μ m, and only ~10% of vacuoles were between 0.75 and 1.5 μ m, with no vacu-

oles >1.5 μ m in diameter. After 24 hr of trophic factor withdrawal, most Purkinje neurons contained very large vacuoles, with ~49% of vacuoles between 0.75 and 1.5 μ m, ~13% of vacuoles between 1.5 and 2.25 μ m, and ~11% of vacuoles >2.25 μ m. Cultures that were preincubated with p75nr antisense oligonucleotides demonstrated a shifted lysosome size profile, with ~70% of vacuoles <0.75 μ m in diameter, ~26% of vacuoles between 0.75 and 1.5 μ m, ~4% of vacuoles between 1.5 and 2.25 μ m, and <1% of vacuoles >2.25 μ m. In contrast, missense oligonucleotides had no effect on the lysosome size profile of Purkinje neurons deprived of trophic support (Fig. 7B). Collectively, the above results indicate that antisense-mediated depletion of p75nr decreases the basal survival of Purkinje neurons in the presence of trophic support. However, under conditions of trophic factor withdrawal, decreasing p75nr provides a survival advantage to the remaining Purkinje neurons. The ability of p75nr to mediate both the survival and death in the same neuron depending on cellular context is consistent with previous reports of its effects on dorsal root ganglion neuron survival (Barrett and Bartlett, 1994; Sorensen et al., 2003).

Overexpression of a truncated p75nr lacking the extracellular domain induces Purkinje neuron autophagy and death in the presence of trophic support

To provide direct evidence that the p75nr can induce autophagy and death in Purkinje neurons, we investigated the effects of adenoviral-mediated overexpression of a myristoylated rat p75nr intracellular domain (p75mICD) protein. This p75nr truncation mutant was used because it lacks the ligand-binding domain, which would complicate the interpretation of results because of the presence of endogenous neurotrophins in these cultures. It has been shown that relatively low expression levels of this p75nr mutant mediate the survival of PC12 cells. In contrast, high levels of p75mICD expression induce efficient PC12 cell death (Roux et al., 2001). Finally, it has been demonstrated that the intracellular domain possesses the potent cell death-inducing activity of p75nr (Majdan et al., 1997; Coulson et al., 2000; Rabi-zadeh et al., 2000; Murray et al., 2003). Cultures were infected with recombinant control CMV or p75mICD adenoviruses at various multiplicities of infection (moi) on day 5 in culture. After incubation for 48 hr, the cultures were fixed and stained with polyclonal antibodies raised against the intracellular domain of rat p75nr (Majdan et al., 1997), followed by a Cy3-conjugated secondary antibody. Increases in p75nr immunoreactivity after infection with the p75mICD adenovirus were primarily and consistently observed in cells with morphologies typical of Purkinje neurons. Semiquantitative analysis of fluorescence images indicated that p75nr expression in p75mICD-infected Purkinje neurons was increased by 3.4-fold compared with uninfected controls or cells infected with control CMV adenovirus. To determine whether overexpression of p75mICD could induce Purkinje neuron death, infected neurons were fixed and stained with calbindin antibodies to quantify Purkinje numbers. Overexpression of p75mICD resulted in a dose-dependent loss of Purkinje neurons, with infection at 50 moi yielding similar levels of Purkinje cell loss, as was observed with trophic factor withdrawal (Fig. 8A). Infection with a control adenovirus at 50 moi did not induce significant Purkinje neuron death (Fig. 8A). To determine whether overexpression of p75mICD could induce autophagic vacuolation in Purkinje neurons, live cell quan-

effects of the various treatments on vacuole size were quantified by measuring the diameters of all visible lysosensor blue-positive vacuoles in 6–12 Purkinje neurons per treatment condition in at least three independent experiments. Usually, the total number of vacuoles measured per condition was between 100 and 200. The size distribution was graphed as a percentage of total vacuoles that were within the indicated size ranges. *G*, A high concentration of NGF (2500 ng/ml) significantly decreased the autophagic vacuolation of Purkinje neurons induced by 24 hr of trophic factor withdrawal. *H*, NGF-neutralizing antibodies significantly increased the vacuolation of Purkinje neurons in control media. *E–H*, ***Significant difference from 25K+S (** $p < 0.01$; * $p < 0.05$). **†Significant difference from 5K–S (** $p < 0.01$; † $p < 0.05$).

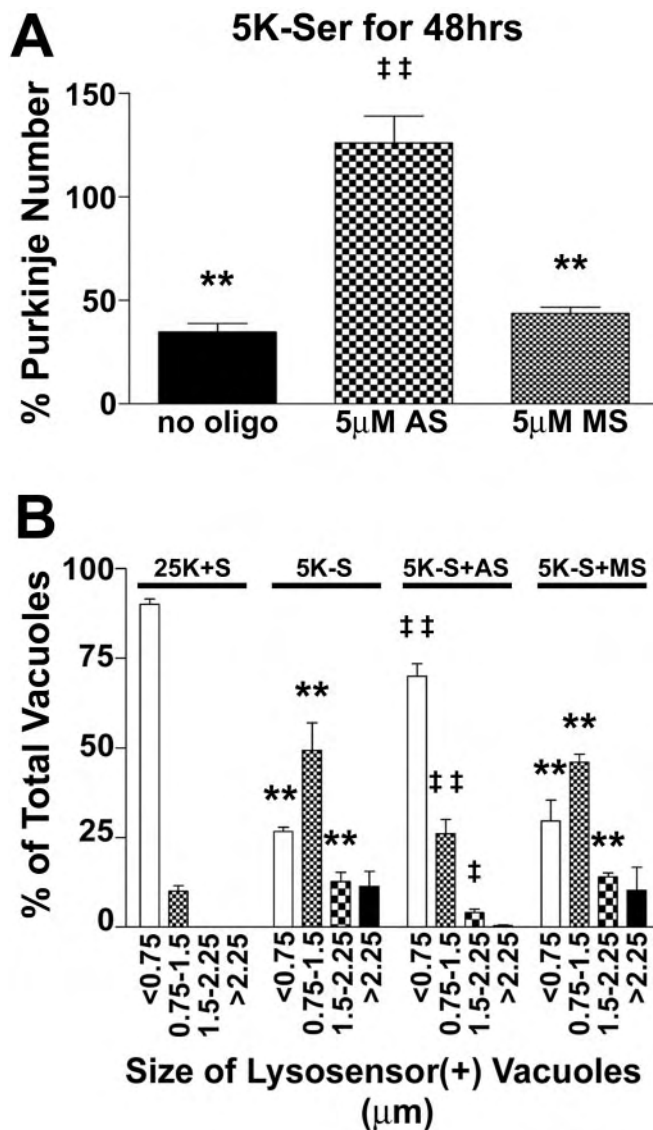


Figure 7. p75ntr antisense inhibits the loss and vacuolation of Purkinje neurons. Purkinje neurons maintained in various conditions were fixed and stained with antibodies to calbindin-D28k. *A*, Quantitation of the effects p75ntr antisense (AS) and missense (MS) oligonucleotides (oligo) on Purkinje neuron numbers expressed as the percentage of the appropriate control demonstrates that p75ntr antisense completely blocks the loss of Purkinje neurons induced by trophic factor withdrawal, whereas missense oligos had no effect on Purkinje survival. Numbers are mean \pm SEM values of at least three independent experiments, each performed in triplicate. *B*, The effects of the various treatments on vacuole size were quantified by measuring the diameters of all visible lysosensor blue-positive vacuoles in 6–12 Purkinje neurons per treatment condition in at least three independent experiments. Usually, the total number of vacuoles measured per condition was between 100 and 200. The size distribution was graphed as a percentage of total vacuoles that were within the indicated size ranges. ***Significant difference from 25K+S (** p < 0.01; * p < 0.05). ††Significant difference from 5K-S (†† p < 0.01; † p < 0.05).

tification of lysosome size was performed (Fig. 8*B*). Purkinje neurons that were infected with 50 moi of p75mICD adenovirus demonstrated significantly increased autophagic vacuolation, with only ~58% of vacuoles <0.75 μ m, ~32% of vacuoles between 0.75 and 1.5 μ m, ~7% of vacuoles between 1.5 and 2.25 μ m, and ~4% of vacuoles >2.25 μ m. Infection with 50 moi of control CMV adenovirus did not significantly increase Purkinje neuron vacuolation. In addition to increasing autophagic vacuolation, p75mICD infection caused notable membrane blebbing and, in some rare cases, nuclear condensation and fragmentation

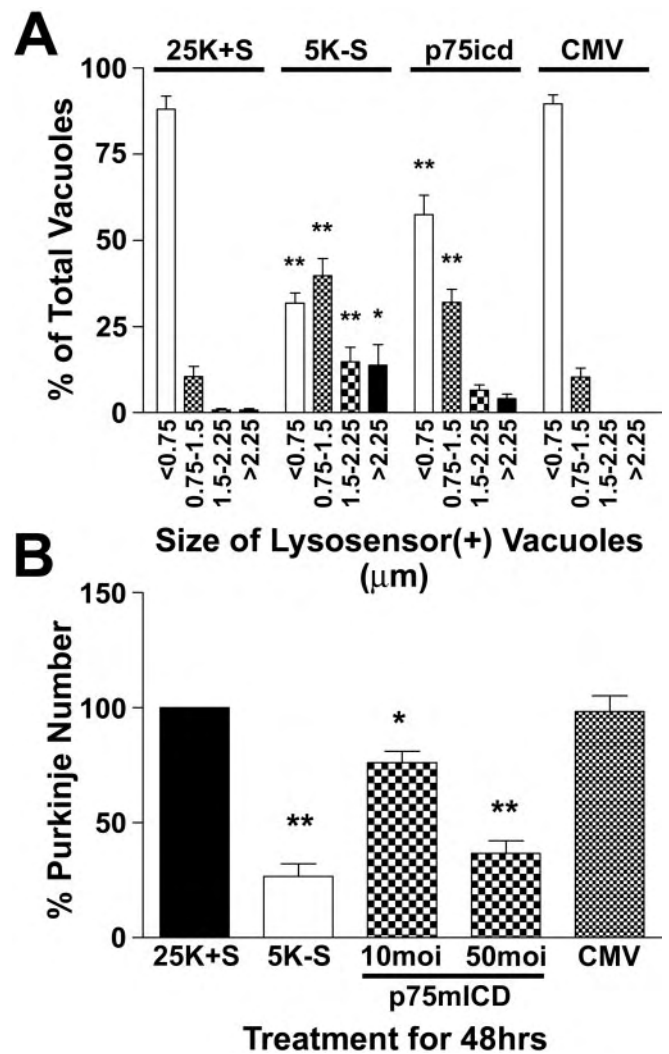


Figure 8. Overexpression of a truncated p75ntr receptor lacking the ligand-binding domain induces the loss and vacuolation of Purkinje neurons. Cultures were subjected to trophic factor withdrawal or adenoviral infection with either control CMV (at 50 moi) or myristoylated intracellular domain p75ntr (at both 10 and 50 moi) adenoviruses on DIV 5. *A*, The cells were fixed and stained with calbindin antibodies to determine Purkinje neuron numbers after the various treatments. *B*, The effects of p75mICD and CMV infection at 50 moi on vacuole size were quantified by measuring the diameters of all visible lysosensor blue-positive vacuoles in 6–12 Purkinje neurons per treatment condition in at least three independent experiments. Usually, the total number of vacuoles measured per condition was between 100 and 200. The size distribution was graphed as a percentage of total vacuoles that were within the indicated size ranges. ***Significant difference from 25K+S (** p < 0.01; * p < 0.05).

in Purkinje neurons. Our observations of increased autophagy with p75mICD expression are consistent with a previous report of p75ntr intracellular domain-induced death being morphologically characterized by increased vacuolation (Coulson et al., 2000), in addition to the regularly reported morphological features of apoptosis.

Discussion

Morphological studies of diseased human postmortem brain consistently reveal signs of increased autophagic activity in degenerating neuronal populations. There are multiple reports in the literature that describe autophagic vacuoles, as well as disturbances in the lysosomal degradative system in neurodegenerative conditions such as Alzheimer's disease (Cataldo et al., 1996; Nixon et al., 2000), Parkinson's disease (Anglade et al., 1997),

Huntington's disease (Kegel et al., 2000; Petersen et al., 2001), prion encephalopathies (Boellaard et al., 1991; Jeffrey et al., 1992), and diffuse Lewy body disease (Zhu et al., 2003). Extensive cytoplasmic vacuole formation, consistent with autophagy, also has been described in degenerating cerebellar Purkinje neurons in models of ischemia (Fessatidis et al., 1993; Barenberg et al., 2001) and in spinocerebellar ataxia 1 transgenic mice (Skinner et al., 2001). Recently, autophagy has been implicated in the death of cerebellar Purkinje neurons in the Lurcher mouse, which suffers from extensive Purkinje neuron degeneration caused by a point mutation in the $\delta 2$ glutamate receptor (Zuo et al., 1997). Two reports have also shown that Lurcher Purkinje neurons demonstrate ultrastructural features of autophagy at a time when they begin to degenerate (Yue et al., 2002; Selimi et al., 2003). In addition, overexpression of the mutant glutamate receptor induced autophagy and death in human embryonic kidney 293 cells (Yue et al., 2002). In the current study, we have shown that autophagy is greatly enhanced in Purkinje neurons that are dying as a result of trophic factor deprivation, and treatments that decrease autophagy are associated with increased survival, lending further support to the hypothesis that enhanced autophagy is involved in Purkinje neuron degeneration. Moreover, we have identified a role for p75^{ntr} as a possible mediator of autophagy and death in Purkinje neurons.

It is generally accepted that the neurotrophins NGF, BDNF, NT-3, and NT-4/5 promote survival and differentiation by binding to their cognate Trk receptors (Ibanez et al., 1992). In contrast, deciphering the role of p75^{ntr} signaling in mediating neurotrophin effects has been complicated by several factors. First, p75^{ntr} shares structural homologies with members of the tumor necrosis factor receptor family of death receptors and lacks intrinsic tyrosine kinase activity. Second, all four neurotrophins are able to bind to p75^{ntr} with similar affinity but display selectivity when binding to the Trk receptors (Klein et al., 1991a,b; Lamballe et al., 1991). Third, p75^{ntr} is often coexpressed with Trk receptors, and neurotrophin effects are dependent on the relative complements of Trk and p75 neurotrophin receptors (for review, see Rabizadeh and Bredesen, 2003). In this context, it has been shown that the presence of p75^{ntr} is required for high-affinity binding of neurotrophins to Trk receptors (Hempstead et al., 1991). Yet another layer of complexity is added when one considers that unprocessed proneurotrophins demonstrate higher-affinity binding to p75^{ntr} but have negligible binding to Trk receptors (Lee et al., 2001). Finally, p75^{ntr} may also function as a coreceptor with the Nogo receptor (Wang et al., 2002) or as a receptor for prion (Della-Bianca et al., 2001) and β -amyloid proteins (Yaar et al., 1997). These complexities in neurotrophin signaling may provide some explanation for the paradoxical roles ascribed to p75^{ntr} in the literature. Expression of p75^{ntr} is capable of inducing death, especially when neurotrophin concentrations are limited (Rabizadeh et al., 1993; Barrett and Georgiou, 1996). In addition, p75^{ntr} signaling can result in death in response to neurotrophin binding (Casaccia-Bonnel et al., 1996; Frade et al., 1996; Kuner and Hertel, 1998; Friedman, 2000). In contrast, other reports suggest that p75^{ntr} plays an important and necessary role in mediating survival in response to neurotrophins (Barrett and Bartlett, 1994; Barrett et al., 1998; DeFreitas et al., 2001; Bui et al., 2002).

In the current report, we provide evidence that p75^{ntr} plays an important role in mediating autophagy and death of cerebellar Purkinje neurons induced by trophic factor withdrawal. The promotion of survival and the reduction of autophagic vacuolation required high concentrations of NGF, suggesting the involve-

ment of p75^{ntr}. TrkA phosphorylation was not correlated with the autophagic vacuolation induced by trophic factor withdrawal or with neuroprotection mediated by NGF. Decreasing available neurotrophin with NGF-neutralizing antibodies induced autophagic vacuolation and death of Purkinje neurons. Antisense to p75^{ntr} decreased autophagy and completely inhibited the loss of Purkinje neurons in response to trophic factor withdrawal. Moreover, adenoviral-mediated overexpression of a myristoylated rat p75^{ntr} intracellular domain protein (p75^{mICD}) resulted in significantly increased autophagic vacuolation that was also accompanied by a significant loss of Purkinje neurons. Finally, our results directly show that Purkinje neuron death induced by either trophic factor withdrawal or p75^{mICD} overexpression is associated with increased autophagic vacuolation, suggesting an important role for autophagy during Purkinje neuron degeneration.

Our results with p75^{ntr} antisense suggest a dual role for p75^{ntr} in mediating both the survival and death of Purkinje neurons. Antisense to p75^{ntr} decreased the survival of Purkinje neurons maintained in healthy conditions. The loss of neurons induced with p75^{ntr} antisense occurred at a time when NGF synthesis becomes detectable, suggesting that p75^{ntr} is required for the basal survival of the cerebellar neurons that is mediated by autocrine and paracrine neurotrophin production in these cultures. In contrast, Purkinje neurons pretreated with p75^{ntr} antisense were completely resistant to death and demonstrated decreased vacuolation in response to trophic factor withdrawal. Collectively, our results suggest that neurotrophin signaling through p75^{ntr} can regulate the survival and death of Purkinje neurons. One can speculate that in the presence of appropriate neurotrophin, signaling from p75^{ntr} can promote Purkinje survival, and decreasing neurotrophin levels can lead to a loss of prosurvival p75^{ntr} signals. However, it is also possible that a loss of appropriate neurotrophins not only leads to a loss of prosurvival signals but also may result in the generation of prodeath signals from p75^{ntr}. This concept of p75^{ntr} as a dependence receptor has been hypothesized by others to explain the paradoxical nature of p75^{ntr} function (Rabizadeh et al., 2000). In addition, our data have not formally ruled out the possibility that trophic factor withdrawal results in an increase of some ligand that promotes prodeath p75^{ntr} signals because there is evidence in the literature that p75^{ntr} may have other ligands or may also function as a coreceptor with other proteins (Yaar et al., 1997; Della-Bianca et al., 2001; Wang et al., 2002).

Despite the evidence suggesting that autophagy is upregulated in neurodegeneration, very little is known about the cellular mechanisms that regulate autophagy in neurons (for review, see Yuan et al., 2003). Several reports suggest that the activation of autophagy contributes to the death of neurons (Xue et al., 1999; Uchiyama, 2001; Borsello et al., 2003; Weeks, 2003). In contrast, other studies indicate a neuroprotective role for autophagy in Huntington's disease and α -synucleinopathies (Qin et al., 2003; Webb et al., 2003). These studies demonstrate that autophagy may be a mechanism for mutant protein degradation and the prevention of plaque formation. Similarly, in cases in which mitochondria are extensively damaged, autophagy may be protective by sequestering and degrading defective mitochondria before they can release death-inducing proteins (Lemasters et al., 2002; Tolkovsky et al., 2002). One can speculate that the degree and specificity of autophagy may determine cell fate. By elucidating the molecular pathways that regulate autophagy, it may be possible to determine which components of autophagy may contribute to neurodegeneration and which may be neuroprotective. In

addition to the questions regarding autophagy as a survival or death mechanism, it will be of great importance to understand the effects of autophagy on neuronal function, such as the formation and maintenance of synapses, the transduction of electrical impulses, and neurotransmitter release.

References

- Anglade P, Vyas S, Javoy-Agid F, Herrero MT, Michel PP, Marquez J, Mouatt-Prigent A, Ruberg M, Hirsch EC, Agid Y (1997) Apoptosis and autophagy in nigral neurons of patients with Parkinson's disease. *Histol Histopathol* 12:25–31.
- Bailey A, Luthert P, Dean A, Harding B, Janota I, Montgomery M, Rutter M, Lantos P (1998) A clinicopathological study of autism. *Brain* 121:889–905.
- Baptista CA, Hatten ME, Blazeski R, Mason CA (1994) Cell-cell interactions influence survival and differentiation of purified Purkinje cells in vitro. *Neuron* 12:243–260.
- Barenberg P, Strahlendorf H, Strahlendorf J (2001) Hypoxia induces an excitotoxic-type of dark cell degeneration in cerebellar Purkinje neurons. *Neurosci Res* 40:245–254.
- Barrett GL, Bartlett PF (1994) The p75 nerve growth factor receptor mediates survival or death depending on the stage of sensory neuron development. *Proc Natl Acad Sci USA* 91:6501–6505.
- Barrett GL, Georgiou A (1996) The low-affinity nerve growth factor receptor p75NGFR mediates death of PC12 cells after nerve growth factor withdrawal. *J Neurosci Res* 45:117–128.
- Barrett GL, Georgiou A, Reid K, Bartlett PF, Leung D (1998) Rescue of dorsal root sensory neurons by nerve growth factor and neurotrophin-3, but not brain-derived neurotrophic factor or neurotrophin-4, is dependent on the level of the p75 neurotrophin receptor. *Neuroscience* 85:1321–1328.
- Bhave SV, Ghoda L, Hoffman PL (1999) Brain-derived neurotrophic factor mediates the anti-apoptotic effect of NMDA in cerebellar granule neurons: signal transduction cascades and site of ethanol action. *J Neurosci* 19:3277–3286.
- Biederbeck A, Kern HF, Elsasser HP (1995) Monodansylcadaverine (MDC) is a specific in vivo marker for autophagic vacuoles. *Eur J Cell Biol* 66:3–14.
- Boellaard JW, Kao M, Schlote W, Diringer H (1991) Neuronal autophagy in experimental scrapie. *Acta Neuropathol (Berl)* 82:225–228.
- Borghesani PR, Alt FW, Bottaro A, Davidson L, Aksoy S, Rathbun GA, Roberts TM, Swat W, Segal RA, Gu Y (2000) Abnormal development of Purkinje cells and lymphocytes in *Atm* mutant mice. *Proc Natl Acad Sci USA* 97:3336–3341.
- Borsello T, Croquelois K, Hornung JP, Clarke PG (2003) *N*-methyl-D-aspartate-triggered neuronal death in organotypic hippocampal cultures is endocytic, autophagic and mediated by the *c-Jun* N-terminal kinase pathway. *Eur J Neurosci* 18:473–485.
- Bui NT, König HG, Culmsee C, Bauerbach E, Poppe M, Kriegelstein J, Prehn JH (2002) p75 neurotrophin receptor is required for constitutive and NGF-induced survival signalling in PC12 cells and rat hippocampal neurons. *J Neurochem* 81:594–605.
- Carter AR, Berry EM, Segal RA (2003) Regional expression of p75NTR contributes to neurotrophin regulation of cerebellar patterning. *Mol Cell Neurosci* 22:1–13.
- Casaccia-Bonnel P, Carter BD, Dobrowsky RT, Chao MV (1996) Death of oligodendrocytes mediated by the interaction of nerve growth factor with its receptor p75. *Nature* 383:716–719.
- Cataldo AM, Hamilton DJ, Barnett JL, Paskevich PA, Nixon RA (1996) Properties of the endosomal-lysosomal system in the human central nervous system: disturbances mark most neurons in populations at risk to degenerate in Alzheimer's disease. *J Neurosci* 16:186–199.
- Cheema SS, Barrett GL, Bartlett PF (1996) Reducing p75 nerve growth factor receptor levels using antisense oligonucleotides prevents the loss of axotomized sensory neurons in the dorsal root ganglia of newborn rats. *J Neurosci Res* 46:239–245.
- Cohen-Cory S, Elliott RC, Dreyfus CF, Black IB (1993) Depolarizing influences increase low-affinity NGF receptor gene expression in cultured Purkinje neurons. *Exp Neurol* 119:165–175.
- Condorelli DF, Dell'Albani P, Timmusk T, Mudo G, Belluardo N (1998) Differential regulation of BDNF and NT-3 mRNA levels in primary cultures of rat cerebellar neurons. *Neurochem Int* 32:87–91.
- Coulson EJ, Reid K, Baca M, Shipham KA, Hulet SM, Kilpatrick TJ, Bartlett PF (2000) Chopper, a new death domain of the p75 neurotrophin receptor that mediates rapid neuronal cell death. *J Biol Chem* 275:30537–30545.
- DeFreitas MF, McQuillen PS, Shatz CJ (2001) A novel p75NTR signaling pathway promotes survival, not death, of immunopurified neocortical subplate neurons. *J Neurosci* 21:5121–5129.
- Della-Bianca V, Rossi F, Armato U, Dal-Pra I, Costantini C, Perini G, Politi V, Della Valle G (2001) Neurotrophin p75 receptor is involved in neuronal damage by prion peptide-(106–126). *J Biol Chem* 276:38929–38933.
- D'Mello SR, Galli C, Ciotti T, Calissano P (1993) Induction of apoptosis in cerebellar granule neurons by low potassium: inhibition of death by insulin-like growth factor I and cAMP. *Proc Natl Acad Sci USA* 90:10989–10993.
- Favaron M, Manev RM, Rimland JM, Candeo P, Beccaro M, Manev H (1993) NMDA-stimulated expression of BDNF mRNA in cultured cerebellar granule neurons. *NeuroReport* 4:1171–1174.
- Ferrer I, Saracibar N, Gonzalez G (1991) Spongiform encephalopathy and multisystemic degeneration. *Neurologia* 6:29–33.
- Fessatidis IT, Thomas VL, Shore DF, Hunt RH, Weller RO (1993) Neuro-pathological features of profoundly hypothermic circulatory arrest: an experimental study in the pig. *Cardiovasc Surg* 1:155–160.
- Frade JM, Rodriguez-Tebar A, Barde YA (1996) Induction of cell death by endogenous nerve growth factor through its p75 receptor. *Nature* 383:166–168.
- Friedman WJ (2000) Neurotrophins induce death of hippocampal neurons via the p75 receptor. *J Neurosci* 20:6340–6346.
- Gatti RA, Vinters HV (1985) Cerebellar pathology in ataxia-telangiectasia: the significance of basket cells. *Kroc Found Ser* 19:225–232.
- Ghez C, Thach WT (2000) The cerebellum. In: *Principles of neuroscience* (Kandel ER, Schwartz JH, Jessell TM, eds), pp 832–852. New York: McGraw-Hill.
- Hempstead BL, Martin-Zanca D, Kaplan DR, Parada LF, Chao MV (1991) High-affinity NGF binding requires coexpression of the *trk* proto-oncogene and the low-affinity NGF receptor. *Nature* 350:678–683.
- Ibanez CF, Ebendal T, Barbany G, Murray-Rust J, Blundell TL, Persson H (1992) Disruption of the low affinity receptor-binding site in NGF allows neuronal survival and differentiation by binding to the *trk* gene product. *Cell* 69:329–341.
- Jeffrey M, Scott JR, Williams A, Fraser H (1992) Ultrastructural features of spongiform encephalopathy transmitted to mice from three species of bovidae. *Acta Neuropathol (Berl)* 84:559–569.
- Jia L, Dourmashkin RR, Allen PD, Gray AB, Newland AC, Kelsey SM (1997) Inhibition of autophagy abrogates tumour necrosis factor alpha induced apoptosis in human T-lymphoblastic leukaemic cells. *Br J Haematol* 98:673–685.
- Kegel KB, Kim M, Sapp E, McIntyre C, Castano JG, Aronin N, DiFiglia M (2000) Huntingtin expression stimulates endosomal-lysosomal activity, endosome tubulation, and autophagy. *J Neurosci* 20:7268–7278.
- Klein R, Jing SQ, Nanduri V, O'Rourke E, Barbacid M (1991a) The *trk* proto-oncogene encodes a receptor for nerve growth factor. *Cell* 65:189–197.
- Klein R, Nanduri V, Jing SA, Lamballe F, Tapley P, Bryant S, Cordon-Cardo C, Jones KR, Reichardt LF, Barbacid M (1991b) The *trkB* tyrosine protein kinase is a receptor for brain-derived neurotrophic factor and neurotrophin-3. *Cell* 66:395–403.
- Klionsky DJ, Emr SD (2000) Autophagy as a regulated pathway of cellular degradation. *Science* 290:1717–1721.
- Koeppen AH (1998) The hereditary ataxias. *J Neuropathol Exp Neurol* 57:531–543.
- Kuner P, Hertel C (1998) NGF induces apoptosis in a human neuroblastoma cell line expressing the neurotrophin receptor p75NTR. *J Neurosci Res* 54:465–474.
- Lamballe F, Klein R, Barbacid M (1991) *trkC*, a new member of the *trk* family of tyrosine protein kinases, is a receptor for neurotrophin-3. *Cell* 66:967–979.
- Lasmezias CI, Deslys JP, Robain O, Jaegly A, Beringue V, Peyrin JM, Fournier JG, Hauw JJ, Rossier J, Dormont D (1997) Transmission of the BSE agent to mice in the absence of detectable abnormal prion protein. *Science* 275:402–405.
- Lee R, Kermani P, Teng KK, Hempstead BL (2001) Regulation of cell survival by secreted proneurotrophins. *Science* 294:1945–1948.
- Legrand C, Clos J (1991) Biochemical, immunocytochemical and morphological evidence for an interaction between thyroid hormone and nerve growth factor in the developing cerebellum of normal and hypothyroid rats. *Dev Neurosci* 13:382–396.
- Leingartner A, Heisenberg CP, Kolbeck R, Thoenen H, Lindholm D (1994) Brain-derived neurotrophic factor increases neurotrophin-3 expression in cerebellar granule neurons. *J Biol Chem* 269:828–830.
- Lemasters JJ, Qian T, He L, Kim JS, Elmore SP, Cascio WE, Brenner DA (2002) Role of mitochondrial inner membrane permeabilization in necrotic cell death, apoptosis, and autophagy. *Antioxid Redox Signal* 4:769–781.

- Liberski PP, Gajdusek DC, Brown P (2002) How do neurons degenerate in prion diseases or transmissible spongiform encephalopathies (TSEs): neuronal autophagy revisited. *Acta Neurobiol Exp (Warsz)* 62:141–147.
- Linseman DA, McClure ML, Bouchard RJ, Laessig TA, Ahmadi FA, Heidenreich KA (2002a) Suppression of death receptor signaling in cerebellar Purkinje neurons protects neighboring granule neurons from apoptosis via an insulin-like growth factor I-dependent mechanism. *J Biol Chem* 277:24546–24553.
- Linseman DA, Phelps RA, Bouchard RJ, Le SS, Laessig TA, McClure ML, Heidenreich KA (2002b) Insulin-like growth factor-I blocks Bcl-2 interacting mediator of cell death (Bim) induction and intrinsic death signaling in cerebellar granule neurons. *J Neurosci* 22:9287–9297.
- Linseman DA, Bartley CM, Le SS, Laessig TA, Bouchard RJ, Meintzer MK, Li M, Heidenreich KA (2003) Inactivation of the myocyte enhancer factor-2 repressor histone deacetylase-5 by endogenous Ca^{2+} /calmodulin-dependent kinase II promotes depolarization-mediated cerebellar granule neuron survival. *J Biol Chem* 278:41472–41481.
- Lowry KS, Murray SS, Coulson EJ, Epa R, Bartlett PF, Barrett G, Cheema SS (2001) Systemic administration of antisense p75(NTR) oligodeoxynucleotides rescues axotomized spinal motor neurons. *J Neurosci Res* 64:11–17.
- Majdan M, Lachance C, Gloster A, Aloyz R, Zeindler C, Bamji S, Bhakar A, Belliveau D, Fawcett J, Miller FD, Barker PA (1997) Transgenic mice expressing the intracellular domain of the p75 neurotrophin receptor undergo neuronal apoptosis. *J Neurosci* 17:6988–6998.
- Marini AM, Rabin SJ, Lipsky RH, Mocchiatti I (1998) Activity-dependent release of brain-derived neurotrophic factor underlies the neuroprotective effect of *N*-methyl-D-aspartate. *J Biol Chem* 273:29394–29399.
- Martinez-Murillo R, Caro L, Nieto-Sampedro M (1993) Lesion-induced expression of low-affinity nerve growth factor receptor-immunoreactive protein in Purkinje cells of the adult rat. *Neuroscience* 52:587–593.
- Mitchener JS, Shelburne JD, Bradford WD, Hawkins HK (1976) Cellular autophagocytosis induced by deprivation of serum and amino acids in HeLa cells. *Am J Pathol* 83:485–491.
- Mount HT, Elkabes S, Dreyfus CF, Black IB (1998) Differential involvement of metabotropic and p75 neurotrophin receptors in effects of nerve growth factor and neurotrophin-3 on cultured Purkinje cell survival. *J Neurochem* 70:1045–1053.
- Munafa DB, Colombo MI (2001) A novel assay to study autophagy: regulation of autophagosome vacuole size by amino acid deprivation. *J Cell Sci* 114:3619–3629.
- Murray SS, Bartlett PF, Lopes EC, Coulson EJ, Greferath U, Cheema SS (2003) Low-affinity neurotrophin receptor with targeted mutation of exon 3 is capable of mediating the death of axotomized neurons. *Clin Exp Pharmacol Physiol* 30:217–222.
- Nixon RA, Cataldo AM, Mathews PM (2000) The endosomal-lysosomal system of neurons in Alzheimer's disease pathogenesis: a review. *Neurochem Res* 25:1161–1172.
- Petersen A, Larsen KE, Behr GG, Romero N, Przedborski S, Brundin P, Sulzer D (2001) Expanded CAG repeats in exon 1 of the Huntington's disease gene stimulate dopamine-mediated striatal neuron autophagy and degeneration. *Hum Mol Genet* 10:1243–1254.
- Qin ZH, Wang Y, Kegel KB, Kazantsev A, Apostol BL, Thompson LM, Yoder J, Aronin N, DiFiglia M (2003) Autophagy regulates the processing of amino terminal Huntingtin fragments. *Hum Mol Genet* 12:3231–3244.
- Rabizadeh S, Bredesen DE (2003) Ten years on: mediation of cell death by the common neurotrophin receptor p75(NTR). *Cytokine Growth Factor Rev* 14:225–239.
- Rabizadeh S, Oh J, Zhong LT, Yang J, Bitler CM, Butcher LL, Bredesen DE (1993) Induction of apoptosis by the low-affinity NGF receptor. *Science* 261:345–348.
- Rabizadeh S, Ye X, Sperandio S, Wang JJ, Ellerby HM, Ellerby LM, Giza C, Andrusiak RL, Frankowski H, Yaron Y, Moayeri NN, Rovelli G, Evans CJ, Butcher LL, Nolan GP, Assa-Munt N, Bredesen DE (2000) Neurotrophin dependence domain: a domain required for the mediation of apoptosis by the p75 neurotrophin receptor. *J Mol Neurosci* 15:215–229.
- Ritvo ER, Freeman BJ, Scheibel AB, Duong T, Robinson H, Guthrie D, Ritvo A (1986) Lower Purkinje cell counts in the cerebella of four autistic subjects: initial findings of the UCLA-NSAC Autopsy Research Report. *Am J Psychiatry* 143:862–866.
- Roux PP, Bhakar AL, Kennedy TE, Barker PA (2001) The p75 neurotrophin receptor activates Akt (protein kinase B) through a phosphatidylinositol 3-kinase-dependent pathway. *J Biol Chem* 276:23097–23104.
- Seglen PO, Gordon PB (1982) 3-Methyladenine: specific inhibitor of autophagic/lysosomal protein degradation in isolated rat hepatocytes. *Proc Natl Acad Sci USA* 79:1889–1892.
- Selimi F, Lohof AM, Heitz S, Lalouette A, Jarvis CI, Bailly Y, Mariani J (2003) Lurcher GRID2-induced death and depolarization can be dissociated in cerebellar Purkinje cells. *Neuron* 37:813–819.
- Shelburne JD, Arstila AU, Trump BF (1973) Studies on cellular autophagocytosis: cyclic AMP- and dibutyryl cyclic AMP-stimulated autophagy in rat liver. *Am J Pathol* 72:521–540.
- Skinner PJ, Vierra-Green CA, Clark HB, Zoghbi HY, Orr HT (2001) Altered trafficking of membrane proteins in purkinje cells of SCA1 transgenic mice. *Am J Pathol* 159:905–913.
- Sorensen B, Tandrup T, Koltzenburg M, Jakobsen J (2003) No further loss of dorsal root ganglion cells after axotomy in p75 neurotrophin receptor knockout mice. *J Comp Neurol* 459:242–250.
- Stromhaug PE, Klionsky DJ (2001) Approaching the molecular mechanism of autophagy. *Traffic* 2:524–531.
- Tolkovsky AM, Xue L, Fletcher GC, Borutaite V (2002) Mitochondrial disappearance from cells: a clue to the role of autophagy in programmed cell death and disease? *Biochimie* 84:233–240.
- Torres-Aleman I, Pons S, Arevalo MA (1994) The insulin-like growth factor I system in the rat cerebellum: developmental regulation and role in neuronal survival and differentiation. *J Neurosci Res* 39:117–126.
- Uchiyama Y (2001) Autophagic cell death and its execution by lysosomal cathepsins. *Arch Histol Cytol* 64:233–246.
- Vaudry D, Falluel-Morel A, Leuillet S, Vaudry H, Gonzalez BJ (2003) Regulators of cerebellar granule cell development act through specific signaling pathways. *Science* 300:1532–1534.
- Wang KC, Kim JA, Sivasankaran R, Segal R, He Z (2002) P75 interacts with the Nogo receptor as a co-receptor for Nogo, MAG and OMgp. *Nature* 420:74–78.
- Watanabe R, Duchon LW (1993) Cerebral amyloid in human prion disease. *Neuropathol Appl Neurobiol* 19:253–260.
- Watake K, Weeber EJ, Xu B, Antalffy B, Yuva-Paylor L, Hashimoto K, Kano M, Atkinson R, Sun Y, Armstrong DL, Sweatt JD, Orr HT, Paylor R, Zoghbi HY (2002) A long CAG repeat in the mouse Sca1 locus replicates SCA1 features and reveals the impact of protein solubility on selective neurodegeneration. *Neuron* 34:905–919.
- Webb JL, Ravikumar B, Atkins J, Skepper JN, Rubinsztein DC (2003) α -Synuclein is degraded by both autophagy and the proteasome. *J Biol Chem* 278:25009–25013.
- Weeks JC (2003) Thinking globally, acting locally: steroid hormone regulation of the dendritic architecture, synaptic connectivity and death of an individual neuron. *Prog Neurobiol* 70:421–442.
- Wetts R, Herrup K (1982) Interaction of granule, Purkinje and inferior olivary neurons in lurcher chimaeric mice. I. Qualitative studies. *J Embryol Exp Morphol* 68:87–98.
- Xue L, Fletcher GC, Tolkovsky AM (1999) Autophagy is activated by apoptotic signalling in sympathetic neurons: an alternative mechanism of death execution. *Mol Cell Neurosci* 14:180–198.
- Yaar M, Zhai S, Pilch PF, Doyle SM, Eisenhauer PB, Fine RE, Gilchrist BA (1997) Binding of beta-amyloid to the p75 neurotrophin receptor induces apoptosis: A possible mechanism for Alzheimer's disease. *J Clin Invest* 100:2333–2340.
- Yan Q, Johnson Jr EM (1988) An immunohistochemical study of the nerve growth factor receptor in developing rats. *J Neurosci* 8:3481–3498.
- Yuan J, Lipinski M, Degtrev A (2003) Diversity in the mechanisms of neuronal cell death. *Neuron* 40:401–413.
- Yue Z, Horton A, Bravin M, DeJager PL, Selimi F, Heintz N (2002) A novel protein complex linking the delta 2 glutamate receptor and autophagy: implications for neurodegeneration in lurcher mice. *Neuron* 35:921–933.
- Zanjani HS, Herrup K, Guastavino JM, Delhaye-Bouchaud N, Mariani J (1994) Developmental studies of the inferior olivary nucleus in staggerer mutant mice. *Brain Res Dev Brain Res* 82:18–28.
- Zhu JH, Guo F, Shelburne J, Watkins S, Chu CT (2003) Localization of phosphorylated ERK/MAP kinases to mitochondria and autophagosomes in Lewy body diseases. *Brain Pathol* 13:473–481.
- Zuo J, De Jager PL, Takahashi KA, Jiang W, Linden DJ, Heintz N (1997) Neurodegeneration in Lurcher mice caused by mutation in delta2 glutamate receptor gene. *Nature* 388:769–773.

Glycogen Synthase Kinase-3 β Phosphorylates Bax and Promotes Its Mitochondrial Localization during Neuronal Apoptosis

Daniel A. Linseman,* Brent D. Butts,* Thomas A. Precht, Reid A. Phelps, Shoshona S. Le, Tracey A. Laessig, Ron J. Bouchard, Maria L. Florez-McClure, and Kim A. Heidenreich

Department of Pharmacology, University of Colorado Health Sciences Center, and Denver Veterans Affairs Medical Center, Denver, Colorado 80262

Glycogen synthase kinase-3 β (GSK-3 β) is a critical activator of neuronal apoptosis induced by a diverse array of neurotoxic insults. However, the downstream substrates of GSK-3 β that ultimately induce neuronal death are unknown. Here, we show that GSK-3 β phosphorylates and regulates the activity of Bax, a pro-apoptotic Bcl-2 family member that stimulates the intrinsic (mitochondrial) death pathway by eliciting cytochrome *c* release from mitochondria. In cerebellar granule neurons undergoing apoptosis, inhibition of GSK-3 β suppressed both the mitochondrial translocation of an expressed green fluorescent protein (GFP)-Bax α fusion protein and the conformational activation of endogenous Bax. GSK-3 β directly phosphorylated Bax α on Ser163, a residue found within a species-conserved, putative GSK-3 β phosphorylation motif. Coexpression of GFP-Bax α with a constitutively active mutant of GSK-3 β , GSK-3 β (Ser9Ala), enhanced the *in vivo* phosphorylation of wild-type Bax α , but not a Ser163Ala mutant of Bax α , in transfected human embryonic kidney 293 (HEK293) cells. Moreover, cotransfection with constitutively active GSK-3 β promoted the localization of Bax α to mitochondria and induced apoptosis in both transfected HEK293 cells and cerebellar granule neurons. In contrast, neither a Ser163Ala point mutant of Bax α nor a naturally occurring splice variant that lacks 13 amino acids encompassing Ser163 (Bax α _{cr}) were driven to mitochondria in HEK293 cells coexpressing constitutively active GSK-3 β . In a similar manner, either mutation or deletion of the identified GSK-3 β phosphorylation motif prevented the localization of Bax to mitochondria in cerebellar granule neurons undergoing apoptosis. Our results indicate that GSK-3 β exerts some of its pro-apoptotic effects in neurons by regulating the mitochondrial localization of Bax, a key component of the intrinsic apoptotic cascade.

Key words: glycogen synthase kinase; cerebellar granule neuron; apoptosis; mitochondria; Bax; phosphorylation

Introduction

Aberrant neuronal apoptosis contributes to the progression of several neurodegenerative disorders (Vila and Przedborski, 2003). Protein kinases are key regulators of neuronal cell fate and can be broadly categorized into anti-apoptotic and pro-apoptotic groups. Anti-apoptotic kinases, including AKT and ERK (extracellular signal-regulated kinase), are activated downstream of neurotrophic factor receptors (Fukunaga and Miyamoto, 1998; Brunet et al., 2001). In contrast, protein kinases that play pro-apoptotic roles in neurons, including JNK (c-Jun NH₂-terminal

kinase) and glycogen synthase kinase-3 β (GSK-3 β), are activated by a variety of neuronal insults (Mielke and Herdegen, 2000; Kaytor and Orr, 2002). In particular, GSK-3 β is a critical activator of cell death in numerous models of neuronal apoptosis (Hetman et al., 2000; Li et al., 2000; Perez et al., 2003; Phiel et al., 2003).

Identification of substrates of GSK-3 β may provide insight into the cellular mechanisms that underlie neurodegeneration. To date, the three most studied substrates of GSK-3 β include the metabolic enzyme glycogen synthase, the microtubule bundling protein tau, and a mediator of the Wnt signaling pathway and cell–cell adhesion, β -catenin (Doble and Woodgett, 2003). Although hyperphosphorylation of tau by GSK-3 β has been implicated in the pathogenesis of Alzheimer's disease (Kaytor and Orr, 2002), the contribution of this phosphorylation event to neuronal death in other models of neurodegeneration is less well established. Moreover, although the GSK-3 β -mediated phosphorylation of β -catenin targets this protein for degradation, phosphorylation-site mutants of β -catenin fail to protect neurons from apoptosis under conditions in which GSK-3 β inhibition is neuroprotective (Hetman et al., 2000). These findings suggest that additional unidentified substrates of GSK-3 β exist that mediate its pro-apoptotic action in neurons.

Received Jan. 21, 2004; revised Sept. 9, 2004; accepted Sept. 27, 2004.

This work was supported by Department of Veterans Affairs Merit Awards (K.A.H. and D.A.L.), Department of Defense Grant USAMRMC 03281009 (K.A.H. and D.A.L.), National Institutes of Health (NIH) Grant NS38619-01A1 (K.A.H.), and the Department of Veterans Affairs Research Enhancement Award Program (K.A.H. and D.A.L.). Molecular Biology Core Services were supported by NIH Diabetes Endocrinology Research Care Grant P30-DK57516. We thank Dr. R. J. Youle (National Institute of Neurological Disorders and Stroke, NIH, Bethesda, MD) for GFP-Bax α , Dr. R. Bertrand (University of Montreal, Montreal, Quebec, Canada) for the Bax α _{cr} construct, and Dr. M. J. Birnbaum (University of Pennsylvania, Philadelphia, PA) for HA-GSK-3 β S9A.

*D.A.L. and B.D.B. contributed equally to this work.

Correspondence should be addressed to Dr. Kim A. Heidenreich, Department of Pharmacology, University of Colorado Health Sciences Center at Fitzsimons, P.O. Box 6511, Mail Stop 8303, Aurora, CO 80045-0511. E-mail: Kim.Heidenreich@UCHSC.edu.

DOI:10.1523/JNEUROSCI.2057-04.2004

Copyright © 2004 Society for Neuroscience 0270-6474/04/249993-10\$15.00/0

Neuronal apoptosis often occurs via an intrinsic apoptotic cascade triggered by the translocation of Bax, a pro-apoptotic Bcl-2 family member, to mitochondria. In response to signals generated by BH3-only Bcl-2 family members, such as Bim and Bid, Bax oligomerizes at the outer mitochondrial membrane and forms a pore that releases cytochrome *c* from the mitochondria (Zong et al., 2001). Cytosolic cytochrome *c* then interacts with Apaf-1 and pro-caspase-9 to form a functional apoptosome that ultimately activates downstream executioner caspases (Zou et al., 1999). Many models of neuronal apoptosis occur via this Bax-dependent mitochondrial pathway (Cregan et al., 1999; Putcha et al., 1999; Selimi et al., 2000; Vila et al., 2001). Yet despite the prevalence of Bax involvement in neuronal apoptosis, the cellular mechanisms that regulate this Bcl-2 family member, particularly the role of phosphorylation, have not been clearly defined.

In the current study, we used primary cultures of cerebellar granule neurons (CGNs) isolated from postnatal rats to investigate the role of GSK-3 β in the regulation of Bax function. CGNs require serum and depolarizing extracellular potassium for their survival *in vitro* and die via a mitochondrial apoptotic cascade when deprived of this trophic support (D'Mello et al., 1993; Linseman et al., 2002). CGN apoptosis is dependent on both Bax translocation to mitochondria and activation of GSK-3 β (Li et al., 2000; Putcha et al., 2002). Thus, this is an ideal cell model in which to examine the interaction of Bax and GSK-3 β during neuronal apoptosis.

Materials and Methods

Reagents. A plasmid encoding an N-terminal green fluorescent protein (GFP) fusion protein of human Bax $_{\alpha}$ was kindly provided by Dr. R. J. Youle (National Institute of Neurological Disorders and Stroke, National Institutes of Health, Bethesda, MD). Enhanced GFP (pEGFP) vector, monoclonal antibody for immunoprecipitation of GFP, and polyclonal living colors antibody for immunoblotting of GFP were from BD Biosciences Clontech (Palo Alto, CA). Tetramethylrhodamine ethyl ester (TMRE) dye and an antibody to cytochrome *c* oxidase subunit IV (COX IV) were from Molecular Probes (Eugene, OR). Monoclonal antibody to the hemagglutinin (HA) epitope tag and polyclonal antibodies to phospho-GSK-3 β (Ser9) and total GSK-3 β were obtained from Cell Signaling Technologies (Beverly, MA). Insulin-like growth factor I (IGF-I), LiCl, Hoechst dye 33258, and 4',6-diamidino-2-phenylindole (DAPI) were from Sigma (St. Louis, MO). GSK-3 β inhibitor II and a specific peptide inhibitor of GSK-3 β were from Calbiochem (San Diego, CA). Monoclonal antibody to the active conformation of Bax (clone 6A7) was purchased from Alexis Biochemicals (San Diego, CA). Recombinant, active GSK-3 β was from Upstate Biotechnology (Charlottesville, VA). [γ -³²P]ATP (3000 Ci/mmol), ³²P as orthophosphate (10 mCi/ml), horseradish peroxidase-linked secondary antibodies, and reagents for enhanced chemiluminescence detection were obtained from Amersham Biosciences (Piscataway, NJ). Empty pcDNA3.1 vector was obtained from Invitrogen (Carlsbad, CA). A plasmid encoding HA-tagged GSK-3 β (Ser9Ala) was provided by Dr. M. J. Birnbaum (University of Pennsylvania, Philadelphia, PA). A plasmid encoding Bax $_{\alpha}$ was provided by Dr. R. Bertrand (University of Montreal, Montreal, Quebec, Canada). FITC- and cyanine 3 (Cy3)-conjugated secondary antibodies for immunofluorescence were from Jackson ImmunoResearch (West Grove, PA).

Cell culture. Rat CGNs were isolated from 7-d-old Sprague Dawley rat pups (15–19 gm), as described previously (Li et al., 2000). Briefly, neurons were plated on 35-mm-diameter plastic dishes coated with poly-L-lysine at a density of 2.0×10^6 cells/ml in basal modified Eagle's medium containing 10% fetal bovine serum, 25 mM KCl, 2 mM L-glutamine, and penicillin (100 U/ml)–streptomycin (100 μ g/ml) (Invitrogen). Cytosine arabinoside (10 μ M) was added to the culture medium 24 hr after plating to limit the growth of non-neuronal cells. Using this protocol, the cultures were ~95% pure for granule neurons. In general, experiments were performed after 6–7 d in culture. Human embryonic kidney 293

(HEK293) cells were maintained in standard DMEM containing 10% fetal calf serum and routinely passaged every 3–4 d.

Transfection of primary CGNs. CGNs were transiently transfected using the Helios Gene-Gun system (Bio-Rad, Hercules, CA). Briefly, 60 μ g of plasmid DNA was precipitated onto 30 mg of 0.6- μ m-diameter gold beads in a CaCl₂–spermidine mixture. The gold/DNA precipitates were washed three times in 100% ethanol and resuspended in 3 ml of ethanol containing 0.05 mg/ml polyvinylpyrrolidone. After thoroughly resuspending the gold/DNA precipitate, it was drawn into ~74 cm of Tefzel tubing, and the beads were allowed to settle to the bottom of the tubing. After 5 min, the ethanol was slowly drawn off while the beads adhered to the tubing. The tubing was dried under nitrogen for an additional 5 min and then cut into ~1.3 cm pieces. These pieces can be stored desiccated at 4°C for ~6 weeks. CGNs to be transfected were seeded at a density of 8×10^5 cells/well on polyethyleneimine-coated glass coverslips in 24-well plates (Corning, Corning, NY). After 5 d in culture, the medium was removed from the wells, and the 1.3 cm lengths of tubing containing the DNA-bound beads were loaded into the Gene-Gun and shot with a burst of ~100 psi helium through a 40 μ m nylon cell strainer placed over the well. The medium was replaced immediately, and cells were grown an additional 48 hr before image analysis. For experiments in which GFP-Bax $_{\alpha}$ was cotransfected with either pcDNA3.1 or HA-GSK-3 β (S9A), the ratio of plasmids coprecipitated onto the gold beads was 60:1 for empty vector or GSK-3 β to the Bax fusion protein.

Transfection of HEK293 cells. HEK293 cells were grown to ~90% confluency in 35-mm-diameter tissue culture plates. Aliquots (500 ng) of the various GFP–Bax plasmids and 4 μ g of either constitutively active HA-GSK3 β Ser9Ala or the empty vector control plasmid (pcDNA3.1) were transiently transfected using the Lipofectamine 2000 reagent (Invitrogen) according to the manufacturer's protocol. Cells were grown for 24 hr, after which they were fixed for microscopic imaging analysis of GFP–Bax localization. For morphological assessment of apoptosis, transfected cells were grown for 48 hr before quantitation of apoptosis.

Quantitation of GFP–Bax localization. CGNs or HEK293 cells, which were transfected with various GFP–Bax plasmids, were washed once with PBS and fixed for 20 min in 4% paraformaldehyde. GFP–Bax localization was assessed in HEK293 cells using a 63 \times water immersion objective. Localization in CGNs was performed under 63 \times oil after adhering the coverslips to glass slides. Cells were examined for GFP fluorescence and were scored as either diffuse (if the staining observed in the FITC channel was diffuse throughout the cell) or mitochondrial (if the staining observed in the FITC channel localized to discrete subcellular locations within the cytoplasm and around the nucleus). Results for HEK293 cells are averages of blinded quantitations from at least three independent experiments per group in which ~200 transfected cells were counted per group per experiment. Data for CGNs represent quantitative analysis of at least three separate experiments in which ~200 transfected CGNs were analyzed per fusion protein under both control and apoptotic conditions.

Immunocytochemistry. CGNs were cultured on polyethyleneimine-coated glass coverslips at a density of $\sim 2.5 \times 10^5$ cells per coverslip. After transfection and incubation as described in Results, cells were fixed in 4% paraformaldehyde and were then permeabilized and blocked in PBS, pH 7.4, containing 0.2% Triton X-100 and 5% BSA. Cells were then incubated for ~16 hr at 4°C with primary antibody diluted in PBS containing 0.2% Triton X-100 and 2% BSA. The primary antibody was aspirated, and the cells were washed five times with PBS. The cells were then incubated with either Cy3-conjugated or FITC-conjugated secondary antibodies and DAPI for 1 hr at room temperature. CGNs were then washed five more times with PBS, and coverslips were adhered to glass slides in mounting medium (0.1% *p*-phenylenediamine in 75% glycerol in PBS). Fluorescent images were captured using a 63 \times oil immersion objective on an Axioplan 2 microscope (Zeiss, Oberkochen, Germany) equipped with a Cooke Sencis deep-cooled CCD camera and a Slidebook software analysis program for digital deconvolution (Intelligent Imaging Innovations, Denver, CO). Quantitation of active Bax immunoreactivity was performed by determining the percentage of CGNs that showed positive punctate staining with the 6A7 monoclonal antibody to the active conformation of Bax. In general, HEK293 cells were stained using an identical protocol, except that they were cultured on 35-mm-diameter

plastic culture dishes and images were captured using a 63 \times water immersion objective.

Live cell imaging of TMRE fluorescence. HEK293 cells were cotransfected with GFP-Bax $_{\alpha}$ and either pcDNA3.1 empty vector or HA-GSK-3 β S9A. At 24 hr after transfection, TMRE (500 nM) and Hoechst dye were added for 30 min, and living cells were imaged using a Cy3 filter to detect TMRE fluorescence.

Preparation of cell extracts. After incubation, the culture medium was aspirated and cells were washed once with 2 ml of ice-cold PBS, pH 7.4, placed on ice, and scraped into lysis buffer (200 μ l/35 mm well) containing 20 mM HEPES, pH 7.4, 1% Triton X-100, 50 mM NaCl, 1 mM EGTA, 5 mM β -glycerophosphate, 30 mM sodium pyrophosphate, 100 μ M sodium orthovanadate, 1 mM phenylmethylsulfonyl fluoride, 10 μ g/ml leupeptin, and 10 μ g/ml aprotinin. Cell debris was removed by centrifugation at 6000 \times g for 3 min, and the protein concentration of the supernatant was determined using a commercially available protein assay kit (Pierce, Rockford, IL). Aliquots (~150 μ g) of supernatant protein were diluted to a final concentration of 1 \times SDS-PAGE sample buffer, boiled for 5 min, and electrophoresed through 10% polyacrylamide gels. Proteins were transferred to polyvinylidene difluoride (PVDF) membranes (Millipore, Bedford, MA) and processed for immunoblot analysis.

Immunoblotting. Nonspecific binding sites were blocked in PBS, pH 7.4, containing 0.1% Tween 20 (PBS-T) and 1% BSA for 1 hr at room temperature. Primary antibodies were diluted in blocking solution and incubated with the membranes for 1 hr. Excess primary antibody was removed by washing the membranes three times in PBS-T. The blots were then incubated with the appropriate horseradish peroxidase-conjugated secondary antibody diluted in PBS-T for 1 hr and were subsequently washed three times in PBS-T. Immunoreactive proteins were detected by enhanced chemiluminescence. The autoluminograms shown are generally representative of at least three independent experiments.

Immunoprecipitation of GFP-Bax. At 16–24 hr after transfection, HEK293 cell lysates were prepared in lysis buffer containing 1% Triton X-100, as described above. Ten microliters of monoclonal antibody against GFP were added to 500 μ l of lysate (~1 μ g/ μ l HEK293 cell protein concentration), and samples were mixed for 4 hr at 4 $^{\circ}$ C by continuous inversion. Agarose-conjugated protein A/G (50 μ l) was added, and samples were mixed for an additional 2 hr. Immune complexes were pelleted and washed for incubation in the *in vitro* kinase assay.

In vitro kinase assay. Pelleted GFP-Bax immune complexes were washed twice with 500 μ l of cell lysis buffer, followed by two more washes in 500 μ l of kinase reaction buffer [8 mM 4-morpholinepropanesulfonic acid (MOPS), pH 7.2, 0.2 mM EDTA, and 10 mM magnesium acetate]. The beads were then resuspended in 20 μ l of kinase buffer, and 50 ng (in a total volume of 10 μ l) of recombinant active GSK-3 β was added, followed by 10 μ Ci of [γ - 32 P]ATP (previously diluted in ATP dilution buffer containing 20 mM MOPS, pH 7.2, 75 mM MgCl $_2$, 25 mM β -glycerophosphate, 5 mM EGTA, 1 mM sodium orthovanadate, 1 mM DTT, and 500 μ M cold ATP). The kinase reaction mixtures were incubated at 30 $^{\circ}$ C for 30 min with continuous mixing at 1400 rpm. Reactions were stopped by adding 50 μ l of 2 \times SDS-PAGE sample buffer and boiling for 5 min. Samples were then resolved on 10% polyacrylamide gels, and proteins were transferred to PVDF membranes and exposed to film for autoradiography. Subsequently, the membranes were immunoblotted with a polyclonal antibody to GFP to assess the immunoprecipitation efficiencies of the various GFP-Bax variants.

In vivo phosphorylation of GFP-Bax $_{\alpha}$ by constitutively active GSK-3 β S9A. HEK293 cell cultures were washed three times in phosphate-free DMEM culture medium and then labeled for 6 hr with 32 P-orthophosphate (final concentration, 1.5 mCi/ml). Unincorporated phosphate was removed, and cells were washed three more times in phosphate-free DMEM. HEK293 cells were then cotransfected with wild-type GFP-Bax $_{\alpha}$, the single Ser163Ala mutant, or the Ser163Ala/Thr167Ala double mutant and either empty vector or constitutively active GSK-3 β S9A. Approximately 16 hr after transfection, the GFP-Bax variants were immunoprecipitated using a GFP monoclonal antibody, as described above. Immune complexes were resolved by SDS-PAGE on a

10% polyacrylamide gel and transferred to PVDF, and phosphorylation was assessed by autoradiography.

Site-directed mutagenesis of GFP-Bax $_{\alpha}$. Site-directed mutagenesis of potential GSK3 β phosphorylation sites within Bax $_{\alpha}$ was performed on the pEGFP-Bax $_{\alpha}$ plasmid using the Quikchange kit from Stratagene (La Jolla, CA). The following primers and annealing temperatures were used (underlined nucleotides indicate mutated site): Ser163Ala: upper primer 5'-GGTTGGGACGGCCTCCTCGCCTACTTTGGGACGCC-3', lower primer 5'-ACCCTGCCGAGGAGCGGATGAAACCCTGC-3', 69 $^{\circ}$ C annealing temperature (5% v/v DMSO was added to the reaction mix); Thr167Ala: upper primer 5'-TCCTCTCCTACTTTGGGGCGCCACGT-3', lower primer 5'-GAGAGGATGAAACCCCGCGGTGCA-3', 78.6 $^{\circ}$ C annealing temperature. The double mutant Ser163Ala/Thr167Ala was constructed using the Ser163Ala pEGFP-Bax $_{\alpha}$ plasmid and the Thr167 upper and lower primers at an annealing temperature of 70 $^{\circ}$ C.

All reactions were performed with the following program: 95 $^{\circ}$ C for 30 sec, appropriate annealing temperature for 1 min, and 72 $^{\circ}$ C for 5 min for 18 cycles.

Quantitation of apoptosis. HEK293 cells were transfected with variants of GFP-Bax in the absence or presence of constitutively active GSK-3 β . At 48 hr after transfection, Hoechst dye was added directly to the wells to stain nuclei and cells were scraped into the culture medium so that all cells were harvested, including those that had detached from the dish. The cells were then pelleted, washed once with PBS, and resuspended in PBS. Nuclear morphology of GFP-positive cells was assessed by fluorescence microscopy. Cells containing chromatin that was condensed and/or fragmented were scored as apoptotic. Approximately 150 transfected cells were quantitated per well, and each construct was transfected into duplicate wells in a total of two separate experiments.

Data analysis. The results shown represent the means \pm SEM for the number (*n*) of independent experiments that were performed. Statistical differences between the means of unpaired sets of data were evaluated by one-way ANOVA, followed by a *post hoc* Dunnett's or Tukey's test. A *p* value of <0.01 was considered statistically significant.

Results

GSK-3 β inhibitors suppress Bax translocation to mitochondria and Bax conformational activation in trophic factor-deprived CGNs

CGNs were transfected with plasmids expressing either GFP or an NH $_2$ -terminal GFP fusion protein of human Bax α (GFP-Bax $_{\alpha}$) (Wolter et al., 1997). Neurons were transfected using gold beads coated with the precipitated plasmid DNA via particle-mediated gene transfer by a Helios Gene-Gun (Wellmann et al., 1999). At 48 hr after transfection, cells were either maintained in control medium containing serum and 25 mM KCl (25K+Ser) or switched to apoptotic medium lacking serum and containing 5 mM KCl (5K-Ser). After an additional 4 hr incubation, neurons were fixed in paraformaldehyde, and nuclei were stained with Hoechst dye. The localization of GFP or GFP-Bax $_{\alpha}$ and nuclear morphology were examined by fluorescence microscopy (Fig. 1). GFP displayed a diffuse distribution over the entire cell body in CGNs cultured in either control or apoptotic medium (Fig. 1A, top). In contrast, the localization of GFP-Bax $_{\alpha}$ changed from a diffuse pattern in control medium to a punctate distribution in apoptotic medium. The punctate localization of GFP-Bax $_{\alpha}$ in apoptotic medium coincided with condensation and fragmentation of the chromatin in CGNs (Fig. 1A, bottom). To confirm that the punctate distribution of GFP-Bax $_{\alpha}$ corresponded to its translocation to mitochondria, CGNs were stained for the integral mitochondrial membrane protein COX IV. In control medium, there was little specific overlap between the localization of GFP-Bax $_{\alpha}$ and COX IV (Fig. 1B, top). While in apoptotic medium, GFP-Bax $_{\alpha}$ showed substantial colocalization with COX IV (Fig. 1B, bottom). These data show that removal of serum and depolarizing extracellular potassium (trophic factor withdrawal)

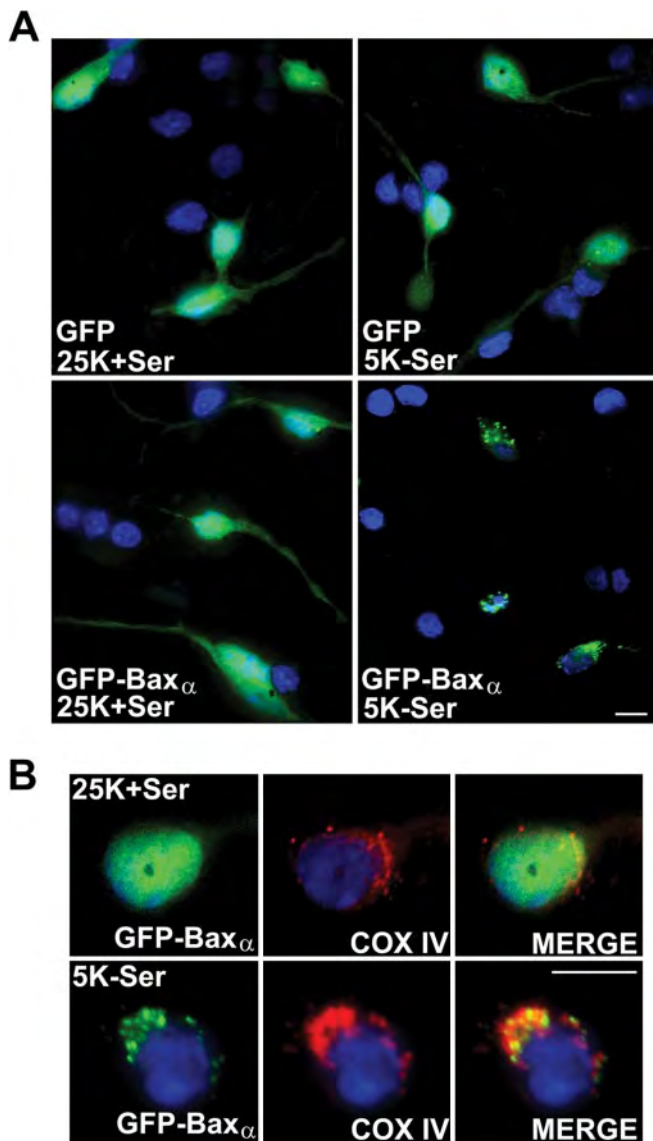


Figure 1. An expressed GFP-Bax α fusion protein translocates to mitochondria in CGNs undergoing apoptosis. *A*, Representative images of CGNs transfected with either GFP or GFP-Bax α and subsequently incubated for 4 hr in either control medium (25 mM KCl with serum; 25K+Ser) or apoptotic medium (5 mM KCl without serum; 5K-Ser). Images show the localization of GFP or GFP-Bax α and nuclear morphology after staining with Hoechst dye (shown in blue). *B*, Neurons transfected with GFP-Bax α were incubated as described in *A*, followed by immunostaining for COX IV to identify mitochondria. Scale bars, 10 μ m.

triggers translocation of GFP-Bax α to mitochondria in CGNs undergoing apoptosis.

Examination of the kinetics of GFP-Bax α translocation revealed a rapid movement of the expressed fusion protein to mitochondria after induction of apoptosis (Fig. 2*A*). In control medium, <30% of the CGNs expressing GFP-Bax α showed a mitochondrial localization of the fusion protein. Within 1 hr of trophic factor deprivation, a significant increase in mitochondrial GFP-Bax α was detectable. After 4 hr of incubation in apoptotic medium, ~70% of the transfected CGNs demonstrated a mitochondrial distribution of GFP-Bax α . Measurement of GSK-3 β activation in CGNs undergoing apoptosis revealed kinetics that closely paralleled the mitochondrial translocation of GFP-Bax α . When dephosphorylation of the inhibitory residue Ser9 was used as an index of GSK-3 β activation, significant stim-

ulation was observed within 1 hr, and nearly complete dephosphorylation occurred after 4 hr of incubation in apoptotic medium (Fig. 2*B*). Thus, the activation of GSK-3 β is temporally correlated with the movement of Bax to mitochondria in CGNs undergoing apoptosis.

To determine whether GSK-3 β activity is required to trigger Bax translocation to mitochondria in CGNs, we evaluated the effects of several distinct GSK-3 β inhibitors on the movement of GFP-Bax α . IGF-I is a known survival factor for CGNs that signals through phosphatidylinositol 3-kinase to activate the anti-apoptotic kinase AKT (D'Mello et al., 1993; Linseman et al., 2002). AKT subsequently phosphorylates and inactivates several pro-apoptotic molecules including Bad, caspase-9, GSK-3 β , and the forkhead transcription factor FKHRL1 (Lawlor and Alessi, 2001). In the case of GSK-3 β , AKT phosphorylates the inhibitory residue Ser9. As shown in Figure 2*C*, IGF-I significantly attenuated the dephosphorylation of GSK-3 β on Ser9 in CGNs switched to apoptotic medium. In addition to IGF-I, we also used a substituted oxadiazole GSK-3 β inhibitor, GSK-3 β inhibitor II (Inh-II; Calbiochem) (Naerum et al., 2002), and the monovalent cation lithium, which is a noncompetitive inhibitor of GSK-3 β that is protective in many models of neuronal apoptosis including CGNs (Linseman et al., 2003). Inclusion of either IGF-I or Inh-II resulted in an ~40% decrease in the (5K-Ser)-induced translocation of GFP-Bax α to mitochondria (Fig. 2*D*). Moreover, the combination of IGF-I and Inh-II did not produce an additive inhibitory effect on GFP-Bax α translocation, suggesting that each of these agents blocks the same signal for Bax movement (i.e., GSK-3 β activation) (Fig. 2*D*). Finally, the noncompetitive GSK-3 β inhibitor lithium was most effective at blocking GFP-Bax α translocation in apoptotic medium (Fig. 2*D*).

We next analyzed the activation of the endogenous Bax protein by immunostaining CGNs with a monoclonal antibody that specifically recognizes the active Bax conformation (clone 6A7) (Hsu and Youle, 1997). CGNs maintained in control medium showed little to no detectable 6A7 staining, whereas neurons in apoptotic medium showed active Bax immunoreactivity (Fig. 2*E*). Moreover, the 6A7 staining often coincided with condensed and/or fragmented chromatin. Inclusion of either the GSK-3 β inhibitor II or a specific phosphopeptide inhibitor of GSK-3 β (Plotkin et al., 2003) significantly inhibited both the conformational activation of endogenous Bax and CGN apoptosis (Fig. 2*F*). In a similar manner, the peptide inhibitor of GSK-3 β also blunted GFP-Bax α translocation to mitochondria in transfected CGNs incubated in apoptotic medium (data not shown). Collectively, these results demonstrate that GSK-3 β activity is necessary to induce the conformational change and mitochondrial translocation of Bax in trophic factor-deprived CGNs.

GSK-3 β directly phosphorylates Bax on Ser163 *in vitro* and *in vivo*

To determine whether Bax is a direct substrate of GSK-3 β , we examined the amino acid sequences of several species variants of Bax α to establish whether they contain any conserved GSK-3 β consensus phosphorylation motifs (Fig. 3*A*). GSK-3 β phosphorylates the consensus site S*/T*XXXS(P)/T(P), where (P) indicates a previously phosphorylated or "primed" serine or threonine residue and the asterisk denotes the site targeted by GSK-3 β (Fiol et al., 1987). Bax α contains a SXXXT motif (residues Ser163 through Thr167) that is conserved in human, rat, mouse, and bovine Bax α (Fig. 3*A*). To ascertain whether Ser163 is phosphorylated by GSK-3 β , we first analyzed the ability of purified GSK-3 β to phosphorylate GFP-Bax α *in vitro*. GFP-Bax α was im-

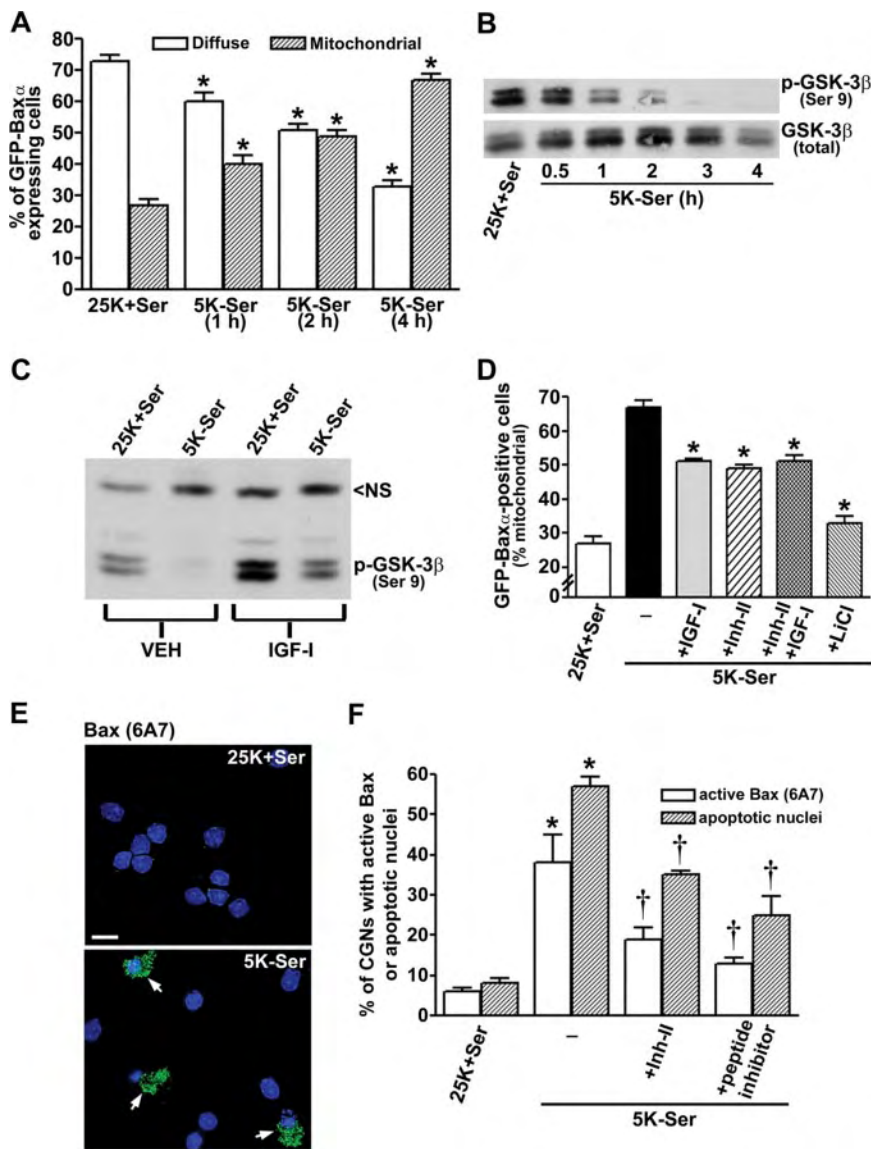


Figure 2. GSK-3 β activity regulates Bax translocation to mitochondria and Bax conformational activation in apoptotic CGNs. *A*, Quantitation of the percentage of GFP-Bax α -expressing cells that demonstrated either a diffuse or mitochondrial localization of the fusion protein. The data shown are from three independent experiments in which \sim 200 transfected CGNs were counted per experiment ($*p < 0.01$ compared with the 25K+Ser control). *B*, Time course of GSK-3 β activation after trophic factor withdrawal in CGNs was measured by dephosphorylation at Ser9 (top blot). Total GSK-3 β was not significantly altered over the duration of the experiment (bottom blot). All subsequent experiments involved a 4 hr incubation in 5K-Ser medium, unless noted otherwise. *C*, Effects of dilute acetic acid vehicle (VEH) or IGF-I (200 ng/ml) on GSK-3 β activation (dephosphorylation) in trophic factor-deprived CGNs. NS, Nonspecific protein detected by the phospho-GSK-3 β antibody, shown as a loading control. *D*, Quantitation of GFP-Bax α -positive CGNs that displayed mitochondrial localization of the fusion protein in either control or apoptotic medium containing IGF-I (200 ng/ml), GSK-3 β inhibitor II (10 μ M), or LiCl (20 mM). The results shown are from three separate experiments in which \sim 200 transfected CGNs were counted per experiment ($*p < 0.01$ compared with 5K-Ser). *E*, Representative images of the activation of endogenous Bax detected immunocytochemically in trophic factor-deprived CGNs using an active conformation-specific monoclonal antibody (clone 6A7). Nuclei are stained with DAPI (shown in blue). Scale bar, 10 μ m. *F*, Quantitation of CGN apoptosis and immunoreactivity for active Bax in cells incubated for 16 hr in control or apoptotic medium containing either GSK-3 β inhibitor II (10 μ M) or a specific peptide inhibitor of GSK-3 β (50 μ M). The data represent the results from three independent experiments in which apoptosis and active Bax immunoreactivity were quantitated in \sim 300 cells per condition per experiment ($*p < 0.01$ compared with 25K+Ser; $^{\dagger}p < 0.01$ compared with 5K-Ser).

munoprecipitated from HEK293 cells at 24 hr after transfection using a monoclonal antibody to GFP. Equivalent amounts of immunoprecipitated GFP-Bax α were then subjected to *in vitro* kinase assays using purified GSK-3 β in the absence or presence of lithium. A small amount of phosphorylation occurred on GFP-Bax α *in vitro* in the absence of GSK-3 β , and this increased mark-

edly when GSK-3 β was added to the kinase reaction (Fig. 3*B*, top). Autophosphorylation of GSK-3 β was also detected during the kinase reaction (Fig. 3*B*, bottom). Both the autophosphorylation of GSK-3 β and the enhanced phosphorylation of GFP-Bax α were blocked by inclusion of lithium. Furthermore, when GFP-Bax α was immunoprecipitated from HEK293 cells that had been cotransfected with a constitutively active mutant of GSK-3 β (S9A), it was less efficiently phosphorylated by GSK-3 β *in vitro* compared with GFP-Bax α immunoprecipitated from cells cotransfected with empty vector (Fig. 3*C*). This latter result suggests that fewer Bax α sites were available for *in vitro* phosphorylation after previous exposure to constitutively active GSK-3 β S9A. Collectively, these findings indicate that GFP-Bax α is a substrate for GSK-3 β both *in vitro* and in intact cells.

Next, we analyzed the ability of GSK-3 β to phosphorylate several site-directed mutants of GFP-Bax α *in vitro*. When the 32 P incorporation into the fusion protein was normalized to the amount of GFP-Bax immunoprecipitated from transfected HEK293 cells, the addition of GSK-3 β induced an \sim 12-fold increase in the phosphorylation of wild-type GFP-Bax α (Fig. 3*D*, compare lanes 1 and 2). A Ser163Ala mutant of GFP-Bax α was not significantly phosphorylated by GSK-3 β *in vitro*, consistent with Ser163 being a major phosphorylation site (Fig. 3*D*, compare lanes 2 and 3). In contrast, GFP-Bax α mutated at the putative priming site, Thr167Ala, was efficiently phosphorylated by GSK-3 β *in vitro* (Fig. 3*D*, lane 4), whereas the double mutant Ser163Ala/Thr167Ala showed substantially decreased phosphorylation relative to wild-type Bax α (Fig. 3*D*, lane 5). Overall, these data indicate that the species-conserved residue Ser163 of Bax α is a substrate for GSK-3 β -mediated phosphorylation *in vitro*. However, phosphorylation of the putative priming residue Thr167 is apparently not necessary for GSK-3 β to target Ser163 *in vitro*.

Finally, to demonstrate that Ser163 of Bax is a substrate for GSK-3 β *in vivo*, we cotransfected 32 P-orthophosphate-labeled HEK293 cells with wild-type GFP-Bax α , the single Ser163Ala mutant, or the Ser163Ala/Thr167Ala double mutant in combination with either empty vector or constitutively active GSK-3 β S9A. Approximately 16 hr after transfection, the GFP-Bax variants were immunoprecipitated, immune complexes were resolved by SDS-PAGE, and phosphorylation was assessed by autoradiography. Cotransfection with GSK-3 β S9A markedly increased the phosphorylation of wild-type GFP-Bax α by approximately fourfold (Fig. 3*E*, compare lanes 1 and 2). In contrast, coex-

active GSK-3 β S9A. Approximately 16 hr after transfection, the GFP-Bax variants were immunoprecipitated, immune complexes were resolved by SDS-PAGE, and phosphorylation was assessed by autoradiography. Cotransfection with GSK-3 β S9A markedly increased the phosphorylation of wild-type GFP-Bax α by approximately fourfold (Fig. 3*E*, compare lanes 1 and 2). In contrast, coex-

pression with constitutively active GSK-3 β did not enhance ^{32}P incorporation into either the single Ser163Ala mutant or the double mutant of GFP-Bax $_{\alpha}$ (Fig. 3E, lanes 3–6). These data strongly suggest that Ser163 of Bax is a principal substrate for GSK-3 β *in vivo* in intact cells.

Constitutively active GSK-3 β drives GFP-Bax $_{\alpha}$ to mitochondria in transfected HEK293 cells and CGNs

To assess the functional consequences of phosphorylation by GSK-3 β , we examined the subcellular distribution of GFP-Bax $_{\alpha}$ in HEK293 cells cotransfected with either empty vector or HA-tagged, constitutively active GSK-3 β S9A. The majority of cells cotransfected with empty vector showed a GFP-Bax $_{\alpha}$ distribution that was diffuse over the entire cell (Fig. 4A, left; B, top). In contrast, cells cotransfected with constitutively active GSK-3 β S9A showed a marked redistribution of GFP-Bax $_{\alpha}$ to organelles that were structurally identifiable as mitochondria (Fig. 4A, right; B, bottom). These structures were confirmed to be mitochondria by colabeling live HEK293 cells with the mitochondrial marker TMRE. Cells cotransfected with GSK-3 β S9A showed significant colocalization of GFP-Bax $_{\alpha}$ with TMRE-stained mitochondria (Fig. 4C). These data indicate that activation of GSK-3 β is sufficient to trigger localization of Bax to mitochondria in transfected HEK293 cells.

Next, we examined the effects of constitutively active GSK-3 β on the localization of GFP-Bax $_{\alpha}$ and induction of apoptosis in CGNs. As described in Figure 1, CGNs cotransfected with GFP-Bax $_{\alpha}$ and empty vector (maintained in control medium) showed a diffuse distribution of the Bax fusion protein and no nuclear condensation (Fig. 5A, B, left). In contrast, CGNs coexpressing GFP-Bax $_{\alpha}$ and HA-GSK-3 β S9A (maintained in control medium) displayed a punctate localization of the Bax fusion protein and demonstrated significant nuclear condensation and fragmentation (Fig. 5A, B, right). Thus, constitutive activation of GSK-3 β promotes Bax localization to mitochondria and induces CGN apoptosis even in the presence of survival medium.

Ser163 is required for GSK-3 β to induce Bax translocation and apoptosis in HEK293 cells

To confirm that the putative GSK-3 β phosphorylation site Ser163 is necessary for Bax localization to mitochondria, we evaluated the ability of constitutively active GSK-3 β to affect the subcellular distribution of various Bax mutants in cotransfected HEK293 cells. Consistent with its relative

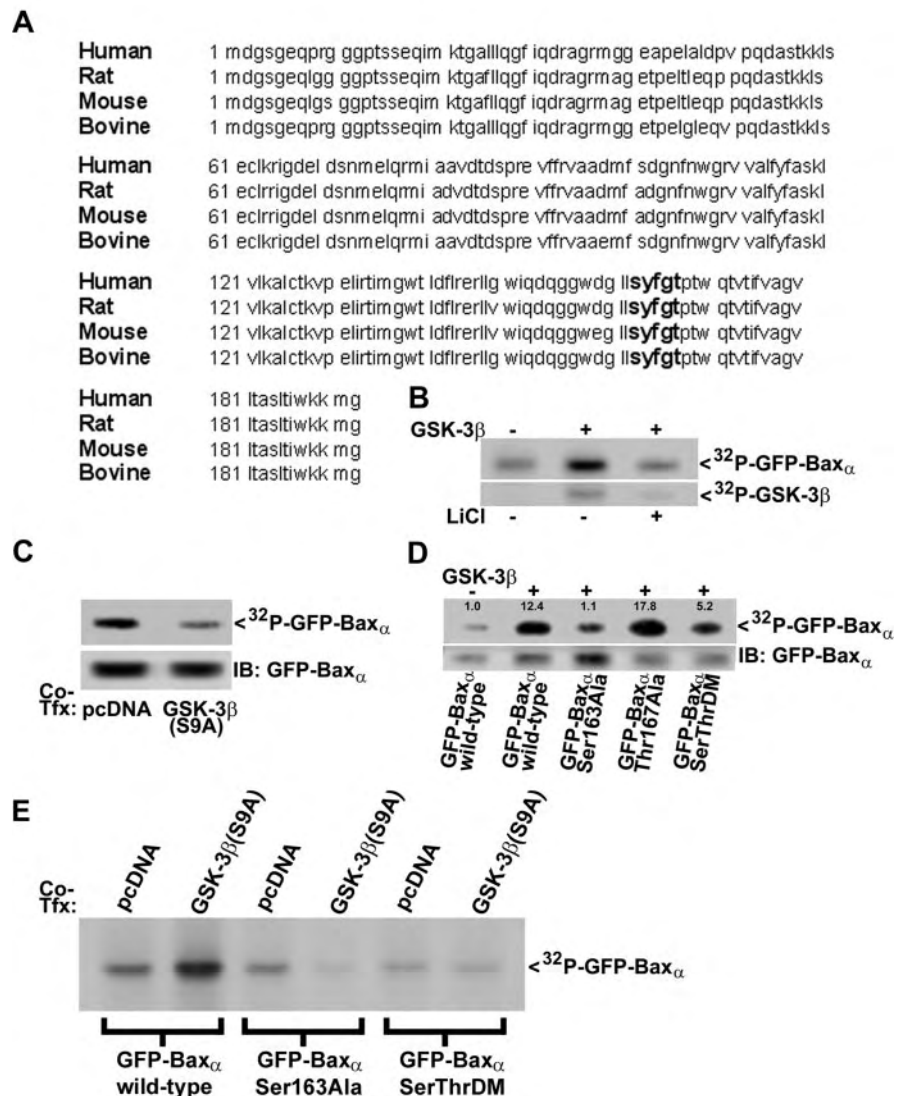


Figure 3. GSK-3 β phosphorylates Bax $_{\alpha}$ on the species-conserved residue Ser163. *A*, Amino acid sequence alignment of Bax $_{\alpha}$ from human (GenBank accession number NP_620116), rat (Q63690), mouse (AAA03622), and bovine (AAC48806). A conserved GSK-3 β consensus phosphorylation motif is highlighted in bold lettering at residues Ser163 to Thr167. *B*, HEK293 cells were transfected with GFP-Bax $_{\alpha}$ as described in Materials and Methods. At 24 hr after transfection, the fusion protein was immunoprecipitated from cell lysates using a GFP monoclonal antibody. Immune complexes were then subjected to *in vitro* kinase assay by incubating for 30 min at 30°C with purified GSK-3 β (50 ng) and [γ - ^{32}P]ATP (10 μCi), in either the absence or the presence of LiCl (20 mM). ^{32}P incorporation into GFP-Bax $_{\alpha}$ (top) and GSK-3 β (bottom) was detected by autoradiography. *C*, GFP-Bax $_{\alpha}$ was immunoprecipitated from HEK293 cells that were cotransfected (Co-Tfx) with either empty vector (pcDNA3.1) or constitutively active GSK-3 β (S9A). Immune complexes were subjected to GSK-3 β *in vitro* kinase assay, and ^{32}P incorporation into GFP-Bax $_{\alpha}$ was detected by autoradiography (top). The membrane was later immunoblotted (IB) for GFP-Bax $_{\alpha}$ using a polyclonal antibody to GFP to demonstrate transfection and immunoprecipitation efficiencies (bottom). *D*, HEK293 cells were transfected with either wild-type GFP-Bax $_{\alpha}$, the site-directed mutants Ser163Ala or Thr167Ala, or the Ser163Ala/Thr167Ala double mutant (SerThrDM). At 24 hr after transfection, the fusion proteins were immunoprecipitated using a GFP monoclonal antibody, and immune complexes were subjected to GSK-3 β *in vitro* kinase assay. The amount of ^{32}P incorporation into each of the fusion proteins (top) was normalized to the densitometric signal of the GFP immunoblot (bottom) to correct for differences in either expression or immunoprecipitation efficiencies. The normalized ratio for wild-type GFP-Bax $_{\alpha}$ in the absence of GSK-3 β was set to 1.0, and all other values are relative to that control. *E*, GFP-Bax $_{\alpha}$ (wild type, the single Ser163Ala mutant, or the Ser163Ala/Thr167Ala double mutant) was immunoprecipitated from ^{32}P -orthophosphate-labeled HEK293 cells that were cotransfected (Co-Tfx) for ~16 hr with either empty vector (pcDNA3.1) or constitutively active GSK-3 β (S9A). Immune complexes were resolved by SDS-PAGE, and ^{32}P incorporation into GFP-Bax $_{\alpha}$ was detected by autoradiography.

inefficiency as a GSK-3 β substrate (Fig. 3D, E), the Ser163Ala/Thr167Ala double mutant of GFP-Bax $_{\alpha}$ failed to localize to mitochondria when cotransfected with GSK-3 β S9A (Fig. 6A). Quantitative analysis of the mitochondrial localization of various

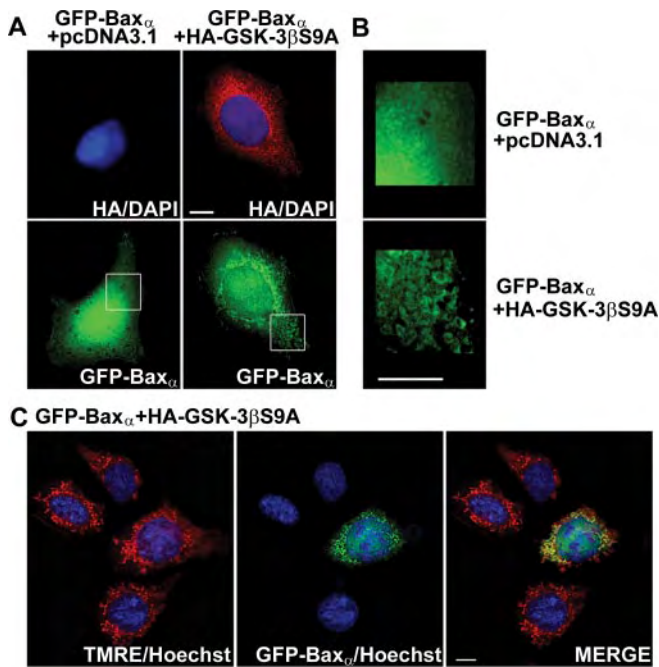


Figure 4. Coexpression of GFP-Bax α with a constitutively active mutant of GSK-3 β (S9A) induces translocation of the Bax fusion protein to mitochondria in transfected HEK293 cells. *A*, HEK293 cells were cotransfected with GFP-Bax α and either empty vector or HA-tagged GSK-3 β S9A. At 24 hr after transfection, cotransfected cells were visualized by staining for the epitope tag using an HA polyclonal antibody and a Cy3-conjugated secondary. *B*, The areas demarcated by the boxes in *A* were enlarged 300% to show fine structure. *C*, HEK293 cells were cotransfected with GFP-Bax α and HA-tagged GSK-3 β S9A. At 24 hr after transfection, cells were incubated for 30 min with Hoechst dye (to stain nuclei) and TMRE to label mitochondria. Live cells were then visualized with a 63 \times water immersion objective, and digitally deconvolved images were obtained using an Axioplan 2 microscope (Zeiss) equipped with a Cooke Sensicam deep-cooled CCD camera and a Slidebook software analysis program for digital deconvolution (Intelligent Imaging Innovations). Cotransfection with GSK-3 β S9A induced a marked redistribution of GFP-Bax α that showed significant colocalization with the mitochondrial marker TMRE. The images shown are representative of data obtained in two independent experiments. Scale bars, 10 μ m.

GFP-Bax α mutants is shown in Figure 6*B*. Cotransfection of wild-type GFP-Bax α with GSK-3 β S9A induced a statistically significant increase in the mitochondrial localization of the fusion protein. In contrast, the single alanine substitution mutants at Ser163 and Thr167, as well as the Ser163/Thr167 double Ala mutant, were predominantly cytosolic regardless of the presence of GSK-3 β S9A.

The above results parallel the phosphorylation data shown in Figure 3*D*, except for the single Thr167Ala mutant that was phosphorylated by GSK-3 β *in vitro* but failed to localize to mitochondria in intact cells. This apparent discrepancy may reflect a physiological necessity for priming in order for Bax to be phosphorylated by GSK-3 β *in vivo*. The high concentration of GSK-3 β added to the *in vitro* kinase reaction most likely circumvented this requirement. Alternatively, it is possible that an additional docking site for GSK-3 β exists on Bax distinct from the phosphorylated threonine at position (+4) relative to Ser163 (Biondi and Nebreda, 2003).

Additional evidence implicating Ser163 as a critical residue in the regulation of Bax function was acquired from analysis of the various Bax isoforms (Oltvai et al., 1993). In particular, a recently described isoform, human Bax σ (Bax σ) (Schmitt et al., 2000), is nearly identical to Bax α , except it lacks residues 159–171, which

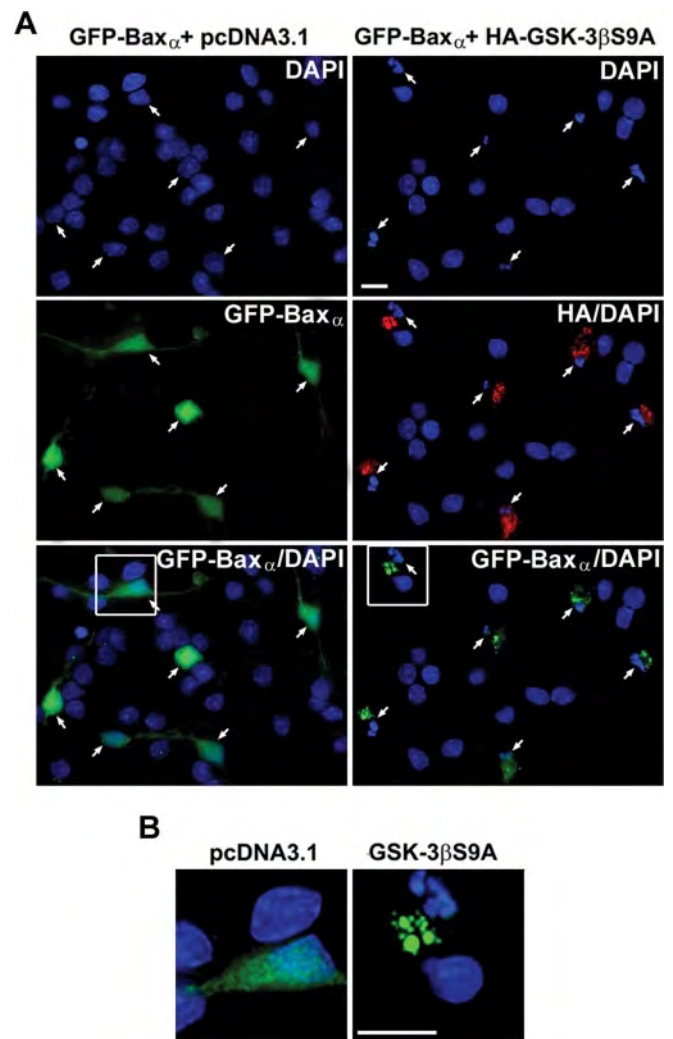


Figure 5. Cotransfection of CGNs with GFP-Bax α and a constitutively active mutant of GSK-3 β (S9A) induces translocation of the Bax fusion protein to mitochondria and triggers CGN apoptosis. *A*, CGNs were cotransfected with GFP-Bax α and either empty vector or HA-tagged GSK-3 β S9A using the Helios Gene-Gun system, as described in Materials and Methods. At 48 hr after transfection, cotransfected cells were maintained in control medium and were visualized by staining for the epitope tag using an HA polyclonal antibody and a Cy3-conjugated secondary antibody. The images shown are composites of four to six fields captured with a 63 \times oil objective to give a representative view of the localization of the Bax fusion protein in the absence or presence of constitutively active GSK-3 β . *B*, The areas demarcated by the boxes in *A* were enlarged 300% to show fine structure. Scale bars, 10 μ m.

encompass the putative GSK-3 β -regulated site Ser163 (Fig. 6*C*). Like the Ser163Ala point mutant of Bax α , HEK293 cells cotransfected with GFP-Bax σ and HA-GSK-3 β S9A demonstrated a diffuse localization of the Bax fusion protein with little accumulation in mitochondria (Fig. 6*B, C*).

Finally, in agreement with the mitochondrial localization of Bax triggering the intrinsic death pathway, the amount of apoptosis induced in transfected HEK293 cells reflected the ability of GSK-3 β S9A to drive wild-type Bax α , but not the Ser163Ala Bax α single mutant, the Ser163Ala/Thr167Ala Bax α double mutant, or Bax σ , to mitochondria (Fig. 6*D*). These data indicate that phosphorylation of Ser163 on Bax by GSK-3 β promotes the localization of Bax to mitochondria and induction of apoptosis in transfected HEK293 cells.

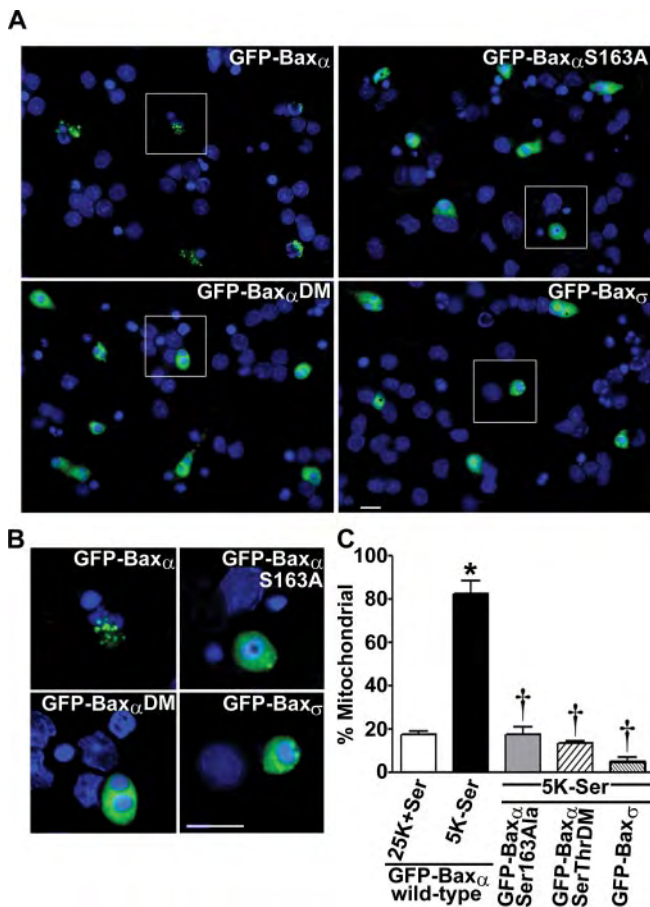


Figure 7. Bax variants lacking Ser163 fail to localize to mitochondria in CGNs undergoing apoptosis. *A*, CGNs were transfected using the Helios Gene-Gun with wild-type GFP-Bax α , the GFP-Bax α Ser163Ala single mutant or the Ser163Ala/Thr167Ala double mutant (DM), or GFP-Bax α . At 48 hr after transfection, neurons were switched to apoptotic medium (5K-Ser) for 4 hr. CGNs were then fixed, and nuclei were stained with Hoechst dye. The images shown are composites of four to six fields captured with a 63 \times oil objective to give a representative view of the localization of the various fusion proteins. *B*, The regions demarcated by the boxes in *A* were enlarged 250% to magnify the fusion protein distributions and nuclear morphologies. *C*, Quantitation of the fraction of transfected CGNs showing a mitochondrial distribution of the GFP-Bax variants [wild-type α , Ser163Ala α , Ser163Ala/Thr167Ala α (SerThrDM), and Bax α] after incubation in either control or apoptotic medium. Data represent the means \pm SEM of at least three separate experiments with each Bax variant in which \sim 200 transfected CGNs were counted per experiment. * $p < 0.01$ compared with wild-type α incubated in control medium; † $p < 0.01$ compared with GFP-Bax α (wild type) in apoptotic medium. Scale bars: *A*, *B*, 10 μ m.

Our finding that Bax is a direct target of GSK-3 β complements a recent study by Watcharasit et al. (2003) showing that GSK-3 β indirectly stimulates the transcription of Bax via regulation of p53 activity. Collectively, these results suggest that GSK-3 β modulates Bax expression and function at the transcriptional and posttranslational levels, respectively, to promote mitochondrial apoptosis.

Where and how GSK-3 β and Bax interact in neurons remains to be investigated. Previous studies examining the interactions of GSK-3 β with β -catenin have revealed that the kinase is brought in close proximity to its substrate by their interactions with the axin–adenomatous polyposis coli scaffold complex (Hart et al., 1998). Similarly, GSK-3 β and tau interact via their common association with cytosolic scaffolding proteins of the 14-3-3 family (Agarwal-Mawal et al., 2003). Because cytosolic Bax was shown recently to interact with 14-3-3 proteins (Nomura et al., 2003), it

is possible that 14-3-3 scaffolds also mediate the interaction of GSK-3 β with Bax.

The current finding that GSK-3 β phosphorylates and regulates Bax function impacts on several recent reports. First, activation of AKT was reported to inhibit Bax conformational change in B-cells subjected to cytokine withdrawal (Yamaguchi and Wang, 2001) and Bax translocation to mitochondria in COS-1 cells incubated with staurosporine (Tsuruta et al., 2002). Although there is no consensus AKT phosphorylation site on Bax, Gardai et al. (2004) recently reported that Bax is phosphorylated in neutrophils on the C-terminal Ser184 in an AKT-dependent manner. Furthermore, they suggest that this phosphorylation event inhibits the pro-apoptotic action of Bax in neutrophils. Our results indicate that the ability of AKT to modulate Bax conformation and movement in these non-neuronal cells may also involve regulation of GSK-3 β activity. Second, Somerville et al. (2001) reported that lithium prevents the conformational change in Bax in human erythroid progenitor cells deprived of growth factors. Although they related this effect to inhibition of GSK-3 β activity, these authors did not show that Bax is a direct substrate of GSK-3 β . Given the coincident activation of Bax and GSK-3 β in many models of apoptosis, it is likely that the interaction of these two molecules acts as a common trigger for activation of the intrinsic death pathway.

Precisely how phosphorylation of Bax by GSK-3 β stimulates Bax movement to mitochondria will require further investigation. There are several potential events that could be influenced by Bax phosphorylation. The phosphorylation may alter the conformation of Bax and facilitate its ability to oligomerize or to incorporate into the outer mitochondrial membrane. Indeed, we found that peptide and non-peptide inhibitors of GSK-3 β activity effectively blocked the conformational change of endogenous Bax induced by trophic factor deprivation in CGNs. Alternatively, phosphorylation may decrease the affinity of Bax for cytosolic anchoring proteins like 14-3-3. Conversely, the affinity of Bax for mitochondrial membrane proteins may be enhanced by phosphorylation, thus promoting its targeting to mitochondria. Additional elucidation of the mechanism by which GSK-3 β -mediated phosphorylation regulates Bax function may reveal novel targets for inhibiting neuronal apoptosis.

References

- Agarwal-Mawal A, Qureshi HY, Cafferty PW, Yuan Z, Han D, Lin R, Paudel HK (2003) 14-3-3 connects glycogen synthase kinase-3 beta to tau within a brain microtubule-associated tau phosphorylation complex. *J Biol Chem* 278:12722–12728.
- Biondi RM, Nebreda AR (2003) Signalling specificity of Ser/Thr protein kinases through docking-site-mediated interactions. *Biochem J* 372:1–13.
- Brunet A, Datta SR, Greenberg ME (2001) Transcription-dependent and -independent control of neuronal survival by the PI3K-Akt signaling pathway. *Curr Opin Neurobiol* 11:297–305.
- Cregan SP, MacLaurin JG, Craig CG, Robertson GS, Nicholson DW, Park DS, Slack RS (1999) Bax-dependent caspase-3 activation is a key determinant in p53-induced apoptosis in neurons. *J Neurosci* 19:7860–7869.
- D’Mello SR, Galli C, Ciotti T, Calissano P (1993) Induction of apoptosis in cerebellar granule neurons by low potassium: inhibition of death by insulin-like growth factor I and cAMP. *Proc Natl Acad Sci USA* 90:10989–10993.
- Doble BW, Woodgett JR (2003) GSK-3: tricks of the trade for a multitasking kinase. *J Cell Sci* 116:1175–1186.
- Fiol CJ, Mahrenholz AM, Wang Y, Roeske RW, Roach PJ (1987) Formation of protein kinase recognition sites by covalent modification of the substrate. Molecular mechanism for the synergistic action of casein kinase II and glycogen synthase kinase 3. *J Biol Chem* 262:14042–14048.
- Fukunaga K, Miyamoto E (1998) Role of MAP kinase in neurons. *Mol Neurobiol* 16:79–95.

- Gardai SJ, Hildeman DA, Frankel SK, Whitlock BB, Frasch SC, Borregaard N, Marrack P, Brattton DL, Henson PM (2004) Phosphorylation of Bax Ser184 by Akt regulates its activity and apoptosis in neutrophils. *J Biol Chem* 279:21085–21095.
- Hart MJ, de los Santos R, Albert IN, Rubinfeld B, Polakis P (1998) Down-regulation of beta-catenin by human axin and its association with the APC tumor suppressor, beta-catenin and GSK3 beta. *Curr Biol* 8:573–581.
- Hetman M, Cavanaugh JE, Kimelman D, Xia Z (2000) Role of glycogen synthase kinase-3 β in neuronal apoptosis induced by trophic withdrawal. *J Neurosci* 20:2567–2574.
- Hsu YT, Youle RJ (1997) Nonionic detergents induce dimerization among members of the Bcl-2 family. *J Biol Chem* 272:13829–13834.
- Kaytor MD, Orr HT (2002) The GSK3 beta signaling cascade and neurodegenerative disease. *Curr Opin Neurobiol* 12:275–278.
- Lawlor MA, Alessi DR (2001) PKB/Akt: a key mediator of cell proliferation, survival and insulin responses? *J Cell Sci* 114:2903–2910.
- Li M, Wang X, Meintzer MK, Laessig T, Birnbaum MJ, Heidenreich KA (2000) Cyclic AMP promotes neuronal survival by phosphorylation of glycogen synthase kinase 3beta. *Mol Cell Biol* 20:9356–9363.
- Linseman DA, Phelps RA, Bouchard RJ, Le SS, Laessig TA, McClure ML, Heidenreich KA (2002) Insulin-like growth factor-I blocks Bcl-2 interacting mediator of cell death (Bim) induction and intrinsic death signaling in cerebellar granule neurons. *J Neurosci* 22:9287–9297.
- Linseman DA, Cornejo BJ, Le SS, Meintzer MK, Laessig TA, Bouchard RJ, Heidenreich KA (2003) A myocyte enhancer factor 2D (MEF2D) kinase activated during neuronal apoptosis is a novel target inhibited by lithium. *J Neurochem* 85:1488–1499.
- Mielke K, Herdegen T (2000) JNK and p38 stress kinases—degenerative effectors of signal-transduction-cascades in the nervous system. *Prog Neurobiol* 61:45–60.
- Naerum L, Norkov-Lauritsen L, Olesen PH (2002) Scaffold hopping and optimization towards libraries of glycogen synthase kinase-3 inhibitors. *Bioorg Med Chem Lett* 12:1525–1528.
- Nomura M, Shimizu S, Sugiyama T, Narita M, Ito T, Matsuda H, Tsujimoto Y (2003) 14-3-3 interacts directly with and negatively regulates pro-apoptotic Bax. *J Biol Chem* 278:2058–2065.
- Oltvai ZN, Millman CL, Korsmeyer SJ (1993) Bcl-2 heterodimerizes *in vivo* with a conserved homolog, Bax, that accelerates programmed cell death. *Cell* 74:609–619.
- Perez M, Rojo AI, Wandosell F, Diaz-Nido J, Avila J (2003) Prion peptide induces neuronal cell death through a pathway involving glycogen synthase kinase 3. *Biochem J* 372:129–136.
- Phiel CJ, Wilson CA, Lee VM, Klein PS (2003) GSK-3alpha regulates production of Alzheimer's disease amyloid-beta peptides. *Nature* 423:435–439.
- Plotkin B, Kaidanovich O, Talior I, Eldar-Finkelman H (2003) Insulin mimetic action of synthetic phosphorylated peptide inhibitors of glycogen synthase kinase-3. *J Pharmacol Exp Ther* 305:974–980.
- Putcha GV, Deshmukh M, Johnson Jr EM (1999) Bax translocation is a critical event in neuronal apoptosis: regulation by neuroprotectants, Bcl-2, and caspases. *J Neurosci* 19:7476–7485.
- Putcha GV, Harris CA, Moulder KL, Easton RM, Thompson CB, Johnson Jr EM (2002) Intrinsic and extrinsic pathway signaling during neuronal apoptosis: lessons from the analysis of mutant mice. *J Cell Biol* 157:441–453.
- Schinzel A, Kaufmann T, Schuler M, Martinalbo J, Grubb D, Borner C (2004) Conformational control of Bax localization and apoptotic activity by Pro168. *J Cell Biol* 164:1021–1032.
- Schmitt E, Paquet C, Beauchemin M, Dever-Bertrand J, Bertrand R (2000) Characterization of Bax-sigma, a cell death-inducing isoform of Bax. *Biochem Biophys Res Commun* 270:868–879.
- Selimi F, Vogel MW, Mariani J (2000) Bax inactivation in lurcher mutants rescues cerebellar granule cells but not purkinje cells or inferior olivary neurons. *J Neurosci* 20:5339–5345.
- Somerville TC, Linch DC, Khwaja A (2001) Growth factor withdrawal from primary human erythroid progenitors induces apoptosis through a pathway involving glycogen synthase kinase-3 and Bax. *Blood* 98:1374–1381.
- Tsuruta F, Masuyama N, Gotoh Y (2002) The phosphatidylinositol 3-kinase (PI3K)-Akt pathway suppresses Bax translocation to mitochondria. *J Biol Chem* 277:14040–14047.
- Vila M, Przedborski S (2003) Targeting programmed cell death in neurodegenerative diseases. *Nat Rev Neurosci* 4:365–375.
- Vila M, Jackson-Lewis V, Vukosavic S, Djaldetti R, Liberatore G, Offen D, Korsmeyer SJ, Przedborski S (2001) Bax ablation prevents dopaminergic neurodegeneration in the 1-methyl-4-phenyl-1,2,3,6-tetrahydropyridine mouse model of Parkinson's disease. *Proc Natl Acad Sci USA* 98:2837–2842.
- Watcharasi P, Bijur GN, Song L, Zhu J, Chen X, Jope RS (2003) Glycogen synthase kinase-3beta (GSK3beta) binds to and promotes the actions of p53. *J Biol Chem* 278:48872–48879.
- Wellmann H, Kaltschmidt B, Kaltschmidt C (1999) Optimized protocol for biolistic transfection of brain slices and dissociated cultured neurons with a hand-held gene gun. *J Neurosci Methods* 92:55–64.
- Wolter KG, Hsu YT, Smith CL, Nechushtan A, Xi XG, Youle RJ (1997) Movement of Bax from the cytosol to mitochondria during apoptosis. *J Cell Biol* 139:1281–1292.
- Yamaguchi H, Wang HG (2001) The protein kinase PKB/Akt regulates cell survival and apoptosis by inhibiting Bax conformational change. *Oncogene* 20:7779–7786.
- Zong WX, Lindsten T, Ross AJ, MacGregor GR, Thompson CB (2001) BH3-only proteins that bind pro-survival Bcl-2 family members fail to induce apoptosis in the absence of Bax and Bak. *Genes Dev* 15:1481–1486.
- Zou H, Li Y, Liu X, Wang X (1999) An APAF-1-cytochrome c multimeric complex is a functional apoptosome that activates procaspase-9. *J Biol Chem* 274:11549–11556.

Inhibition of Rac GTPase triggers a c-Jun- and Bim-dependent mitochondrial apoptotic cascade in cerebellar granule neurons

Shoshona S. Le,^{*,1} F. Alexandra Loucks,^{*,1} Hiroshi Udo,[†] Sarah Richardson-Burns,[‡] Reid A. Phelps,^{*} Ron J. Bouchard,^{*} Holger Barth,[§] Klaus Aktories,[¶] Kenneth L. Tyler,^{*,‡} Eric R. Kandel,[†] Kim A. Heidenreich^{***} and Daniel A. Linseman^{***}

^{*}Research Service, Veterans Affairs Medical Center, Denver, Colorado, USA

[†]Howard Hughes Medical Institute, Columbia University, New York, New York, USA

[‡]Department of Neurology, University of Colorado Health Sciences Center, Denver, Colorado, USA

[§]Department of Pharmacology and Toxicology, University of Ulm, Ulm, Germany

[¶]Institut für Experimentelle und Klinische Pharmakologie und Toxikologie der Albert-Ludwigs-Universität Freiburg, Germany

^{***}Department of Pharmacology and Neuroscience Program, University of Colorado Health Sciences Center, Denver, Colorado, USA

Abstract

Rho GTPases are key transducers of integrin/extracellular matrix and growth factor signaling. Although integrin-mediated adhesion and trophic support suppress neuronal apoptosis, the role of Rho GTPases in neuronal survival is unclear. Here, we have identified Rac as a critical pro-survival GTPase in cerebellar granule neurons (CGNs) and elucidated a death pathway triggered by its inactivation. GTP-loading of Rac1 was maintained in CGNs by integrin-mediated (RGD-dependent) cell attachment and trophic support. *Clostridium difficile* toxin B (ToxB), a specific Rho family inhibitor, induced a selective caspase-mediated degradation of Rac1 without affecting RhoA or Cdc42 protein levels. Both ToxB and dominant-negative N17Rac1 elicited CGN apoptosis, characterized by cytochrome *c* release and activation of

caspase-9 and -3, whereas dominant-negative N19RhoA or N17Cdc42 did not cause significant cell death. ToxB stimulated mitochondrial translocation and conformational activation of Bax, c-Jun activation, and induction of the BH3-only protein Bim. Similarly, c-Jun activation and Bim induction were observed with N17Rac1. A c-jun N-terminal protein kinase (JNK)/p38 inhibitor, SB203580, and a JNK-specific inhibitor, SP600125, significantly decreased ToxB-induced Bim expression and blunted each subsequent step of the apoptotic cascade. These results indicate that Rac acts downstream of integrins and growth factors to promote neuronal survival by repressing c-Jun/Bim-mediated mitochondrial apoptosis.

Keywords: Bax, BH3-only, c-jun N-terminal protein kinase, neuronal survival, Rho GTPase.

J. Neurochem. (2005) **94**, 1025–1039.

Apoptosis is a form of programmed cell death that plays an essential role in the development of the central nervous system by mediating the removal of redundant neuronal populations (Lossi and Merighi 2003). However, aberrant neuronal apoptosis contributes to the onset and progression of several devastating neurodegenerative disorders, including Parkinson's disease and amyotrophic lateral sclerosis (Inoue *et al.* 2003; Tatton *et al.* 2003). Consequently, identification of molecular pathways that regulate neuronal apoptosis is key to developing novel therapeutics that slow or halt these neurodegenerative diseases.

One well-studied *in vitro* system used to investigate neuronal apoptosis is cultured cerebellar neurons from early (day 7) post-natal rats. Cerebellar granule neurons (CGNs)

Received February 16, 2005; revised manuscript received April 12, 2005; accepted April 13, 2005.

Address correspondence and reprint requests to Daniel A. Linseman, Denver Veterans Affairs Medical Center, Research Service-111H, 1055 Clermont Street, Denver, CO 80220, USA.

E-mail: Dan.Linseman@UCHSC.edu

¹These authors contributed equally to the manuscript.

Abbreviations used: BSA, bovine serum albumin; CGNs, cerebellar granule neurons; COXIV, cyt C oxidase subunit IV; cyt C, cytochrome *c*; ECM, extracellular matrix; JNK, c-jun N-terminal protein kinase; K⁺_{ex}, extracellular potassium; LTox, *Clostridium sordellii* lethal toxin; PBS, phosphate-buffered saline; SDS-PAGE, sodium dodecyl sulfate – polyacrylamide gel electrophoresis; ToxB, *Clostridium difficile* toxin B.

require both serum-derived growth factors (e.g. insulin-like growth factor-I) and depolarization-mediated Ca^{2+} influx for their survival *in vitro* (D'Mello *et al.* 1993). CGNs deprived of serum growth factors and depolarizing extracellular potassium (K^+_{ex}) undergo a rapid cell death that involves induction of the BH3-only protein, Bim, and activation of an intrinsic (mitochondrial) apoptotic cascade (Gerhardt *et al.* 2001; Linseman *et al.* 2002b).

In addition to growth factors and activity-dependent Ca^{2+} influx, neurons also depend on survival signals originating at sites of cell attachment to the extracellular matrix (ECM). Cell–matrix adhesion is mediated via binding of heterodimeric integrin receptors to their ECM ligands. The activated (ligand-bound) integrins stimulate multiple survival signals, including AKT- and ERK-dependent pathways, by interacting with partner proteins via their cytoplasmic domains (Stupack and Cheresch 2002).

Rho family GTPases are monomeric G-proteins that act as key transducers of integrin/ECM signaling (Parise *et al.* 2000; Schwartz and Shattil 2000; Arthur *et al.* 2002) and growth factor signaling (Huang and Reichardt 2003; Burrige and Wennerberg 2004). These G-proteins are involved in a diverse array of biological functions, including cytoskeletal dynamics, membrane trafficking, cell cycle progression, gene transcription, adhesion, migration, and cell survival (Etienne-Manneville and Hall 2002; Burrige and Wennerberg 2004). The three most studied family members include RhoA, Rac1, and Cdc42.

Despite the essential roles that Rho family GTPases play in mediating survival signaling by integrins and growth factors, the potential of these G-proteins to promote neuronal survival has largely been unexplored. We have previously utilized Clostridial toxins, which act as highly specific inhibitors of Ras and Rho family GTPases (Busch and Aktories 2000), to demonstrate a critical function for these G-proteins in maintaining CGN survival (Linseman *et al.* 2001a). In particular, *Clostridium difficile* toxin B (ToxB) and *Clostridium sordellii* lethal toxin (LTox), are large Clostridial toxins that specifically mono-glucosylate a critical threonine residue conserved in the switch 1 region of Ras and Rho family members. The substrate specificities for these two toxins include Rho, Rac, and Cdc42 for ToxB and Rac, Cdc42 (to a lesser extent than Rac), Ras, and Rap for LTox (Just *et al.* 1995; Genth *et al.* 1996; Popoff *et al.* 1996; Hofmann *et al.* 1998; Djouder *et al.* 2000). Incubation of CGNs with either of these toxins induces substantial apoptosis, whereas the Rho-specific inhibitor, *Clostridium botulinum* C3 fusion toxin (Barth *et al.* 1998), does not promote CGN death. From these data, we previously concluded that Clostridial toxins with overlapping specificities for inhibiting Rac and Cdc42 GTPases are capable of inducing apoptosis of CGNs, suggesting a key role for one or both of these specific G-proteins in promoting CGN survival (Linseman *et al.* 2001a).

In the present study, we have utilized adenoviral dominant-negative mutants of RhoA, Rac1, and Cdc42 to explicitly identify Rac as the essential pro-survival GTPase in CGNs. In addition, we have elucidated a death pathway triggered in CGNs by antagonism of Rac and determined that it is dependent on a c-Jun-driven induction of Bim and the subsequent activation of a mitochondrial apoptotic cascade. Our findings suggest a critical role for Rac as an endogenous suppressor of c-Jun/Bim-dependent mitochondrial apoptosis in healthy neurons.

Experimental procedures

Materials

Reagents for measurement of GTP-bound Rac, including agarose-conjugated PAK-protein binding domain, were obtained from Upstate Biotechnology (Charlottesville, VA, USA) and Cytoskeleton Inc. (Denver, CO, USA). Monoclonal antibodies to Rac1 (clone 102; 1 : 1000), Rho (clone 55; 1 : 250), Cdc42 (clone 44; 1 : 250), and a polyclonal to cyt C oxidase subunit IV (COXIV) were from BD Biosciences Clontech (Palo Alto, CA, USA). *C. difficile* toxin B was isolated and prepared as previously described (von Eichel-Streiber *et al.* 1987). Hoechst dye number 33258 and 4',6-diamidino-2-phenylindole (DAPI) were from Sigma (St Louis, MO, USA). SB203580, SP600125, the pan-caspase inhibitors, Boc-Asp(OMe)-FMK and zVAD-FMK, the caspase-9-selective inhibitor, zLEHD-FMK, the proteasome inhibitor, MG132, and RGD and RAD peptides were from Calbiochem (San Diego, CA, USA). Rabbit polyclonal antibodies to Bim (FL-198; 1 : 250) and cytochrome *c* (H-104; 1 : 200) were obtained from Santa Cruz Biotechnology (Santa Cruz, CA, USA). Polyclonal antibodies to the active fragment of caspase-9 were purchased from Santa Cruz (H-83; 1 : 200 for western blotting) and from Cell Signaling Technology (1 : 500; Beverly, MA) for immunocytochemistry. Polyclonal antibodies to active caspase-3 were from Santa Cruz (H-227; 1 : 250 for western blotting) and Promega (rabbit pAb; 1 : 500; Madison, WI, USA) for immunocytochemistry. A plasmid encoding an amino-terminal GFP fusion protein of human Bax_s was kindly provided by Dr R. J. Youle (NINDS, NIH, Bethesda, MD, USA). Monoclonal antibody to the active conformation of Bax (clone 6A7; 1 : 1000) was purchased from Alexis Biochemicals (San Diego, CA, USA). Rabbit polyclonal antibody to c-Jun (1 : 1000) was from Cell Signaling Technology. Horseradish peroxidase-linked secondary antibodies and reagents for enhanced chemiluminescence detection were obtained from Amersham Biosciences (Piscataway, NJ, USA). Cy3-conjugated secondary antibodies for immunofluorescence were from Jackson Immunoresearch Laboratories (West Grove, PA, USA).

CGN culture

Rat CGNs were isolated from 7-day-old Sprague–Dawley rat pups (15–19 g) as described previously (Li *et al.* 2001). Briefly, neurons were plated on 35-mm diameter plastic dishes coated with poly-L-lysine at a density of 2.0×10^6 cells/mL in basal modified Eagle's medium containing 10% fetal bovine serum, 25 mM KCl, 2 mM L-glutamine, and penicillin (100 units/mL)/streptomycin (100 µg/mL) (Life Technologies, Grand Island, NY, USA). Cytosine

arabinoside (10 μM) was added to the culture medium 24 h after plating to limit the growth of non-neuronal cells. These cultures are highly homogeneous, consisting of approximately 95–98% cerebellar granule neurons (CGNs) with the remainder being primarily made up of Purkinje neurons (Linseman *et al.* 2002a). In general, experiments were performed after 6–7 days in culture.

Cell lysis and immunoblotting

Following incubation, the culture medium was aspirated, cells were washed once with 2 mL of ice-cold PBS (pH 7.4), placed on ice and scraped into lysis buffer (200 μL /35-mm well) containing 20 mM HEPES (pH 7.4), 1% Triton X-100, 50 mM NaCl, 1 mM EGTA, 5 mM β -glycerophosphate, 30 mM sodium pyrophosphate, 100 mM sodium orthovanadate, 10 $\mu\text{g}/\text{mL}$ leupeptin, and 10 $\mu\text{g}/\text{mL}$ aprotinin. In the case of subcellular fractionation to isolate a mitochondrial pellet, CGNs were lysed and fractionated according to the manufacturer's directions using a commercially available mitochondria/cytosol fractionation kit (Alexis Biochemicals). Cell debris was removed by centrifugation at 600 *g* for 3 min and the protein concentration of the supernatant was determined using a commercially available protein assay kit (Pierce, Rockford, IL, USA). Aliquots (~80 μg) of supernatant protein were diluted to a final concentration of 1 \times sodium dodecyl sulfate – polyacrylamide gel electrophoresis (SDS–PAGE) sample buffer, boiled for 5 min, and electrophoresed through 12.5 or 15% polyacrylamide gels. Proteins were transferred to polyvinylidene difluoride (PVDF) membranes (Amersham Biosciences) and processed for immunoblot analysis.

Non-specific binding sites were blocked in phosphate-buffered saline (PBS; pH 7.4) containing 0.1% Tween 20 (PBS-T) and 1% bovine serum albumin (BSA) for 1 h at room temperature (22°C). Primary antibodies were diluted in blocking solution and incubated with the membranes for 1 h. Excess primary antibody was removed by washing the membranes three times in PBS-T. The blots were then incubated with the appropriate horseradish peroxidase-conjugated secondary antibody diluted in PBS-T for 1 h and were subsequently washed three times in PBS-T. Immunoreactive proteins were detected by enhanced chemiluminescence. Autoluminograms shown are generally representative of at least three independent experiments.

BD PowerBlot™ analysis

CGN lysates were pooled from three separate cell isolations following incubation for 24 h with either vehicle (2 $\mu\text{g}/\text{mL}$ BSA, final concentration) or ToxB (40 ng/mL , final concentration). Lysates were prepared according to the manufacturer's instructions followed by western blotting with a PowerBlot™ array of over 1000 monoclonal antibodies (BD Biosciences). Raw data in the form of image files of the actual blots and densitometric measurements of the immunoreactive proteins were obtained from the manufacturer. The blots and densitometric results shown for Rac1, RhoA, and Cdc42 are representative of a 2 \times 2 comparison of duplicate control and ToxB lysates.

Adenoviral preparation and infection

Adenoviral dominant-negative Rho family GTPases were constructed as previously described (Allen *et al.* 2002). Briefly, Rac1, RhoA, and Cdc42 were cloned from a mouse cDNA library. Dominant-negative (T17N or T19N) mutations were generated by

PCR-based site-directed mutagenesis. Adenoviral GFP, GFP/N17Rac1, GFP/N17Cdc42, and GFP/N19RhoA were generated using the AdEasy system (Qbiogene Inc., Carlsbad, CA, USA). The produced adenoviruses express both GFP and the respective dominant-negative Rho family mutant. CGN cultures were infected on day 4 *in vitro* with adenoviruses at a final titer of 50 infectious particles per cell. Using these conditions, the adenoviruses infected approximately 15–20% of the CGNs in the cultures. At 72 h post-infection, CGNs were fixed in paraformaldehyde and nuclei were stained with Hoechst dye for quantitation of apoptosis. Alternatively, cell lysates of infected cells were prepared for immunoblot analysis. Because of the mechanisms involved in infecting primary neurons, CGNs require at least 48 h for infection to be effective (based on visualization of GFP fluorescence). Therefore, infecting them for 72 h is essentially equivalent to exposing the cells for approximately 24 h to the dominant negative mutant.

Rac GTP-binding assays

CGNs were either deprived of serum and depolarizing K^+ for up to 4 h, detached from the culture plate by scraping for various times from 15 min to 4 h, or incubated for 8 h with one of two small peptides, H-Gly-Arg-Ala-Asp-Ser-Pro-OH (RAD; negative control, 10 mM) or H-Gly-Arg-Gly-Asp-Ser-Pro-OH (RGD; 10 mM). Cells were lysed by homogenization in a high (10 mM) Mg^{2+} buffer and the lysates were briefly pelleted to remove cell debris. A small aliquot of the resulting supernatant was immediately removed for detection of total Rac1 protein. To detect GTP-bound Rac1, agarose beads bound to a GST-PAK-protein binding domain were added to the remaining supernatant according to the manufacturer's instructions (Upstate Biotechnology). The supernatants were then mixed by inversion for 1 h at 4°C and the pelleted beads were washed three times with Mg^{2+} lysis buffer. Aliquots of the original cell lysates and the PAK-precipitates were subjected to SDS–PAGE through 15% polyacrylamide gels, transferred to PVDF membranes, and immunoblotted for Rac1.

Quantitation of apoptosis

Treated neurons were fixed in 4% paraformaldehyde and nuclei were stained with Hoechst dye. Cells were scored as apoptotic if they contained chromatin that was condensed and/or fragmented. In general, approximately 500 cells from at least two fields of a 35-mm well were scored and each treatment was performed in duplicate in a minimum of three independent experiments. For the cultures infected with adenoviral dominant-negative Rho family GTPases, approximately 100 infected cells (GFP-positive neurons) were quantitated per coverslip, and each adenovirus was infected into triplicate coverslips in a total of four separate experiments.

Immunocytochemistry

CGNs were cultured on polyethyleneimine-coated glass cover slips at a density of approximately 5 \times 10⁵ cells per coverslip. Following adenoviral infection and/or incubation as described in Results, cells were fixed in 4% paraformaldehyde and were then permeabilized and blocked in PBS (pH 7.4) containing 0.2% Triton X-100 and 5% BSA. Cells were then incubated for approximately 16 h at 4°C with primary antibody diluted in PBS containing 0.2% Triton X-100 and 2% BSA. The primary antibody was aspirated and the cells were

washed five times with PBS. The cells were then incubated with Cy3-conjugated secondary antibodies and DAPI for 1 h at room temperature. CGNs were then washed five more times with PBS and coverslips were adhered to glass slides in mounting medium (0.1% *p*-phenylenediamine in 75% glycerol in PBS). Fluorescent images were captured using a 63 \times oil immersion objective on a Zeiss Axioplan 2 microscope equipped with a Cooke Sencicam deep-cooled CCD camera and a Slidebook software analysis program for digital deconvolution (Intelligent Imaging Innovations Inc., Denver, CO, USA).

Gene-gun transfection

CGNs were transiently transfected using the Helios Gene-Gun system (Bio-Rad, Hercules, CA, USA). Briefly, 60 μ g of plasmid DNA was precipitated onto 30 mg of 0.6 μ m-diameter gold beads in a CaCl₂/spermidine mixture. The gold/DNA precipitates were washed three times in 100% ethanol, and re-suspended in 3 mL of ethanol containing 0.05 mg/mL polyvinylpyrrolidone. After thoroughly re-suspending the gold/DNA precipitate, it was drawn into approximately 74 cm of Tefzel tubing and the beads were allowed to settle to the bottom of the tubing. After 5 min, the ethanol was slowly drawn off while the beads adhered to the tubing. The tubing was dried under nitrogen for an additional 5 min and then cut into approximately 1.3-cm pieces. CGNs to be transfected were seeded at a density of 8×10^5 cells/well on polyethyleneimine-coated glass coverslips in 24-well plates. After 5 days in culture, the medium was removed from the wells and the 1.3-cm lengths of tubing containing the DNA-bound beads were loaded into the Gene-Gun and shot with a burst of ~ 100 p.s.i. helium through a 40- μ m nylon cell strainer placed over the well. The medium was immediately replaced and cells were grown an additional 48 h before exposure to ToxB and subsequent image analysis of the localization of either GFP alone or the GFP-Bax fusion protein.

Results

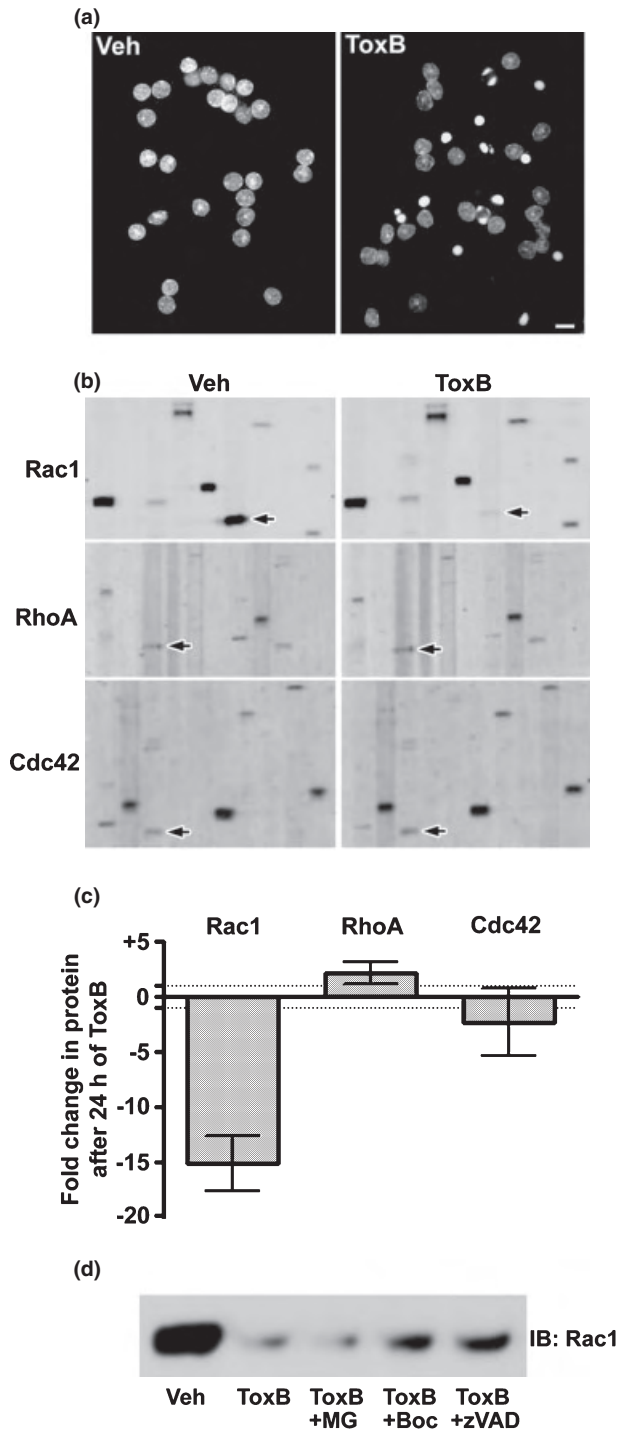
ToxB induces a specific caspase-mediated degradation of Rac1 in CGNs undergoing apoptosis

To define the relative pro-survival contributions of Rac and Cdc42 GTPases in CGNs, we examined the protein expression of the various Rho family members during ToxB-induced apoptosis. As previously reported (Linseman *et al.* 2001a), CGNs incubated for 24 h with ToxB showed a marked increase in the percentage of cells with condensed and/or fragmented nuclei, consistent with an apoptotic mechanism of cell death (Fig. 1a). After 24 h of incubation with either vehicle or ToxB, CGN lysates were prepared and electrophoresed through polyacrylamide gels for analysis using the BD PowerBlotTM screen (BD Biosciences). Representative immunoblots are shown in Fig. 1(b) that include areas of the membranes which were probed with monoclonal antibodies against either Rac1, RhoA, or Cdc42 (indicated by the arrows). Incubation with ToxB induced a striking decrease in the amount of Rac1 detected in CGN lysates (Fig. 1b, upper panels, see arrows). In contrast,

neither RhoA nor Cdc42 showed any notable reduction in immunoreactivity in lysates from CGNs exposed to ToxB (Fig. 1b, middle and lower panels, see arrows). Semiquantitative densitometric analysis of the PowerBlotTM data is shown in Fig. 1(c). Incubation with ToxB for 24 h induced an approximately 15-fold reduction in the immunoreactivity of Rac1, but had no demonstrable effect on the content of either RhoA or Cdc42. Furthermore, the marked loss of Rac1 GTPase observed in CGNs exposed to ToxB was not affected by an inhibitor of the 26S proteasome, MG132, but was partially blocked by co-incubation with the pan-caspase inhibitors, Boc-Asp(OMe)-FMK or zVAD-FMK (Fig. 1d). In agreement with a recent report that identified Rac1 as a caspase substrate in lymphoma cells (Zhang *et al.* 2003), the current data suggest that the effects of the glucosylation of Rac by ToxB are potentially augmented by the caspase-mediated degradation of this G-protein in CGNs. Thus, although ToxB glucosylates and inhibits all three Rho family members, Rho, Rac and Cdc42 (Just *et al.* 1995), Rac1 GTPase is the sole member degraded by caspases following its glucosylation in CGNs, likely resulting in a prolonged functional inhibition of this particular G-protein.

Adenoviral expression of dominant-negative Rac1 induces CGN apoptosis

Given the specific caspase-mediated degradation of Rac1 observed in ToxB-treated CGNs, and the fact that Rac1 is a common substrate for two Clostridial toxins (ToxB and LTox) that each induce apoptosis of CGNs (Linseman *et al.* 2001a), we postulated that Rac is the major pro-survival Rho family GTPase in these neurons. To test this hypothesis, we infected CGN cultures with adenoviruses expressing either GFP alone or in combination with dominant-negative mutants of either RhoA (N19), Rac1 (N17), or Cdc42 (N17). At 72 h post-infection, CGNs were fixed and stained with Hoechst dye to identify nuclear morphology. Infection with adenoviral GFP had essentially no effect on the survival of CGNs with less than 10% of the GFP-expressing cells undergoing apoptosis after 72 h (Fig. 2a, upper panels, and Fig. 2b). In contrast, adenoviral-mediated expression of N17Rac1 with GFP induced a significant (approximately 5.8-fold) increase in CGN apoptosis when compared with GFP alone, which was characterized by marked nuclear condensation and fragmentation (Fig. 2a, lower panels, and Fig. 2b). Although both N17Cdc42 and N19RhoA tended to enhance the apoptosis of CGNs, the effects of these dominant-negative GTPases did not reach statistical significance at 72 h post-infection (Fig. 2b). The differential effects of these dominant-negative GTPase mutants on CGN survival strongly corroborate our previous data obtained using Rho GTPase-specific inhibitory toxins (Linseman *et al.* 2001a), and establish Rac as a major pro-survival GTPase in CGNs.



Rac activity is maintained by trophic support and integrin-mediated cell attachment in CGNs

Rho family GTPases are activated downstream of both integrin and growth factor receptor stimulation (Marcoux and Vuori 2003). Moreover, both integrin- and growth factor-dependent signals contribute to neuronal survival (Gary and Mattson 2001; Linseman *et al.* 2002b; Gary *et al.* 2003). To

Fig. 1 ToxB induces apoptosis and elicits a selective caspase-mediated degradation of Rac1 GTPase in CGNs. (a) CGNs were incubated for 24 h in complete medium (containing serum and 25 mM KCl) in the presence of either vehicle (Veh; 2 μ g/mL BSA in PBS) or ToxB (40 ng/mL). Following incubation, cells were fixed in paraformaldehyde and nuclei were stained with Hoechst dye. CGNs exposed to ToxB showed marked nuclear condensation and fragmentation characteristic of apoptosis. Scale bar, 10 μ m. (b) Representative immunoblots of lysates obtained from CGNs incubated as described in (a). The blots shown were obtained from the BD PowerBlot™ (see Experimental procedures for details) using specific monoclonal antibodies against Rac1 (upper blots), RhoA (middle blots), or Cdc42 (lower blots). The immunoreactive Rho family GTPases are indicated by the arrows. Other protein bands apparent on the membranes represent adjacent lanes of the PowerBlot™ that were probed for distinct proteins and are shown to give an indication of the overall equality of protein loading. (c) The fold change in protein content induced by 24 h of ToxB treatment for each of the Rho family members blotted for in (b) is shown. Data represent the means \pm range of duplicate PowerBlot™ comparisons for each GTPase. The dotted lines indicate no change (-1 to $+1$ fold). (d) CGNs were exposed for 8 h to ToxB in the absence or presence of either a pan-caspase inhibitor (Boc-Asp(OMe)-FMK; 200 μ M or zVAD-FMK; 200 μ M) or a proteasome inhibitor (MG132; 10 μ M). Following incubation, cell lysates were immunoblotted for Rac1.

add further support that Rac1 activity is important for CGN survival, we assessed the relative contributions of integrins or trophic support in the activation of Rac1 by examining the effects of cell detachment or trophic factor deprivation on Rac1 GTP-binding using a PAK-based pull-down assay (Benard *et al.* 1999). Consistent with a growth factor receptor-dependent pathway for Rac1 activation in CGNs, removal of serum and depolarizing K^+ induced a significant loss of Rac GTP-loading in attached CGNs (Fig. 3a). Similarly, detachment from the culture dish led to a rapid loss of GTP-bound Rac1 (Fig. 3b), and this effect occurred more quickly than that observed upon trophic factor withdrawal. These data show that active (GTP-bound) Rac1 is maintained in CGNs by both trophic factor stimulation and cell attachment to the ECM.

Cell adhesion and subsequent signal transduction is often activated by integrins and can occur in conjunction with growth factor receptor stimulation (Gibson *et al.* 2005). Integrins mediate cell attachment via recognition of an Arg-Gly-Asp (RGD) motif on ECM ligands like fibronectin (Takagi 2004). To determine if the effects of cell attachment on Rac activity in CGNs are integrin-mediated, we utilized RGD-containing inhibitory peptides. The RGD peptides compete with RGD-containing ECM proteins for integrin binding, thereby reducing integrin signaling. It has previously been shown that RGD peptides inhibit integrin stimulation of Rho family GTPases (Yang *et al.* 1999). CGNs incubated for 8 h with RGD peptides showed a marked decrease in GTP-bound Rac1 relative to cells incubated with the negative control peptide, RAD (Fig. 3c). These results indicate that Rac1 activity is maintained in

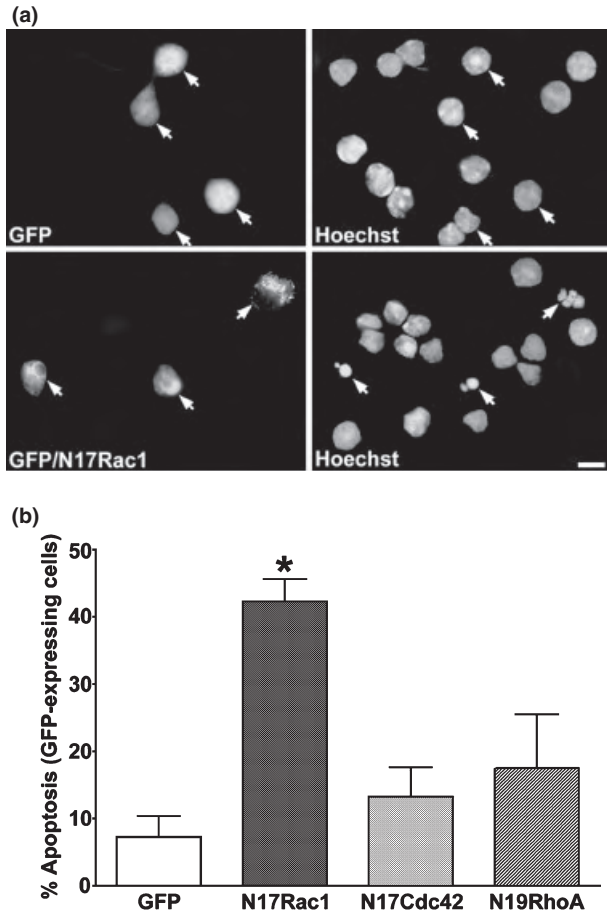


Fig. 2 Adenoviral expression of N17Rac1 induces apoptosis of CGNs: dominant-negative mutants of RhoA or Cdc42 do not cause significant cell death. (a) On day 4 *in vitro*, CGN cultures were infected with adenovirus expressing either GFP alone or in combination with dominant-negative N17Rac1. At 72 h post-infection, CGNs were fixed in paraformaldehyde and nuclei were stained with Hoechst dye. Images shown represent composites of two fields each for GFP or GFP/N17Rac1. Infected cells are indicated by the arrows. CGNs infected with adenovirus expressing GFP alone showed large intact nuclei characteristic of healthy cells (upper panels). In contrast, CGNs infected with adenovirus expressing N17Rac1 displayed marked chromatin condensation and fragmentation indicative of apoptotic cell death (lower panels). Note that non-infected cells in the N17Rac1 condition remained healthy. Scale bar, 10 μ m. (b) Quantitation of CGN apoptosis in GFP-expressing cells following 72 h of infection with adenoviruses expressing either GFP alone or in combination with dominant-negative mutants of Rac1, Cdc42, or RhoA at a final titer of 50 infectious particles per cell. Using these conditions, each of the adenoviruses infected approximately 15–20% of the CGNs in the cultures. The results shown represent the means \pm SEM for four experiments, each conducted on triplicate coverslips in which approximately 100 GFP-positive CGNs were counted per condition per coverslip. *Significantly different from adenoviral GFP alone ($p < 0.01$).

CGNs via integrin signaling downstream of cell attachment (and trophic stimulation).

ToxB and N17Rac1 each trigger cytochrome *c* release and activation of caspases-9 and -3 in CGNs

Previous work has shown that CGNs deprived of serum and depolarizing K^+ _{ex} undergo apoptosis that involves activation of an intrinsic mitochondrial pathway (Gerhardt *et al.* 2001; Linseman *et al.* 2002b). To determine if CGN death induced by the inhibition of Rac GTPase proceeds by a similar mechanism, we analyzed the ability of ToxB or N17Rac1 to trigger mitochondrial cytochrome *c* (cyt C) release. Subcellular fractionation of CGN lysates showed that the vast majority of cyt C in vehicle-treated cells was localized to the mitochondrial pellet along with the integral mitochondrial membrane protein, COXIV (Fig. 4a, first and second lanes). Incubation with ToxB for 24 h resulted in a marked decrease in cyt C immunoreactivity in the mitochondrial pellet and a coincident appearance of several high molecular weight bands in the cytosolic fraction that were detected by the cyt C antibody (Fig. 4a, third and fourth lanes, see arrowheads). We postulate that these high molecular weight forms of cyt C may represent ubiquitin conjugates of the released protein as has previously been observed for yeast cyt C (Pearce and Sherman 1997). Regardless of the precise nature of these high molecular weight forms of cyt C, it is clear from the substantial loss of immunoreactivity in the mitochondrial pellet that the majority of cyt C was indeed released from mitochondria in CGNs exposed to ToxB.

In addition to subcellular fractionation, cyt C localization was also assessed by immunocytochemical methods. CGNs incubated with vehicle showed a cyt C distribution that was punctate and perinuclear in agreement with its localization to mitochondria (Fig. 4b, upper panels). In contrast, CGN cultures exposed to ToxB for 24 h displayed cells that had condensed and fragmented chromatin accompanied by a diffuse distribution of cyt C over the entire cell body, consistent with its release into the cytoplasm (Fig. 4b, lower panels, see arrows). In a similar manner, many CGNs which were infected with adenovirus expressing GFP and N17Rac1 showed a nearly complete loss of cyt C immunoreactivity that was coincident with condensed nuclei at 72 h post-infection, consistent with an extremely diffuse distribution of cyt C in the apoptotic cells (Fig. 4c, see arrows). Note that uninfected surrounding cells showed punctate cyt C staining localized in the perinuclear region and contained large intact nuclei. In addition, CGNs expressing GFP alone did not have condensed nuclei at 72 h, and the cyt C remained localized in the mitochondria (data not shown). These results indicate that CGN apoptosis induced by either ToxB or N17Rac1 proceeds via the release of cyt C from mitochondria.

Once cyt C is released from mitochondria, it interacts with apoptosis-activating factor-1 (Apaf-1) and pro-caspase-9 to form an oligomeric apoptosome structure that activates the

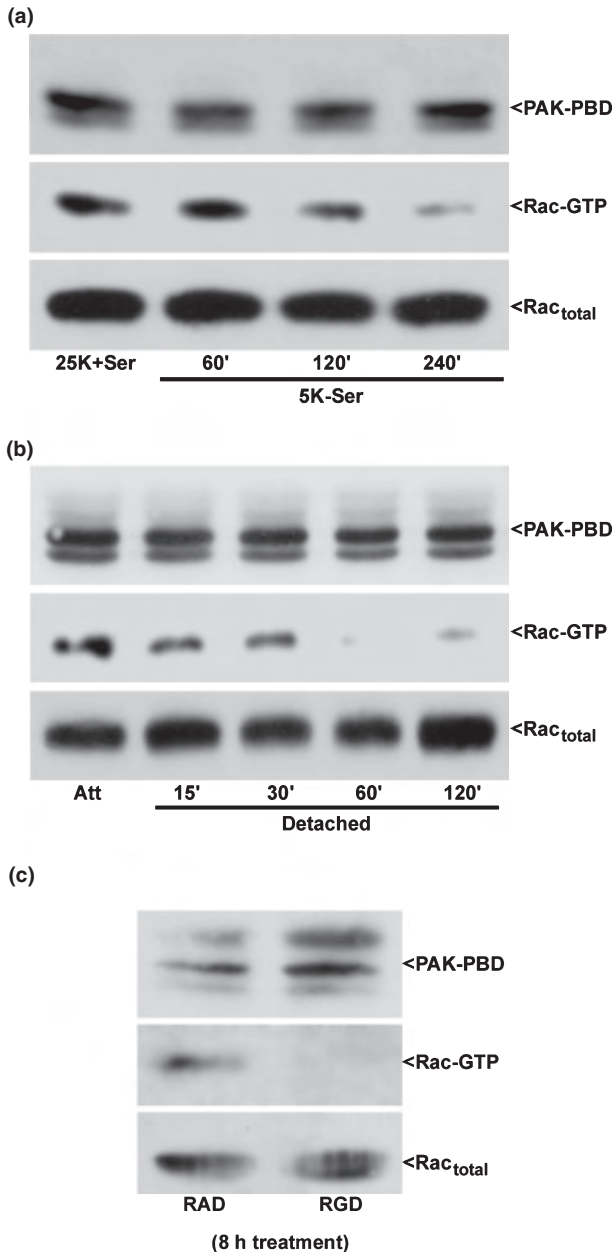


Fig. 3 Rac1 GTP-loading is maintained in CGNs by trophic support and integrin-mediated cell attachment. CGNs were incubated under either attached conditions (a) in trophic factor-deprived medium containing 5 mM KCl and lacking serum (5K-Ser) for up to 4 h, detached conditions (b) for up to 2 h in medium containing 25 mM KCl and serum (25K + Ser), or incubated with RAD or RGD peptides (c) for 8 h. Following incubation, CGNs were immediately lysed on ice into a high Mg^{2+} buffer. Cell debris was removed by brief centrifugation and a small aliquot of the resulting lysate was separated for quantitation of total Rac in each sample. The remaining cell lysates were incubated for 1 h with an excess of the protein binding domain of the Rac effector, PAK (PAK-PBD), bound to agarose beads. The pellet was washed three times with lysis buffer and samples were electrophoresed through 15% polyacrylamide gels. Proteins were transferred to PVDF membranes which were immunoblotted with a monoclonal antibody against Rac1 and an HRP-conjugated secondary antibody. Immunoreactive Rac1 protein was detected using standard ECL techniques. GTP-loaded Rac was brought down in the PAK-PBD precipitation (middle blots). The PAK-PBD is detected non-specifically by the secondary antibody and is shown as a control for equal loading (upper blots). The total Rac in each lysate is also shown as a loading control as no significant loss is detected in Rac protein under these conditions (bottom blots). The blots shown are representative of results obtained in three separate experiments. Att, attached control.

no active caspase staining was detected in CGNs expressing GFP alone (data not shown). Essentially every N17Rac1 GFP-positive cell that showed condensed and/or fragmented chromatin was immunoreactive for active caspase-9 or -3. Moreover, CGN apoptosis induced by a 24-h incubation with ToxB ($40 \pm 4\%$ apoptosis with ToxB vs. $8 \pm 2\%$ apoptosis with vehicle, mean \pm SEM, $n = 3$, $p < 0.01$ vs. vehicle) was significantly suppressed by co-incubation with either a pan-caspase inhibitor [Boc-Asp(OMe)-FMK, $9 \pm 1\%$ apoptosis, $p < 0.01$ vs. ToxB alone] or a caspase-9 selective inhibitor (zLEHD-FMK, $13 \pm 2\%$ apoptosis, $p < 0.01$ vs. ToxB alone). Thus, CGN apoptosis triggered by the inhibition of Rac with either ToxB or N17Rac1 involves the cyt C-mediated activation of caspase-9 and -3.

ToxB elicits Bax translocation to mitochondria and conformational activation of Bax in CGNs

Cyt C is released from mitochondria via an oligomeric channel containing the multidomain Bcl-2 family member, Bax (Antonsson *et al.* 2000). Bax is normally sequestered in the cytoplasm of healthy cells via binding to 14-3-3 scaffolding proteins and translocates to mitochondria in response to apoptotic stimuli (Nomura *et al.* 2003). In CGNs transfected via gene gun with GFP-Bax (Wolter *et al.* 1997), distribution of the fusion protein changed from a diffuse pattern in vehicle-treated cells (Fig. 6a, upper panels, see arrows and Fig. 6b, left panel) to a punctate mitochondrial localization following ToxB treatment (Fig. 6a, middle panels, see arrows and Fig. 6b, middle panel). The redistribution of GFP-Bax to mitochondria following ToxB

intrinsic initiator caspase, caspase-9 (Zou *et al.* 1999). Therefore, we next examined CGNs exposed to ToxB or N17Rac1 for the appearance of the intrinsic initiator caspase-9 and the executioner caspase-3. Using antibodies that detect the cleaved (active) fragments of caspase-9 and -3, we found that CGNs incubated for 24 h with ToxB showed activation of each of these proteases (Figs 5a and b, respectively). Similarly, many CGNs expressing N17Rac1 (identified by GFP fluorescence) showed apoptotic nuclear morphology in conjunction with positive staining using antibodies that specifically detect the cleaved forms of caspase-9 and -3 (Figs 5c and d, respectively), but

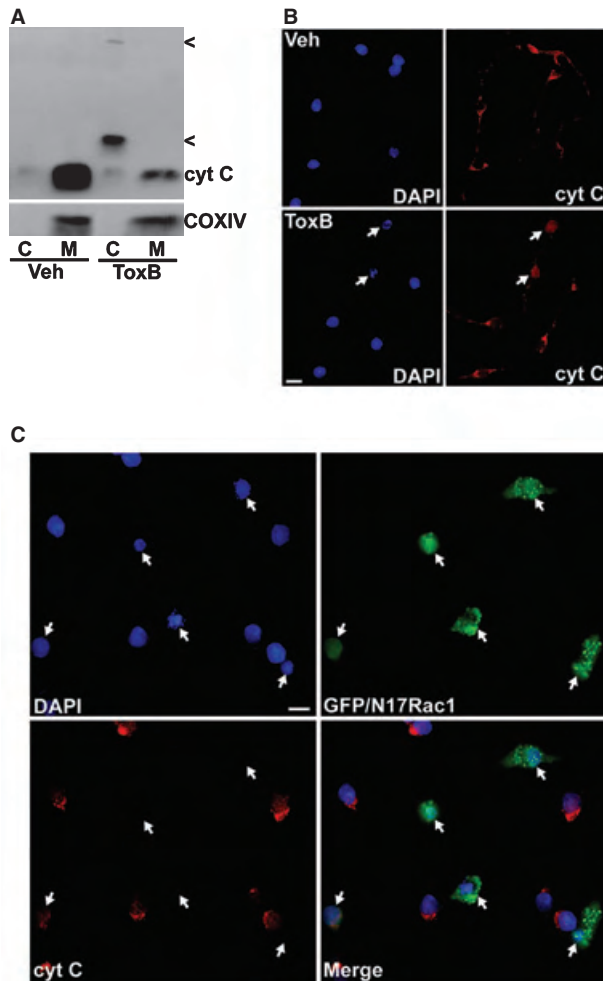


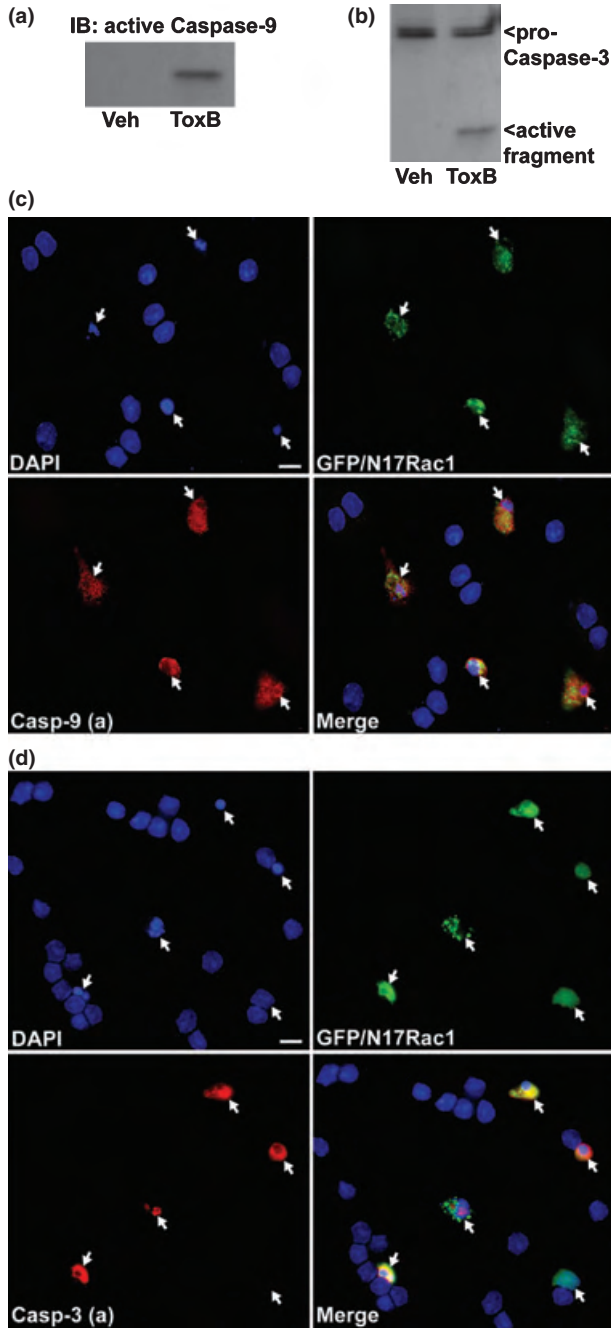
Fig. 4 ToxB and N17Rac1 each trigger cytochrome *c* release from mitochondria in CGNs. (a) CGNs were incubated for 24 h in complete medium (containing serum and 25 mM KCl) in the presence of either vehicle (Veh; 2 μ g/mL BSA in PBS) or ToxB (40 ng/mL). Following incubation, cell lysates were fractionated into cytosolic (C) and mitochondrial (M) subcellular fractions as described in Experimental procedures. Equivalent amounts of cytosolic (20 μ g) and mitochondrial (40 μ g) fractions from Veh- or ToxB-treated cells were subjected to SDS-PAGE and immunoblotted for cytochrome *c* (cyt C). The membranes were then stripped and re-probed for the integral mitochondrial membrane protein, cyt C oxidase subunit IV (COXIV), to verify the purity of the subcellular fractions. Note that the amount of cyt C detectable in mitochondrial fractions was significantly less in ToxB-treated CGNs, although the amount of immunoreactive COXIV was similar to Veh. The cyt C released into the cytosolic fraction in the ToxB-treated cells did not appear at the same molecular weight as that detected in the mitochondrial fractions, but instead it displayed several higher molecular weight forms (indicated by <) which may reflect ubiquitination of the cytoplasmic cyt C. The blots shown are illustrative of data from two independent experiments. (b) CGNs were exposed to Veh or ToxB as described in (a). After 24 h, cells were fixed with paraformaldehyde, blocked and permeabilized in 5% BSA and 0.2% Triton X-100, and incubated with a polyclonal antibody to cyt C. Localization of cyt C was detected using a Cy3-conjugated secondary antibody and nuclei were stained with DAPI. Veh-treated CGNs showed healthy nuclei and cyt C localization that was mostly perinuclear consistent with mitochondria (upper panels). In contrast, a significant fraction of the CGNs exposed to ToxB displayed fragmented nuclei and a diffuse distribution of cyt C over the entire cell body (lower panels, see arrows). The images shown are indicative of those from three separate experiments. Scale bar, 10 μ m. (c) CGNs were incubated for 72 h after infection with adenovirus expressing GFP and N17Rac1 (at a final titer of 50 infectious particles per cell). Following infection, cells were stained for cyt C, as described in (b). The merged image shows that the majority of GFP- and N17Rac1-positive cells (indicated by the arrows) had condensed or fragmented nuclear morphology and lacked detectable cyt C staining, whereas surrounding uninfected cells were largely healthy and displayed significant perinuclear cyt C. The essentially complete loss of cyt C staining in the N17Rac1-expressing cells likely reflects the diffuse distribution of the protein over such a prolonged time post-infection. The images shown are composites of three different fields of CGNs infected with adenoviral GFP/N17Rac1. Scale bar, 10 μ m.

exposure occurred in conjunction with substantial nuclear condensation and fragmentation. In contrast, ToxB did not cause a significant redistribution of the control protein, GFP, which maintained a relatively diffuse localization throughout the entire cell body despite the fact that significant apoptosis was induced (Fig. 6a, lower panels, see arrows and Fig. 6b, right panel).

In addition to mitochondrial translocation, upon induction of apoptosis Bax also undergoes a conformational change that exposes an amino-terminal epitope detected by a specific monoclonal (6A7) antibody (Hsu and Youle 1998). CGN cultures incubated with vehicle showed little-to-no detectable immunoreactivity with the Bax 6A7 antibody (Fig. 6c, left panel). However, CGNs exposed to ToxB showed marked positive staining with the active conformation-specific Bax antibody in conjunction with chromatin condensation and fragmentation (Fig. 6c, right panel). These results show that ToxB-mediated inactivation of Rac GTPase stimulates Bax translocation to mitochondria while concurrently promoting a conformational change in Bax that is commonly associated with its cyt C-releasing activity.

ToxB and N17Rac1 each promote c-Jun activation and Bim induction in CGNs: inhibition of c-Jun and Bim activation by the pyridinyl imidazole SB203580

Conformational activation and mitochondrial translocation of Bax is stimulated by pro-apoptotic BH3-only proteins that neutralize the activities of anti-apoptotic Bcl-2 family members (Bouillet *et al.* 2002). Various isoforms of Bim, a BH3-only protein, play a significant role in several models of neuronal apoptosis (Putcha *et al.* 2001; Linseman *et al.* 2002b; Napankangas *et al.* 2003). In response to diverse apoptotic stimuli, Bim expression is up-regulated at the transcriptional level. One of the key signaling pathways that promotes Bim transcription involves the c-jun N-terminal



protein kinase (JNK)-mediated phosphorylation of c-Jun (Harris and Johnson 2001; Whitfield *et al.* 2001). As we previously have shown (Linseman *et al.* 2001a), incubation of CGNs with ToxB induced a rapid increase in the phosphorylation (detected as a decrease in electrophoretic mobility) and expression of c-Jun (Fig. 7a), effects that were largely prevented by the pyridinyl imidazole JNK/p38 MAPK inhibitor, SB203580 (Fig. 7b) (Coffey *et al.* 2002). Consistent with c-Jun stimulating Bim transcription, ToxB also induced a marked increase in the expression of Bim_s (the

Fig. 5 ToxB and N17Rac1 each promote activation of caspases-9 and -3 in CGNs. (a) CGNs were incubated for 24 h in complete medium (containing serum and 25 mM KCl) in the presence of either vehicle (Veh; 2 μg/mL BSA in PBS) or ToxB (40 ng/mL). After incubation, cell lysates were resolved by SDS-PAGE on 15% polyacrylamide gels and proteins were transferred to PVDF membranes. The blots were then probed with an antibody that specifically detects the cleaved (active) form of caspase-9. (b) CGNs were treated exactly as described in (a) and lysates were western blotted with an antibody that recognizes both the pro- and cleaved (active) forms of caspase-3. The blots shown in (a) and (b) are representative of results obtained in three separate experiments. (c) CGNs were incubated for 72 h after infection with adenovirus expressing GFP and N17Rac1 (at a final titer of 50 infectious particles per cell). Following infection, cells were fixed in paraformaldehyde, blocked and permeabilized in 5% BSA and 0.2% Triton X-100, and immunostained with an antibody that specifically detects the active (cleaved) form of caspase-9 [Casp-9 (a)] and a Cy3-conjugated secondary antibody. Nuclei were stained with DAPI. The merged image shows that GFP- and N17Rac1-positive cells (indicated by the arrows) had condensed or fragmented nuclear morphology and displayed significant immunoreactivity for active caspase-9, whereas surrounding uninfected cells were largely healthy and devoid of active caspase-9. (d) CGNs were infected as described in (c) and were then immunostained for active (cleaved) caspase-3 [Casp-3 (a)]. As described above, most of the GFP- and N17Rac1-positive cells (indicated by the arrows) showed marked chromatin condensation and fragmentation and stained positively for active caspase-3. The images shown in (c) and (d) are composites of three to four different fields of CGNs infected with adenoviral GFP/N17Rac1. Ad-GFP control data not shown. Scale bars, 10 μm.

short isoform of Bim) which was similarly blocked by SB203580 (Fig. 7c). Finally, both an increased phosphorylation of c-Jun and induction of Bim were also observed in CGNs infected with N17Rac1 as compared with cells infected with the GFP control adenovirus (Fig. 7d). These data show that antagonism of Rac activity in CGNs promotes a robust c-Jun-dependent induction of the BH3-only protein, Bim_s.

SB203580 significantly inhibits ToxB-induced Bax activation, cytochrome *c* release, and caspase activation in CGNs

To determine if the c-Jun-dependent induction of Bim is necessary for initiation of the mitochondrial apoptotic pathway elicited in CGNs by ToxB, we examined the effects of SB203580 on Bax conformational change, cyt C release, and caspase activation. The enhanced immunoreactivity for conformationally active Bax (i.e. positive 6A7 antibody staining) induced by ToxB was significantly suppressed by co-incubation with SB203580 (Fig. 8a). Concurrently, inclusion of SB203580 substantially decreased the number of condensed and/or fragmented nuclei observed in ToxB-treated CGN cultures. Moreover, co-incubation with SB203580 prevented the ToxB-induced loss of cyt C from the mitochondrial pellet and inhibited the cleavage of

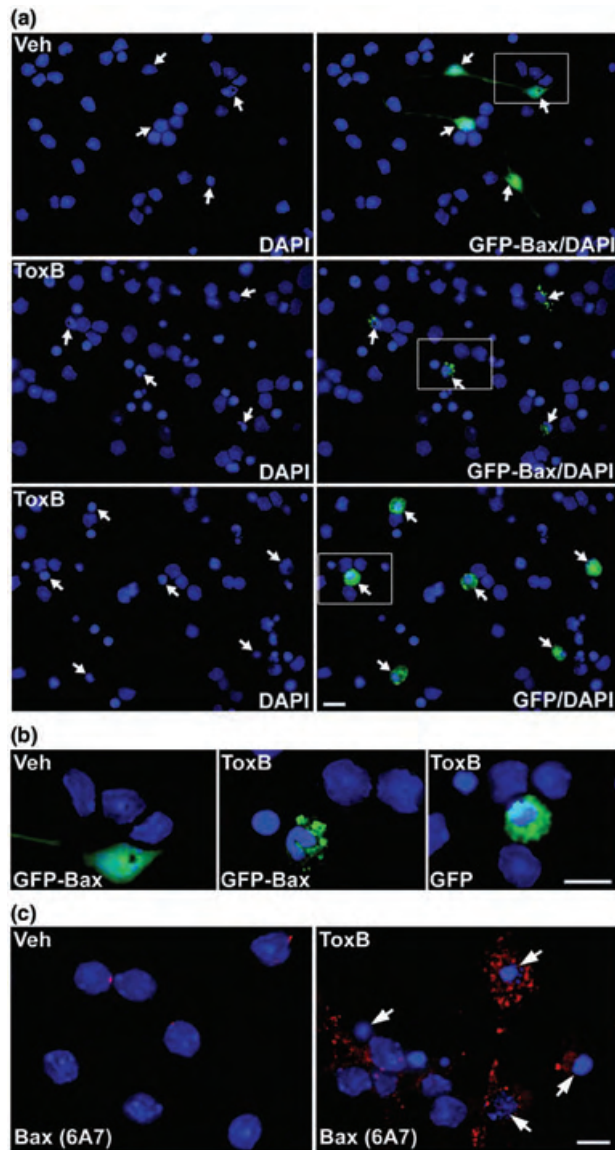


Fig. 6 ToxB elicits translocation of a GFP-Bax fusion protein to mitochondria and conformational activation of endogenous Bax in CGNs. (a) On day 5 *in vitro*, CGNs were transfected with either GFP alone or a GFP-Bax fusion protein using a helium-powered gene gun, as described in Experimental procedures. At 48 h post-transfection, cells were exposed for 24 h to either vehicle (Veh; 2 μg/mL BSA in PBS) or ToxB (40 ng/mL). CGNs were then fixed in paraformaldehyde and nuclei were stained with DAPI. The expressed GFP-Bax fusion protein had a diffuse distribution in the predominantly healthy CGNs incubated with Veh (upper panels). In contrast, cells exposed to ToxB demonstrated marked nuclear condensation and fragmentation, and GFP-Bax staining that was punctate and consistent with localization to mitochondria (middle panels). In CGNs transfected with GFP alone, ToxB still induced substantial apoptosis; however, GFP maintained a distribution that encompassed the entire cell unlike the more localized distribution of GFP-Bax under these conditions (lower panels). The images shown are representative of results from two experiments. Transfected cells in each panel are indicated by the arrows. Scale bar, 10 μm. (b) The areas demarcated by the boxes in (a) have been enlarged 300% to enhance the visualization of GFP-Bax or GFP. (c) Untransfected CGNs were incubated with either Veh or ToxB for 24 h and cells were fixed and immunostained with a monoclonal antibody (clone 6A7) that specifically detects the active conformation of Bax. Active endogenous Bax was visualized in a punctate mitochondrial distribution using a Cy3-conjugated anti-mouse secondary antibody (indicated by the arrows). Scale bar, 10 μm.

caspase-9 and -3 to the active fragments (Fig. 8b). Thus, in CGNs in which Rac has been inactivated, a c-Jun-driven induction of Bim lies upstream of a Bax-dependent mitochondrial death pathway.

The anthracycline, SP600125, a JNK-specific inhibitor, significantly blocks ToxB-induced c-Jun phosphorylation, Bim induction, and CGN apoptosis

As SB203580 inhibits both JNK and p38 MAP kinase activities, we evaluated the effects of a more selective JNK inhibitor, SP600125 (Bennett *et al.* 2001), on c-Jun phosphorylation and the subsequent apoptotic cascade elicited by ToxB in CGNs. In agreement with the results obtained for SB203580, SP600125 significantly suppressed the ToxB-induced phosphorylation and increased expression of c-Jun (Fig. 9a). Furthermore, the induction of Bim was also

significantly blocked by inclusion of SP600125 (Fig. 9b), providing further evidence that the Bim-initiated apoptotic cascade is mediated by c-Jun. Finally, quantitation of CGN apoptosis revealed that co-incubation of ToxB with SP600125 significantly decreased the number of neurons with condensed and/or fragmented nuclei (Fig. 9c). Thus, the JNK-specific inhibitor, SP600125, protects CGNs from apoptosis induced by the Rac-inhibitory ToxB.

Discussion

Several previous studies have demonstrated a significant role for integrin/ECM and growth factor signaling in promoting neuronal survival. Integrin-mediated signaling was recently shown to protect cultured hippocampal neurons from glutamate- or staurosporine-induced toxicity (Gary and Mattson 2001; Gary *et al.* 2003). Moreover, disruption of ECM proteins, either by gene deletion or infusion of ECM-neutralizing proteins or antibodies, exacerbated neuronal death *in vivo* in response to focal ischemia or excitotoxicity (Sakai *et al.* 2001; Chen *et al.* 2003). Growth factors also play a key role in neuronal survival. For example, we have shown that IGF-I promotes neuronal survival by blocking FKHRL1-dependent transcription of Bim, thereby suppressing apoptosis (Linseman *et al.* 2002b). Collectively, these findings illustrate a critical function for integrin/ECM and growth factor signaling in maintaining neuronal survival both *in vitro* and *in vivo*.

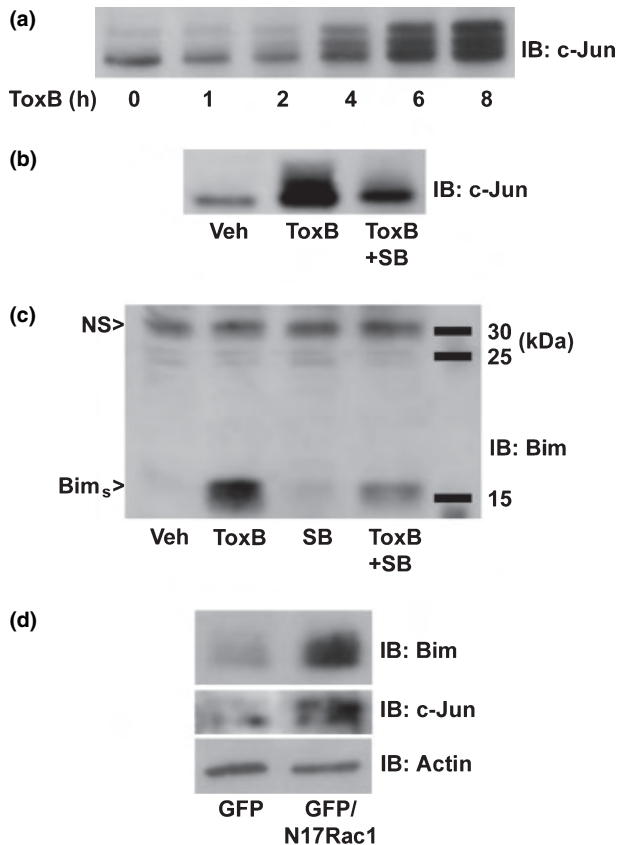


Fig. 7 ToxB and N17Rac1 each stimulate c-Jun activation and induction of Bim in CGNs: inhibition of ToxB-induced Bim expression by the pyridinyl imidazole, SB203580. (a) CGNs were incubated for up to 8 h with ToxB (40 ng/mL) and cell lysates were immunoblotted (IB) with a polyclonal antibody to c-Jun. The decreased mobility of c-Jun observed with increasing duration of ToxB exposure is indicative of activating phosphorylation. (b) CGNs were incubated for 6 h with either BSA/PBS vehicle (Veh) or ToxB \pm SB203580 (SB; 20 μ M). Following treatment, CGN lysates were immunoblotted for c-Jun. (c) CGNs were incubated for 6 h as described in (b). Cell lysates were then immunoblotted with a polyclonal antibody that detects an approximately 15-kDa isoform of Bim, Bim short (Bim_s). (d) CGNs were infected with either adenoviral GFP alone or in combination with N17Rac1. At 96 h post-infection, cell lysates were obtained and immunoblotted for c-Jun, Bim_s, and actin (as a loading control). NS, non-specific protein bands that are detected by the antibodies and are shown as loading controls.

Yet despite the fact that Rho family GTPases are key downstream effectors of integrin activation and growth factor signaling, little is known about the role of these G-proteins in regulating neuronal survival. Several elegant studies by Bazenet and colleagues have shown that Rac/Cdc42 GTPases promote the apoptotic death of NGF-deprived sympathetic neurons by stimulating two distinct MAP kinase kinases, apoptosis signal-regulating kinase 1 (ASK1) and mixed lineage kinase 3 (MLK3), upstream of JNK/c-Jun

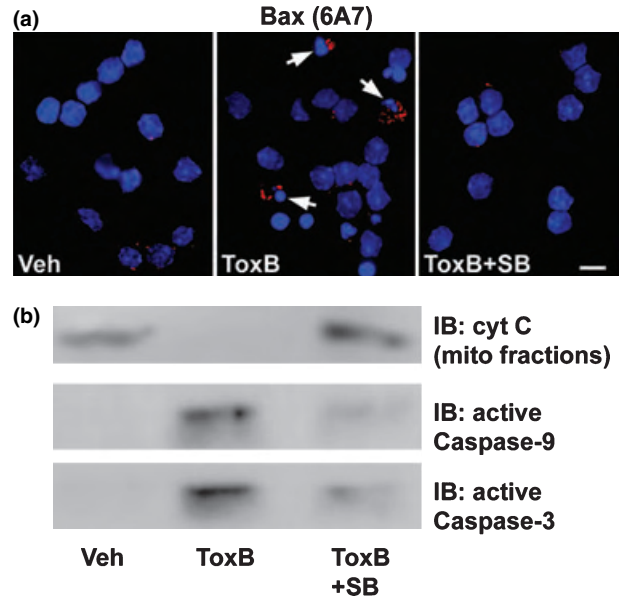


Fig. 8 The pyridinyl imidazole, SB203580, inhibits mitochondrial apoptotic signaling induced by ToxB in CGNs. (a) CGNs were incubated for 24 h with either vehicle (Veh; 2 μ g/mL BSA in PBS) or ToxB (40 ng/mL) \pm SB203580 (SB; 20 μ M). Following incubation, cells were immunostained with a monoclonal antibody to the active conformation of Bax (clone 6A7) and nuclei were stained with DAPI. The arrows indicate cells that stained positively for active Bax. Scale bar, 10 μ m. (b) CGNs were incubated exactly as described in (a) and either mitochondrial fractions were immunoblotted (IB) for cyt C or whole cell lysates were probed for active caspase-9 or -3. The blots shown are each indicative of data obtained in three separate experiments.

activation (Bazenet *et al.* 1998; Kanamoto *et al.* 2000; Mota *et al.* 2001). Furthermore, it was shown that p75-regulated activation of Rac induced JNK after withdrawal of NGF in rat oligodendrocytes, supporting a pro-apoptotic role of Rac (Harrington *et al.* 2002). Other studies, however, suggest that the pro-apoptotic activity of Rho family GTPases observed in sympathetic neurons and oligodendrocytes is not consistently seen in all types of neurons. For example, previous work by several groups correlated a loss of plasma membrane-associated Rho family GTPases with induction of apoptosis in primary cortical neurons and brain neuroblasts (Tanaka *et al.* 2000; Garcia-Roman *et al.* 2001; Meske *et al.* 2003). Each of these studies utilized inhibitors of 3-hydroxy-3-methylglutaryl-CoA reductase (statins) to block the isoprenylation and membrane localization of Ras and Rho GTPases. More recently, Kobayashi *et al.* (2004) demonstrated that targeted dominant-negative mutants of either Rho or Rho kinase significantly enhance the apoptosis of spinal motor neurons *in vivo* during embryonic development. In addition, it was recently shown that Rac1 also plays a primary role in the survival of motor neurons; the juvenile-onset form of amyotrophic lateral sclerosis is caused by

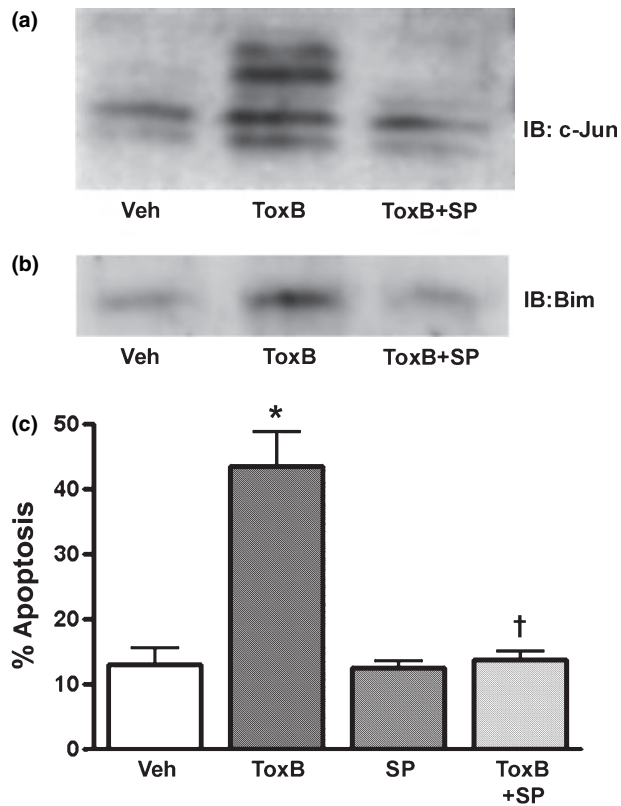


Fig. 9 The JNK-specific inhibitor, SP600125, significantly blocks c-Jun phosphorylation, Bim induction, and apoptosis in ToxB-treated neurons. (a) CGNs were incubated for 8 h with ToxB (40 ng/mL) \pm SP600125 (20 μ M). Cell lysates were then immunoblotted with a polyclonal antibody for c-Jun. Activation of phosphorylation is seen by the decreased mobility of c-Jun in a time-dependent manner upon incubation with ToxB. (b) CGNs were incubated as above in (a) for 8 h. The cell lysates were then immunoblotted with a polyclonal antibody that detects Bim_s, approximately 15 kDa. (c) CGNs were incubated as described above for 24 h. The cells were then fixed with paraformaldehyde and stained with Hoechst to visualize nuclei. The cells incubated with SP600125 showed a significant decrease in apoptosis. The results shown represent the means \pm SEM of three experiments with approximately 400 cells counted per condition in each experiment. *Significantly different from Veh-treated cells ($p < 0.01$). †Significantly different from ToxB-treated cells ($p < 0.01$).

truncation and loss of function of the Rac1 GEF, alsinLF (Kanekura *et al.* 2005). The above studies indicate that, as has been previously described for non-neuronal cells (Murga *et al.* 2002), the relative pro-survival or pro-apoptotic effects of Rho family GTPases in neurons are cell-type specific.

Consistent with several prior studies which showed a pro-survival role for Rho family GTPases in specific neuronal populations, we have previously reported that CGNs undergo apoptosis following incubation with Clostridial toxins that inhibit Rac/Cdc42 GTPases (Linseman *et al.* 2001a). Here, we utilized adenoviral dominant-negative Rho family

GTPases to identify Rac as the major pro-survival GTPase in CGNs, as significant apoptosis was induced by N17Rac1 but not dominant-negative mutants of RhoA or Cdc42. Although we cannot conclude irrefutably that Cdc42 does not play at least a minor role in CGN survival, our data provide strong evidence that Rac is the major pro-survival Rho family GTPase in these neurons. First, although dominant-negative mutants of Rac and Cdc42 can compete for the same guanine nucleotide exchange factors (GEFs), and therefore may have inhibitory effects that overlap on pathways downstream of one another, this lack of selectivity was not observed in CGNs where apoptosis was significantly elevated following infection with adenoviral N17Rac1 but not N17Cdc42 (see Fig. 2). The differential sensitivity of CGN survival to dominant-negative Rac versus dominant-negative Cdc42 was observed despite the fact that both adenoviruses appeared to infect the neurons equally based on GFP fluorescence.

Second, although Rac was a substrate for caspases in CGNs incubated with ToxB, Cdc42 was not degraded by caspases in this model (see Fig. 1). Therefore, while de novo Cdc42 synthesis could potentially overcome the effects of ToxB glucosylation over time (i.e. as the catalytic activity of ToxB diminishes), newly synthesized Rac would continually be degraded by caspases. The specificity of the caspase-mediated degradation for Rac versus Cdc42 further supports a major pro-survival role for Rac in CGNs.

Third, we previously showed that incubation with *C. sordellii* LTox mimicks the effects of ToxB on CGN apoptosis (Linseman *et al.* 2001a). While LTox definitely overlaps with ToxB in the glucosylation of Rac, it has been reported to inhibit Cdc42 in some cell-free assays (Genth *et al.* 1996; Hofmann *et al.* 1998) but not in others (Popoff *et al.* 1996). Moreover, LTox is generally regarded as a more potent inhibitor of Rac than Cdc42 within cells, further suggesting that it is the inhibition of Rac rather than Cdc42 that ultimately triggers CGN apoptosis.

Finally, we show that Rac1 activity (GTP-loading) is significantly decreased in CGNs deprived of serum and depolarizing K^+ _{ex} (see Fig. 3a). In contrast, Cdc42 activity as measured by increased tyrosine phosphorylation of the specific Cdc42 effector, ACK-1 (Linseman *et al.* 2001b), is sustained under these conditions (data not shown). These results indicate that, while loss of Rac activity is coincident with induction of apoptosis, Cdc42 activity is regulated independently of apoptotic signals. Collectively, these findings indicate that Rac is the major Rho family GTPase involved in promoting CGN survival and any role for Cdc42 is likely secondary.

Given that ToxB or N17Rac1 each induce CGN apoptosis in the presence of serum and depolarizing K^+ _{ex}, our data also suggest that loss of Rac function is not compensated for by trophic support. Moreover, we have previously shown that CGN apoptosis induced by Rac inactivation with either ToxB

or LTox is not mimicked by direct disruption of F-actin using the actin ADP-ribosylation factor, *C. botulinum* C2 toxin (Linseman *et al.* 2001a), indicating that the pro-survival action of Rac is independent of its effects on the actin cytoskeleton. Our current research is focused on identifying the effectors downstream of Rac that promote CGN survival.

Antagonism of Rac in CGNs using either ToxB or N17Rac1 triggered the release of cyt C from mitochondria and activation of the intrinsic initiator, caspase-9, and the executioner, caspase-3. Moreover, CGNs incubated with ToxB showed a c-Jun-dependent induction of the BH3-only protein, Bim, and mitochondrial translocation and conformational activation of Bax. c-Jun activation and Bim induction were similarly observed in CGNs infected with adenoviral N17Rac1. The pyridinyl imidazole JNK/p38 inhibitor, SB203580, and the JNK-specific inhibitor, SP600125, suppressed c-Jun activation, Bim induction and mitochondrial apoptosis in CGNs exposed to ToxB. These results show that inactivation of Rac GTPase is sufficient to induce a c-Jun/Bim-dependent mitochondrial apoptotic pathway in CGNs that are maintained in full trophic support (i.e. serum and depolarizing K^+_{ex}). Thus, serum-derived growth factors and depolarization-mediated calcium influx do not provide a buffer against c-Jun activation and Bim induction in the face of Rac inactivation. These data suggest that Rho family GTPases, and specifically Rac in CGNs, regulate the transcriptional control of Bim at the level of c-Jun phosphorylation. Although many studies have indicated that Rac/Cdc42 GTPases act as upstream activators of JNK/c-Jun signaling (Bazenet *et al.* 1998), others have recently reported that these G-proteins can also suppress the JNK pathway via PAK-mediated phosphorylation of the MAP kinase kinase, MEKK1 (Gallagher *et al.* 2002). Therefore, whether Rac GTPase positively or negatively regulates the JNK/c-Jun pathway in a given cell type likely depends on the specific MAP kinase kinase kinases present. The ability of PAK to antagonize c-Jun activation and, as a result, to inhibit Bim induction, complements its direct phosphorylation and inhibition of another BH3-only protein, Bad (Schurmann *et al.* 2000). Thus, Rac signaling through PAK may act as a key pro-survival pathway in some types of neurons by suppressing BH3-only protein-dependent mitochondrial apoptosis.

Finally, a recent study by Reginato *et al.* (2003) demonstrated that Bim is strongly induced in epithelial cells by cell detachment, and down-regulation of Bim using RNA interference prevents detachment-induced apoptosis or anoikis. These authors further showed that the up-regulation of Bim during cell detachment was because of loss of β 1 integrin ligation to the ECM and down-regulation of EGF receptor signaling to the ERK pathway. In this context, several groups have recently shown that Bim is targeted for degradation following ERK-mediated phosphorylation (Ley *et al.* 2003; Marani *et al.* 2004). Given that Rac1 has previously been

shown to transduce signals from the ECM-ligated β 1 integrin to the ERK MAP kinase pathway (Hirsch *et al.* 2002), it will be interesting to determine if inactivation of Rac in CGNs leads to suppression of the ERK pathway and if this effect contributes to the consequential increase in Bim expression that ultimately triggers neuronal apoptosis.

In conclusion, we have shown that inactivation of Rac GTPase, using either *C. difficile* toxin B or dominant negative N17Rac1, provokes apoptosis of primary cultured CGNs. The apoptosis induced by antagonism of Rac function occurs via a Bim-dependent mitochondrial death pathway that is significantly inhibited by blockade of c-Jun activation. Our findings that Rac is a key pro-survival molecule for CGNs complement those of Kobayashi *et al.* (2004) and Kanekura *et al.* (2005) who recently showed a critical role for Rho and Rac, respectively, in motor neuron survival. Elucidation of the pro-survival signals generated by Rho family GTPases in neurons is key to understanding how integrin-mediated adhesion and growth factors suppress neuronal apoptosis.

Acknowledgements

This work was supported by a Department of Veterans Affairs Merit Review Entry Program (MREP) Award (to DAL) and a Department of Defense Grant USAMRMC no. 03281009 (to DAL and KAH). The authors thank Tracey Laessig and Brent Butts for technical assistance.

References

- Allen M. P., Linseman D. A., Udo H., Xu M., Schaack J. B., Varnum B., Kandel E. R., Heidenreich K. A. and Wierman M. E. (2002) Novel mechanism for gonadotropin-releasing hormone neuronal migration involving Gas6/Ark signaling to p38 mitogen-activated protein kinase. *Mol. Cell Biol.* **22**, 599–613.
- Antonsson B., Montessuit S., Lauper S., Eskes R. and Martinou J. C. (2000) Bax oligomerization is required for channel-forming activity in liposomes and to trigger cytochrome c release from mitochondria. *Biochem. J.* **345**, 271–278.
- Arthur W. T., Noren N. K. and Burrige K. (2002) Regulation of Rho family GTPases by cell–cell and cell–matrix adhesion. *Biol. Res.* **35**, 239–246.
- Barth H., Hofmann F., Olenik C., Just I. and Aktories K. (1998) The N-terminal part of the enzyme component (C2I) of the binary *Clostridium botulinum* C2 toxin interacts with the binding component C2II and functions as a carrier system for a Rho ADP-ribosylating C3-like fusion toxin. *Infect. Immun.* **66**, 1364–1369.
- Bazenet C. E., Mota M. A. and Rubin L. L. (1998) The small GTP-binding protein Cdc42 is required for nerve growth factor withdrawal-induced neuronal death. *Proc. Natl Acad. Sci. USA* **95**, 3984–3989.
- Benard V., Bohl B. P. and Bokoch G. M. (1999) Characterization of rac and cdc42 activation in chemoattractant-stimulated human neutrophils using a novel assay for active GTPases. *J. Biol. Chem.* **274**, 13 198–13 204.
- Bennett B. L., Sasaki D. T., Murray B. W. *et al.* (2001) SP600125, an anthracycline inhibitor of Jun N-terminal kinase. *Proc. Natl Acad. Sci. USA* **98**, 13 681–13 686.

- Bouillet P., Strasser A., Bouillet P., Cory S., Zhang L. C., Strasser A. and Adams J. M. (2002) BH3-only proteins – evolutionarily conserved proapoptotic Bcl-2 family members essential for initiating programmed cell death: degenerative disorders caused by Bcl-2 deficiency prevented by loss of its BH3-only antagonist Bim. *J. Cell Sci.* **115**, 1567–1574.
- Burridge K. and Wennerberg K. (2004) Rho and Rac take center stage. *Cell* **116**, 167–179.
- Busch C. and Aktories K. (2000) Microbial toxins and the glycosylation of rho family. GTPases. *Curr. Opin. Struct. Biol.* **10**, 528–535.
- Chen Z. L., Indyk J. A. and Strickland S. (2003) The hippocampal laminin matrix is dynamic and critical for neuronal survival. *Mol. Biol. Cell* **14**, 2665–2676.
- Coffey E. T., Smiciene G., Hongisto V., Cao J., Brecht S., Herdegen T. and Courtney M. J. (2002) c-Jun N-terminal protein kinase (JNK) 2/3 is specifically activated by stress, mediating c-Jun activation, in the presence of constitutive JNK1 activity in cerebellar neurons. *J. Neurosci.* **22**, 4335–4345.
- D'Mello S. R., Galli C., Ciotti T. and Calissano P. (1993) Induction of apoptosis in cerebellar granule neurons by low potassium: inhibition of death by insulin-like growth factor I and cAMP. *Proc. Natl Acad. Sci. USA* **90**, 10 989–10 993.
- Djouder N., Prepens U., Aktories K. and Cavalie A. (2000) Inhibition of calcium release-activated calcium current by Rac/Cdc42-inactivating clostridial cytotoxins in RBL cells. *J. Biol. Chem.* **275**, 18 732–18 738.
- von Eichel-Streiber C., Harperath U., Bosse D. and Hadding U. (1987) Purification of two high molecular weight toxins of *Clostridium difficile* which are antigenically related. *Microb. Pathog.* **2**, 307–318.
- Etienne-Manneville S. and Hall A. (2002) Rho GTPases in cell biology. *Nature* **420**, 629–635.
- Gallagher E. D., Xu S., Moomaw C., Slaughter C. A. and Cobb M. H. (2002) Binding of JNK/SAPK to MEKK1 is regulated by phosphorylation. *J. Biol. Chem.* **277**, 45 785–45 792.
- Garcia-Roman N., Alvarez A. M., Toro M. J., Montes A. and Lorenzo M. J. (2001) Lovastatin induces apoptosis of spontaneously immortalized rat brain neuroblasts: involvement of nonsterol isoprenoid biosynthesis inhibition. *Mol. Cell Neurosci.* **17**, 329–341.
- Gary D. S. and Mattson M. P. (2001) Integrin signaling via the PI3-kinase-Akt pathway increases neuronal resistance to glutamate-induced apoptosis. *J. Neurochem.* **76**, 1485–1496.
- Gary D. S., Milhavel O., Camandola S. and Mattson M. P. (2003) Essential role for integrin linked kinase in Akt-mediated integrin survival signaling in hippocampal neurons. *J. Neurochem.* **84**, 878–890.
- Genth H., Hofmann F., Selzer J., Rex G., Aktories K. and Just I. (1996) Difference in protein substrate specificity between hemorrhagic toxin and lethal toxin from *Clostridium sordellii*. *Biochem. Biophys. Res. Commun.* **229**, 370–374.
- Gerhardt E., Kugler S., Leist M., Beier C., Berliocchi L., Volbracht C., Weller M., Bahr M., Nicotera P. and Schulz J. B. (2001) Cascade of caspase activation in potassium-deprived cerebellar granule neurons: targets for treatment with peptide and protein inhibitors of apoptosis. *Mol. Cell Neurosci.* **17**, 717–731.
- Gibson R. M., Craig S. E., Heenan L., Tourmier C. and Humphries M. J. (2005) Activation of integrin $\alpha 5\beta 1$ delays apoptosis of Ntera2 neuronal cells. *Mol. Cell Neurosci.* **28**, 588–598.
- Harrington A. W., Kim J. Y. and Yoon S. O. (2002) Activation of Rac GTPase by p75 is necessary for c-Jun N-terminal kinase-mediated apoptosis. *J. Neurosci.* **22**, 156–166.
- Harris C. A. and Johnson E. M. Jr (2001) BH3-only Bcl-2 family members are coordinately regulated by the JNK pathway and require Bax to induce apoptosis in neurons. *J. Biol. Chem.* **276**, 37 754–37 760.
- Hirsch E., Barberis L., Brancaccio M. *et al.* (2002) Defective Rac-mediated proliferation and survival after targeted mutation of the $\beta 1$ integrin cytodomain. *J. Cell Biol.* **157**, 481–492.
- Hofmann F., Busch C. and Aktories K. (1998) Chimeric clostridial cytotoxins: identification of the N-terminal region involved in protein substrate recognition. *Infect. Immun.* **66**, 1076–1081.
- Hsu Y. T. and Youle R. J. (1998) Bax in murine thymus is a soluble monomeric protein that displays differential detergent-induced conformations. *J. Biol. Chem.* **273**, 10 777–10 783.
- Huang E. J. and Reichardt L. F. (2003) Trk receptors: roles in neuronal signal transduction. *Annu. Rev. Biochem.* **72**, 609–642.
- Inoue H., Tsukita K., Iwasato T. *et al.* (2003) The crucial role of caspase-9 in the disease progression of a transgenic ALS mouse model. *EMBO J.* **22**, 6665–6674.
- Just I., Selzer J., Wilm M., von Eichel-Streiber C., Mann M. and Aktories K. (1995) Glucosylation of Rho proteins by *Clostridium difficile* toxin B. *Nature* **375**, 500–503.
- Kanamoto T., Mota M., Takeda K., Rubin L. L., Miyazono K., Ichijo H. and Bazenet C. E. (2000) Role of apoptosis signal-regulating kinase in regulation of the c-Jun N-terminal kinase pathway and apoptosis in sympathetic neurons. *Mol. Cell Biol.* **20**, 196–204.
- Kanekura K., Hashimoto Y., Kita Y., Sasabe J., Aiso S., Nishimoto I. and Matsuoka M. (2005) A Rac1/phosphatidylinositol 3-kinase/Akt3 anti-apoptotic pathway, triggered by AlsinLF, the product of the ALS2 gene, antagonizes Cu/Zn-superoxide dismutase (SOD1) mutant-induced motoneuronal cell death. *J. Biol. Chem.* **280**, 4532–4543.
- Kobayashi K., Takahashi M., Matsushita N., Miyazaki J., Koike M., Yaginuma H., Osumi N., Kaibuchi K. and Kobayashi K. (2004) Survival of developing motor neurons mediated by Rho GTPase signaling pathway through Rho-kinase. *J. Neurosci.* **24**, 3480–3488.
- Ley R., Balmanno K., Hadfield K., Weston C. and Cook S. J. (2003) Activation of the ERK1/2 signaling pathway promotes phosphorylation and proteasome-dependent degradation of the BH3-only protein, Bim. *J. Biol. Chem.* **278**, 18 811–18 816.
- Li M., Linseman D. A., Allen M. P., Meintzer M. K., Wang X., Laessig T., Wierman M. E. and Heidenreich K. A. (2001) Myocyte enhancer factor 2A and 2D undergo phosphorylation and caspase-mediated degradation during apoptosis of rat cerebellar granule neurons. *J. Neurosci.* **21**, 6544–6552.
- Linseman D. A., Laessig T., Meintzer M. K., McClure M., Barth H., Aktories K. and Heidenreich K. A. (2001a) An essential role for Rac/Cdc42 GTPases in cerebellar granule neuron survival. *J. Biol. Chem.* **276**, 39 123–39 131.
- Linseman D. A., Heidenreich K. A. and Fisher S. K. (2001b) Stimulation of M3 muscarinic receptors induces phosphorylation of the Cdc42 effector activated Cdc42Hs-associated kinase-1 via a Fyn tyrosine kinase signaling pathway. *J. Biol. Chem.* **276**, 5622–5628.
- Linseman D. A., McClure M. L., Bouchard R. J., Laessig T. A., Ahmadi F. A. and Heidenreich K. A. (2002a) Suppression of death receptor signaling in cerebellar Purkinje neurons protects neighboring granule neurons from apoptosis via an insulin-like growth factor I-dependent mechanism. *J. Biol. Chem.* **277**, 24 546–24 553.
- Linseman D. A., Phelps R. A., Bouchard R. J., Le S. S., Laessig T. A., McClure M. L. and Heidenreich K. A. (2002b) Insulin-like growth factor-I blocks Bcl-2 interacting mediator of cell death (Bim) induction and intrinsic death signaling in cerebellar granule neurons. *J. Neurosci.* **22**, 9287–9297.
- Lossi L. and Merighi A. (2003) *In vivo* cellular and molecular mechanisms of neuronal apoptosis in the mammalian CNS. *Prog. Neurobiol.* **69**, 287–312.

- Marani M., Hancock D., Lopes R., Tenev T., Downward J. and Lemoine N. R. (2004) Role of Bim in the survival pathway induced by Raf in epithelial cells. *Oncogene* **23**, 2431–2441.
- Marcoux N. and Vuori K. (2003) EGF receptor mediates adhesion-dependent activation of the Rac GTPase: a role for phosphatidylinositol 3-kinase and Vav2. *Oncogene* **22**, 6100–6106.
- Meske V., Albert F., Richter D., Schwarze J. and Ohm T. G. (2003) Blockade of HMG-CoA reductase activity causes changes in microtubule-stabilizing protein tau via suppression of geranylgeranylpyrophosphate formation: implications for Alzheimer's disease. *Eur. J. Neurosci.* **17**, 93–102.
- Mota M., Reeder M., Chernoff J. and Bazenet C. E. (2001) Evidence for a role of mixed lineage kinases in neuronal apoptosis. *J. Neurosci.* **21**, 4949–4957.
- Murga C., Zohar M., Teramoto H. and Gutkind J. S. (2002) Rac1 and RhoG promote cell survival by the activation of PI3K and Akt, independently of their ability to stimulate JNK and NF- κ B. *Oncogene* **21**, 207–216.
- Napankangas U., Lindqvist N., Lindholm D. and Hallbook F. (2003) Rat retinal ganglion cells upregulate the pro-apoptotic BH3-only protein Bim after optic nerve transection. *Brain Res. Mol. Brain Res.* **120**, 30–37.
- Nomura M., Shimizu S., Sugiyama T., Narita M., Ito T., Matsuda H. and Tsujimoto Y. (2003) 14-3-3 interacts directly with and negatively regulates pro-apoptotic Bax. *J. Biol. Chem.* **278**, 2058–2065.
- Parise L. V., Lee J. and Juliano R. L. (2000) New aspects of integrin signaling in cancer. *Semin. Cancer Biol.* **10**, 407–414.
- Pearce D. A. and Sherman F. (1997) Differential ubiquitin-dependent degradation of the yeast apo-cytochrome c isozymes. *J. Biol. Chem.* **272**, 31 829–31 836.
- Popoff M. R., Chaves-Olarte E., Lemichez E. *et al.* (1996) Ras, Rap, and Rac small GTP-binding proteins are targets for *Clostridium sordellii* lethal toxin glucosylation. *J. Biol. Chem.* **271**, 10 217–10 224.
- Putcha G. V., Moulder K. L., Golden J. P., Bouillet P., Adams J. A., Strasser A. and Johnson E. M. (2001) Induction of BIM, a proapoptotic BH3-only BCL-2 family member, is critical for neuronal apoptosis. *Neuron* **29**, 615–628.
- Reginato M. J., Mills K. R., Paulus J. K., Lynch D. K., Sgroi D. C., Debnath J., Muthuswamy S. K. and Brugge J. S. (2003) Integrins and EGFR coordinately regulate the pro-apoptotic protein Bim to prevent anoikis. *Nat. Cell Biol.* **5**, 733–740.
- Sakai T., Johnson K. J., Murozono M., Sakai K., Magnuson M. A., Wieloch T., Cronberg T., Isshiki A., Erickson H. P. and Fassler R. (2001) Plasma fibronectin supports neuronal survival and reduces brain injury following transient focal cerebral ischemia but is not essential for skin-wound healing and hemostasis. *Nat. Med.* **7**, 324–330.
- Schurmann A., Mooney A. F., Sanders L. C., Sells M. A., Wang H. G., Reed J. C. and Bokoch G. M. (2000) p21-activated kinase 1 phosphorylates the death agonist bad and protects cells from apoptosis. *Mol. Cell Biol.* **20**, 453–461.
- Schwartz M. A. and Shattil S. J. (2000) Signaling networks linking integrins and rho family GTPases. *Trends Biochem. Sci.* **25**, 388–391.
- Stupack D. G. and Cheresch D. A. (2002) Get a ligand, get a life: integrins, signaling and cell survival. *J. Cell Sci.* **115**, 3729–3738.
- Takagi J. (2004) Structural basis for ligand recognition by RGD (Arg-Gly-Asp)-dependent integrins. *Biochem. Soc. Trans.* **32**, 403–406.
- Tanaka T., Tatsuno I., Uchida D. *et al.* (2000) Geranylgeranyl-pyrophosphate, an isoprenoid of mevalonate cascade, is a critical compound for rat primary cultured cortical neurons to protect the cell death induced by 3-hydroxy-3-methylglutaryl-CoA reductase inhibition. *J. Neurosci.* **20**, 2852–2859.
- Tatton W. G., Chalmers-Redman R., Brown D. and Tatton N. (2003) Apoptosis in Parkinson's disease: signals for neuronal degradation. *Ann. Neurol.* **53**, S61–S70.
- Whitfield J., Neame S. J., Paquet L., Bernard O. and Ham J. (2001) Dominant-negative c-Jun promotes neuronal survival by reducing BIM expression and inhibiting mitochondrial cytochrome c release. *Neuron* **29**, 629–643.
- Wolter K. G., Hsu Y. T., Smith C. L., Nechushtan A., Xi X. G., Youle R. J., Hsu Y. T., Wolter K. G. and Youle R. J. (1997) Movement of Bax from the cytosol to mitochondria during apoptosis: cytosol-to-membrane redistribution of Bax and Bcl-X(L) during apoptosis. *J. Cell Biol.* **139**, 1281–1292.
- Yang W., Lin Q., Guan J. L. and Cerione R. A. (1999) Activation of the Cdc42-associated tyrosine kinase-2 (ACK-2) by cell adhesion via integrin β 1. *J. Biol. Chem.* **274**, 8524–8530.
- Zhang B., Zhang Y. and Shacter E. (2003) Caspase 3-mediated inactivation of rac. GTPases promotes drug-induced apoptosis in human lymphoma cells. *Mol. Cell Biol.* **23**, 5716–5725.
- Zou H., Li Y., Liu X. and Wang X. (1999) An APAF-1/cytochrome c multimeric complex is a functional apoptosome that activates procaspase-9. *J. Biol. Chem.* **274**, 11 549–11 556.

Endoplasmic reticulum stress and trophic factor withdrawal activate distinct signaling cascades that induce glycogen synthase kinase-3 β and a caspase-9-dependent apoptosis in cerebellar granule neurons

J.L. Brewster,^{a,b,c,*} D.A. Linseman,^{a,b} R.J. Bouchard,^{a,b} F.A. Loucks,^{a,b} T.A. Precht,^{a,b}
E.A. Esch,^c and K.A. Heidenreich^{a,b}

^aDepartment of Pharmacology, University of Colorado Health Sciences Center, Denver, CO 80262, USA

^bVeterans Affairs Medical Center, Denver, CO 80220, USA

^cNatural Science Division, Pepperdine University, Malibu, CA 90263-4321, USA

Received 3 February 2006; revised 12 April 2006; accepted 24 April 2006
Available online 9 June 2006

Loss of trophic or activity-dependent survival signals is commonly recognized as a stimulus for neuronal apoptosis and may play a significant role in neurodegeneration. Recent data have also implicated endoplasmic reticulum (ER) stress as an important factor in some neurodegenerative conditions. However, whether shared or unique apoptotic cascades are activated by trophic factor withdrawal (TFW) versus ER stress in primary neurons has not previously been investigated. In primary cultures of rat cerebellar granule neurons (CGNs), the ER stressor brefeldin A activated a discrete pathway involving the following: (1) stimulation of the ER resident kinase PERK, (2) enhanced phosphorylation of the translation initiation factor eIF2 α , and (3) increased expression and nuclear localization of the transcription factor Gadd153/CHOP. ER stress-induced CGN apoptosis was blocked by an antagonist of IP₃ receptor-mediated Ca²⁺ release, 2-aminoethoxydiphenyl borate (2-APB), and by expression of ER-targeted Bcl-2. In contrast, CGN apoptosis elicited by TFW (i.e., removal of serum and depolarizing extracellular potassium) did not display any ER stress component nor was it blocked by either 2-APB or ER-Bcl-2. Despite these apparent differences, both brefeldin A and TFW induced dephosphorylation (activation) of glycogen synthase kinase-3 β (GSK-3 β). Moreover, inhibitors of GSK-3 β (IGF-I, lithium)

and caspase-9 (LEHD-fmk) significantly protected CGNs from apoptosis induced by either ER stress or TFW. These data indicate that ER stress and TFW elicit distinct signals that activate GSK-3 β and intrinsic apoptosis in neurons.

© 2006 Elsevier Inc. All rights reserved.

Keywords: Cerebellar granule neurons; Endoplasmic reticulum stress; Apoptosis; Trophic factor withdrawal; Glycogen synthase kinase-3 β ; Inositol 1,4,5-trisphosphate receptor; Bcl-2; Gadd153/CHOP

Introduction

The apoptotic death of neurons is a necessary process to remove redundant neuronal populations during nervous system development. However, when abnormally regulated, apoptosis contributes to a variety of neurodegenerative diseases. The molecular triggers for apoptosis induction include the loss of essential cellular survival signals from the extracellular milieu, excitotoxic or oxidative stress, severe DNA damage, organelle dysfunction, and receptor-mediated death signaling (Adams, 2003). Apoptotic signaling involves both extrinsic and intrinsic/stress-induced pathways. The extrinsic pathway is induced via death receptors [FasR/CD95, tumor necrosis factor (TNF) receptor, TRAIL/DR-5] that, upon ligand binding, initiate a caspase-8-mediated proteolytic cascade. Intrinsic death signaling involves apoptotic events that are induced by changes in outer mitochondrial membrane permeability, resulting in the release of soluble, pro-apoptotic signaling molecules (cytochrome *c*, Smac/Diablo, Omi, AIF) from the mitochondrial intermembrane space. The release of cytochrome *c* to the cytosol activates a caspase-9-mediated proteolytic cascade via formation of the apoptosome (a proteolytically active complex of caspase-9, cytochrome *c*, and Apaf-1).

Abbreviations: 2-APB, 2-aminoethoxydiphenyl borate; A β , amyloid β ; APP, amyloid precursor protein; BA, brefeldin A; CGN, cerebellar granule neuron; DAPI, 4,6-diamidino-2-phenylindole; DMEM, Dulbecco's modified Eagles medium; ER, endoplasmic reticulum; FITC, fluorescein-5-isothiocyanate; GSK-3 β , glycogen synthase kinase-3 β ; IGF-I, insulin-like growth factor-I; IP₃, inositol 1,4,5-trisphosphate; mPT, mitochondrial permeability transition; NFT, neurofibrillary tangles; NF- κ B, nuclear factor- κ B; PBS, phosphate-buffered saline; PKB, protein kinase B; PP2A, protein phosphatase 2A; SERCA, sarcoplasmic/ER Ca²⁺ ATPase; TFW, trophic factor withdrawal.

* Corresponding author. Natural Science Division, Pepperdine University, 25255 Pacific Coast Highway, Malibu, CA 90263-4321, USA. Fax: +1 310 506 4785.

E-mail address: Jay.Brewster@pepperdine.edu (J.L. Brewster).

Available online on ScienceDirect (www.sciencedirect.com).

In addition to death receptors and mitochondria, the endoplasmic reticulum (ER) is capable of rapidly inducing apoptosis in response to specific stress signals. These stresses include the accumulation of improperly folded proteins within the ER (Rutkowski and Kaufman, 2004), perturbation of ER Ca^{2+} uptake/release (Chen et al., 2004b; Scorrano et al., 2003), and/or the improper processing of specific surveillance proteins within the ER (Hong et al., 2004). ER stress can induce an initial adaptive cellular response, known as the unfolded protein response or UPR, through induction of (1) the Ire1 transmembrane kinase/endoribonuclease, (2) the PERK (PKR-like endoplasmic reticulum kinase) transmembrane kinase, or (3) ATF6-mediated signaling (Rutkowski and Kaufman, 2004). eIF2 α can be phosphorylated by PERK during ER stress, inhibiting recycling of eIF2 α following translation initiation. This arrests most translation initiation within the cell and enables a UPR-directed recovery from ER stress. However, unmitigated ER stress ultimately overwhelms the cell, leading to apoptotic death. The capability of ER stress to induce intrinsic apoptosis is well documented but is incompletely understood (Boyce and Yuan, 2006). One potential mechanism of ER crosstalk with the mitochondria is Ca^{2+} release from ER stores, mediated by the ER-localized inositol 1,4,5-trisphosphate (IP_3) receptors and regulated by ER-localized Bcl-2, Bax, and Bak (Hanson et al., 2004; Scorrano et al., 2003). Ca^{2+} signaling is a central component of ER-initiated mitochondrial depolarization and release of apoptogenic factors (Scorrano et al., 2003; Thomenius and Distelhorst, 2003; Verkhatsky and Toescu, 2003).

Recent studies have revealed ER stress-induced apoptotic signaling in neurodegenerative diseases. Alzheimer's disease can result from mutations in two ER resident membrane proteins, presenilin (PS) 1 and 2, proteins in the γ -secretase complex. Mutations in PS1 or PS2 can elevate proteolytic processing of amyloid precursor protein (APP) in the ER, increasing the production of the cytotoxic product of APP proteolysis, amyloid beta ($\text{A}\beta$). These mutations have been shown to dampen adaptive ER stress signaling, to elevate neuronal sensitivity to an ER stress-induced apoptosis, and to cause dysregulation of both ER and cytosolic Ca^{2+} concentrations (Demuro et al., 2005; Katayama et al., 2004; Takuma et al., 2005). An additional group of neurodegenerative disorders whose path to apoptotic death appears to include an ER signaling component is the CAG (polyglutamine) repeat expansion diseases, which include Kennedy's disease and spinocerebellar ataxias (Thomas et al., 2005). These diseases display an accumulation of toxic protein aggregates in the affected neurons. The complex signaling capabilities of the ER, enabling adaptation and recovery from cellular stress or, alternatively, stimulating apoptotic progression, makes it a central focus of current research into the cell biology of neurodegenerative disease.

Rat cerebellar granule neurons (CGNs) are an excellent source of primary neurons for studies of neuronal apoptosis. Maintaining these cells in the presence of depolarizing concentrations of extracellular potassium (25 mM KCl or 25K) sustains cellular survival signals (D'Mello et al., 1993). A trophic factor withdrawal (TFW) apoptotic phenotype is induced in these cells by lowering the concentration of extracellular potassium (5 mM KCl or 5K). This results in the rapid activation of mitochondrial apoptosis via the induced expression of a BH3-only protein, Bim (Linseman et al., 2002; Putcha et al., 2001) and translocation of Bax to mitochondria (Linseman et al., 2004). Currently, only a few studies have examined ER stress signaling in primary neurons, and

little is known about the involvement of the ER in TFW-induced apoptosis of CGNs. In this study, we examined whether shared or distinct apoptotic signaling pathways are activated by TFW versus ER stress in CGNs. We report that CGNs utilize canonical ER stress-induced apoptotic pathway components to activate apoptosis when exposed to ER stressors, and that these ER signaling mechanisms are not activated during TFW-induced apoptosis. Inhibition of IP_3 receptor-mediated Ca^{2+} release from the ER was sufficient to rescue CGNs from ER stress-induced but not TFW-induced apoptosis. Moreover, we show that despite their distinct proximal signaling events, TFW and ER stress both activated the pro-apoptotic kinase, glycogen synthase kinase-3 β (GSK-3 β), and triggered a caspase-9-dependent apoptotic cascade in CGNs.

Results

eIF2 α phosphorylation distinguishes ER stress from TFW in CGNs

Initially, we performed a comparative screen of canonical ER stress-activated signals induced in CGNs by either thapsigargin or TFW. Cultured rat CGNs were transferred to 5K medium to induce TFW or thapsigargin was added to induce ER stress. Thapsigargin is a cell-permeable inhibitor of sarcoplasmic/ER Ca^{2+} ATPase (SERCA) pumps, generating an arrest of ER Ca^{2+} uptake from the cytosol. Thapsigargin is known to induce a robust ER stress signal in a variety of cell types. Proteins were extracted after an acute 8-h exposure and used in immunoblot analyses (Kinexus Protein Screen; Fig. 1).

In examining the expression or activation of select protein targets during thapsigargin treatment, CGNs displayed a marked phosphorylation of eIF2 α at serine-52 (Fig. 1). In contrast, CGNs subjected to TFW displayed no increase in eIF2 α phosphorylation relative to control conditions. Neither ER stress nor TFW induced detectable changes in the cellular content of the ER-chaperones,

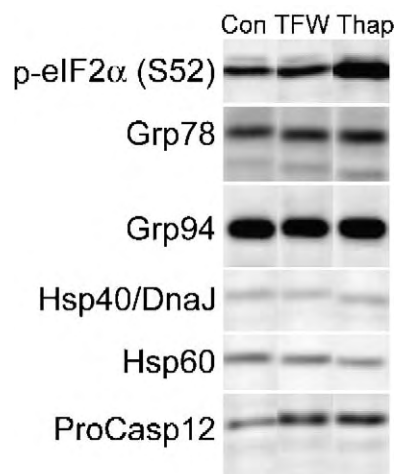


Fig. 1. eIF2 α is differentially inactivated in response to apoptotic stimuli. To compare CGNs experiencing ER stress and TFW, we treated cultures with thapsigargin (Thap, 20 μM) or TFW medium. Following an 8-h incubation, lysates were isolated, and a select group of known stress signaling targets was analyzed by Kinexus Bioinformatics Corporation (Vancouver, BC, Canada). The eIF2 α antibody is specific for the inactive, phosphorylated form of this initiation factor (Ser52). eIF2 α was phosphorylated in response to ER stress but not TFW.

Grp78 and Grp94, nor did they induce the heat shock chaperones, Hsp40/DnaJ and Hsp60. An examination of the ER-associated caspase-12 revealed no evidence of the cleaved (active) form of the protease, although procaspase-12 is clearly expressed in CGNs. Thus, in response to thapsigargin, CGNs display an ER stress response that is characterized by induction of eIF2 α phosphorylation in the absence of any apparent increase in either the expression of ER chaperones or the processing of pro-caspase-12. Moreover, TFW does not elicit eIF2 α phosphorylation, suggesting a lack of ER stress following this apoptotic stimulus.

ER stressors induce apoptosis in CGNs

To further characterize CGN apoptosis following ER stress, we used three separate agents to perturb ER function and activate ER stress response: tunicamycin, an inhibitor of N-linked glycosylation; brefeldin A, an inhibitor of ER to Golgi transport; and thapsigargin. At the indicated time points, CGNs were fixed, stained with DAPI, and scored for apoptotic nuclei (Fig. 2A). CGNs displayed differential sensitivity to each of the ER stressors with brefeldin A generating the most robust apoptotic response. To

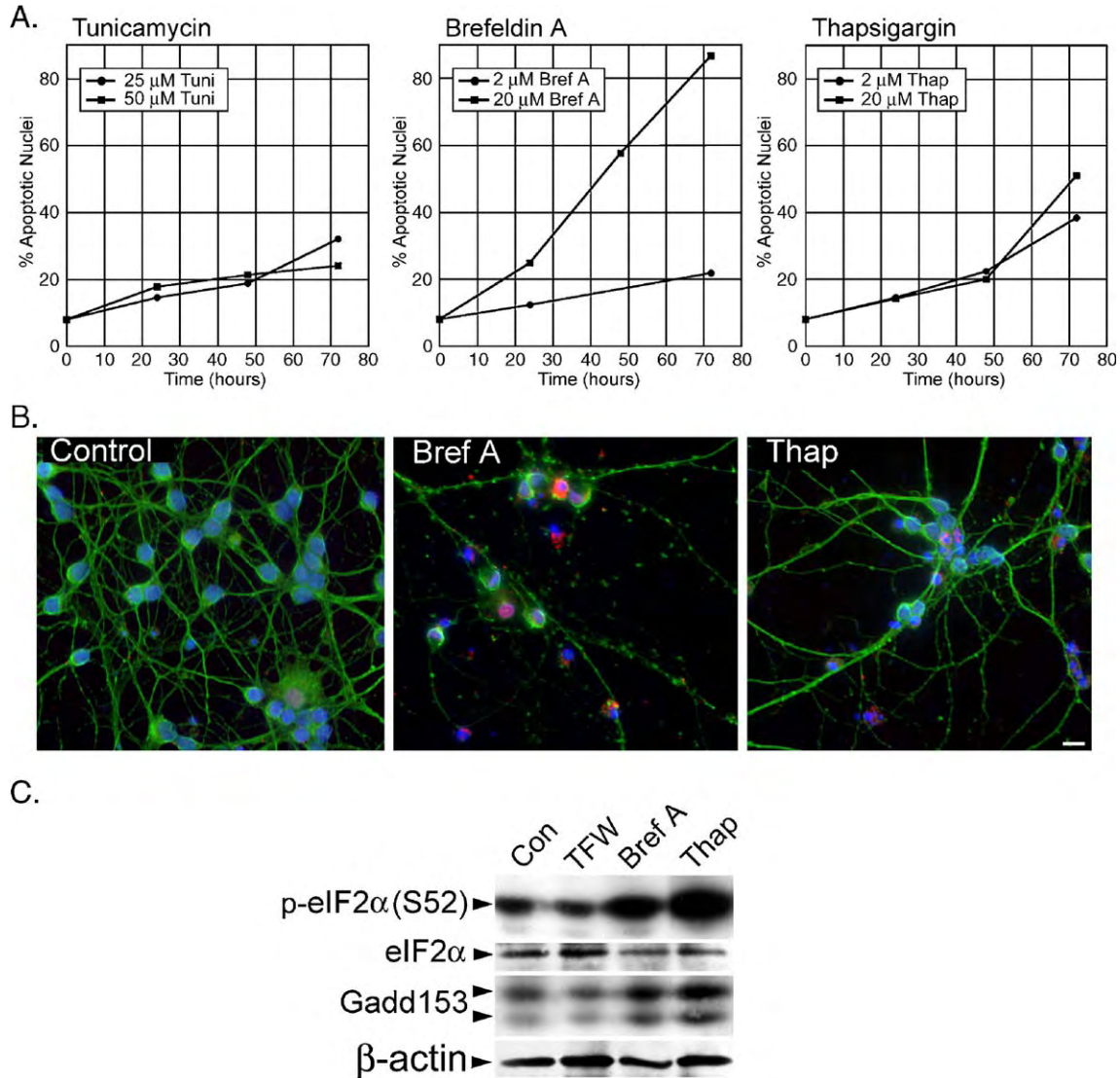


Fig. 2. Characterization of apoptosis activation in CGNs undergoing ER stress. (A) CGN cultures were grown in the presence of ER stress-inducing toxins to assess apoptotic activation over a period of 72 h. ER stress inducers included tunicamycin (25 or 50 μ M), brefeldin A (2 or 20 μ M), and thapsigargin (2 or 20 μ M). At the indicated time points, CGNs were fixed in 4% paraformaldehyde and nuclei were stained with DAPI. The percentage of apoptotic nuclei was determined using fluorescence microscopy. (B) Immunocytochemistry was performed to assess activation of caspase-3 and the integrity of cellular microtubule networks. CGNs were cultured for 24 h in the presence or absence of brefeldin A (Bref A, 20 μ M) or thapsigargin (Thap, 20 μ M). Cells were then fixed in 4% paraformaldehyde, permeabilized, and analyzed via immunocytochemistry (see Experimental methods). Cells were incubated with primary antibodies to detect active caspase-3 (rabbit polyclonal, red) and tubulin (mouse monoclonal, green). Secondary antibodies were Cy3-conjugated anti-rabbit and FITC-conjugated anti-mouse conjugates. Nuclei were stained using DAPI (blue). Scale bar is 20 μ m. (C) Immunoblot analysis of CGN cell lysates was performed to assess expression of Gadd153/CHOP and phosphorylation of eIF2 α during ER stress. CGNs were cultured for 12 h in the presence or absence of brefeldin A (Bref A, 20 μ M), thapsigargin (Thap, 5 μ M), or TFW medium. Lysates were prepared from treated cells and proteins analyzed by immunoblot analysis. Analysis of β -actin is included as a loading control.

evaluate morphological indices of apoptosis, we performed immunocytochemistry after 24 h of ER stress to measure caspase-3 activation and disruption of the cytoskeleton. An antibody specific for the cleaved (active) form of caspase-3 (Cy3) and an anti-tubulin antibody (FITC) were used to examine cells exposed to ER stressors. CGNs with condensed or fragmented nuclei consistently stained positively for caspase-3 activity and displayed a deteriorated microtubule cytoskeleton (Fig. 2B). Using these morphological criteria, brefeldin A was again shown to induce the strongest apoptotic response in CGNs.

To confirm that brefeldin A was inducing CGN apoptosis via an ER stress pathway, we next examined its effects on Gadd153/CHOP induction and eIF2 α phosphorylation. Gadd153 dimerizes with C/EBP β to bind DNA and regulate the expression of pro-death and pro-survival genes (Marciniak et al., 2004; Wang et al., 1998; Yamaguchi and Wang, 2004). Elevated expression, phosphorylation, and nuclear localization of the Gadd153 transcription factor has been associated with ER stress-induced apoptosis in non-neuronal cell lines (Marciniak et al., 2004; Oyadomari and Mori, 2004; Yamaguchi and Wang, 2004). As is shown (Fig. 2C), a 12-h exposure to either brefeldin A or thapsigargin resulted in a robust phosphorylation of eIF2 α relative to the TFW and control samples. Densitometry was performed to identify the ratio of phosphorylated eIF2 α to total eIF2 α under each condition. When normalized to control neurons, brefeldin A and thapsigargin were shown to generate an 80% (1.8-fold) and 140% (2.4-fold) increase in eIF2 α phosphorylation (respectively). TFW-treated neurons showed a 35% reduction in eIF2 α phosphorylation. Gadd153 expression was induced by both ER stressors but showed no increase following TFW induction. These data indicate that brefeldin A, like thapsigargin, induces eIF2 α phosphorylation and Gadd153 expression, consistent with ER stress-induced CGN apoptosis. In contrast, TFW shows no ER stress component, displaying neither eIF2 α phosphorylation nor increased Gadd153 expression.

ER stress, but not TFW, induces PERK activation and enhanced Gadd153/CHOP localization within the nucleus

Gadd153 is observed in the cytosol and nucleus of non-stressed cells (Cui et al., 2000) and displays increased expression and prominent nuclear localization during ER stress (Lorz et al., 2004). PERK is an ER resident transmembrane kinase that is known to autophosphorylate on the cytoplasmic kinase domain in response to accumulated unfolded proteins in the ER lumen. Activated PERK is capable of phosphorylating several cytosolic proteins including eIF2 α (Rutkowski and Kaufman, 2004). Gadd153 localization and PERK activation (phosphorylation) were assessed immunocytochemically in CGNs exposed to either TFW or brefeldin A (Fig. 3A). Control neurons displayed a cytosolic localization of Gadd153 (Cy3-red), only weak reactivity with phospho-PERK (active; FITC-green) antibodies, and uncondensed nuclei (DAPI-blue). TFW generated apoptotic nuclei (DAPI-blue), but no significant change in either Gadd153 localization or PERK phosphorylation. However, brefeldin A-treated CGNs displayed a clear redistribution of Gadd153 to the nucleus (Cy3-red) coincident with diminished cytosolic staining and condensed apoptotic nuclei (DAPI-blue). Translocation of Gadd153 to the nucleus is consistent with an ER stress-induced transcriptional response mediated by Gadd153. Moreover, the activated, phosphorylated form of PERK (Thr980) showed a bright, punctate, perinuclear localization in brefeldin A-treated cells, consistent with its activation within the

ER (FITC-green). As a control for brefeldin A-induced stress that might be independent of ER stress, cells were exposed to brefeldin A in the presence of actinomycin D, a potent transcriptional blocker that dramatically lowers protein synthesis in the ER. Actinomycin D-treated neurons did not display Gadd153 translocation to the nucleus or enhanced PERK phosphorylation following exposure to brefeldin A (data not shown).

Co-localization studies were used to determine if the phospho-PERK-reactive staining observed in brefeldin A-treated CGNs was indeed localized to the ER. CGNs were transfected with a plasmid encoding an ER-specific red fluorescent protein (KDEL ER-retention motif, pDsRed2-ER). As lipid-based transfection is highly toxic to primary neurons, a gene gun strategy was employed. Plasmid-coated gold pellets were shot into the adherent CGNs using a high-pressure burst of helium gas, and cells were exposed to experimental treatments 24 h later. Transfected cells exhibited a membranous, peri-nuclear red fluorescence, consistent with ER localization and morphology (Fig. 3B). Control and brefeldin A-treated, ER-red transfected cells were analyzed for phospho-PERK intensity and localization. Whereas control cells displayed essentially no phospho-PERK reactivity, brefeldin A-treated cells displayed a punctate staining as was previously observed, and this fluorescence co-localized with vesicularized ER in apoptotic cells (Fig. 3B, lower panels). Collectively, the data presented thus far show that brefeldin A induces PERK activation, enhanced phosphorylation of eIF2 α , and translocation of Gadd153/CHOP to the nucleus of CGNs. In contrast, neurons subjected to TFW are indistinguishable from controls with regard to these ER stress-specific characteristics.

IP₃ receptor-mediated Ca²⁺ release is required for ER stress-induced apoptosis but not TFW-induced apoptosis of CGNs

It is believed that the release of Ca²⁺ from the ER plays a central role in the activation of mitochondrial apoptosis. Mediators of the pro-apoptotic release of ER Ca²⁺ have not been well characterized, although pro-apoptotic Bcl-2 family members (Bax and Bak) have been shown to deplete ER Ca²⁺ when overexpressed (Scorrano et al., 2003). IP₃ receptors are known to activate endogenous, store-operated Ca²⁺ release from the ER in response to cytosolic IP₃ signaling and ER stress (Szabadkai and Rizzuto, 2004). To evaluate IP₃ receptor-based Ca²⁺ release as a component of apoptotic signaling in CGNs, we utilized 2-aminoethoxydiphenyl borate (2-APB), a cell-permeable IP₃ antagonist and inhibitor of IP₃-mediated Ca²⁺ release from the ER (Maruyama et al., 1997). Neurons were cultured in the presence/absence of 20 μ M 2-APB and exposed to either TFW or brefeldin A for 24 h (Fig. 4A). In control cells, 20 μ M 2-APB was mildly cytotoxic, elevating the percentage of apoptotic cells by ~10% over a period of 24 h. In brefeldin A-treated samples, 2-APB significantly inhibited the ER stress-induced activation of apoptosis, reducing the number of apoptotic cells from ~54% (BA) to ~17% (BA + 2-APB) over a 24-h exposure. In contrast, TFW induced an apoptotic morphology in ~69% of the neurons, and inclusion of 2-APB displayed no ability to block this apoptotic signal (~89% apoptotic). Thus, 2-APB-mediated protection from neuronal apoptosis was specific for ER stress signaling.

2-APB has not, to our knowledge, previously been shown to block an ER stress-induced apoptosis. Thus, we chose to examine the affect of 2-APB upon cells undergoing a well-characterized ER stress that results in apoptosis. tsBN7 hamster fibroblasts carry a temperature-sensitive mutation in a subunit of the ER-localized oligosaccharyltransferase complex (Sanjay et al., 1998) and display a

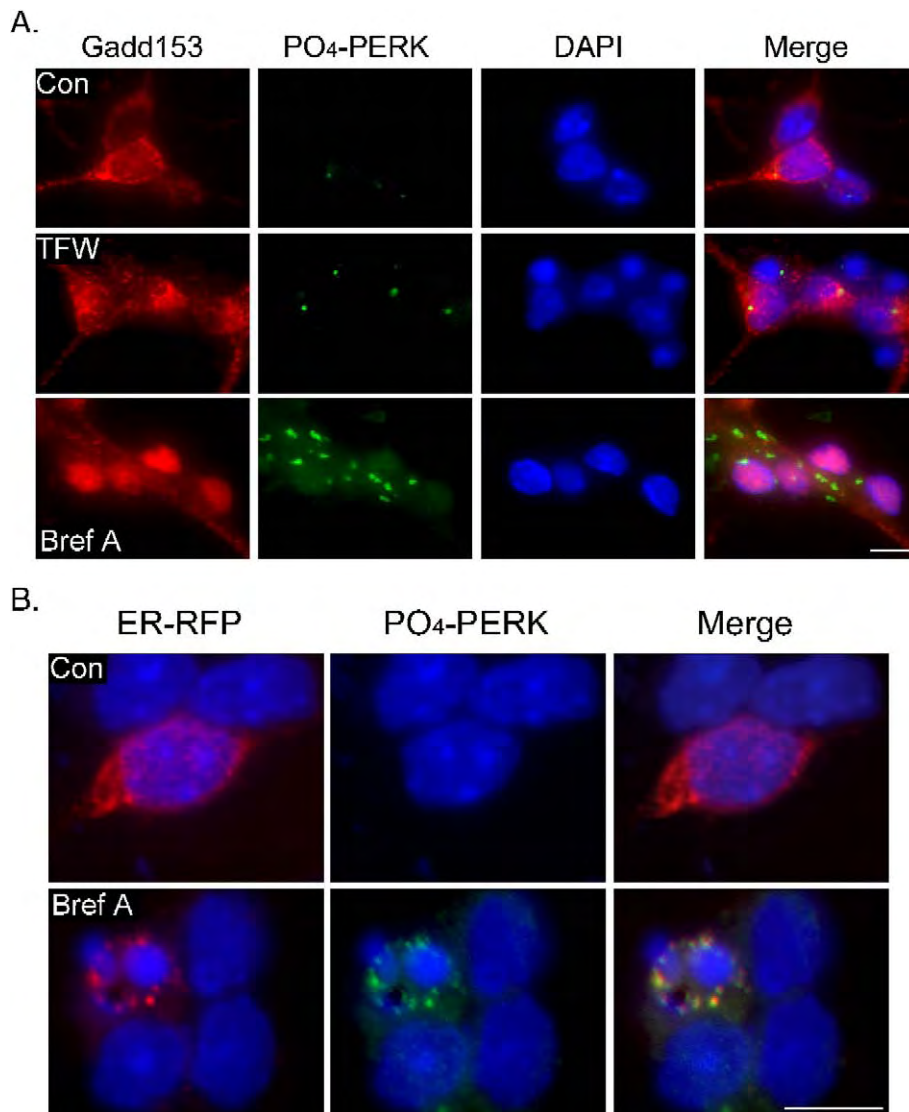


Fig. 3. Immunocytochemical analysis of Gadd153/CHOP translocation and PERK activation downstream of ER stress and TFW. (A) CGNs were seeded onto polyethyleneimine-treated glass coverslips, then transferred to control media (\pm brefeldin A, 20 μ M), or TFW media for 12 h. Fixed cells were permeabilized and then incubated with antibodies to CHOP/Gadd153 (mouse monoclonal) and phosphorylated (active) PERK (rabbit polyclonal). Bound antibodies were detected with Cy3-conjugated anti-mouse and FITC-conjugated anti-rabbit secondary antibodies. Nuclei were stained using DAPI (blue). Brefeldin A-treated cells displayed a clear translocation of CHOP/Gadd153 (red) to the nucleus and an increase in phosphorylated PERK (green). TFW induced neither of these effects, although apoptotic nuclei were clearly observed. Scale bar is 10 μ m. (B) Gene gun-mediated transfection of CGNs was used to evaluate the cellular localization of phosphorylated PERK relative to the endoplasmic reticulum (ER). CGNs were seeded onto coverslips and transfected with pDsRed2-ER (ER-RFP, see Experimental methods) using plasmid-coated gold beads and the Helios Gene-Gun apparatus (Bio-Rad, Hercules CA, USA). Plasmid-bearing cells display a red fluorescence in the ER. Transfected cells were allowed 24 h for recovery and were then shifted to control media (\pm brefeldin A, 20 μ M) for 12 h. Immunolocalization of phosphorylated PERK (green) was performed as described above and revealed a clear co-localization of phosphorylated PERK with the ER. Scale bar is 10 μ m.

temperature-induced defect in N-linked glycosylation, which activates ER-stress signaling, and a mitochondria-dependent apoptotic death (Niederer et al., 2005). At the restrictive temperature of 39.5°C, tsBN7 cells displayed a marked induction of apoptotic death (Fig. 4B), increasing from \sim 7% apoptosis observed in non-stressed cells to \sim 20% (24 h) and then \sim 35% (30 h). When 2-APB (20 or 50 μ M) was included in the medium, the restrictive temperature induced only a modest increase in apoptotic cells. For example, after 30 h at the restrictive temperature, cells containing 50 μ M 2-APB displayed only \sim 9% apoptosis. Thus, inhibition of IP₃ receptor-mediated Ca²⁺ release is sufficient to inhibit an ER stress-induced apoptosis in both

primary rat neurons and hamster fibroblasts but is unable to inhibit neuronal apoptosis elicited by TFW.

ER-targeted Bcl-2 selectively inhibits brefeldin A-induced CGN apoptosis

Bcl-2 is a well-known, anti-apoptotic resident of the mitochondrial outer membrane. Bcl-2 proteins associate with pro-apoptotic proteins such as Bax and Bak, inhibiting their capacity to permeabilize the outer mitochondrial membrane and enable the release of apoptosis-inducing mitochondrial components such as

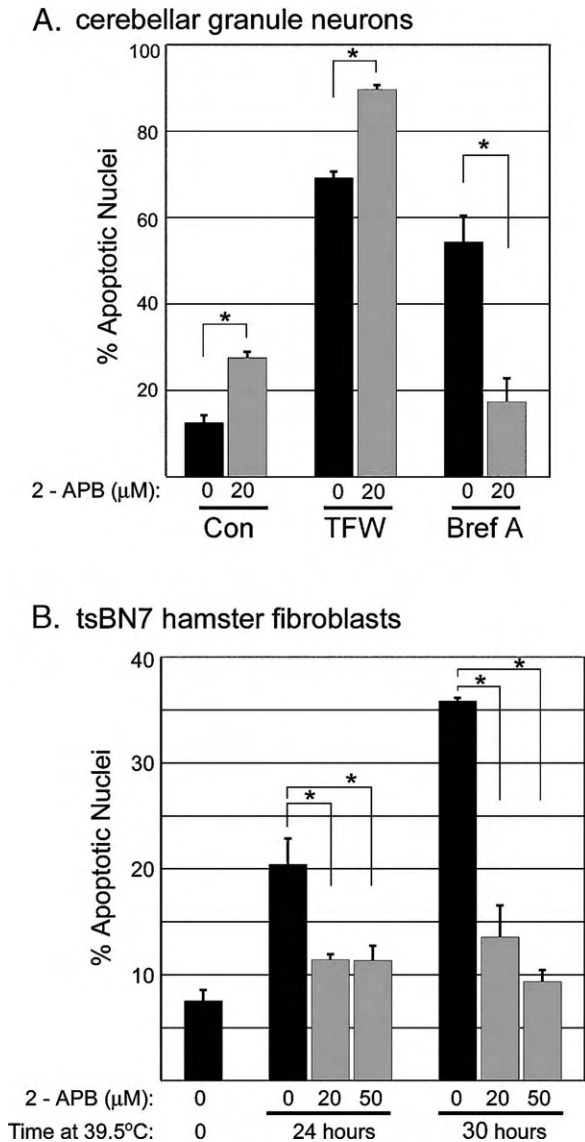


Fig. 4. An IP_3 receptor-mediated Ca^{2+} release is required for ER stress-induced apoptosis, but not TFW-induced apoptosis. (A) CGNs were cultured for 12 h in the presence or absence of brefeldin A (Bref A, 20 μ M) or TFW. Duplicate samples, \pm 2-aminoethoxydiphenyl borate (2-APB, 20 μ M), were generated to assess involvement of IP_3 R-mediated Ca^{2+} release in the activation of apoptosis under each condition. Following incubation, cells were fixed in 4% paraformaldehyde and stained with DAPI. Apoptosis was scored by examination of nuclear morphology. 2-APB significantly elevated apoptotic counts in control cells and TFW-treated cells revealing a mild toxicity of this agent. In cells experiencing ER stress, 2-APB inhibited the activation of apoptosis. The data shown represent the mean \pm SEM for at least three independent experiments, and an asterisk (*) denotes statistical difference among treatments ($P < 0.05$) using a one-way ANOVA test. (B) Hamster fibroblast cells (tsBN7) were cultured at 39.5°C to induce ER stress (\pm 2-APB, 20 μ M or 50 μ M). Cells were then fixed, stained, and counted as described in panel A. 2-APB was sufficient to inhibit ER stress-induced apoptosis in either cell type but did not inhibit TFW-induced apoptosis.

cytochrome *c* (Kuwana and Newmeyer, 2003). A small percentage of native Bcl-2 exists in the membrane of the ER, and overexpression of ER-targeted Bcl-2 (Bcl-2_{ER}) has been shown to perturb stress-induced Ca^{2+} release from the ER (Distelhorst and

Shore, 2004). A recent report has shown Bcl-2_{ER} to interact directly with the IP_3 receptor and to inhibit IP_3 -activated Ca^{2+} release from the ER (Chen et al., 2004b). Thus, if Bcl-2_{ER} and 2-APB both perturb IP_3 receptor-mediated Ca^{2+} release, they should display a similar specificity for arresting ER-dependent apoptotic signals.

Neurons were transfected with a plasmid encoding either a Bcl-2/GFP fusion protein or GFP only. Plasmid-coated pellets were shot onto coverslips with attached primary neurons. ER stress or TFW was induced for a period of 12 h and neurons were subsequently fixed, stained with DAPI, and examined using fluorescence microscopy. Overexpression of wild-type Bcl-2 was found to inhibit both TFW- and brefeldin A-induced apoptosis. This result is difficult to interpret as Bcl-2 is known to act at both the mitochondria and the ER, but it does reveal both apoptotic signals to act via a Bcl-2-regulated process. Attempts to express a mitochondria-specific Bcl-2 in CGNs were unsuccessful, presumably because of the toxicity of high levels of mitochondrial Bcl-2 that have been noted previously (Wang et al., 2001). An ER-specific Bcl-2 was used in subsequent experiments to examine the capacity of Bcl-2_{ER} to inhibit apoptotic signaling. The Bcl-Cb5 fusion protein contains Bcl-2 fused to the C-terminus of rat cytochrome B5, which targets the fusion protein to the ER membrane (Thomenius and Distelhorst, 2003; Wang et al., 2001). Neurons expressing Bcl-2_{ER}/GFP displayed fluorescence in a perinuclear pattern, consistent with ER localization, whereas cells expressing the GFP control protein displayed an evenly distributed cytosolic localization (Fig. 5A). Neurons expressing GFP alone displayed a normal induction of apoptotic morphology following exposure to brefeldin A or TFW activation (~40% apoptosis at 12 h). Neurons expressing the Bcl-2_{ER}/GFP fusion protein displayed a clear reduction in brefeldin A-induced apoptosis (~19%), but no inhibition of 5K-induced apoptosis (~39%). Bcl-2_{ER} provides a significant protection for CGNs experiencing ER stress, but not those experiencing TFW.

TFW and brefeldin A-induced apoptosis is blocked by IGF-I and GSK-3 β inhibitors

Insulin-like growth factor-I (IGF-I) blocks CGN apoptotic activation following TFW (Linseman et al., 2002). IGF-I interacts with the IGF-I receptor to induce cellular survival via activation of phosphatidylinositol-3 (PI_3) kinase and subsequent Akt/PKB signaling, elevated expression of the anti-apoptotic Bcl-2 and Bcl-X_L proteins, and diminished expression of the pro-apoptotic Bax, Bim, and Bcl-X_S proteins (Heidenreich, 2003; Linseman et al., 2002). To determine if IGF-I has a similar influence upon the brefeldin A-induced apoptotic signal, we exposed CGNs to apoptosis-inducing conditions in the presence/absence of IGF-I. Exposure to TFW or brefeldin A induced apoptotic nuclei in ~67% and ~52% of the neurons, respectively, whereas control neurons displayed ~10% apoptosis (Fig. 6A). IGF-I protected CGNs from both TFW- and brefeldin A-induced apoptosis, reducing apoptosis to ~20% and 10%, respectively. This result reveals, for the first time in this study, a shared component of neuronal apoptosis induction utilized by these distinct stressors.

One target of IGF-induced neuroprotection is the pro-apoptotic kinase GSK-3 β , whose activity is inhibited by Akt-mediated phosphorylation at Serine-9. GSK-3 β is a complex cellular kinase, regulating a variety of processes including glycogen metabolism, Wnt signaling during development, cell proliferation, and apopto-

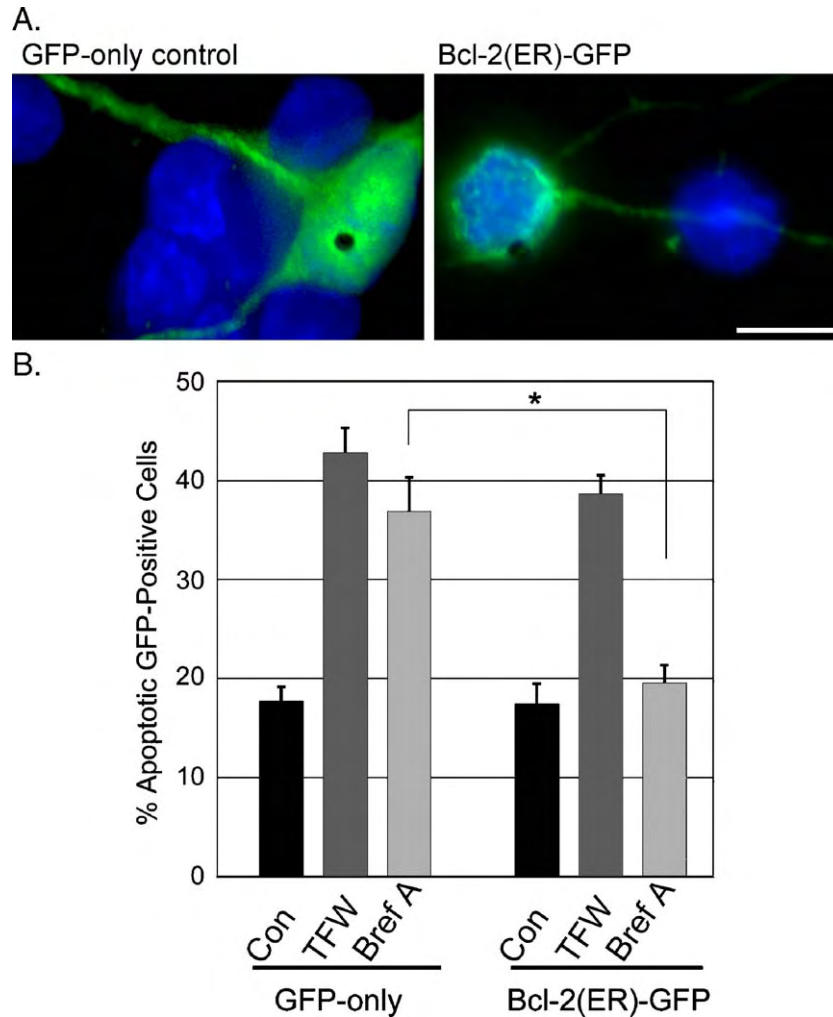


Fig. 5. Overexpression of an ER-localized Bcl-2 inhibits ER stress-induced apoptosis, but not TFW-induced apoptosis. (A) Gene gun-mediated transfection was used to generate CGNs expressing an ER-specific Bcl-2-GFP fusion protein or a GFP control protein. CGNs were seeded onto coverslips and transfected with pGFP-Bcl-2-Cb5 or pGFP (GFP-only control plasmid) using the Helios Gene-Gun, as described previously. Plasmid-bearing CGNs displayed green fluorescence in a peri-nuclear pattern, consistent with ER localization (GFP-Bcl-2-Cb5) or a generalized cytosolic localization (GFP-only). Nuclei are stained with DAPI (blue). In transfected cells, the gold beads are typically visible (see arrows). Scale bar is 10 μ m. (B) Apoptosis was assessed in CGNs expressing high levels of Bcl-2 in the ER. Transfected CGNs were cultured in control medium (\pm brefeldin A, 20 μ M) or TFW media for a period of 12–14 h. Apoptotic cells were clearly visible as cells displaying neurite deterioration, nuclear condensation, and fragmentation. The data shown represent the mean \pm SEM for at least three independent experiments, and an asterisk (*) denotes statistical difference among treatments ($P < 0.05$) using a one-way ANOVA test. Bcl-2_{ER} inhibited apoptosis in cells experiencing ER stress but did not inhibit apoptosis in cells experiencing TFW.

sis (Frame and Cohen, 2001). The kinase activity of GSK-3 β can be blocked in vivo with the addition of lithium to the cell culture medium as a potent, non-competitive inhibitor (Hongisto et al., 2003). LiCl (20 mM) addition protected CGNs from apoptosis induced by either TFW or brefeldin A, displaying populations of neurons that were phenotypically indistinguishable from the 25K control cells (Fig. 6A). Consistent with inhibitors of GSK-3 β blocking apoptosis induced by TFW or ER stress, both TFW (Fig. 6B) and brefeldin A (Fig. 6C) elicited a marked acute dephosphorylation (activation) of GSK-3 β . In the case of TFW, GSK-3 β dephosphorylation was detected as early as 1 h after 5K treatment, consistent with our previous data (Linseman et al., 2004). In brefeldin A-treated CGNs, GSK-3 β dephosphorylation was somewhat delayed but was prominent after 8 h. GSK-3 β dephosphorylation was detectable in brefeldin A-treated CGNs by either loss of a band with decreased mobility in blots probed with a GSK-3 β antibody (Fig. 6C, left blot) or loss of phospho-GSK-3 β in blots

probed with a phospho-Ser9-specific antibody (Fig. 6C, right blot). Densitometry was performed to quantify the ratio of phospho-GSK-3 β /total-GSK-3 β in TFW- or brefeldin A-treated neurons relative to control neurons. TFW generated a 70% reduction in GSK-3 β phosphorylation within two h, and brefeldin A generated a 93% reduction in GSK-3 β phosphorylation within 8 h. Thus, activation of GSK-3 β is a shared component of both TFW and ER stress apoptotic induction in CGNs.

TFW and ER stress each induce CGN apoptosis via a caspase-9-dependent pathway

To confirm that TFW and ER stress apoptotic signals were transduced through the intrinsic death pathway, we evaluated the role of the mitochondrial initiator, caspase-9, in CGN apoptosis elicited by each of these stressors. Immunocytochemistry of CGNs exposed to TFW and brefeldin A revealed a clear activation of

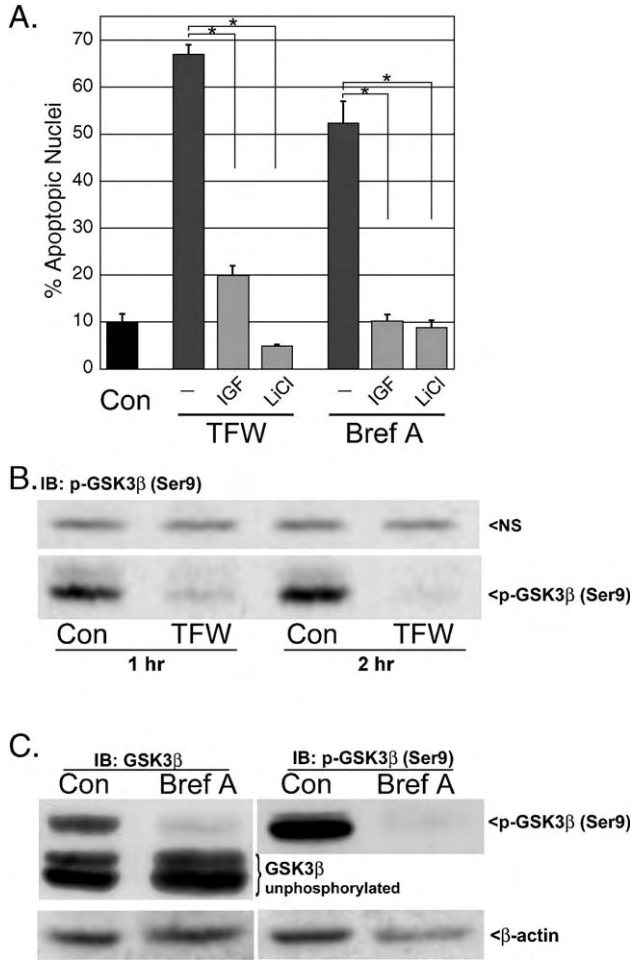


Fig. 6. Distinct apoptosis signaling pathways downstream of ER stress and TFW converge at GSK-3β. (A) CGNs were incubated for 24 h in control medium (\pm brefeldin A, 20 μ M) or TFW medium. LiCl (20 mM) or insulin-like growth factor-I (IGF-I, 200 ng/ml) were evaluated for their ability to inhibit apoptotic activation in TFW and brefeldin A-treated CGNs. Following incubation, cells were fixed in 4% paraformaldehyde, and nuclei were stained with DAPI. The percentage of apoptotic nuclei was determined using fluorescence microscopy, scoring \sim 500 cells/experimental replicate. The data shown represent the mean \pm SEM for at least three independent experiments, and an asterisk (*) denotes statistical difference among treatments ($P < 0.05$) using a one-way ANOVA test. (B, C) CGNs were incubated in control medium (\pm brefeldin A, 20 μ M) for 8 h or TFW medium for 1–2 h. Proteins from cellular lysates were resolved by SDS–PAGE, transferred to PVDF membranes, and immunoblotted with a GSK-3β or a phospho-specific GSK-3β (Ser9) antibody. Dephosphorylation at serine 9 indicates activation of GSK-3β signaling. The GSK-3β antibody detects unphosphorylated GSK-3β as well as phospho-GSK-3β (Ser9). The GSK-3β antibody reveals a decrease in phospho-GSK-3β (Ser9) and a slight increase in unphosphorylated GSK-3β (left panel). A decrease in phospho-GSK-3β (Ser9) was also detected using the phospho-specific GSK-3β (Ser9) antibody (right panel). (B) NS = non-specific band detected by the p-GSK-3β antibody that is shown as a loading control. (C) Both blots were stripped and re-probed with an antibody to β -actin to show equal loading.

caspase-9 activity and the coincident condensation/fragmentation of cellular nuclei (Fig. 7A). To evaluate if caspase-9 activity was required for apoptotic induction under these conditions, LEHD, we used a potent competitive and irreversible peptide inhibitor selective for caspase-9. Cultures were exposed to the indicated stressor for 24 h in the presence or absence of cell-permeable LEHD, and apoptotic

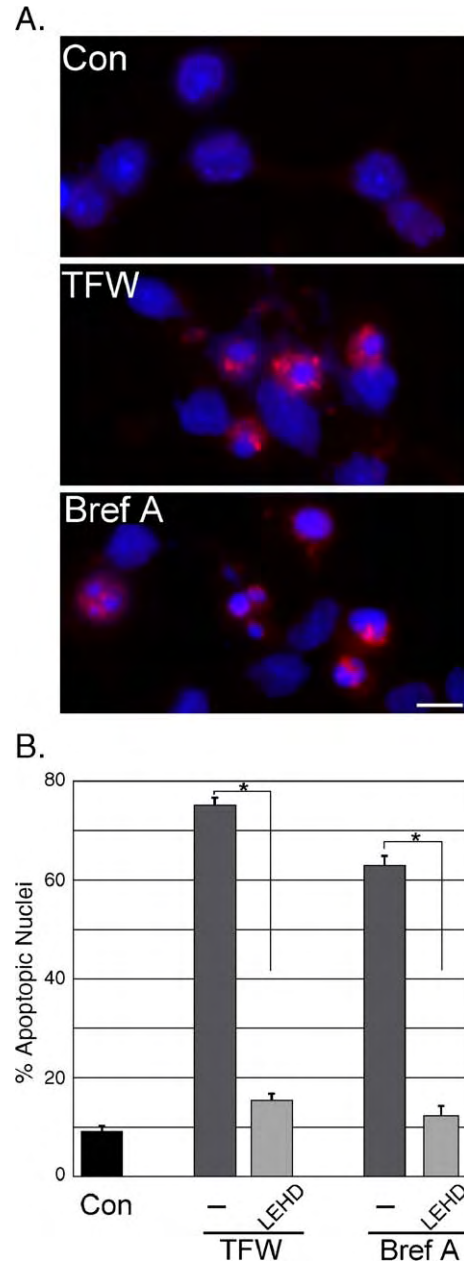


Fig. 7. Brefeldin A and TFW initiate apoptosis via caspase-9 activity. (A) CGNs were seeded onto glass coverslips, and then cultured in control medium (\pm brefeldin A, 20 μ M), or TFW medium for 16 h. Samples were fixed, permeabilized, and incubated with an antibody to active caspase-9 (rabbit polyclonal, Cy3 anti-rabbit secondary antibody). Nuclei were stained using DAPI. Both brefeldin A and TFW-treated samples displayed a robust activation of caspase-9 staining and apoptotic nuclear morphology. Scale bar is 10 μ m. (B) To assess the role of caspase-9 in the apoptosis of CGNs experiencing ER stress or TFW, we used a caspase-9 inhibitor. CGNs were cultured for 24 h in control medium (\pm brefeldin A, 20 μ M) or TFW medium. Replicate samples contained a cell-permeable inhibitor of caspase-9 activity, z-LEHD-fmk (LEHD, 100 μ M). After incubation, cells were fixed in 4% paraformaldehyde and stained with DAPI. Samples were scored for apoptosis as previously described. The data shown represent the mean \pm SEM for at least three independent experiments, and an asterisk (*) denotes statistical difference among treatments ($P < 0.05$) using a one-way ANOVA test. LEHD inhibited both TFW- and ER stress-induced apoptosis, revealing caspase-9 to be required for the activation of apoptosis under these conditions.

nuclei were quantified using fluorescence microscopy (Fig. 7B). Apoptosis induced by either TFW or brefeldin A was nearly completely blocked by caspase-9 inhibition revealing both apoptotic signals to require the activation of caspase-9 for neuronal death.

Discussion

The activation of cellular apoptosis in CGNs can result from a diverse array of cellular signals and stresses. In this study, we have characterized the mechanism of apoptosis activation during endoplasmic reticulum stress, and the status of ER stress pathways when neuronal apoptosis is induced by TFW. Brefeldin A, a known ER stressor, was shown to induce clear indications of ER signaling, caspase activation, neurite degeneration, and nuclear degradation. ER stress signaling was revealed as phosphorylation of eIF2 α and PERK, accompanied by increased expression and nuclear localization of Gadd153/CHOP. TFW generated none of the above stress signals despite a robust activation of caspase activity and apoptosis. Thus, ER stress activates an initial signal that is distinct from that activated by TFW. Both ER stress and TFW were found to induce dephosphorylation (activation) of GSK-3 β , a central cellular kinase that regulates apoptosis in CGNs. GSK-3 β inhibition was sufficient to block apoptosis activation under either condition. Furthermore, both ER stress and TFW were shown to require the activation of caspase-9 to induce apoptosis. Thus, despite originating from distinct cellular signals, both ER stress and TFW activate apoptotic signals that ultimately converge on GSK-3 β and caspase-9 to induce the intrinsic apoptotic pathway (Fig. 8).

This work reveals IP₃ receptors to contribute an essential component of ER-induced apoptotic signaling in CGNs. The ER

can induce apoptosis via the mPT, and although the mechanism is not well understood, it is clear that Ca²⁺ release from the ER followed by elevated cytosolic Ca²⁺ can induce the mPT and subsequent apoptotic death (Assefa et al., 2004). A depletion of luminal ER Ca²⁺ stores is protective against several apoptotic insults that utilize the intrinsic pathway, consistent with a central role for ER Ca²⁺ release in activating the mPT (Distelhorst and Shore, 2004). IP₃ receptors have been a focal point for studies on pro-apoptotic Ca²⁺ release from the ER. Diminished expression of IP₃ receptor isoforms is protective against apoptotic activation (Hanson et al., 2004), and recent evidence has identified suppression of IP₃ receptor-1 expression as the key anti-apoptotic mode of action for the transcription factor, nuclear factor- κ B (NF- κ B) (Camandola et al., 2005). In addition, IP₃ receptors that “leak” Ca²⁺ are generated by caspase-3-mediated proteolysis (Assefa et al., 2004) and by interaction with cytosolic cytochrome *c* (Boehning et al., 2005). The expression of high levels of Bcl-2 in the ER has been shown to protect against several forms of apoptosis (Thomenius and Distelhorst, 2003), and recent evidence has shown Bcl-2_{ER} to interact directly with IP₃ receptors to dampen Ca²⁺ release during stress (Chen et al., 2004b). In this work, both Bcl-2_{ER} and an IP₃ receptor antagonist were sufficient to block apoptosis activation in CGNs experiencing ER stress but were unable to block TFW-induced apoptosis. These data are consistent with IP₃ receptors playing an essential role in ER stress-specific apoptosis signaling.

GSK-3 has been traditionally associated with the regulation of glycogen metabolism, although in recent years it has become clear that GSK-3 is a key regulator of a diversity of cellular processes. In vitro studies have revealed GSK-3 to phosphorylate 18 different transcription factors, over 20 different enzymes, and 10 different structural proteins (Jope and Johnson, 2004). The differential affinity of GSK-3 for these targets is regulated by pre-phosphorylation of substrates by other kinases, the requirement for GSK-3 binding partners to mediate substrate interaction, and the subcellular localization of active GSK-3. Cellular mechanisms regulated by GSK-3 include survival signaling, microtubule organization and function, cellular metabolism, and the activation of apoptosis. GSK-3 α and GSK-3 β refer to two separate genes encoding nearly identical proteins, with GSK-3 β being highly expressed in neurons (Mukai et al., 2002).

GSK-3 β activity is associated with neuronal apoptotic signaling (Chen et al., 2004a; Hongisto et al., 2003; Loberg et al., 2002; Murphy, 2004; Stoica et al., 2003), and has recently been shown to be induced by ER stress (Chen et al., 2004a; Kim et al., 2005; Song et al., 2002). Inhibition of GSK-3 β is via phosphorylation, mediated by the survival factor-induced signaling of protein kinase A (PKA) (Mingtau et al., 2000), protein kinase B (PKB/AKT) (Dudek et al., 1997), and/or the ribosomal S6 kinase. TFW inhibits survival pathway signaling and releases GSK-3 β inhibition to induce cellular apoptosis (Chin et al., 2005). In human SH-SY5Y neuroblastoma cells, ER stress signaling induces protein phosphatase 2A (PP2A)-dependent dephosphorylation of GSK-3 β , and the subsequent GSK-3 β -dependent induction of apoptosis (Chen et al., 2004a). Qu et al. (2004) showed that ER stress activates GSK-3 β activity in non-neuronal cells lines, but they found that activity to be protective against DNA damage-induced apoptosis. In their study, GSK-3 β phosphorylated cytosolic p53, inhibiting its pro-apoptotic translocation to the nucleus following DNA damage. Pro-apoptotic substrates for GSK-3 β have not been well-characterized, although we have recently shown GSK-3 β to phosphorylate Bax in response to TFW, inducing Bax translocation to the

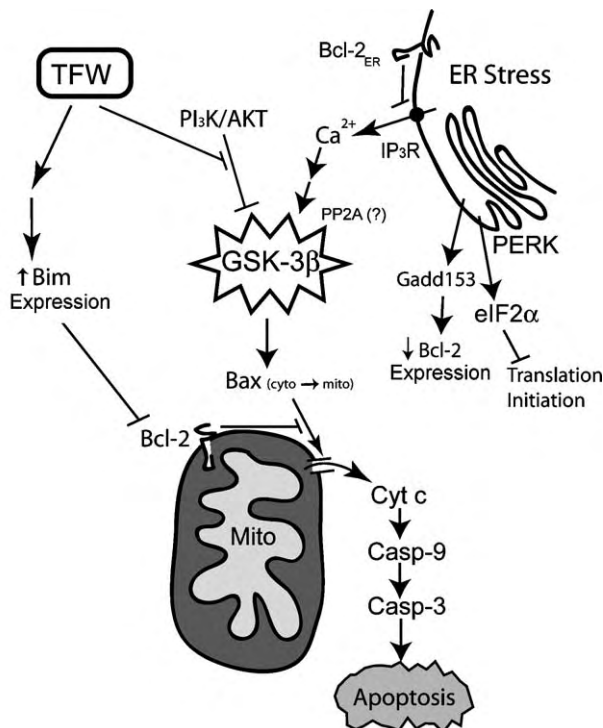


Fig. 8. A model of TFW and ER stress signaling convergence to induce intrinsic CGN apoptosis.

mitochondria and activating cellular apoptosis (Linseman et al., 2004). In this work, we have found both ER stress and TFW to induce GSK-3 β dephosphorylation in CGNs, and we have shown the addition of a GSK-3 β inhibitor (lithium) to be sufficient to block the activation of apoptosis under either condition. These results are consistent with GSK-3 β or an upstream activator of GSK-3 β , serving as a site of convergence for neuronal signals activating the intrinsic apoptotic pathway.

GSK-3 β activation has been linked to the neuronal apoptosis associated with neurodegenerative disease (Jope and Johnson, 2004). We have revealed a connection between ER stress signaling and GSK-3 β activation in CGNs. This supports models that include ER dysfunction as a key initial event in familial Alzheimer's disease and identifies GSK-3 β activity as a possible downstream target of ER stress signaling in affected neurons. ER Ca²⁺ homeostasis is perturbed in neurons accumulating A β protein, or neurons overexpressing the PS1 allele associated with inherited Alzheimer's disease (Paschen and Mengesdorf, 2005). In addition to A β protein accumulation, Alzheimer's disease is defined by the neuronal accumulation of hyperphosphorylated tau protein, which results in the formation of intra-neuronal filamentous aggregates known as neurofibrillary tangles (NFT). GSK-3 β activity is elevated in neurons developing NFT or displaying a degenerative phenotype (Pei et al., 1999), and in vitro studies have identified tau to be phosphorylated by GSK-3 β (Jope and Johnson, 2004). In addition, overexpression of GSK-3 β in transgenic mice or cell culture models induces the hyperphosphorylation of tau, and neuronal apoptosis (Lucas et al., 2001; Takashima et al., 1998). The discovery that GSK-3 β may serve as a site of apoptotic signaling convergence for both TFW and ER stress elevates the importance of examining therapeutic interventions to inhibit/perturb GSK-3 signaling in affected neurons.

Experimental methods

Reagents

Brefeldin A, thapsigargin, SB203580, and 2-aminoethoxydiphenylborate (2-APB) were purchased from Calbiochem (San Diego, CA, USA). Rabbit polyclonal antibodies to eIF2 α , phospho-eIF2 α , phospho-PERK, phospho-GSK-3 β (Ser 9), active (cleaved fragment) caspase-3, β -actin, and Grp78/Bip were purchased from Cell Signaling (Madison, WI, USA). Monoclonal antibodies to Gadd153/CHOP and rabbit polyclonal antibodies to Bim were purchased from Santa Cruz Biotechnology (Santa Cruz, CA, USA). Monoclonal antibodies to active caspase-9 were purchased from Alexis Biochemicals (San Diego, CA, USA). Tunicamycin, insulin-like growth factor-I (IGF-I), monoclonal antibodies to β -tubulin, *p*-phenylenediamine, and 4,6-diamindino-2-phenylindole (DAPI) were from Sigma (St. Louis, MO, USA). Fluorescein-5-isothiocyanate (FITC)-conjugated and Cy3-conjugated secondary antibodies for immunocytochemistry were purchased from Jackson ImmunoResearch Laboratories (West Grove, PA, USA). The ER subcellular localization plasmid (pDsRed2-ER) was purchased from BD Biosciences/Clontech (Palo Alto, CA, USA). The ER-targeted Bcl-2-GFP fusion protein expression vector (pGFP-Bcl-2-Cb5) and GFP-only vector (pGFP) are described in a previous publication (Wang et al., 2001).

CGN culture

Cerebellar granule neurons were dissociated from 7-day-old Sprague–Dawley rat pups as previously described (Linseman et al., 2002). Neurons were plated at a density of 2.0×10^6 cells/ml onto poly-L-lysine-treated plastic cell culture dishes. Initial plating was in 25K medium composed of

basal modified Eagles medium containing 10% fetal bovine serum, 25 mM KCl, 2 mM L-glutamine, 100 U/ml penicillin, and 100 μ g/ml streptomycin (Invitrogen, Grand Island, NY). One day after initial seeding, cultures were treated with cytosine arabinoside (10 μ M) to limit the growth of non-neuronal cells. All experiments were performed on cultures 6–8 days after initial harvest. This protocol reproducibly generates a highly enriched population of granule neurons (95–97%). Time points for each experiment are in reference to the time at which enriched cultures are shifted to experimental conditions. For most experiments, enriched cultures were transferred into high potassium (25K) serum-free medium at initiation of the experiment—identified as control medium. To induce the TFW apoptotic phenotype, we shifted cells to low potassium (5K) serum-free medium.

Quantification of apoptotic cells

After the specified treatment of neuronal cultures, cells were fixed with 4% paraformaldehyde (20 min), gently rinsed with phosphate-buffered saline (PBS), and stained with DAPI (1 μ g/ml). Cells were then examined using fluorescence microscopy and scored as apoptotic if the cells displayed a condensed or fragmented nucleus. Untreated cultures of CGNs typically exhibit ~5–10% apoptotic nuclei. Each well of treated cells was evaluated independently, counting 400–600 cells to determine the percentage of apoptotic cells in each well. All data sets presented are the average of at least three separate experiments. Apoptotic assessment of tsBN7 cells was identical to CGNs with the exception of the cell culture medium used, which was Dulbecco's modified Eagles medium (DMEM), 10% fetal bovine serum, 1 \times non-essential amino acids, 100 U/ml penicillin, and 100 μ g/ml streptomycin.

Protein isolation/immunoblots

To isolate proteins for immunoblot analysis, we rinsed neurons gently with PBS and lysed it in a solution of 95°C SDS lysis solution (10 mM Tris–HCl pH 7.4, 1.0% sodium dodecyl sulfate, 1 mM sodium orthovanadate). Lysates were transferred into microfuge tubes, heated at 95°C for 30 s, and passed 10 \times through a 25-gauge syringe needle to decrease viscosity. Protein concentration was then determined using a BCA protein assay kit from Pierce Biotechnology (Rockford, IL, USA). Kinexus Bioinformatics Corporation (Vancouver, BC, Canada) performed initial immunoblot screens to assess ER stress- and 5K-induced changes in cellular signaling. The Kinexus methodology for controlling loading includes protein assay before electrophoresis and an analysis of total lane intensity, including space between bands, after immunoblotting (each lane is probed for multiple protein targets). All other immunoblots were performed as previously described (Linseman et al., 2002). Densitometry of chemiluminescent immunoblots was performed using a FluorChemSP imaging system and AlphaEaseFC software (Alpha Innotech, San Leandro, CA). The phosphorylation of eIF2 α and GSK-3 β was quantified using immunoblot densitometry data of phosphorylated and non-phosphorylated forms of each protein for each lysate. To reveal fold-changes in phosphorylation, the ratio of phosphorylated to non-phosphorylated protein was determined for control and treated neurons. This was then expressed as a percentage of induction or repression for each treatment, relative to control samples.

Immunocytochemistry

For immunocytochemistry and gene gun-based transfection, CGNs were seeded at a density of $\sim 2.5 \times 10^5$ cells/ml onto polyethyleneimine-treated glass coverslips. Coverslip-attached neurons were exposed to experimental conditions, fixed in 4% paraformaldehyde, gently rinsed with PBS (pH 7.4), and were then permeabilized/blocked for ~1 h in a PBS solution containing 0.2% Triton X-100 and 5% bovine serum albumin (BSA). The blocking solution was aspirated and replaced with a PBS solution containing 0.2% Triton X-100, 2% BSA, and primary antibody. Coverslips were incubated ~16 h in the primary antibody solution (4°C). The primary antibody solution was then aspirated, the coverslips washed

5× with PBS, and a secondary antibody solution was added containing a Cy3- or FITC-conjugated secondary antibody and DAPI (1 µg/ml). After a 1-h incubation, coverslips were again washed 5× with PBS and were then mounted onto slides in a small volume of mounting medium of Fluoromount G (Fisher, Pittsburgh, PA, USA) and 0.1% *p*-phenylenediamine. Fluorescence images were captured using a Zeiss Axioplan 2 microscope equipped with a Cooke Sencam deep-cooled CCD camera and Slidebook software analysis program for digital deconvolution (Intelligent Imaging Innovations, Denver, CO, USA).

Gene gun transfection of primary CGNs

CGNs were transiently transfected using the Helios Gene-Gun system (Bio-Rad, Hercules, CA, USA) according to the manufacturer's protocol. Individual plasmids were precipitated onto 0.6-µm-diameter gold beads in a CaCl₂/spermidine mixture. The beads were washed 3× with 100% ethanol and resuspended in ethanol containing 0.05 mg/ml polyvinylpyrrolidone. The suspension was drawn into Tefzel tubing, and the beads were then allowed to settle within the tubing (~5 min). The ethanol was then removed, and the beads were dried using nitrogen gas. The tubing was chopped into short (1.3 cm) pieces, which could then be inserted into the barrel of the gene gun for transfection experiments. Transfections were performed 5 or 6 days after harvesting of the CGNs. All media were removed from the coverslip, and the beads were shot through a 40-µm strainer onto the coverslip using a burst of helium gas (100 psi). The medium was replaced immediately, and the neurons were cultured for 24 h before initiating any experimental condition. In gene gun experiments, transgenic neurons were identified by fluorescence microscopy, and then scored for apoptotic morphology, as defined by nuclear condensation and the degeneration of neurites. Experiments were performed in triplicate from three independent CGN preparations, scoring ~400 neurons/condition for each experiment.

Data analysis

Data points shown represent mean ± standard error of the mean (SEM) for the replicated experimental treatments. Statistically significant differences between data points were determined using a one-way ANOVA test. Statistically significant differences between data points are annotated with an asterisk. By convention, a *P* value of <0.05 was considered statistically significant.

Acknowledgments

The authors would like to thank Clark Distelhorst (Case Western Reserve University, School of Medicine, Cleveland, OH) for his generosity with regard to sharing Bcl-2 plasmids. In addition, we thank Brent Butts, Shoshona Le, Tracy Laessig, and Maria McClure for their assistance and advice on this project. This work was supported by the Department of Veterans Affairs Merit Awards (K.A.H.), the Department of Defense Grant USAMRMC 03281009 (K.A.H. and D.A.L.), the National Institutes of Health (NIH) Grant NS38619-01A1 (K.A.H.), and the Department of Veterans Affairs Research Enhancement Award Program (K.A.H. and D.A.L.), and by an NIH-AREA grant GMO65139-01 (J.L.B.). Molecular Biology Core Services were supported by NIH Diabetes Endocrinology Research Care Grant P30-DK57516.

References

- Adams, J.M., 2003. Ways of dying: multiple pathways to apoptosis. *Genes Dev.* 17, 2481–2495.
- Assefa, Z., Bultynck, G., Szlufcik, K., Kasri, N.N., Vermassen, E., Goris, J., Missiaen, L., Callewaert, G., Parys, J.B., DeSmedt, H., 2004. Caspase-3-induced truncation of type 1 inositol trisphosphate receptor accelerates apoptotic cell death and induces inositol trisphosphate-independent calcium release during apoptosis. *J. Biol. Chem.* 279, 43227–43236.
- Boehning, D., van Rossum, D.B., Patterson, R.L., Snyder, S.H., 2005. A peptide inhibitor of cytochrome *c*/inositol 1,4,5-trisphosphate receptor binding blocks intrinsic and extrinsic cell death pathways. *Proc. Natl. Acad. Sci. U. S. A.* 102, 1466–1471.
- Boyce, M., Yuan, J., 2006. Cellular response to endoplasmic reticulum stress: a matter of life or death. *Cell Death Differ.*, 1–11 (online-ahead of publication, Jan 6).
- Camandola, S., Cutler, R.G., Gary, D.S., Milhavel, O., Mattson, M.P., 2005. Suppression of calcium release from inositol 1,4,5-trisphosphate-sensitive stores mediates the anti-apoptotic function of nuclear factor-κB. *J. Biol. Chem.* 280, 22287–22296.
- Chen, G., Bower, K.A., Ma, C., Fang, S., Thiele, C.J., Luo, J., 2004. Glycogen synthase kinase 3β (GSK3β) mediates 6-hydroxydopamine-induced neuronal death. *FASEB J.* 18, 1162–1164.
- Chen, R., Valencia, I., Zhong, F., McColl, K.S., Roderick, H.L., Bootman, M.D., Berridge, M.J., Conway, S.J., Holmes, A.B., Mignery, G.A., Velez, P., Distelhorst, C.W., 2004. Bcl-2 functionally interacts with inositol 1,4,5-trisphosphate receptors to regulate calcium release from the ER in response to inositol 1,4,5-trisphosphate. *J. Cell Biol.* 166, 193–203.
- Chin, P.C., Majdzadeh, N., D'Mello, S.R., 2005. Inhibition of GSK3β is a common event in neuroprotection by different survival factors. *Brain Res. Mol. Brain Res.* 137, 193–201.
- Cui, K., Coutts, M., Stahl, J., Sytkowski, A.J., 2000. Novel interaction between the transcription factor CHOP (Gadd153) and the ribosomal protein FTE/S3a modulates erythropoiesis. *J. Biol. Chem.* 275, 7591–7596.
- Demuro, A., Mina, E., Kaye, R., Milton, S.C., Parker, I., 2005. Calcium dysregulation and membrane disruption as a ubiquitous neurotoxic mechanism of soluble amyloid oligomers. *J. Biol. Chem.* 280, 17294–17300.
- Distelhorst, C.W., Shore, G.C., 2004. Bcl-2 and calcium: controversy beneath the surface. *Oncogene* 23, 2875–2880.
- D'Mello, S.R., Galli, C., Ciotti, T., Calissano, P., 1993. Induction of apoptosis in cerebellar granule neurons by low potassium: inhibition of death by insulin-like growth factor I and cAMP. *Proc. Natl. Acad. Sci. U. S. A.* 90, 10989–10993.
- Dudek, H., Datta, S.R., Franke, T.F., Birnbaum, M.J., Yao, R., Cooper, G.M., Segal, R.A., Kaplan, D.R., Greenberg, M.E., 1997. Regulation of neuronal survival by the serine-threonine protein kinase Akt. *Science* 275, 661–665.
- Frame, S., Cohen, P., 2001. GSK3 takes centre stage more than 20 years after its discovery. *Biochem. J.* 359, 1–16.
- Hanson, C.J., Bootman, M.D., Roderick, H.L., 2004. Cell Signaling: IP3 receptors channel calcium into cell death. *Curr. Biol.* 14, 933–935.
- Heidenreich, K.A., 2003. Molecular mechanisms of neuronal cell death. *Ann. N. Y. Acad. Sci.* 991, 237–250.
- Hong, M., Luo, S., Baumeister, P., Huang, J.M., Gogia, R.K., Li, M., Lee, A.S., 2004. Underglycosylation of ATF6 as a novel sensing mechanism for activation of the unfolded protein response. *J. Biol. Chem.* 279, 11354–11363.
- Hongisto, V., Smeds, N., Brecht, S., Herdegen, T., Courtney, M.J., Coffey, E.T., 2003. Lithium blocks the c-Jun stress response and protects neurons via its action on glycogen synthase kinase-3. *Mol. Cell Biol.* 23, 6027–6036.
- Jope, R.S., Johnson, G.V.W., 2004. The glamour and gloom of glycogen synthase kinase-3. *Trends Biochem. Sci.* 29, 95–102.
- Katayama, T., Imaizumi, K., Manabe, T., Hitomi, J., Kudo, T., Tohyama, M., 2004. Induction of neuronal death by ER stress in Alzheimer's disease. *J. Chem. Neuroanat.* 28, 67–78.
- Kim, A.J., Shi, Y., Austin, R.C., Werstuck, G.H., 2005. Valproate protects cells from ER stress-induced lipid accumulation and apoptosis by inhibiting glycogen synthase kinase-3. *J. Cell Sci.* 118, 89–99.

- Kuwana, T., Newmeyer, D.D., 2003. Bcl-2-family proteins and the role of mitochondria in apoptosis. *Curr. Opin. Cell Biol.* 15, 691–699.
- Linseman, D.A., Phelps, R.A., Bouchard, R.J., Le, S.S., Laessig, T.A., McClure, M.L., Heidenreich, K.A., 2002. Insulin-like growth factor-I blocks Bcl-2 interacting mediator of apoptosis (Bim) induction and intrinsic death signaling in cerebellar granule neurons. *J. Neurosci.* 22, 9287–9297.
- Linseman, D.A., Butts, B.D., Precht, T.A., Phelps, R.A., Le, S.S., Laessig, T.A., Bouchard, R.J., Heidenreich, K.A., 2004. Glycogen synthase kinase-3beta phosphorylates Bax and promotes its mitochondrial localization during neuronal apoptosis. *J. Neurosci.* 24, 9993–10002.
- Loberg, R.D., Vesely, E., Brosius, F.C., 2002. Enhanced glycogen synthase kinase-3beta activity mediates hypoxia-induced apoptosis of vascular smooth muscle cells and is prevented by glucose transport and metabolism. *J. Biol. Chem.* 277, 41667–41673.
- Lorz, C., Justo, P., Sanz, A., Subira, D., Egido, J., Ortiz, A., 2004. Paracetamol-induced renal tubular injury: a role for ER stress. *J. Am. Soc. Nephrol.* 15, 380–389.
- Lucas, J.J., Hernandez, F., Gomez-Ramos, P., Moran, M.A., Hen, R., Avila, J., 2001. Decreased nuclear beta-catenin, tau hyperphosphorylation and neurodegeneration in GSK-3beta conditional transgenic mice. *EMBO J.* 20, 27–39.
- Marciniak, S.J., Yun, C.Y., Oiyadomari, S., Novoa, I., Zhang, Y., Jungreis, R., Nagata, K., Harding, H.P., Ron, D., 2004. CHOP induces death by promoting protein synthesis and oxidation in the stressed endoplasmic reticulum. *Genes Dev.* 18, 3066–3077.
- Maruyama, T., Kanaji, T., Nakade, S., Kanno, T., Mikoshiba, K., 1997. 2-APB, 2-aminoethoxydiphenyl borate, a membrane-penetrable modulator of Ins (1,4,5), P3-induced Ca²⁺ release. *J. Biochem.* 122, 498–505.
- Mingtau, L., Xiaomin, W., Meintzer, M.K., Laessig, T.A., Birnbaum, M.J., Heidenreich, K.A., 2000. Cyclin AMP promotes neuronal survival by phosphorylation of glycogen synthase kinase 3beta. *Mol. Cell. Biol.* 20, 9356–9363.
- Mukai, F., Ishiguro, K., Sano, Y., Fujita, S.C., 2002. Alternative splicing isoform of tau protein kinase I/glycogen synthase kinase 3beta. *J. Neurochem.* 81, 1073–1083.
- Murphy, E., 2004. Inhibit GSK-3beta and there's heartbreak ahead. *J. Clin. Invest.* 113, 1526–1528.
- Niederer, K.E., Morrow, D.K., Gettings, J.L., Irick, M., Krawiecki, A., Brewster, J.L., 2005. Cypermethrin blocks a mitochondria-dependent apoptotic signal initiated by deficient N-linked glycosylation within the endoplasmic reticulum. *Cell. Signal.* 17, 177–186.
- Oiyadomari, S., Mori, M., 2004. Roles of CHOP/GADD153 in endoplasmic reticulum stress. *Cell Death Differ.* 11, 381–389.
- Paschen, W., Mengesdorf, T., 2005. Endoplasmic reticulum stress response and neurodegeneration. *Cell Calcium* 38, 409–415.
- Pei, J.J., Braak, E., Grundle-Iqbal, I., Tqbal, K., Winblad, B., Cowburn, A.D., 1999. Distribution of active glycogen synthase kinase 3beta (GSK3beta) in brains staged for Alzheimer disease neurofibrillary changes. *J. Neuropathol. Exp. Neurol.* 58, 1010–1019.
- Putcha, G.V., Moulder, K.L., Golden, J.P., Bouillet, P., Adams, J.A., Strasser, A., EJohnson, M.J., 2001. Induction of Bim, a pro-apoptotic BH3-only Bcl-2 family member, is critical for neuronal apoptosis. *Neuron* 29, 615–628.
- Qu, L., Huang, S., Baltzis, D., Rivas-Estilla, A.M., Pluquet, O., Hatzoglou, M., Koumenis, C., Taya, Y., Yoshimura, A., Koromilas, A.E., 2004. Endoplasmic reticulum stress induces p53 cytoplasmic localization and prevents p53-dependent apoptosis by a pathway involving glycogen synthase kinase-3b. *Genes Dev.* 18, 261–277.
- Rutkowski, D.T., Kaufman, R.J., 2004. A trip to the ER: coping with stress. *Trends Cell Biol.* 14, 20–28.
- Sanjay, A., Fu, J., Kreibich, G., 1998. DAD1 is required for the function and the structural integrity of the oligosaccharyltransferase complex. *J. Biol. Chem.* 273, 26094–26099.
- Scorrano, L., Oakes, S.A., Opferman, J.T., Cheng, E.H., Sorcinelli, M.D., Pozzan, T., Korsmeyer, S.J., 2003. BAX and BAK regulation of endoplasmic reticulum Ca²⁺: a control point for apoptosis. *Science* 300, 135–139.
- Song, L., DeSarno, P., Jope, R.S., 2002. Central role of glycogen synthase kinase-3beta in endoplasmic reticulum stress-induced caspase-3 activation. *J. Biol. Chem.* 277, 44701–44708.
- Stoica, B.A., Movsesyan, V.A., Lea, P.M., Faden, A.I., 2003. Ceramide-induced neuronal apoptosis is associated with desphosphorylation of Akt, BAD, FKHR, GSK-3beta, and induction of the mitochondrial-dependent intrinsic caspase pathway. *Mol. Cell Neurosci.* 22, 365–382.
- Szabadkai, G., Rizzuto, R., 2004. Participation of endoplasmic reticulum and mitochondrial calcium handling in apoptosis: more than just neighborhood? *FEBS* 567, 111–115.
- Takashima, A., Honda, T., Yasutake, K., Michel, G., Murayama, O., Murayama, M., Ishiguro, K., Yamaguchi, H., 1998. Activation of tau protein kinase I/glycogen synthase kinase-3beta by amyloid beta peptide (25–35). *Neurosci. Res.* 32, 317–323.
- Takuma, K., Yan, S.S., Stern, D.M., Yamada, K., 2005. Mitochondrial dysfunction, endoplasmic reticulum stress, and apoptosis in Alzheimer's disease. *J. Pharmacol. Sci.* 97, 312–316.
- Thomas, M., Yu, Z., Dadgar, N., Varambally, S., Yu, J., Chinnaiyan, A.M., Lieberman, A.P., 2005. The unfolded protein response modulates toxicity of the expanded glutamine androgen receptor. *J. Biol. Chem.* 280, 21264–21271.
- Thomenius, M.J., Distelhorst, C.W., 2003. Bcl-2 on the endoplasmic reticulum: protecting the mitochondria from a distance. *J. Cell Sci.* 116, 4493–4499.
- Verkhatsky, A., Toescu, E.C., 2003. Endoplasmic reticulum Ca²⁺ homeostasis and neuronal death. *J. Cell. Mol. Med.* 7, 351–361.
- Wang, X.Z., Kuroda, M., Sok, J., Batchvarova, N., Kimmel, R., Chung, P., Zinsner, H., Ron, D., 1998. Identification of novel stress-induced genes downstream of CHOP. *EMBO J.* 17, 3619–3630.
- Wang, N.S., Unkila, M.T., Reineks, E.Z., Distelhorst, C.W., 2001. Transient expression of wild-type or mitochondrially targeted Bcl-2 induces apoptosis, whereas transient expression of endoplasmic reticulum-targeted Bcl-2 is protective against Bax-induced cell death. *J. Biol. Chem.* 276, 44117–44128.
- Yamaguchi, H., Wang, H.G., 2004. CHOP is involved in endoplasmic reticulum stress-induced apoptosis by enhancing DR5 expression in human carcinoma cells. *J. Biol. Chem.* 279, 45495–45502.